Solubility of Arsenic in multi-component systems

From the microscopic to the macroscopic scale

Promotor: Prof. Dr. Willem H. van Riemsdijk
Hoogleraar Bodemscheikunde en Chemische Bodemkwaliteit

Samenstelling promotiecommissie:

Prof. Dr. Ir. Cees J.N. Buisman
Wageningen Universiteit

Dr. Ir. David G. Kinniburgh
British Geological Survey, Wallingford, UK

Prof. Dr. Ir. Bart A. Koelmans
Wageningen Universiteit

Dr. Ir. Timo J. Heimovaara
Technische Universiteit Delft

Dit onderzoek is uitgevoerd binnen de onderzoekschool SENSE

Solubility of Arsenic in multi-component systems

From the microscopic to the macroscopic scale

Monika Stachowicz

Proefschrift

ter verkrijging van de graad van doctor

op gezag van de rector magnificus

van Wageningen Universiteit

Prof. Dr. M. J. Kropff

in het openbaar te verdedigen

op donderdag 1 november 2007

des morgens te elf uur in de Aula.

Stachowicz, Monika

Solubility of Arsenic in multi-component systems. From the microscopic to the macroscopic scale.

Ph.D. thesis Wageningen University, Wageningen, the Netherlands 2007.
-With references. – With summary in English and Dutch.

ISBN 978-90-8504-765-0

Abstract

Stachowicz, M. (2007) **Solubility of Arsenic in multi-component systems. From the microscopic to the macroscopic scale.**

Doctoral thesis, Wageningen University, the Netherlands

Arsenic in groundwater has generated one of the most important problems with respect to the quality of drinking water in the modern world. The discovery of arsenic contamination in groundwater around the world has stimulated the scientific community to initiate research activities. For a better understanding of what conditions in nature cause naturally elevated arsenic concentrations as well as for designing better treatment techniques an increase in our fundamental knowledge on the interaction of arsenic in complex environmental matrices with iron oxides is essential.

The aim of this thesis has been to answer several questions related with identifying the chemical and geochemical processes responsible for arsenic (de)contamination of water. The research tactics have included 3 sequential steps: (1) obtaining adsorption datasets for mono-component and multi-component systems simulating relevant groundwater field situations; (2) interpretation of these data with a molecular based adsorption model and to apply the model in order to predict the adsorption behavior of arsenic for a very wide range of chemical compositions as they are observed in the field; (3) providing quantitative understanding of the behavior of arsenic in natural waters. In Chapter 2 of this thesis the adsorption of As(III) and As(V) on goethite has been studied as a function of pH and loading. This section gives insight into the basic factors that influence the surface speciation of an adsorbed arsenic ion for both arsenite and arsenate. Since natural systems are very complex some macro-elements, often found in high-As-groundwater, could potentially be relevant for the release of arsenic. Chapter 3 and 4 provide the knowledge on major macro elements and their effect on the behavior of As. In Chapter 3 of this thesis attention is paid mainly to the effects of carbonate on the arsenic sorption. Our goal was to establish a direct link between the presence of bicarbonate and the release of As(V) and As(III) in goethite systems using a pH and concentration range that is relevant for field situations. In Chapter 4 the adsorption of As(III) and As(V) on goethite in the presence of Mg^{2+}, Ca^{2+}, PO_4^{3-}, HCO_3^- has been studied, using 'single-, dual- and triple-ion' systems. The information on As adsorption on goethite has created a scientific basis for Chapter 5, in which the arsenic adsorption and the primary charging behavior of goethite and HFO is modeled in a coherent manner using the CD model approach. This resulted in one set of adsorption parameters, common for both materials. All data were modeled using the CD model incorporating the

available structural information of both the surface and the adsorbed species. Chapter 6 of this thesis uses the information that has been developed in the preceding chapters to perform a scenario/sensitivity analysis of arsenic behavior for Bangladesh conditions. The aim is to asses as good as possible for the present state of the art the factors and processes that govern the arsenic behavior in such aquifers. This knowledge may contribute to the long-term solutions for arsenic problems, such as an optimization of arsenic removal from drinking water as well as a methodology to guide the positioning of new arsenic-free wells.

Key words: arsenic, arsenite, As(III), arsenate, As(V), adsorption, goethite, HFO, iron oxides, CD model, charge distribution, surface speciation, quantum chemical calculations, spectroscopy, Bangladesh

Content

1
Introduction

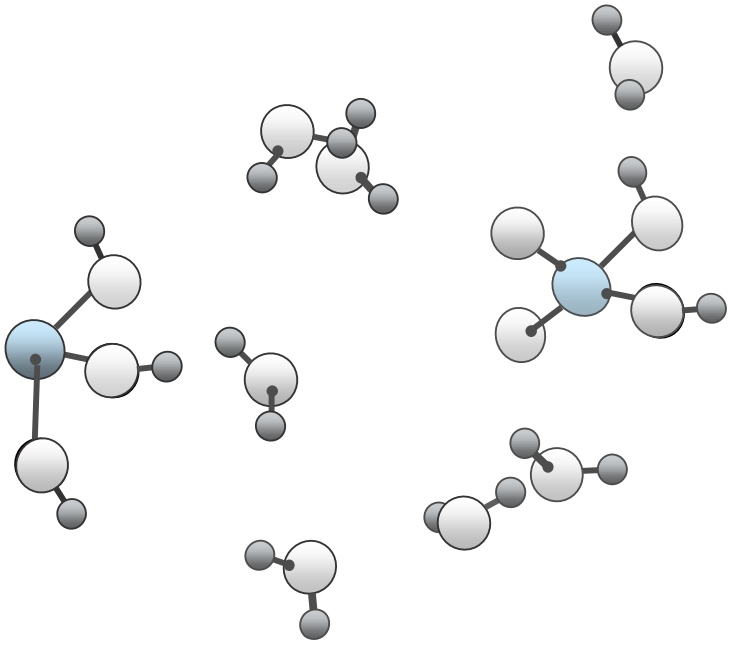

General

Arsenic contamination in groundwater has been recognized in many aquifers in Asia (Bangladesh, China, India), South America (Argentina, Bolivia, Chile), North America (USA, Mexico) and Europe (Greece, Germany, England, Netherlands)(BGS and DPHE 2001; Mandal and Suzuki 2002). In most cases arsenic is a naturally occurring pollutant. Its presence has generated one of the most important problems with respect to the quality of drinking water in the modern world.

In 1970s, many countries in Asia, led by an aspiration to attain a microbiologically safe water source, made a large-scale shift from surface water to groundwater as a water resource (Frankerberger 2002). For years groundwater seemed like a secure solution for widespread water demand. Less than two decades later "the arsenic crisis" emerged (Alaerts and Khouri 2004).

Groundwater contamination with arsenic quickly became a key-issue on political agendas around the world, as it turned out that the number of people affected by this problem worldwide is increasing. In Bangladesh alone it is estimated that tens of millions of people are affected by too high concentrations of arsenic in drinking water (Mandal, Chowdhury et al. 1996; Chakraborti, Biswas et al. 1999; BGS and DPHE 2001; Chakraborti, Rahman et al. 2002). The subject remains highly relevant, since chronic exposure to arsenic in drinking water poses serious health risks, such as: cancer in lungs, bladder, kidney, skin and other skin changes (Gomez-Caminero, Howe et al. 2001; Chakraborti, Rahman et al. 2002). Until now, the actual impact of arsenic exposure on human health has not been accurately evaluated. Taking into account the length of the exposure in the areas affected by arsenic contamination with regard to the latency period of human cancer (Yoshida, Yamauchi et al. 2004), it is certainly possible that this process will require as much as several decades of research to complete. Several millions of people have been already diagnosed with chronic arsenism, and a number of skin cancer cases has been already reported (Yoshida, Yamauchi et al. 2004).

The need to initiate immediate remedial actions has brought many governments to costly investments in new technological solutions. At the same time, the modern water remediation technologies can serve only as a temporary strategy. They directly eliminate health risks caused by drinking contaminated water, nonetheless they also produce immediate toxic wastes (BGS and

DPHE 2001) followed by long-term disposal problems. For countries like Bangladesh or India the technological solution will not ease the problem as long as the public supply of treated water is limited. The population extracts water locally from tube-wells reaching subsurface alluvial aquifers, which happen to be often contaminated with naturally occurring arsenic. Locating an alternative source of safe water is not easy, because the degree of contamination varies widely even within very short distances(BGS and DPHE 2001; Mandal and Suzuki 2002).

There is a tendency to lower the limit for arsenic in drinking water in the western legislations. At first, increased health risks have been reported in association with ingestion of drinking water of arsenic concentrations exceeding 50µg/l (Gomez-Caminero, Howe et al. 2001). Since 1994 World Health Organization (WHO) recommends 10 µg/l as a maximum level content of arsenic in drinking water (Nickson, McArthur et al. 2000). The actual value differs among countries, according to the national drinking water quality standards determined by related legislation. In Bangladesh the limit is now 50, in Europe-10 (BGS and DPHE 2001) and in the USA it will become as low as 5 µg/l (Frankerberger 2002). However, the lower we set the quality standards, the more difficult it is to meet them technically.

The discovery of arsenic contamination in groundwater around the world has stimulated the scientific community to initiate research activities. The data obtained in field studies point to iron oxides as a source of arsenic in water. Besides, most of the water purification and waste treatment techniques related with arsenic contamination are either based on co-precipitation with iron oxides (Sparks 1995; Han, Zimbron et al. 2003) and/or adsorption on iron oxides (Arienzo, Adamo et al. 2002; Katsoyiannis and Zouboulis 2002; Deschamps, Ciminelli et al. 2003; Manna, Dey et al. 2003; Su and Puls 2003; Zeng 2003). For a better understanding of what conditions in nature cause naturally elevated arsenic concentrations, as well as for designing better treatment techniques, an increase in our fundamental knowledge on the interaction of arsenic in complex environmental matrices with iron oxides is essential. In Chapter 2 of this thesis the adsorption of As(III) and As(V) on goethite has been studied as a function of pH and loading. This section gives insight into the basic factors that influence the surface speciation of an adsorbed arsenic ion for both arsenite and arsenate. Adsorption edges have been measured for both species for different loadings (Fig.1) and linked to the experimentally observed surface speciation using spectroscopy, which can be found in the literature. The data were modeled using the CD model incorporating the available structural information of both the surface and the adsorbed species.

The results of quantum chemical calculations (Fig.2), that are used to derive an *a priori* estimated CD value have been compared with the results of the modeling of the adsorption data using spectroscopic information on $As(OH)_3$ binding to iron oxides.

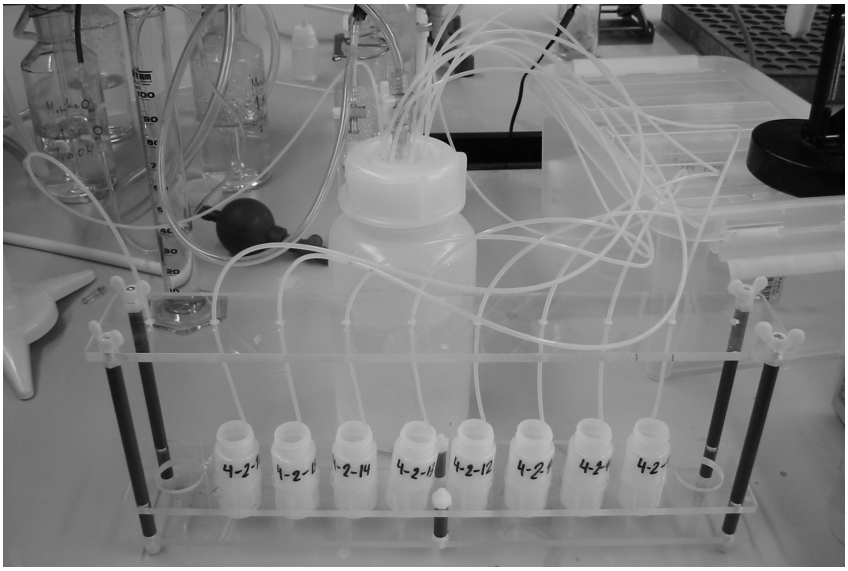

Fig. 1. Experimental set-up for sorption experiments.

The amount of mobile arsenic at field conditions is often linked to the amount of iron found by oxalate extraction (BGS and DPHE 2001). It is believed, that the oxalate-extractable Fe is related to oxide material with a high reactive surface area (Roden and Zachara 1996), and for this reason HFO has been considered a useful proxy for 'field' conditions. The information on As adsorption on goethite has created a scientific basis for Chapter 5, in which the arsenic adsorption and the primary charging behavior of goethite and HFO are modeled in a coherent manner, using the CD model approach. This resulted in one set of adsorption parameters, common for both materials.

Since natural systems are very complex some macro-elements, often found in high-As-groundwater, could potentially be relevant for the release of arsenic. Moreover, the effectiveness of water treatment techniques may be optimized if the understanding of the multi-component interactions is available. Chapter 3 and 4 provide the knowledge on major macro elements and

their effect on the behavior of As. In Chapter 3 of this thesis attention is paid mainly to the effects of carbonate on the arsenic sorption (Fig.1.).

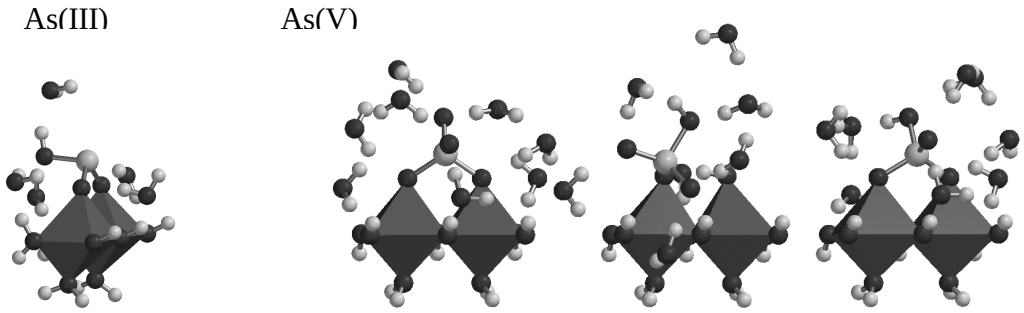

Fig.2. The MO/DFT optimized geometries of As(III) (one structure shown) and As(V) complexes (three structures) used to describe the adsorption of As(III) and As(V) on goethite".

Our goal was to establish a direct link between the presence of bicarbonate and the release of As(V) and As(III) in goethite systems, using a pH and concentration range that is relevant for field situations. In Chapter 4 the adsorption of As(III) and As(V) on goethite in the presence of Mg^{2+}, Ca^{2+}, PO_4^{3-}, HCO_3^- has been studied, using 'single-, dual- and triple-ion' systems.

Arsenic contamination of groundwater has been widely studied (Chowdhury, Basu et al. 1999; BGS and DPHE 2001; Harvey, Swartz et al. 2002; Smedley and Kinniburgh 2002; Swartz, Blute et al. 2004; Harvey, Swartz et al. 2005; Zheng, van Geen et al. 2005). Consequently, a number of explanatory theories have been generated. However, until now the exact combination of natural biological and geochemical processes and conditions, that cause mobilization of arsenic compounds from the solid to the aqueous phase, is unclear. Chapter 6 of this thesis uses the information that has been developed in the preceding chapters to perform a scenario/sensitivity analysis of arsenic behavior for Bangladesh conditions. The aim is to asses as good as possible for the present state of the art the factors and processes that govern the arsenic behavior in such aquifers.

The aim of my project as a whole has been to answer several questions related with identifying the chemical and geochemical processes responsible for arsenic (de)contamination of water. The research tactics have included 3 sequential steps: (1) obtaining adsorption datasets for

mono-component and multi-component systems simulating relevant groundwater field situations; (2) interpretation of these data with a molecular based adsorption model and the application of the model in order to predict the adsorption behavior of arsenic for a very wide range of chemical compositions, as they are observed in the field; (3) providing quantitative understanding of the behavior of arsenic in natural waters.

This knowledge may contribute to the long term solutions for arsenic problems, such as an optimization of arsenic removal from drinking water, as well as a methodology to guide the positioning of new arsenic-free wells (Nickson, McArthur et al. 2000).

2

Surface Speciation of As(III) and As(V) in Relation to Charge Distribution

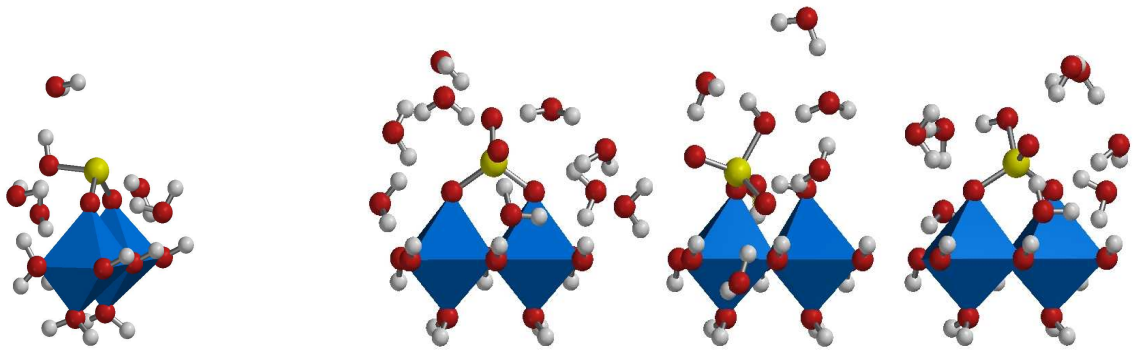

Stachowicz M., Hiemstra T., and van Riemsdijk W. H. (2006) Surface Speciation of As(III) and As(V) in relation to charge distribution. *J. Colloid Interface Sci.* **302**(1), 62-75.

Abstract

The adsorption of As(III) and As(V) on goethite has been studied as function of pH and loading. The data can be successfully described with the charge distribution (CD) model (extended Stern option) using realistic species observed by EXAFS. The CD values have been derived theoretically. Therefore, the Brown bond valence approach has been applied to MO/DFT optimized geometries of a series of hydrated complexes of As(III) and As(V) with Fe(III)(hydr)oxide. The calculated ionic CD values have been corrected for the effect of dipole orientation of interfacial water, resulting in overall interfacial CD coefficients that can be used to describe the surface speciation as function of pH and loading. For As(III), the main surface species is a bidentate complex and a minor contribution of a monodentate species is found, which is in agreement with EXAFS. The CD values have also been fitted. Such an analysis of the adsorption data resulted in the same surface species. The fitted CD values for the bidentate complex points to the presence of strong As-O bonds with the surface and a weaker As-OH bond with the free OH ligand. This agrees quantitatively with the MO/DFT optimized geometry. Interpretation of free fitted CD values for As(V) binding suggests that the main surface species is a non protonated bidentate complex (B) with a contribution of a singly protonated surface complex (MH) at sub neutral pH and high loading. In addition, a protonated bidentate surface complex (BH) may be present. The same species are found if the theoretical CD values are used in the data analysis. The pH dependency of surface speciation is strongly influenced by the charge attribution of adsorbed species to the electrostatic surface plane while the effect of loading is primarily controlled by the amount of charge attributed to the 1-plane, illustrating the different action of the CD value. The MO/DFT geometry optimizations furthermore suggests that for As(V) the B, MH and BH surface complexes may have very similar As-Fe distances which may complicate the interpretation of EXAFS data.

1. Introduction

Metal (hydr)-oxides are omnipresent in nature. They may contribute to the control of the mobility and bioavailability of many elements in the environment via adsorption and desorption processes. Ion binding properties of metal (hydr)-oxides are strongly determined by the structure of the surface and the structure of the surface complexes formed. The microscopic binding modes and structures of surface complexes have been widely studied using various in-situ techniques such as X-ray Spectroscopy like XANES, EXAFS and XRS (Hayes et al., 1987) and InfraRed spectroscopy (Tejedor-Tejedor and Anderson, 1990; Sun and Doner, 1996; Eggleston et al., 1998). Incorporation of the microscopic information, i.e. the structure(s) of the adsorbed entities, in the interpretation of macroscopic adsorption characteristics, is vital for a valid modeling of transport processes and the bioavailability of toxic elements in the environment.

Surface speciation is not a static concept. The binding mode of ions may for instance change as function of the local conditions. It is well known that ligands of surface complexes may protonate or deprotonate. This process is usually not captured by EXAFS, but may be part of IR studies. Surface complexation modeling (SCM) can be a tool to trace changes in surface speciation due to proton exchange reactions. It can only be reliable if the model and preferably the parameters are tightly linked to the microscopic structure of surface complexes involved. This requirement is very important since surface complexation models have a thermodynamic basis that allows description of adsorption data with hypothetical species, if type and number of species can be freely chosen without constraints.

The CD model (Hiemstra et al., 1996) is a typical example of a SCM that is founded in a structural approach and that can link experimentally determined structures to parameter values. An essential parameter in this respect is the charge distribution (CD), which will strongly determine the pH dependency of the adsorption. The ionic charge distribution is related to the structure of the complexes. Recently (Hiemstra and van Riemsdijk, 2006), it was shown that the introduction of ionic charge in the interface may lead to an electrostatic feedback, as result of the orientation of water dipoles in the created electrostatic field. This feedback depends on the type

of species formed and is usually small. The overall electrostatic energy is the combination of both processes. The value of the CD may be used to constrain the type of surface species present, as was recently shown for the adsorption of CO_3^{2-} on goethite. Based on the CD value derived for the carbonate adsorption, it has been hypothesized (Hiemstra et al., 2004) that CO_3^{2-} is mainly bound as a bidentate complex. The dominance of this complex was confirmed in a combined study of ATR-FTIR and MO/DFT calculations (Bargar et al., 2005).

Surface speciation is not only affected by pH. Another factor is surface loading. For instance, it has been shown for phosphate adsorption to iron hydroxides (Tejedor-Tejedor and Anderson, 1990; Arai and Sparks, 2001) that the relative intensity of various IR bands is not only determined by pH, but that it is also affected by the total phosphate loading of the systems. An example of the change in the structure of surface complexes with loading is found for Cd(II) binding to goethite and hydrous ferric oxide (HFO). At low loading, Cd(II) may bind at surfaces in complexes with edge linkage, whereas at high loading also double corner complexes are formed (Spadini et al., 1994; Venema et al., 1997; Spadini et al., 2003; Boily et al., 2005). The last example is for Zn(II) adsorption on silica. An interesting phenomenon has been reported. It is claimed that the Zn(II) ion changes its primary coordination number CN from 6 to 4 as function of loading (Roberts et al., 2003).

Arsenite ($As(OH)_3$) and arsenate (AsO_4^{-3}) are typical examples of adsorbed oxyanions that have been studied frequently over the last decade with EXAFS. A series of authors have studied the surface structure of As(V), adsorbed on goethite (FeOOH) ((Fendorf et al., 1997)). This was also done for As(III) (Manning et al., 1998; Farquhar et al., 2002; Manning et al., 2002; Ona-Nguema et al., 2005). As pointed out by Ona-Nguema et al.(Ona-Nguema et al., 2005), EXAFS results are susceptible to incorrect interpretation due to the limitations of the technique and the literature may not give unambiguous answers as to the exact surface speciation. For instance for As(V), different conditions have been applied in the measurements and different conclusions have been drawn with respect to the types of species that are found to be present. Besides uncertainty in the transformation of the spectral data to reliable electron shells, interpretation of the meaning of the measured speciation in relation to the speciation measured under other experimental conditions (pH, loading, ionic strength, *etcetera*) is difficult without a proper insight in the factors that determine the speciation.

In this paper, we will concentrate on the mechanisms that may determine the change in surface speciation. We will analyze new adsorption data for As(III) and As(V) adsorption on goethite. The data will be modeled using the CD model. We will evaluate the charge distribution obtained in relation to available structural information. The ionic charge distribution for the surface complexes involved will be derived from the geometry of the surface complexes, using the Brown bond valence concept (Brown, 1978; Brown and Altermatt, 1985). These structures will be calculated using molecular orbital calculations applying density functional theory (MO/DFT). The ionic charge distributions derived will be corrected for the dipole effect (Hiemstra and van Riemsdijk, 2006). These results will be used in the CD model. The use of calculated CD values, if reliable, has the practical advantage that the number of adjustable parameters will be strongly reduced. In fact only the binding constant has to be derived for the adsorption data. In this paper, we will focus on the processes that determine the surface speciation. It will be shown why and how surface speciation changes with conditions and to what extent speciation obtained with spectroscopy in various experiments can be interpreted in one general picture.

2. Experimental

2.1. Goethite material

Goethite material used in this study was prepared according to Hiemstra et al.(1989b). Fresh solution of $Fe(NO_3)_3$, dissolved in ultra pure water, 5 dm^3 of 0.5 M, was slowly titrated with 2.5 M NaOH to a pH of 12. Base was added at a rate of 10 cm^3/ min. The suspension was aged at 60 ^oC during about 100 hours and then dialyzed with doubly distilled water until the electric conductivity (EC) was lower than 10 μS/cm. The specific BET-surface area of goethite measured by N_2 gas adsorption was 98 m^2/g. The material was characterized in an acid-base titration experiment for three salt levels: 3.0 10^{-3} M, 1.2 10^{-2} M and 0.1 M $NaNO_3$ by means of a computer-controlled titrator. The initial goethite concentration used in the titration experiment was 16.5 g/L.

For the determination of adsorption edges, the stock of the goethite suspension was diluted with ultra pure water to a concentration of approximately 20.0 g/L. The pH was adjusted to 5.5 and the suspension was purged with moist, cleaned N_2 overnight to remove CO_2.

2.2. Reagents solutions

We prepared the stock solutions ($NaAsO_2$, $NaHAsO_4$ and $NaNO_3$) using 'analytical grade' chemicals (Merck). The solutions were diluted with ultra pure water (≈ 0.018 dS/m) and later stored in polyethylene bottles to avoid silica contamination. In order to avoid CO_2 contamination, all solutions were prepared with pre-boiled water and under N_2 atmosphere. Concentrations of the stock solutions were determined by means of ICP-AES. The solution of 0.100 M NaOH was prepared CO_2-free from Titrasol and stored in a plastic bottle to avoid silica contamination and placed in a dessicator to avoid CO_2 contamination. The solution of 0.100 M HNO_3 was prepared from Titrasol and stored in a glass bottle to avoid contamination by organic material.

2.3. Adsorption experiments

Adsorption experiments were carried out in gas-tight 23.6 ml bottles of low-density polyethylene (Rietra et al., 2001) with fixed amounts of salt, goethite, arsenite and arsenate at different pH values. The pH was adjusted with 0.0100 M or 0.100 M HNO_3 or NaOH. The experiments were done in the pH range 3-11. All solutions were added to the bottles under N_2 atmosphere to prevent CO_2 contamination. The bottles were equilibrated for 24 hours in a shaker in a constant temperature room (~22 ^oC). Next, the bottles were centrifuged and the samples of the supernatant were taken for the ICP-MS analysis. The pH was measured in the bottles after re-suspension of goethite. The total concentrations of components in each bottle, representing one data point, were calculated based on the amounts and concentrations of the solutions added. We used two initial concentrations of As(III), 0.55 and 0.67 mM and three goethite concentrations (3.00, 5.00 and 10.00 g/L), which resulted in five initial surface As(III) loadings (2.23, 1.87, 1.12, 0.68 and 0.51 $\mu mol/m^2$). The initial concentration of As(V) was 0.50 mM and three goethite concentrations were used i.e. 3.0, 5.0 and 10.0 g/L, resulting in three initial As(V) loadings (1.70, 1.02, and 0.51 $\mu mol/m^2$). All background electrolyte concentrations were 0.10 M $NaNO_3$. The total volume of the suspension in each individual bottle was 20.0 ml. The amount of adsorbed arsenite and arsenate was calculated as the difference between the total initial arsenite or arsenate concentration and the measured equilibrium concentration.

2.4. Quantum chemical calculations

The geometries of surface complexes of arsenite and arsenate were calculated using software of Wavefunction (Spartan'04) (Devlin and Buch, 1997). The geometry optimizations were done using density functional theory (DFT). Pseudo potentials, defined in Spartan'04 as LACVP+** (Los Alamos Core Valence Potentials), were used. This set comprises the 6-31+G** basis set for main group elements H-Ar. For As(III), the final geometry was calculated with different models, including BP86, B3LYP, BLYP, EDF1 and a Local (SVWN) model (Kong et al., 2000). The calculated geometry has been interpreted with the Brown bond valence approach (Brown and Altermatt, 1985), in order to obtain the charge distribution value of the complexes. For As(V), only the BP86 model was applied. All calculations were done on hydrated structures.

2.5. Surface complexation modeling

The surface complexation modeling was done with ECOSAT (Keizer and van Riemsdijk, 1998) and FIT (Kinniburgh, 1993). The CD model (Hiemstra and van Riemsdijk, 1996) has been used for modeling the ion adsorption behavior on goethite.

3. Results and Discussion

3.1. Primary charge

The goethite of this study has been prepared simultaneously with the goethite of Weng et al. (Weng et al., 2005) and Rahnemaie et al. (Rahnemaie et al., 2006). The same methods were used, resulting in very similar surface areas. The charging behavior of these goethite materials has been measured separately. The data can be analyzed for a given double layer structure.

Rahnemaie et al. (Rahnemaie et al., 2006) have studied the charging behavior of goethite for a wide range of electrolytes. The position of the individual types of electrolyte ions in the double layer profile was traced with the CD approach for outer sphere complexation. The charge of the various electrolyte ions was allowed to be located in the compact part of the double layer between a minimum distance of approach and the head end of the diffuse double layer (DDL). A critical reevaluation of the data indicates that the charge of most electrolyte ions is approximately at the same position in the compact part of the double layer (Hiemstra and van Riemsdijk, 2006). The extensive data set can also be described using a classical approach, locating the ion charge on

a single electrostatic position (Hiemstra and van Riemsdijk, 2006). A simultaneous description of all data is only possible if the head end of the diffuse double layer (DDL) is separated from the minimum distance of approach of electrolyte ions by a layer of some width. Charge separation between the minimum distance of approach of outer sphere complexes and electrolyte ions in DDL is essential. This model can be classified as an Extended Stern (ES) model (Westall and Hohl, 1980). The data analysis showed that the capacitance of the outer Stern layer (C_2 ~ 0.7 F/m^2) is quite close to the capacitance of the inner layer (C_1~0.9 F/m^2). This picture has recently also been suggested by Sverjensky (Sverjensky, 2005). It has been suggested (Hiemstra and van Riemsdijk, 2006), that the charge separation may be due to ordering of water molecules near the surface. As a consequence, the location of electrolyte ions may change in discrete steps in the structured water layer when approaching the surface. Such stepwise changes have for instance been observed experimentally for the double layer on mica surfaces (Israelachvili and Wennerstrom, 1996).

Three types of surface groups exist on the main 110 face and 100 face (Weidler et al., 1996) of goethite: singly coordinated ≡ FeOH(H), doubly coordinated ≡ Fe_2OH, and triply coordinated ≡ $Fe_3O(H)$ (Hiemstra and van Riemsdijk, 1996). It is assumed that the primary charging behavior of goethite is caused by the protonation of the singly (≡ $FeOH^{-1/2}$) and triply (≡ $Fe_3O^{-1/2}$) coordinated surface oxygens, according to the following reactions (Hiemstra and van Riemsdijk, 1996):

$$\equiv FeOH^{-0.5} + H^{+1} \Leftrightarrow \equiv FeOH_2^{+0.5} \qquad \log K_{FeOH}$$

$$\equiv Fe_3O^{-0.5} + H^{+1} \Leftrightarrow \equiv Fe_3OH^{+0.5} \qquad \log K_{Fe3O}$$

The various batches of goethite material produced ((Weng et al., 2005), (Rahnemaie et al., 2006) and this study), have comparable charging properties, but slight differences exist in the experimental PZC value (9.0-9.3) and capacitance of the Stern layer (C_1= 0.85-0.92 F/m^2). The goethite used for our experiments had a PZC of 9.2 and the charging behavior could be described with C_1=0.85±0.01 F/m^2. The parameters are given in Table 1.

Table1. Table of surface species of H^+, Na^+ and NO_3^{-1} based on data of (Rahnemaie et al., 2006). The charge allocation (z) and the affinity constants were derived from modeling of the goethite titration data of (Rahnemaie et al., 2006) using the extended Stern model. The fitted capacitance of the first Stern layer C_1 = 0.85±0.01. The capacitance of the second Stern layer (C_2= 0.75±0.11 F/m^2) is from (Hiemstra and van Riemsdijk, 2006). The site density of reactive surface groups (FeOH=3.45/nm^2 and Fe_3O=2.7/nm^2) were taken from the literature (Hiemstra and van Riemsdijk, 1996).

Surface species	≡ FeOH	≡ Fe_3O	Δz_0	Δz_1	Δz_2	H^+	Na^+	NO_3^-	logK
≡ $FeOH^{-1/2}$	1	0	0	0	0	0	0	0	0.00
≡ $FeOH_2^{+1/2}$	1	0	1	0	0	1	0	0	9.20
≡ $FeOH^{-1/2}\cdots Na^+$	1	0	0	1	0	0	1	0	-0.60
≡ $FeOH_2^{+1/2}\cdots NO_3^-$	1	0	1	-1	0	1	0	1	8.52
≡ $Fe_3O^{-1/2}$	0	1	0	0	0	0	0	0	0.00
≡ $Fe_3OH^{+1/2}$	0	1	1	0	0	1	0	0	9.20
≡ $Fe_3O^{-1/2}\cdots Na^+$	0	1	0	1	0	0	1	0	-0.60
≡ $Fe_3OH^{+1/2}\cdots NO_3^{-1}$	0	1	1	-1	0	1	0	1	8.52

3.2. Arsenite, As(III)

3.2.1. Two surface species

The solution chemistry of arsenite is relatively simple. At high pH, arsenite is present as $H_2AsO_3^{1-}$ (aq). In the pH range below pH=9.24 (i.e. $logK_H$), a non-charged, trigonal $As(OH)_3$(aq) species is dominant (Frankerberger, 2002). This species may adsorb, forming predominantly a bidentate complex in which two of the ligands interact with a Fe(III) of the solid instead of proton. This may lead to redistribution of the As(III) charge in the complex. Preliminary CD modeling suggests that some positive charge may shift towards the surface. If the individual adsorption edges, which differ in As(III) loading, are analyzed with the CD model, one observes a decrease in the fitted CD value (Δz_0) with the increase of loading (Fig.1), if the presence of only the bidentate species is assumed. The fitting result may change if the presence of an additional surface species assumed, i.e. besides the presence of a bidentate complex, also a monodentate surface complex. In this second analysis, we assume that the charge attribution of As(III) to the surface is twice as high for the bidentate (B) surface complex compared to the monodentate (M) surface complex, since the bidentate ≡ $Fe_2O_2As(III)OH$ complex has two oxygen atoms common with the surface while it is only one for the monodentate ≡ $FeOAs(III)(OH)_2$ complex. With this

assumption, all data could be described very well and the fitted CD value for the bidentate complex becomes independent of the loading (Δz_0 = 0.28±0.03 v.u., Δz_1 = -0.28±0.03 v.u.), as shown in Fig.1.

The above assumption of the presence of a second surface species may agree with the spectroscopic observations (EXAFS) presented in literature (Table 2). Bidentate double corner complexes (^{2}C) are found to be dominant with a minor contribution of monodentate complexes (^{1}V-complexes). The longer As-Fe distance (≈ 355±5 pm) in the spectra is representative for the ^{1}V complex. The As-Fe distance in the bidentate complex is ≈ 334±3 pm. The reported coordination number for both complexes differs and is qualitatively in agreement with the type of complex that is suggested, i.e. CN=1 for a monodentate complex and CN=2 for a bidentate complex.

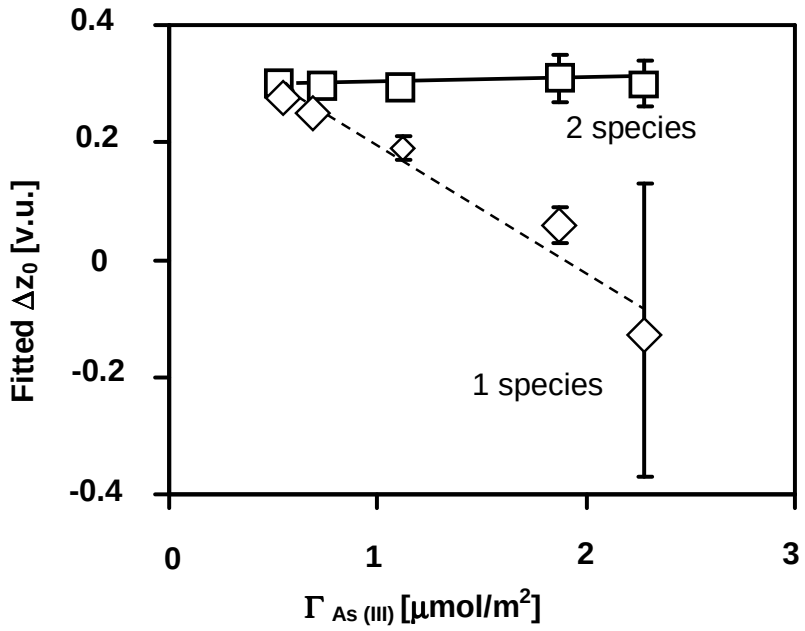

Fig.1. The fitted charge attribution to the surface plane (Δz_0) of a bidentate As(III) surface complex, found by modeling As(III) adsorption data for various loading (Γ). Assuming the presence of only a bidentate As(III) surface complex, the CD decreases with increase in surface loading (the trend is shown as dashed line). In case of the presence of two surface species, a monodentate and a bidentate surface complex, the charge attribution value Δz_0 for bidentate complex formation becomes independent of the loading (the trend is shown as full line).

In the above analysis, the CD values are fitted. However, it will be an advantage if the CD can be derived independently, for instance from an analysis of the structure of a surface complex. The structure of a complex can be found by MO/DFT optimization of the geometry and the calculated bond lengths can be interpreted as bond valence charge.

Recently (Hiemstra and van Riemsdijk, 2006), it has been shown that the introduction of charge in the interface by an ion (n_0, $n_{1,}$) and additionally protons (n_{H0}, n_{H1}), may results in an electrostatic feedback due to the orientation of water molecules in the Stern layer. To derive the overall interfacial charge distribution (Δz_0, Δz_1) the dipole contribution can be combined with the calculated ionic charge distribution found from analysis of the MO/DFT optimized geometry.

Table 2. The experimental coordination number CN and distances R (pm) reported in literature for As(III) complexation by goethite.

Reference	**CN_{As-O}**	**R_{As-O}**	**CN_{As-Fe}**	**R_{As-Fe}**	**Conditions**
Manning et al. 1998	3.06±0.03	179±0.8	2.57±0.01	334±3 357*[1]	pH = 6.4-8.6 I = 10^{-3} M NaCl $\Gamma \geq 1.9$ μmol/m^2
Manning et al. 2002	3.10	178	2.00 1.00	334 346	pH ≥ 5 I = very low $\Gamma = 0.75$ μmol/m^2
Farquhar et al. 2002	4.0	178	2.0	331 -	pH = 6 ± 0.5 I = very low $\Gamma = 0.2$ μmol/m^2
Ona-Nguema et al. 2005	3.19	177±1	1.4 0.4	334±5 355±5	pH = 10.4 I = 0.1 M NaCl $\Gamma = 1.7$ μmol/m^2 Anoxic conditions

*[1] The second shell at d_{As-Fe} = 357 pm improved the fit of the spectra.

3.2.2. Quantum chemical geometry calculations

As a starting point, we defined a cluster with two Fe oxide octahedrons with the appropriate multiplicity. The cluster serves as a template to mimic the goethite mineral. The initial geometry of the octahedrons is set equal to the geometry found for goethite (Hazemann et al., 1991). Additional protons were added to obtain the zero-charged cluster $Fe_2(OH)_6(OH_2)_4$ (z=0). The defined O-H distances were set at 104 pm. In the zero charge cluster, the Fe and OH ions form a kind of central plane with OH_2 groups on top on both sides (Fig 2).

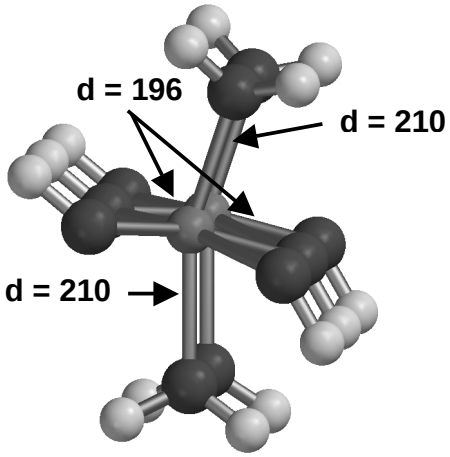

Fig.2. Two Fe (III)-O octahedra with Fe-O distances (pm) and angles as found in goethite (α-FeOOH).

The bidentate As(III) complex was defined by exchanging both H_2O molecules on the top of the cluster against O ligands that are coordinated to As(III). The As(III) is in addition coordinated to a free OH ligand. The exchanged OH_2 ligand on top of each octahedron represents a protonated singly coordinated surface group at the 110 face of goethite. To mimic the influence of hydration, the free OH ligand in the coordination sphere of the adsorbed As(III) was allowed to interact with three water molecules via H bridges (O-H···O). In addition, we defined a hydrogen bond between each common O ligand in the Fe-O-As(III) bond and an additional water molecule. Two additional protons are present to make a zero charged cluster. These protons were located at two singly coordinated OH groups of the central $Fe(OH)_6$ plane. Preliminary calculations showed that these protons were needed to get chemically stable hydration water. Without these protons, dissociation of two water molecules occurred. The protons became bound to most basic OH groups of the central plane in the cluster. As an example, the BP86 optimized As(III) bidentate cluster is shown in Fig.3. The relevant distances in the various optimized structures of the As(III) bidentate complex using different MO/DFT models have been given in Table 3. For the monodentate complex, only one model (BP 86) calculation has been done (Table 4).

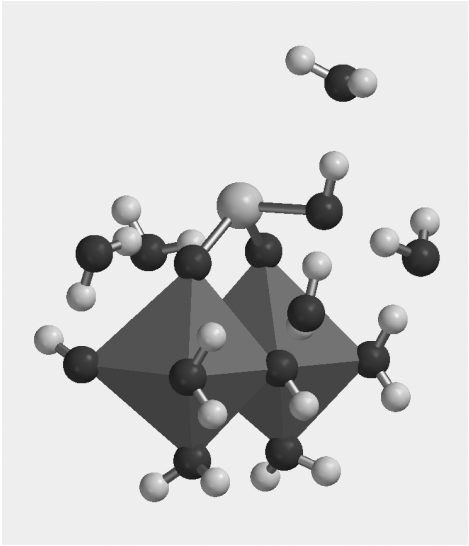

Fig.3. Two Fe(III)-O(H) octahedra with a bidentate arsenite complex on top that is hydrated. The geometry has been optimized with the BP86 model. The overall charge of the cluster is zero.

The calculated distances for the bidentate complex (*d*) can be compared with a previous approximation given in literature usijg various MO/DFT methods . These results are comparable with the exception of the reported average Fe-O distances of about 180 pm. They are very short compared to our optimized value of 196 pm (Table 3), which falls within the range of expected values for singly coordinated OH(H) groups on the surface of goethite. The difference is probably due to our choice to constrain the lower part of both Fe-O octahedrons to the geometry found in goethite ($Fe(OH)_4(OH_2)_2(OH_2)_2$ moiety, Fig 3).

It is interesting to notice that the calculated Fe-As distances in the hydrated bidentate structure fall within the range of distances observed with EXAFS for As(III) adsorbed to goethite (Table 3). For the monodentate complex (Table 4) a larger value is calculated than the observed ($\Delta d_{As\text{-}Fe}$ =20pm). An additional MO/DFT calculation in which the position of the Fe ion of the $Fe(OH)_4(OH_2)_2(OH_2)_2$ moiety (lower part of the octahedron) was allowed to relax, resulted in a Fe-As distance of 365 pm, which is closer ($\Delta d_{As\text{-}Fe}$ =10pm) to the experimental value.

Table 3. The calculated averages and variations (±) in distances (pm) in the geometry of hydrated arsenite bidentate complexes optimized with various MO/DFT models. The bond lengths can be interpreted with the Brow bond values approach resulting in the ionic charge allocation (n_0+$n_{H0,}$ n_1+n_{H1}).

Method	**Local**	**EDF1**	**BP86**	**BLYP**	**B3LYP**	**Exp**
As-OH[*1]	186.1	189.6	191.0	190.3	186.7	178[*2]
O-As[*1]	174.6	176.5	178.0	176.8	176.6	178[*2]
O-As[*1]	178.1	177.0	178.0	178.7	174.7	178[*2]
Fe-O	192±3.5	197±2.0	196±1.8	198±1.5	195±2.5	196[*3]
Fe-As	334±0.6	339±0.7	340±0.6	342±1.5	337±1.5	335±5[*4]
R_0	179.3	180.6	181.9	181.5	179.0	178.9[*5]
n_0+n_{H0}[*6]	+0.17+0	+0.22+0	+0.22+0	+0.21+0	+0.19+0	
n_1+n_{H1}[*6]	-0.17+0	-0.22+0	-0.22+0	-0.21+0	-0.19+0	

[*1] As-OH refers to the bond with the free OH ligand and O-As to the bond with the common oxygen.
[*2] EXAFS data for As(III) adsorbed to goethite d_{As-O} = 179 pm (Manning et al., 1998) d =178 (Manning et al., 2002), d=177±1 pm (Ona-Nguema et al., 2005), d=178 pm (Farquhar et al., 2002). EXAFS data for the As-O distance of $As(OH)_3$ (aq) d = 177 pm (Ramirez-Solis et al., 2004).
[*3] Distance present in the goethite structure without relaxation.
[*4] EXAFS data for the Fe-As distance d = 338±2 pm (Manning et al., 1998) d =334(Manning and Suarez, 2000), d=335±5 (Ona-Nguema et al., 2005), d=331pm (Farquhar et al., 2002).
[*5] Average R_0 for As(III) in minerals (Brown and Altermatt, 1985).
[*6] The calculation method for the ionic charge distribution is given in the Appendix.

Table 4. The calculated distances (pm) in the geometry of a hydrated monodentate arsenite complex optimized with the BP86 model and the ionic charge allocation.

distance	**BP86**	**Exp**
As-OH[*1]	186.6	178[*2]
As-OH[*1]	182.3	178[*2]
O-As[*1]	179.7	178[*2]
Fe-O	212	196[*3]
Fe-As	375	355±5[*4]
R_0	182.8	178.9[*5]
n_0+n_{H0}[*6]	+0.09+0	
n_1+n_{H1}[*6]	-0.09+0	

[*1-6] see Table 3

3.2.3. The charge distributions

The geometries of Table 3 and 4 can be interpreted in terms of charge distribution using the Brown bond valence concept. According to Brown (Brown and Altermatt, 1985), the bond valence *s* is related to the distance *R* as:

$$s = e^{-(R-R_0)/b} \qquad [1]$$

in which b is a constant (b=37 pm) and R_0 is the element specific parameter. The value of R_0 is chosen such that the sum of the bond valences around the As(III) ion corresponds to the formal valence (z=+3). The various R_0 values calculated for the optimized structure are close to the R_0 value found for minerals, indicating that the average As-OH distance is accurately predicted. The calculated bond valences can be transformed into ionic charge distribution values ($n_0 + n_{H0}$, $n_1 + n_{H1}$) (see Appendix). The calculated ionic CD values (based on Brown bond valences) differ from the CD values based on the Pauling concept with equal distribution. The Pauling bond valence concept results in $\Delta z_0 = 0$ and $\Delta z_1 = 0$ v.u. The quantum chemical calculations show that in the As(III) complexes the charge becomes asymmetrically distributed. The arsenic-oxygen bond length is shortened for the bonds with the common oxygens of the complex while the bond length of the free (OH) ligand is made relatively longer. It implies that more charge should be attributed to the surface. The calculated amount is about 0.20±0.03 v.u. for the bidentate complex (Table 3). The calculated ionic charge distribution for the monodentate complex (Table 4) is 0.09 v.u., which is almost half of the value found for the bidentate complex (0.22 v.u.) with the same MO/DFT model (BP86).

The above derived ionic charge distribution coefficients ($n_0 + n_{H0}$ and $n_1 + n_{H1}$) can be corrected for the electrostatic dipole effect that is induced by the introduction of charge in the interface. This correction results in the overall charge distribution coefficients (Δz_0, Δz_1), which is calculated according to Hiemstra and van Riemsdijk (Hiemstra and van Riemsdijk, 2006) as:

$$\Delta z_0 = n_0 + n_{H0} - \phi(n_0 + n_{H0} + \Sigma n_{ref} z_{ref}) \qquad [2]$$

and

$$\Delta z_1 = n_1 + n_{H1} - \phi(n_0 + n_{H0} + \Sigma n_{ref} z_{ref}) \qquad [3]$$

in which n_0 and n_1 are the charge attributions to respectively the 0 and 1-plane of the ion species defined in the reaction equation and n_{H0} and n_{H1} is the charge attributed to the 0- and 1-plane of any additional protons formulated in the reaction equation. The factor ϕ is a proportionality constant ($\phi \sim 0.17$) and n_{ref} is the number of reference groups used in the reaction and z_{ref} is the charge of these reference group(s).

Application of eq.[2] and [3] will be illustrated for the As(III) adsorption. The formation of the mono- and bidentate surface complex can be given as a reaction of $As(OH)_3(aq)$ with respectively one or two singly coordinated surface groups (n_{ref} =1 or n_{ref} =2) with charge z_{ref} (-1/2 v.u.)

$$1 \equiv FeOH^{-1/2} + As(OH)_3^0(aq) \Leftrightarrow \equiv FeO^{-1/2+n_0}As(OH)_2^{n_1} + 1\ H_2O(l) \qquad [4]$$

$$2 \equiv FeOH^{-1/2} + As(OH)_3^0(aq) \Leftrightarrow \equiv Fe_2O_2^{-1+n_0}AsOH^{n_1} + 2\ H_2O(l) \qquad [5]$$

The adsorbing species is $As(OH)_3^0$ (aq), which is uncharged, i.e. the sum $n_0+n_1 = 0$. No additional proton charges are involved (n_{H0} =0 v.u. and n_{H1}=0 v.u.). The calculated interfacial charge distribution coefficients (Δz_0, Δz_1) based on the calculated ionic charge distribution is given in Table 5. The difference between the values of Δz_0, Δz_1 and n_0+n_{H0}, n_1+n_{H1} represents the dipole correction. These corrections are relatively large (respectively 0.07 ± 0.01 and 0.14 ± 0.01 v.u) compared to the ionic charge distribution (0.09 and 0.20 ± 0.03 v.u.).

In the above calculations, the CD values are based on the geometry of a relatively small cluster. It may be expected that a larger cluster and another arrangement of the water molecules may lead to difference in the details of the geometry. However, we do not expect that this will lead to a considerable difference in calculated CD distribution coefficients since it has been suggested (Hiemstra and van Riemsdijk, 2006) that the MO/DFT calculated charge distribution (CD) is relatively insensitive to the exact structure of the metal octahedra that are directly involved in the complexation.

Table 5. The calculation of the interfacial CD coefficients Δz_0 and Δz_1 (v.u.) based on the calculated ion charge distribution derived from MO/DFT optimized geometries with corrections for the dipole energy changes using eq. [2] and [3] for a bidentate complex (B) and a monodentate complex (M).

Complex	**B**	**M**
n_0	+0.20±0.03	+0.09
n_1	-0.20±0.03	-0.09
n_{H0}	0	0
n_{H1}	0	0
$\Sigma n_{ref}. z_{ref}$	-1	-0.5
Δz_0*	+0.34±0.03	+0.16
Δz_1*	-0.34±0.03	-0.16

*Includes dipoles correction using $\phi = 0.17$

The CD values for PO_4 obtained from structures with and without relaxation of the iron octahedrons were found not to be significantly different at the 0.03 v.u. level of accuracy (Hiemstra and van Riemsdijk, 2006). This contrasts with the presence of absence of hydration water, which leads to larger differences (Rahnemaie et al., 2006).

3.2.4. Surface complexation modeling

The above predicted charge distribution values can be compared with the fitted charge distributions. The fitted CD values found for the bidentate surface complex varied for the different experiments between 0.26 and 0.31 v.u. Simultaneous modeling of the adsorption data for all loadings resulted in an average fitted CD value of Δz_0=0.28 ± 0.03 and Δz_1=-0.28 ±0.03 v.u. for the bidentate complex. The value for the monodentate complex has been set to half of those values, i.e. Δz_0=0.14 ± 0.02 and Δz_1=-0.14 ±0.02 v.u.. Unfortunately, the data did not allow a separate derivation of the CD of the monodentate complex with a sufficient accuracy, probably because of the relatively small contribution of this species. Within the uncertainty, the experimental CD (Δz_0, Δz_1) is almost equal to the values predicted (Table 5). We note that the predicted charge distribution depends on the MO/DFT method used (Table 3), but may depend in these calculations on the number and location of the water molecules used for hydration

(Hiemstra and van Riemsdijk, 2006) as well. For an iron-silicate complex, this variation was about 0.03 v.u.

We have used the predicted CD values of Table 5 to describe the adsorption data and we have fitted the corresponding affinity constants. In Fig. 4, the results of the adsorption experiments for five different experiments are given, expressed in the logarithms of the As(III) equilibrium concentrations as a function of pH. The corresponding affinity constants for bidentate and monodentate complex formation are given in Table 6. The data can be described very well ($R^2 = 0.967$).

Table 6. Table of surface species for As(III) with the charge distribution (Table 5) and the affinity constants (log*K*), optimized by fitting of the adsorption data.

Species	≡ FeOH	≡ Fe_3O	Δz_0	Δz_1	Δz_2	$As(OH)_3$	log*K**
≡ $FeOAs(OH)_2$	1	0	0.16 ± 0.02	-0.16 ± 0.02	0	1	4.91 ± 0.05
≡ Fe_2O_2 AsOH	2	0	0.34 ± 0.03	-0.34 ± 0.03	0	1	7.26 ± 0.01

*NB, only the log*K* value is used as adjustable parameter.

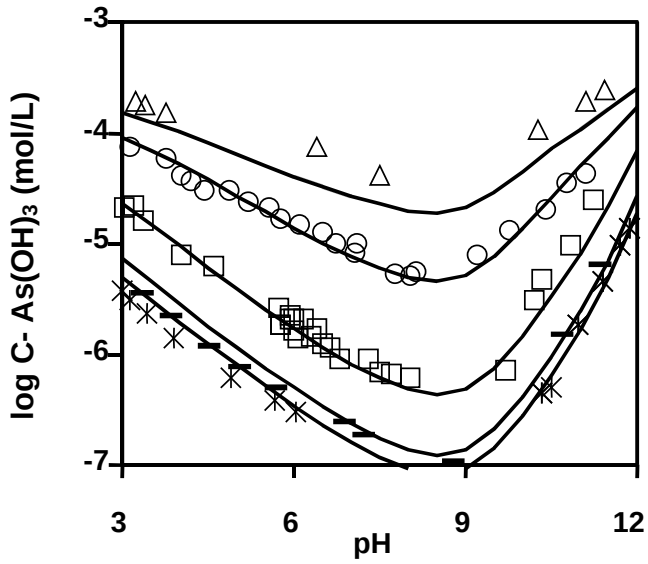

Fig.4. The equilibrium concentration of As(III) in the presence of goethite in 0.1 M $NaNO_3$. Symbols represent the experimental data for the five different initial arsenite loadings i.e. 2.23 (triangles), 1.87 (circles), 1.12 (squares), 0.68 (stripes) and 0.51 (stars) μmol/m^2. Lines are calculated with the fitted log*K* values (Table 6).

3.2.5. As(III) surface speciation

Once the parameters have been derived, we can focus on the question how the surface speciation is expected to change as a function of pH and loading. During the preliminary modeling, we experienced that the largest difference between the data and the calculated curve occurred at low pH and high As(III) loading if we used only a bidentate complex. It indicates that the monodentate species is probably most active under these conditions. In Fig.5, we show the calculated change of the surface speciation as function of pH and as function of loading. The highest contribution of the monodentate species is indeed found at low pH and high loading (Fig.5). The ruling factors behind this behavior are to be discussed.

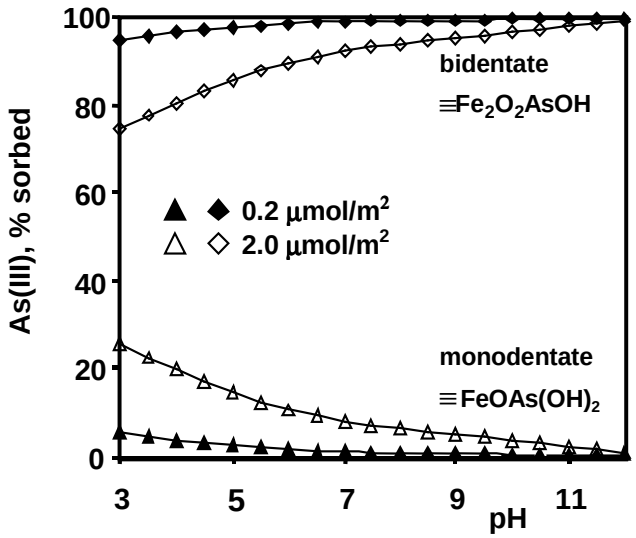

Fig.5. The surface speciation of As(III). Lines with closed symbols show the calculated surface speciation for a low surface loading (about 0.2 μmol/m^2) and the lines with open symbols are for high loading (2 μmol/m^2) at 0.1M $NaNO_3$. Bidentate (≡Fe_2O_2AsOH) is the dominant species over the whole pH range. The contribution of the monodentate complex is low but increases at low pH values and high loading.

3.2.6. pH dependency

The monodentate species has only one ligand common with the surface, which implies less charge interaction with the surface in comparison to the bidentate complex. Introduction of positive charge in the surface leads to the release of protons. In case of monodentate complexes, the release of protons (*p*) will be less than in case of a bidentate species.

A different proton release for mono- and bidentate reactions will lead to a different pH dependency of the formation reactions. To illustrate this, we formulate an equation for the overall thermodynamic reaction describing the interaction of $As(OH)_3$ (aq) with a protonated surface SH:

$$\equiv SH_m + As(OH)_3^0(aq) \Leftrightarrow \equiv SH_{m-p}As(OH)_3^{-p} + p\ H^+(aq) \qquad [6]$$

Equation [6] shows that a higher H^+ concentration will most strongly suppress the As(III) binding of a surface species with a large release of protons (p). This is the surface complex that contributes most charge to the 0-plane (the bidentate complex). The smaller value of p for the monodentate complexes will relatively favor the formation of the monodentate complex at acid conditions.

3.2.7. Loading

A second feature of the change in surface speciation is related to the loading. Fig.5 shows that increase in loading will lead to a relatively higher contribution of the monodentate surface complexes. This can be understood based on electrostatics. As pointed out by Hiemstra and Van Riemsdijk (Hiemstra and van Riemsdijk, 1999), the competition of ions is, in many cases, mainly due to electrostatic interactions. At a given pH, the potential of the 1-plane is most sensitive to change in loading since this location is not buffered by proton charge, in contrast to the surface. With increase of loading, the potential in the 1-plane will increasingly counteract the binding of species via the charge introduced by adsorbing species. The species which will induce the lowest amount of charge in the 1-plane will be relatively favored. In our example, this is the monodentate surface complex, i.e. it will be relatively more important at high loading (Fig.5).

A different model approach for As(III) has recently been proposed by Sverjenski et al. (Sverjensky, 2005). The authors described the As(III) adsorption with the following reaction: $2SOH^0 + 2H^+ + AsO_2OH^{2-} \Leftrightarrow S_2^{2+}$ ---$(AsO_2OH)^{2-} + 2H_2O$. This reaction implies a charge distribution with n_0=+2 v.u. and n_1=-2 v.u. resulting from the assumption in their model that the charge of the protons is located in the 0-plane and the charge of the arsenite ion in the β-plane (TL model), where also the outer sphere complexes of the electrolyte ions are placed. The location for the As(III) moiety is difficult to understand from a spectroscopic point of view. The

created charge distribution is then corrected by an extremely large charge of 2 v.u., in their opinion due to the potential dependent change in dipole energy coming from the release of 2 H_2O molecules from the surface plane, which leads in total to Δz_0=0 v.u. and Δz_1=0 v.u.. The proposed interpretation of the dipole correction strongly differs from ours and is related to two different types of water molecules. In the model of Sverjenski et al. (Sverjensky, 2005), the potential dependent dipole energy is related to water molecules that coordinate strongly with the metal ions of the solid, while in our approach the dipole orientation is related to weakly bound water molecules present in the Stern layer. According to our opinion, the orientation of coordinative water molecules of the solid is independent of strength of the field radiating from the surface in contrast to the water dipoles present in the Stern layer. We note that we are not able to describe our experimental data with Δz_0=0 v.u. and Δz_1=0 v.u. We found on average Δz_0=+0.31±0.03 v.u. and Δz_1=-0.31±0.03 v.u.

3..3. Arsenate, As(V)

In the natural pH range, arsenate dominantly exists in solution as $H_2AsO_4^{-1}$ (between pH 2.2 and 6.9 and as $HAsO_4^{-2}$ (pH 6.9-12.2) (Frankerberger, 2002). Arsenate (V) in solution is fourfold coordinated with oxygen. The As-O bond length is quite sensitive to protonation as can be shown with quantum chemical calculations resulting in an As-OH bond length of 182±6 pm and an As-O bond length of approximately 166±4 pm (Boily, 2003). According to EXAFS measurements (Grafe and Sparks, 2005), the aqueous AsO_3OH^{-2} ion in solution has a mean As-O bond length of 169 pm and a fourfold coordination with oxygen (CN=4.6).

A large series of EXAFS measurements on the As(V) binding to goethite has been done (Table 7). Three important shells have been reported. The most important shell is present at 335 pm. This is interpreted as the formation of double corner complexes (^{2}C). In addition, a shell at 285 pm has been found. Originally, it has been attributed (Manceau, 1995) to As(V) complex formation at the edge (^{1}E) of the Fe octahedra of the solid. Recently, it has been claimed that this shell is a result of As-O-O-As multiple scattering (Sherman and Randall, 2003). The shell with a large distance of about 360 pm has been attributed to the formation of a monodentate surface complex (^{1}V).

Table 7. The experimental distances R (pm) and coordination number CN reported in literature for As(V) complexation by goethite.

Reference	**CN_{As-O}**	**R_{As-O}**	**CN_{As-Fe}**	**R_{As-Fe}**	**Conditions**
Waychunas et al. 1993*[1]			-	-	pH = 8
			ΣCN<4	325	I = 10^{-1} M ?
				360	Γ =1 - 2 μmol/m^2?
Fendorf et al. 1997*[2]	3.7±0.1	166	0.9±0.3	285	pH = 6, 8 & 9
			1.3±0.3	324	I = 10^{-1} M $NaNO_3$
			0.7±0.3	359	Γ = 2.0, 1.6 & 1.2 μmol/m^2
Foster et al. 1998*[3]	5.1	169	-	-	pH = 5
			3.0±0.3	330	I = 10^{-1} M $NaNO_3$
			1.6±0.3	350	Γ ~ 2-10 g As /kg goethite
Manning et al.2002	4.0	170	-	-	pH ≤ 5
			2	336±6	I = very low
			1	353±6	Γ = 0.75 μmol/m^2
Farquhar et al. 2002	4.0	169	0.5	293	pH = 6 ± 0.5
			1.0	330	I = low
			-	-	Γ = 0.4 μmol/m^2
Sherman & Randall	1.0	163	-	-	pH = 3.9 ± 0.05
2003*[4]	3.0	170	2	330	I = 0.1 M $NaClO_4$
			-	-	Γ = 1.16 μmol/m^2

*[1] Possible increase of double corner binding ^{2}C (d =325 pm) relatively to single corner binding ^{1}V (d= 360pm)
*[2] Favorable monodentate binding ^{1}V (d= 360pm) at lowest surface coverage / highest pH.
*[3] personal communication.
*[4] The As-Fe shell at about 285 pm is probably due to As-O-O-As multiple scattering (MS).

In the past, following the example of phosphate, As(V) adsorption on goethite has been modeled with the CD model using three surface species; i.e. a bidentate (≡ $Fe_2O_2AsO_2$), a protonated bidentate surface species (≡ Fe_2O_2AsOOH)(Hiemstra and van Riemsdijk, 1999; Antelo et al., 2005), and a monodentate (≡ $FeOAsO_3$).

3.3.1. Quantum chemical geometry calculations

For the MO/DFT calculations, the zero-charged cluster $Fe_2(OH)_6(OH_2)_4$ (z=0) was used (Fig.2). Three different As(V) complexes were defined by the exchange of one or two water molecules, representative for singly coordinated surface groups on the 110 face of goethite. These complexes are a non-protonated bidentate ≡ $Fe_2O_2AsO_2$, a protonated bidentate ≡ Fe_2O_2AsOOH and a protonated monodentate ≡ $FeOAsO_2OH$ complex. Hydration was mimicked by interaction of each free ligand of As(V) with two or three water molecules via H bridges (O-H···O). In

addition, we defined a hydrogen bond between each common O ligand in Fe-O-As(V) bond and an additional water molecule. The geometries were optimized using the BP86 model option. The relevant geometry data are given in Table 8.

The BP86-MO/DFT calculations result in quite some variation in the As(V)-O bond length that is due to the interaction of these oxygens with the Fe(III) ion of the solid or a proton. In the EXAFS analysis, usually only one average distance is reported. This average distance of about 168±2 pm is almost equal to the calculated As-O distance of the free oxygen ligand(s) in the complexes, but is systematically different from the average distance (172.4±0.5 pm). This leads to a higher R_0 (182.2 pm) than found for minerals.

Table 8. The calculated average and variation (±) in distances (pm) in the geometry of hydrated arsenate complexes optimized with the DFT-B86 model.

Complex	Bi	Exp	BiH	Exp	MH	Exp
n-H_2O	8	-	8	-	7	-
-O-As	175.7	168±2[*1]	173.3	168±2[*1]	173.7	168±2[*1]
-O-As	175.5	168±2[*1]	172.7	168±2[*1]	-	-
As-O	175.3	168±2[*1]	-	-	169.2	168±2[*1]
As-O	169.7	168±2[*1]	168.9	168±2[*1]	170.4	168±2[*1]
As-OH	-	-	177.8	168±2[*1]	184.4	168±2[*1]
Fe-O	199±0.3	196[*2]	202±0.6	196[*2]	213	196[*2]
Fe-As	333±1.0	330±5[*3]	330±0.0	330±5[*3]	329	355±5[*3]
R_0	181.8	176.7[*4]	181.3	176.7[*4]	182.2	176.7[*4]
$n_{H0}+n_0$[*5]	+2-1.64	-	+2-1.50	-	+1-0.74	-
n_1+n_{H1}[*6]	-1.36+0	-	-1.50+1	-	-2.26+1	-

[*1] EXAFS data for As-O are between = 166 and d = 170 pm, see Table 7.
[*2] Distance present in the goethite structure without relaxation.
[*3] EXAFS data for Fe-As see Table 7
[*4] R_0 value based on average As-O distance of 168 pm, As(V) in minerals (R_0 =176.7) (Brown and Altermatt, 1985).
[*5, *6] an example of the calculation is given Appendix

Sherman and Randall (Sherman and Randall, 2003) have optimized the geometry of some Fe-As(V) complexes with MO/DFT. Their computational approach differs from ours. The As(V)

complexes were non-hydrated and the iron octahedrons were allowed to relax freely. The IR optimized structures are two types of doubly protonated bidentate complexes ≡ $Fe_2O_2As(OH)_2$, i.e. edge or double corner sharing, and a doubly protonated monodentate complex ≡ $FeOAsO(OH)_2$, i.e. single corner sharing. Our interpretation of these reported structures with the Brown bond valence approach gives an average R_0 value of 182±2 pm, which is equal to the average number (182±0.5 pm) found in our calculations. A very remarkable and important difference is the Fe-As distance. For the double corner complex, we find the same Fe-As distance which corresponds to the main distance observed with EXAFS. However, the Fe-As distances in the protonated monodentate complexes are totally different.

In our calculation, the Fe-O-As bond gets an angle of 116 ^{o}, whereas the Fe-O-As bond is almost linear in the monodentate complex (^{1}V) calculated by Sherman and Randall (Sherman and Randall, 2003). It is interesting to notice that bending of the Fe-O-As bond is also found for scorodite ($FeAsO_4(OH_2)_2$, s), an iron-arsenate mineral with a six fold coordination of Fe (Kitahama et al., 1975; Hawthorne, 1976). This mineral has single corner sharing, as in the calculated complex. The difference in bond angle leads to a very different prediction of the As-Fe distance which may have important consequences. If our calculated Fe-As distance is representative for monodentate complexation, interpretation of the EXAFS shell at about 330 pm can be ambiguous and the shell found can be due to mono- as well as bidentate complex formation. We note that for gibbsite, Ladeira et al. (Ladeira et al., 2001) did not calculate an important difference between the metal -As(V) distance in the single (309 pm) and double corner (318 pm) complexes (EXAFS $d_{Al\text{-}As(V)}$ =319 pm).

Arsenate and phosphate have similar electronic structures and properties. Optimization of the hydrated structure of a protonated monodentate complex of PO_4 (Rahnemaie et al.) resulted, as for AsO_4, in a relatively short Fe-P distance of 317 pm, which is of the same order as the Fe-P distance in the bidentate complex ($d_{Fe\text{-}P}$=325 pm). In this calculation, the Fe-O-P bond was also bended. This has also been reported for the protonated monodentate complex optimized with MO/DFT by Kwon and Kubicki (Kwon and Kubicki, 2004). In other words, the very comparable results for AsO_4 and PO_4 support the proposition that differentiation between a bidentate complex and a protonated monodentate complex for AsO_4 is at present very uncertain on the basis of only an experimental distance observed with EXAFS.

3.3.2. Surface complexation modeling

The adsorption data of our experiments at various As(V) loading are given in Fig.6. According to the general interpretation of EXAFS spectroscopy data for As(V), bidentate complex formation can be considered as most important and it has been suggested (Hiemstra and van Riemsdijk, 1999) that the adsorption data can be described assuming only the presence of protonated and non-protonated bidentate complexes. In a first approach, we modeled our data using only $\equiv Fe_2O_2AsO_2$ and $\equiv Fe_2O_2AsOOH$. The reactions can be formulated as:

$$2 \equiv FeOH^{-1/2} + 2H^+(aq) + AsO_4^{-3}(aq) \Leftrightarrow \equiv Fe_2O_2^{-1+n_0+2}AsO_2^{n_1} + 2\ H_2O(l) \qquad [7]$$

$$2 \equiv FeOH^{-1/2} + 3H^+(aq) + AsO_4^{-3}(aq) \Leftrightarrow \equiv Fe_2O_2^{-1+n_0+2}AsOOH^{n_1+1} + 2\ H_2O(l) \qquad [8]$$

in which n_0+n_1=-3 v.u.

The log*K* and CD values for the formation of both species have been derived by fitting, yielding respectively the charge distribution coefficients of Δz_0=0.35 ± 0.02 v.u. and Δz_1=-1.65 ±0.02 v.u. for the formation of $\equiv Fe_2O_2AsO_2$ and Δz_0= 0.33 ± 0.03 v.u. and Δz_1=-1.33 ±0.03 v.u. for the formation of $\equiv Fe_2O_2AsOOH$ (R^2=0.98). For the protonated species, the fitted CD value is far from the theoretical CD calculated assuming a Pauling distribution, i.e. Δz_0=0.5 v.u. and Δz_1=-1.5+1=-0.5 v.u. (the latter value includes the proton charge present on one of the outer ligands). The fitted CD value (Δz_0= 0.33 & Δz_1=-1.33), is more representative for the formation of a protonated monodentate instead of a protonated bidentate complex. The Pauling CD value of the protonated monodentate complex is Δz_0= 0.25 and Δz_1=-1.25. Therefore, we assumed in the next approach, besides the presence of a bidentate species ($\equiv Fe_2O_2AsO_2$), also the presence of a protonated monodentate species ($\equiv FeOAsO_2OH$). The reaction for $\equiv FeOAsO_2OH$ is given as:

$$1 \equiv FeOH^{-1/2} + 2H^+(aq) + AsO_4^{-3}(aq) \Leftrightarrow \equiv FeO^{-1/2+n_0+1}AsO_2OH^{n_1+1} + 1\ H_2O(l) \qquad [9]$$

The experimental data can be described reasonably well (R^2=0.98) and the fitted CD values are Δz_0=0.69±0.02 v.u., Δz_1=-1.69±0.02 v.u. for the bidentate species and Δz_0=0.33±0.03 v.u., Δz_1=-1.33±0.03 v.u. for the protonated monodentate species. At first glimpse, the values are

not too different from the Pauling CD values, which are respectively Δz_0=0.5 v.u. & Δz_1=-1.5 v.u. and Δz_0=0.25 v.u. & Δz_1=-2.25+1=-1.25 v.u. for a bidentate and a protonated-monodentate surface species. We experienced that in the above approach the number of degrees of freedom to get a good description of the data is already high if two species are chosen. Introduction of a third surface species, in combination with a free fit of the CD values, does not lead to an improved description of the data and does not point to the presence of an additional species. For a further modeling of the adsorption data, we followed the same approach as described above for As(III), using predicted CD coefficients. This reduces the number of adjustable parameters from 4 to 2.

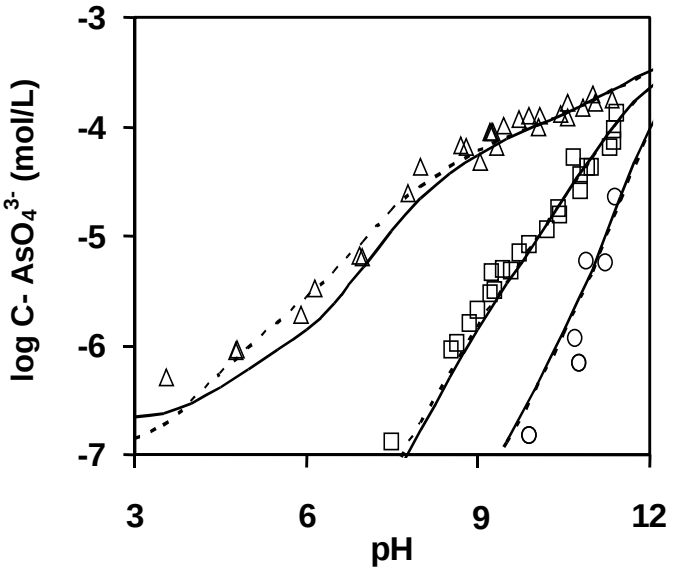

Fig.6. Equilibrium concentrations of As(V) in the presence of goethite (log scale). The initial As(V) concentration was 0.50 mM. Symbols represent experimental data for three goethite concentrations, i.e. 3 g/L (triangles), 5 g/L (squares), and 10 g/L (circles). Full lines show the simulation with fitted affinity constants (Table 10) assuming the presence of two surface species (option I). Dashed lines show the simulation assuming three surface species (option II).

Correction of the ionic CD values (n_0+n_{H0}, n_1+n_{H1}) for the dipole effect results in the overall charge distribution coefficients (Δz_0, Δz_1), given in Table 9. The fitted affinity constants are in Table 10 for two different options, i.e. using B and MH (option I) or B, BH and MH (option II). The new data analysis reveals that only two surface species are needed to describe the data. The calculated adsorptions are given in Fig.6 as solid lines. The quality of the fit remains

good (R^2=0.97), using only two adjustable parameters. The fitting shows that we are not able to distinguish between both model options. As will be shown in the next paragraph, this is due to the dominance of the bidentate species. The contribution of other complexes is relatively low in our experiments.

In the above approaches, the reactions of arsenite (eq. [4-5]) and arsenate (eq. [7-9]) are assumed to take place with singly coordinated surface groups (≡ $FeOH^{-0.5}$). Triply coordinated surface groups (≡ $Fe_3O^{-0.5}$) are supposed not to form inner sphere complexes. This is rationalized on the theorem that over saturation of charge of common oxygen ligand(s) in the innersphere complex (> 0 v.u.) will lead to unstable structures (Bargar et al., 1997).

Table 9. The calculation of the interfacial CD coefficients Δz_0 and Δz_1 (v.u.) based on the calculated ion charge distribution derived from the MO/DFT optimized geometries with corrections for the dipole energy changes using eq. [2] and [3].

Complex	**B**	**BH**	**MH**
n_0	-1.64	-1.50	-0.74
n_1	-1.36	-1.50	-2.26
n_{H0}	2	2	1
n_{H1}	0	1	1
$\Sigma n_{ref}.\ z_{ref}$	-1	-1	-0.5
Δz_0	+0.47	+0.58	+0.30
Δz_1	-1.47	-0.58	-2.30

Table10. Table of surface species for As(V). The affinity constants (log*K*) were optimized by fitting of the adsorption data (option I- two surface species, option II- three species). The charge distribution (CD) values were calculated from the MO/DFT optimized structures (Table 9).

	Species	≡ FeOH	≡ Fe_3O	Δz_0	Δz_1	Δz_2	H^+	AsO_4^{3-}	log*K*
Option I R^2=0.97	≡ $FeOAsO_2OH$	1	0	0.30	-1.30	0	2	1	26.76 ± 0.05
	≡ $Fe_2O_2\,AsO_2$	2	0	0.47	-1.47	0	2	1	29.28 ± 0.02
Option II R^2=0.97	≡ $FeOAsO_2OH$	1	0	0.30	-1.30	0	2	1	26.62 ± 0.12
	≡ $Fe_2O_2\,AsO_2$	2	0	0.47	-1.47	0	2	1	29.29 ± 0.02
	≡ $Fe_2O_2\,AsOOH$	2	0	0.58	-0.58	0	3	1	32.69 ± 0.32

3.3.3. As(V) surface speciation

The above parameter sets (Table 10) can be used to calculate the surface speciation. The speciation for our experimental conditions is shown in Fig.7 for option II. The calculations show that the main surface species is the non-protonated bidentate (B) surface complex ≡ $Fe_2O_2AsO_2$. It is dominantly present in our experiments at all pH values (pH 4-10) and loading conditions studied (Γ~0.5-1.7 umol/m^2).

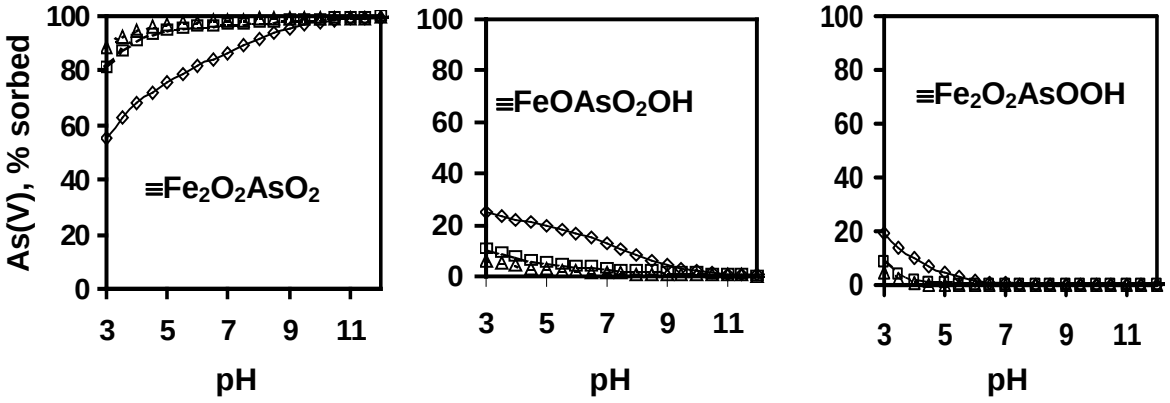

Fig.7. The surface speciation of As(V) calculated using option II. The symbols show the surface speciation for three initial surface loadings 1.70 (diamonds), 1.02 (squares) and 0.51 μmol/m^2 (triangles) in 0.1M $NaNO_3$. Bidentate (≡ $Fe_2O_2AsO_2$) is the dominant species; however, the monodentate (≡ $FeOAsO_2OH$) is becoming increasingly important at lower pH. The presence of the monodentate is more pronounced for higher loadings.

Another surface species is the protonated monodentate (MH) ≡ $FeOAsO_2OH$ complex. This species is found in the sub-neutral pH range below pH<~7. If the presence of a protonated bidentate complex is assumed, this species is only found at very low pH (pH< ~3-5). As can be seen from the experiment, unfortunately almost no data are present in this pH range. Differentiation between both protonated surface species is very uncertain and the data can be described almost equally well using the combination B-MH and B-MH-BH (see also Fig. 6).

3.3.4. pH dependency and loading effect

The above calculations show that the non-protonated bidentate surface species is in all cases dominant. As follows from Fig.7, this is particularly true for a low surface coverage (Γ) as has been used for instance in the experiments of Farquhar et al. (Farquhar et al., 2002) and

Manning et al. (Manning et al., 2002) (Γ_{As}= 0.4-0.75 μmol/m^2, Table7). With increase of loading, the situation will change. According to our calculations, a higher surface coverage, leads to an increasing presence of the (protonated) monodentate species. We have calculated the expected surface speciation for the experiments of Sherman and Randall (Sherman and Randall, 2003) and Fendorf et al. (Fendorf et al., 1997) with the parameters derived in the above given approach (option I). The experiments of Sherman and Randall (Sherman and Randall, 2003) have been done at pH=3.9 and a loading of $\Gamma_{As} \approx 1.2$ μmol/m^2 . According to our prediction, only a small fraction is present as monodentate surface complex (~10 %). The most important species is the non-protonated bidentate complex (~90%) For the experimental conditions of Fendorf et al.(Fendorf et al., 1997), we calculate for pH 6, 8 and 9 respectively a contribution of ~30, ~11 and ~5% of the MH surface complex. These authors (Fendorf et al., 1997) claimed the presence of a monodentate complex on the basis of a feature in the spectrum at ~360 pm. As discussed above, it is possible that this shell is not due to the presence of the MH surface species, if the B and MH species have almost indistinguishable Fe-As distances (Table 8).

The formation reactions of B (eq.[7]) and MH (eq.[9]) are written with the same number of protons, whereas the last one increases at low pH at the expense of the other (Fig.7). It nicely illustrates that the pH dependency should not be judged on the basis of the number of protons in the formation reaction alone. What counts is the number of protons that are co-adsorbed with the binding of the species. The proton co-adsorption is very strongly determined by the average location of the charge in the interface, in particular the charge attributed to the surface. In case of the formation of the MH species, the net amount of charge added to the surface is 0.3 v.u. (Table 9) which is smaller than that for the B surface species (0.5 v.u.). The higher attribution of positive charge results in a lower proton co-adsorption, which implies that the bidentate complex becomes less favorable at low pH than binding of the protonated monodentate species.

With respect to the effect of loading, one should focus on the amount of charge that is introduced in the 1-plane. The B species introduces more negative charge (-1.47 v.u.) in the 1-plane than the MH species (-1.30 v.u.), as follows from Table 9. As argued above for As(III), it leads to more accumulation of charge when the B species is adsorbed and as a result the potential in the 1-plane will change faster than in case of MH binding. It is important to remember that the potential in the 0-plane is almost not affected by adsorption, due to the buffering by the protons bound at the surface groups, i.e. the electrostatic effect of loading is mainly due to changes in the

1-plane. The MH species introduces less charge in the 1-plane (Table 9), which implies that this species is favored with increase in As(V) loading. In general, the species that introduces the lowest amount of charge in the 1-plane is more favored at high loading.

4. Conclusions

- Adsorption of As(III) and As(V) on goethite can be described successfully with the CD model incorporating available structural information. The charge distribution values can be calculated with the Brown bond valence approach using the MO/DFT optimized geometries of surface complexes in combination with a correction for change in dipole orientation. In case of As(III), the dipole correction is relatively large compared to the ionic charge distribution.
- CD modeling reveals that the main As(III) surface species is a bidentate complex. At low pH and high loading also a monodentate complex is present as a minor species. This agrees with EXAFS data. The fitted CD of the bidentate complex points to the presence of asymmetry in the charge distribution, i.e. positive charge is directed to the surface ligands (Δz_0 = + 0.28 v.u.). This conclusion is supported by the results of MO/DFT calculations ($n_0 = 0.20 \pm 0.03$ v.u.) and the expected dipole correction (0.14 v.u.).
- Interpretation of free fitted CD values for As(V) adsorption suggests the presence of a bidentate complex as the main species and some contribution of a protonated species. The use of theoretical CD values for As(V) reveals the presence of two or three main surface species, i.e. a dominant non-protonated bidentate (B) present over a wide range of pH values, and a protonated monodentate complex (MH) formed at sub neutral pH values. At very low pH, a protonated bidentate complex (BH) may also contribute.
- The MO/DFT calculations suggest that the main As(V) surface species (B, BH and MH) may have very comparable As-Fe distances which may complicate the interpretation of EXAFS data.
- Surface speciation of the adsorbed species is a function of conditions such as pH and loading. The pH dependency of adsorption is strongly related to the charge that is introduced in the surface plane, since this factor has a strong influence of the proton co-adsorption and is thermodynamically linked to the pH dependency of adsorption. The

charge attribution to the 1-plane is important when trying to understand the effect of loading on the internal competition of the various surface species. A surface species that introduces a lower amount of charge in 1-plane is more favored at high loading.

- With increase in loading, monodentate complexes of As(III) increases relatively to the bidentate complexation. For As(V), the protonated monodentate is more favored than the bidentate complexation at high loading.

5. Appendix

The MO/DFT approach allows the calculation of the distances between atoms in the structure of the complex (Tables 3, 4 & 8). These distances can be interpreted with the Brown bond valence concept, which describes the relationship between the calculated distances *R* and the bond valence *s* (eq.[1]). The bond valences can be used to calculate the remaining formal charge present on the ligands of the 0- and 1-plane, i.e. the formal ionic charge distribution (n_0+n_{H0}, n_1+$n_{H1)}$, which can be corrected for the dipole effect using eq.[2] & [3]. The calculation procedure is illustrated below for As(III) and As(V).

In case of an As(III) bidentate complex, the As-OH and O-As distances, calculated with MO/DFT (BP86), are respectively are *R* = 191.0, 178.0 and 178.0 pm (Table 3). The corresponding Brown bond valence *s* can be calculated using a R_0 value that results in a bond valence sum (Σs) that is equal to the formal valence of As (Σs=+3 v.u.). Application of eq.[1] with the appropriate R_0 value (Table 3) gives respectively *s* = 0.88, 1.11 and 1.11 v.u. The bidentate complex has two bonds with the surface, each attributing +1.11 v.u. to the 0-plane. Also the charge of two OH^- groups is located in the 0-plane (-1 v.u. each). The total ionic charge $n_{0,}$ introduced in the surface with reaction eq.[5], equals $n_0 = 2\ s_{As\text{-}O} + 2\ z_{OH} = 2 * 1.11 + 2 * -1 =$ +0.22 v.u. Because the $As(OH)_3$ species is neutral, the sum n_0+n_1= 0 v.u., which leads to n_1=-0.22 v.u. In reaction equation [5], no additional protons are formulated, i.e. n_{H0}=0 v.u. and n_{H1}=0 v.u. resulting in n_0+n_{H0}= +0.22 v.u. and n_1+n_{H1}= +0.22 v.u. This ionic charge distribution can be corrected for the effect of dipole orientation using eq.[2] and [3], leading to the overall CD values Δz_0 and Δz_1 (Table 5).

In case of an As(V) bidentate complex, the calculated O-As distance corresponding to the bonds with the surface are R = 175.7 pm and 175.5pm (Table 8). Brown bond valence equation (eq.[1]) with the appropriate value of R_0 leads bond valences of respectively s = 1.18 and +1.19 v.u. Also the charge of two oxygens is attributed to the surface, resulting in $n_0 = \Sigma\, s_{As\text{-}O} + 2\, z_O$ = 1.18+1.19 + 2 * -2 = -1.64 v.u. Based on the charge of the As(V) species, we have n_0+n_1=-3 v.u., leading to n_1= -1.36 v.u. According to the adsorption reaction [eq.7], two additional protons are involved which are located in the 0-plane, i.e. n_0+n_{H0}= +0.36 v.u. and n_1+n_{H1}= -1.36 v.u. Also this ionic charge distribution can be corrected for the effect of dipole orientation (eq.[2],[3]), giving the overall CD values Δz_0 and Δz_1 of Table 9.

3

The Arsenic -Bicarbonate Interaction on Goethite Particles

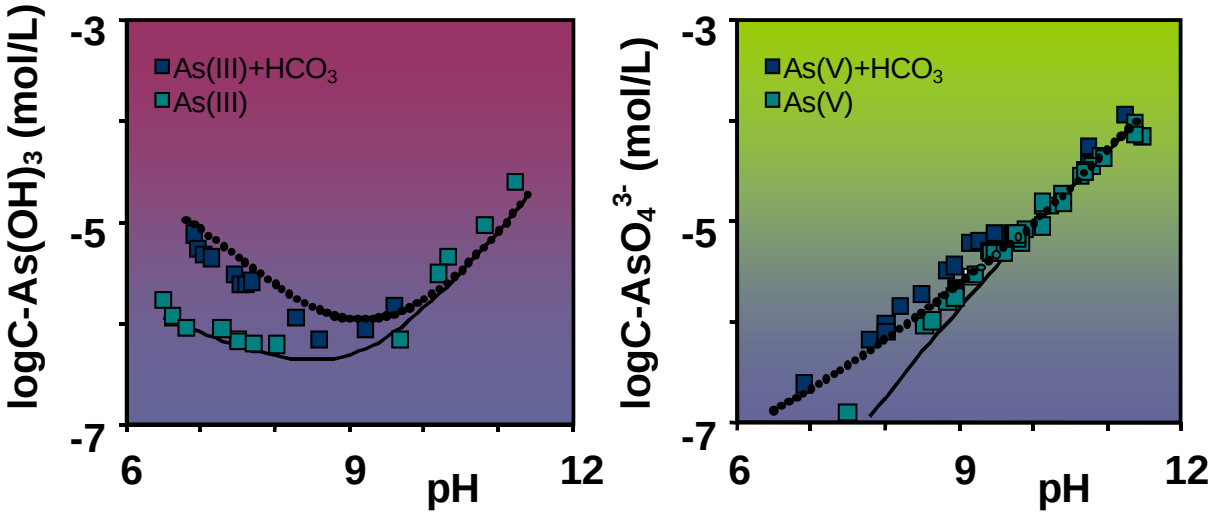

Stachowicz M., Hiemstra T., and van Riemsdijk W. H. (2007) Arsenic and bicarbonate adsorption on goethite. *Environ. Sci. Technol.* **41**(16), p. 5620-5625.

Abstract

The As(V) and As(III) interaction with HCO_3 has been studied for goethite systems using a pH and As concentration range that is relevant for field situations. Our study shows that dissolved bicarbonate may act as a competitor for both As(V) and As(III). In our closed systems, the largest effect of bicarbonate occurs at the lowest experimental pH values (pH~6.5), which is related to the pH dependency of the carbonate adsorption process. The experimental data have been modeled with the charge distribution (CD) model. The CD-model was separately parameterized for goethite with 'single ion' adsorption data of HCO_3, As(III), and As(V). The competitive effect of HCO_3 on the As(III) and As(V) release could be predicted well. Application of the model shows that the natural As loading of aquifer materials (~ < 0.01-0.1 µmol/m^2 or <1-5 mg/kg) is at least about >1-2 orders of magnitude smaller than the As loading based on the competition of As-HCO_3 alone. It indicates that another, very prominent competitor, like phosphate and natural organic matter, will strongly contribute to the control of As in natural systems.

1. Introduction

Arsenic contamination in groundwater has been reported for many aquifers in Asia, South America, North America and Europe (BGS and DPHE, 2001; Mandal and Suzuki, 2002). The presence of arsenic is problematic since a chronic exposure to arsenic in drinking water creates serious health risks, such as cancer in lungs, bladder, kidney, and skin and also other skin changes (Gomez-Caminero et al., 2001; Chakraborti et al., 2002). In natural waters, arsenic is found mostly in the inorganic form (Inskeep et al., 2002). Under intermediate redox conditions, it may be present in the oxidized form as arsenate, As(V), and/or in its reduced form as arsenite, As(III) (Smedley and Kinniburgh, 2002). While in many countries the arsenic content in water exceeding 10 μg/L is considered as a health threat, the aqueous concentrations of arsenic can range from <0.5 up to even 5000 μg/L (BGS and DPHE, 2001) in these aquifers.

A large number of chemical and biogeochemical processes have been proposed that may explain the mobilization of arsenic compounds (Harvey et al., 2005). High arsenic concentrations in groundwater are often accompanied by (bi)carbonate concentrations exceeding 300 mg/L (BGS and DPHE, 2001; Garcia-Sanchez et al., 2005). So far however, the literature sources give contradictory information on what the relation is, if any (Nickson et al., 1998; BGS and DPHE, 2001). Binding to minerals, in particular metal oxides, has been proposed to play a key role in understanding the origin of the high As levels in groundwater systems. It has been argued that high arsenic concentrations can be explained by the competitive action of bicarbonate (Appelo et al., 2002; Anawar et al., 2004). Like arsenate and arsenite (Wilkie and Hering, 1996; Raven et al., 1998; Dixit and Hering, 2003; Arai et al., 2004), (bi)carbonate may adsorb strongly to iron oxides (Villalobos and Leckie, 2000; Villalobos and Leckie, 2001) and therefore, it may influence the speciation and mobility of arsenic. For this reason, the effects of carbonate on the arsenic sorption are particularly important to understand.

The competitive interaction of bicarbonate with adsorbed arsenate (AsO_4) has only been studied experimentally by Arai et al. (Arai et al., 2004), for Fe_2O_3 systems purged with argon or air. The authors found suppression as well as enhancement of the As(V) binding. Some pseudo-

equilibrium data suggest, according to the authors, a very small effect that is only present at the highest pH levels (pH~8). However, one may notice that in contrast to the conditions in groundwater systems, a very high As(V) concentration (~0.4 mM) and a low CO_2 pressure was used.

The arsenic content of sediments is related to the presence of iron (BGS and DPHE, 2001; Swartz et al., 2004). With respect to the choice of the Fe(III) oxide materials in adsorption studies, ferrihydrite is generally assumed to be the major Fe(III) hydroxide in oxidized and slightly reduced sediments. However, a recent study using Mössbauer spectroscopy for a large variety of lake sediments (van der Zee et al., 2003) showed that the iron oxide fraction consisted (except in one case) of nanogoethite particles, not ferrihydrite. The particles are estimated to be 5 nm or smaller (van der Zee et al., 2003). Nanogoethite particles were also identified as the major iron fraction in two marine sediments, even under anoxic conditions. The amount of nanogoethite, determined in a soil with Mössbauer spectroscopy agreed with the amount of ammonium-oxalate extractable iron oxide (Thompson et al., 2006). This latter fraction is usually interpreted as resulting from ferrihydrite (Roden and Zachara, 1996), but may also refer to nanogoethite (Thompson et al., 2006). The above suggests that goethite can be considered as a simple proxy to improve our understanding of the ion interactions in soils and sediments that have predominantly Fe(III) oxides. Nevertheless, it is important to note that at strong reduction Fe(III) (hydr)oxides may significantly transform into for instance magnetite (Fe_3O_4), siderite ($FeCO_3$), or pyrite (FeS_2) which are thermodynamically stable at a low pe value. In that case, a relatively large acid-soluble Fe(II)/Fe(III) ratio, e.g. 0.3-0.9 (Horneman et al., 2004) can be observed.

As(III) can be a dominant species in groundwater (Smedley and Kinniburgh, 2002). Therefore, the influence of bicarbonate on the As release will not only be measured in the present study for As(V) but also for As(III). As(III)-(bi)carbonate interaction is expected because Meng et al. (Meng et al., 2002) have found less removal of As(III) from groundwater by iron oxide in case of the presence of HCO_3. Moreover, Radu et al. (Radu et al., 2005) found in a column study with iron oxide coated sand that an increase of the partial pressure of $CO_2(g)$ has a more distinct influence on the mobility of As(III) than of As(V) at pH 7.

Kim et al. (Kim et al., 2000) hypothesized that the release of As(III) can be due to the formation of aqueous As(III)-carbonate complexes. Formation of such complexes has recently

been confirmed by Neuberger et al. (Neuberger and Helz, 2005), but these complexes are negligible at (bi)carbonate concentrations found in most natural waters. In case of extraction with high HCO_3 concentrations (0.1-1.2M $NaHCO_3$) (Anawar et al., 2004), arsenite-carbonate complexes may contribute to the As(III) release.

Given the arsenic water contamination concern and the debate on the origin of arsenic (Nickson et al., 1998; Appelo et al., 2002; Harvey et al., 2002; Smedley and Kinniburgh, 2002), as well as the correlation found with bicarbonate (BGS and DPHE, 2001; Garcia-Sanchez et al., 2005) and also the absence of strong experimental data, it is important to establish quantitatively the effects of the presence of bicarbonate on the arsenic adsorption by iron oxides. We will study the direct link between the presence of bicarbonate and the release of As(V) and As(III) in goethite systems using a pH and concentration range that is relevant for field situations. The data will be compared with model predictions using the charge distribution (CD) model, which will be parameterized separately with adsorption data from 'single'-ion systems of As(III),As(V) (Stachowicz et al., 2006), and CO_3 (Villalobos and Leckie, 2000).

2. Experimental

2.1. Goethite material

Goethite material was prepared according to Hiemstra et al. (1989a). The specific N_2-BET-surface area is 98 m^2/g. The material has been characterized in an acid-base titration experiment (Stachowicz et al., 2006). The PZC is 9.2.

2.2. Reagents solutions

Stock solutions were prepared CO_2-free from 'analytical grade' chemicals (Merck) and pre-boiled ultra pure water (≈0.018 dS/m) under N_2 atmosphere (except $NaHCO_3$) and stored in polyethylene bottles, avoiding silica contamination. The As concentrations were standardized against commercial stock solutions using ICP-AES,. The solution of 0.100 M NaOH was prepared CO_2-free from Titrasol and stored in a plastic bottle, which was placed in a dessicator to avoid respectively silicate and carbonate contamination. The solution of 0.100 M HNO_3 was prepared from Titrasol and stored in a glass bottle to avoid contamination by organic material.

The pH of a goethite stock suspension diluted with ultra pure water to 20 g/L adjusted to 5.5 and the suspension was purged with moist N_2 overnight to remove CO_2.

2.3. Arsenic-bicarbonate competition experiments

Adsorption experiments were carried out in gas-tight 23.6 ml bottles of low-density polyethylene (Rietra et al., 2001). Appropriate fixed volumes of 2 M $NaNO_3$ solution, 20g/L goethite, and 11 mM arsenite or 10 mM arsenate were added to each bottle. To create a pH range, variable amounts of 0.1 M acid or base and water were added. All solutions were added to the bottles under a moist N_2 atmosphere. Any 0.2 M bicarbonate solution was added at the end, without N_2 flushing, and the bottles were immediately closed. The final volume was 20.0 ml. The bottles were equilibrated for 24 hours in a shaker at room temperature (~22 ^oC). Next, the bottles were centrifuged and the samples of the supernatant were taken for the ICP-MS analysis. The pH was measured in the bottle after re-suspension of the goethite.

2.4. Calculations

The total concentrations of the components in each bottle, representing one data point, were calculated based on the amounts and concentrations of the solutions added and used as input in the surface complexation model. The amount of carbonate present as CO_2 in the gas phase of the bottles (3.6 ml gas per 20 ml solution) was found from chemical equilibrium calculations and taken into account during modeling. All the model calculations have been done with recent versions of ECOSAT (Keizer and van Riemsdijk, 1998) and FIT (Kinniburgh, 1993).

3. Results and discussion

The effect of (bi)carbonate on the adsorption of arsenate, $H_xAsO_4^{-3+x}$, in batch experiments is given in Fig.1. The total bicarbonate concentration used was 0.01 M. This value was selected to reflect the average groundwater concentration in Bangladesh, i.e. ~0.008 M (460 mg/L). To get a constant background electrolyte level, the experiment was done in 0.1 M $NaNO_3$. The experimental pH range was limited to pH $\geq$ 6.5 to minimize the amount of CO_2 in the gas phase above the suspension. Our calculations show that, for the conditions mentioned, less than 6.5% of the bicarbonate added was present in the gas phase. The added amount of As(V) results

in relevant arsenic concentrations in the pH range of interest. Under our experimental conditions, bicarbonate has influence on the adsorption of As(V) particularly in the lowest part of the pH range (Fig.1).

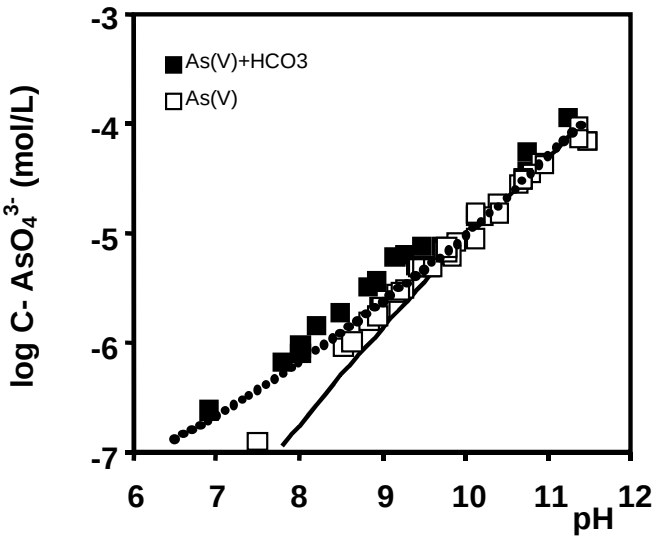

Fig.1. The logarithm of the equilibrium concentrations of As(V) as function of pH in the absence (open symbols) and presence (closed symbols) of 0.01 M (bi)carbonate in 0.1 M $NaNO_3$ - goethite systems (5 g/L) with an initial As(V) concentration of 0.50 mM equivalent with 1.0 μmol/m^2. The full model line is calculated using parameters fitted for 'single' ion systems. The dotted model line is a pure model prediction for the competitive system.

A pH of about 7 is typical for the groundwater systems of Bangladesh, but values well above 8 can also be found in other aquifers with elevated As concentrations like in Spain (Garcia-Sanchez et al., 2005). The observed effect of (bi)carbonate on the As (V) concentration is rather limited which agrees with other results. Radu et al. (Radu et al., 2005) examined the influence of CO_2(g) on As(V) mobility at pH 7 in column experiments and found no effect of carbonate at low partial pressures of CO_2(g) corresponding to 3.6 mM or less total carbonate. At a very high P_{CO2} (10^{-1} bar), equivalent with 23 mM total carbonate, a decrease in the As(V) adsorption (11%) was observed. These observations illustrate the high affinity character of the As(V) binding in comparison to (bi)carbonate.

The effect of the presence of bicarbonate in case of As(III) is given in Fig.2. Similar as for As(V), the presence of (bi)carbonate increased the arsenite concentration in solution, particularly

evident in the pH range relevant for Bangladesh groundwater. In our experiments, the As(III) concentration increased about 10 times at the lowest pH value due to the presence of 0.01 M bicarbonate.

As(V) and As(III) differ in competition with HCO_3. Such differences may depend on pH and loading and can only be interpreted in detail if the competition can be quantified in a model.

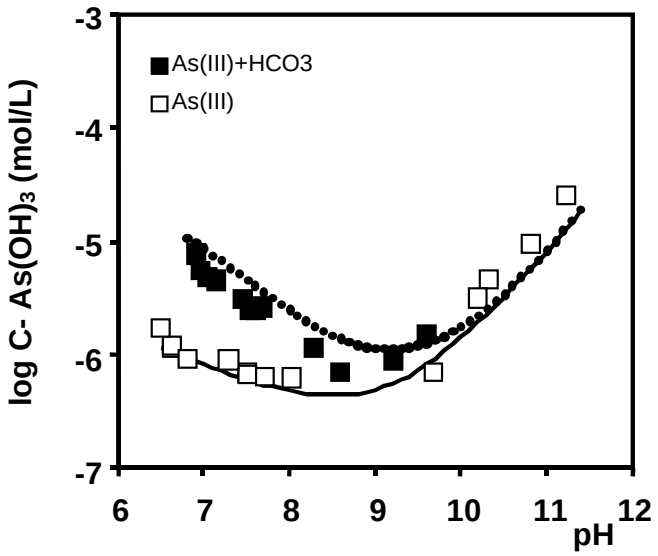

Fig.2. The logarithm of the equilibrium concentrations of As(III) as function of pH in the absence (open symbols) and presence (closed symbols) of 0.01 M (bi)carbonate in 0.1 M $NaNO_3$ - goethite systems (5 g/L) with an initial As(III) concentration of 0.55 mM equivalent with 1.1 μmol/m^2. The full model line is calculated using parameters fitted for 'single' ion systems. The dotted model line is a pure model prediction for the competitive system.

4. Modeling and predicting the As concentrations

For modeling of the data, we first describe the adsorption model and the relevant reactions. After parameterization on the adsorption data of 'single' ion systems ('pseudo-monocomponent' adsorption data), the effect of bicarbonate on the arsenic adsorption will be predicted and compared with the data.

4.1. Double layer model

At an oxide surface, electrolyte ions can form outer sphere complexes (ion pairs) that usually are located at the minimum distance of approach. The simplest representative model approach is known as the Basic Stern (BS) model (Westall and Hohl, 1980). Recently, a refinement of this double layer picture has been suggested (Hiemstra and van Riemsdijk, 2006) based on the analysis of a consistent set of titration data obtained for goethite in the presence of various types of electrolyte ions comprising Li^+, Na^+, K^+, Cs^+, NO_3^-, and Cl^- (Rahnemaie et al., 2006). The data analysis shows that the head end of the diffuse double layer (DDL) is separated from the minimum distance of approach of electrolyte ions by a second Stern layer with a capacitance of C_2=0.9±0.3 F/m^2 (Hiemstra and van Riemsdijk, 2006), resulting in model known as the Extended Stern (ES) approach (Westall and Hohl, 1980). According to Hiemstra and Van Riemsdijk (Hiemstra and van Riemsdijk, 2006), this double layer structure is due to the alignment of water molecules near the surface in 2 to 3 water layers, as can be observed spectroscopically (Toney et al., 1995; Weidler et al., 1998; Fenter and Sturchio, 2004; Catalano et al., 2006).

4.2. Primary charge

Electron microscopy shows for our goethite preparations needle-shaped particles. Such particles have predominantly 110/100 and 001/021 faces (Weidler et al., 1998; Manceau et al., 2000; Gaboriaud and Ehrhardt, 2003). Three types of surface groups exist on these goethite faces, i.e. singly ≡ FeOH(H), doubly ≡ Fe_2OH, and triply ≡ $Fe_3O(H)$ coordinated surface oxygens (Hiemstra et al., 1996). The assumption for goethite is that the primary charging behavior is caused by the protonation of ≡ $FeOH^{-1/2}$ and ≡ $Fe_3O^{-1/2}$ according to (Hiemstra and van Riemsdijk, 1996):

$$\equiv FeOH^{-1/2} + H^+(aq) \Leftrightarrow \equiv FeOH_2^{+1/2} \qquad \log K_{FeOH} \qquad [1]$$

$$\equiv Fe_3O^{-1/2} + H^+(aq) \Leftrightarrow \equiv Fe_3OH^{+1/2} \qquad \log K_{Fe3O} \qquad [2]$$

The proton affinity constant of both reactions have been set equal to the value of the PZC (9.2). The site densities of reactive surface groups are N_s(FeOH)=3.45/nm^2 and N_s(Fe_3O)=2.7/nm^2 (Hiemstra and van Riemsdijk, 1996). The ion pair formation of these surface groups is defined in

Table 1. The titration data can be described with the ES model using a fitted inner Stern layer capacitance of C_1 = 0.85 ± 0.01 F/m^2 (Stachowicz et al., 2006). The outer capacitance is set at C_2=0.75 F/m^2 (Hiemstra and van Riemsdijk, 2006).

Table1. Table defining the surface species of H^+, Na^+, NO_3^-, Cl^-, As(III), As(V) and HCO_3^-.

Surface species	≡ FeOH	≡ Fe_3O	Δz_0 [*1]	Δz_1 [*1]	Δz_2	log*K*[*2]
≡ $FeOH^{-1/2}$	1	0	0	0	0	0.00
≡ $FeOH_2^{+1/2}$	1	0	1	0	0	9.2
≡ $FeOH^{-1/2}\cdots Na^+$	1	0	0	1	0	-0.60
≡ $FeOH_2^{+1/2}\cdots NO_3^{-1}$	1	0	1	-1	0	9.2-0.68=8.52
≡ $FeOH_2^{+1/2}\cdots Cl^{-1}$	1	0	1	-1	0	9.2-0.45=8.75
≡ $Fe_3O^{-1/2}$	0	1	0	0	0	0.00
≡ $Fe_3OH^{+1/2}$	0	1	1	0	0	9.2
≡ $Fe_3O^{-1/2}\cdots Na^+$	0	1	0	1	0	-0.60
≡ $Fe_3OH^{+1/2}\cdots NO_3^{-1}$	0	1	1	-1	0	9.2-0.68=8.52
≡ $Fe_3OH^{+1/2}\cdots Cl^{-1}$	0	1	1	-1	0	9.2-0.45=8.75
≡ $FeOAsO_2OH$	1	0	0.30	-1.30	0	26.62
≡ $Fe_2O_2AsO_2$	2	0	0.47	-1.47	0	29.29
≡ Fe_2O_2AsOOH	2	0	0.58	-0.58	0	32.69
≡ $FeOAs(OH)_2$	1	0	0.16	-0.16	0	4.91
≡ Fe_2O_2AsOH	2	0	0.34	-0.34	0	7.26
≡ Fe_2O_2CO	2	0	0.68	-0.68	0	22.33 ± 0.01

[*1] The charge allocation (Δz) for the arsenic and carbonate species are from respectively (Stachowicz et al., 2006) and (Hiemstra and van Riemsdijk, 2006).
[*2] The log*K* values for Na^+, NO_3^- and Cl^- are from (Hiemstra and van Riemsdijk, 2006)). The log*K* values for As(V) and As(III) are from (Stachowicz et al., 2006). The log*K* for the carbonate species has been found in this study by optimizing the data of (Villalobos and Leckie, 2000)), for open (log*K*= 22.34 ±0.01, R^2= 0.970) and closed systems (log*K*= 22.32 ±0.01, R^2= 0.972).

4.3. CD model

Near a surface, the gradient of the electrostatic potential is usually very large. In this gradient, innersphere complexes are located. To calculate the overall electrostatic interaction, the charge is distributed over two electrostatic positions (0- and 1-plane) each with its own electrostatic potential (Hiemstra and van Riemsdijk, 1996). This charge distribution (CD) approach is used in the modeling of the arsenic and (bi)carbonate adsorption.

4.4. Adsorption of As(III) and As(V)

The surface complexation of As(III) has been studied for goethite with Extended X-ray Absorption Fine Structure (EXAFS) (Fendorf et al., 1997; Manning et al., 1998; Farquhar et al., 2002; Ona-Nguema et al., 2005). The data show that As(III) is predominantly bound as a binuclear bidentate surface complex. At a very high loading, some formation of monodentate complexes is observed. The reactions with singly coordinated surface groups (Sun and Doner, 1996) can be formulated respectively as:

$$2\equiv FeOH^{-1/2} + As(OH)_3(aq) \Leftrightarrow \equiv (FeO)_2^{-1+\Delta z_0} AsOH^{\Delta z_1} + 2\,H_2O\,(l) \qquad [3]$$

$$1\equiv FeOH^{-1/2} + As(OH)_3(aq) \Leftrightarrow \equiv FeO^{-1/2+\Delta z_0} As(OH)_2^{\Delta z_1} + 1\,H_2O\,(l) \qquad [4]$$

in which the sum of the charge distribution values is zero ($\Delta z_0+\Delta z_1=0$).

The charge distribution within the complex can be established with a bond valence analysis (Brown and Altermatt, 1985) of the geometry of the surface complexes (Hiemstra and van Riemsdijk, 2006). The geometry of hydrated iron-arsenite complexes can be found by molecular orbital calculations (MO) using density functional theory (DFT) (Stachowicz et al., 2006). To establish the interfacial CD coefficient, a correction is required for changes in the dipole orientation of water molecules adsorbed in the inner Stern layer (Hiemstra and van Riemsdijk, 2006). An independent calculation of the CD values has the practical advantage that the number of adjustable parameters is reduced by a factor 2 in the modeling. The approach has been applied to the modeling of the As(III) adsorption on goethite (Stachowicz et al., 2006). The CD values and affinity constants are given in Table 1. These parameters can also describe the As(III) behavior reported previously by Dixit and Hering (Dixit and Hering, 2003), after a limited adjustment of the log$K$ values of $\Delta\log K \approx -0.4$.

In the past, following the example of phosphate, As(V) adsorption on goethite was modeled using three surface species, *i.e.* a monodentate, bidentate, and protonated bidentate surface complex (Hiemstra and van Riemsdijk, 1999). This approach was also used by Antelo et al. (Antelo et al., 2005). Recently (Stachowicz et al., 2006), the adsorption of As(V) has been described using CD values found from the MO/DFT optimized geometries of hydrated iron-arsenate species. Application of these theoretical CD values (corrected for dipole effects) in the

analysis of the adsorption data results in a set of affinity constants (Stachowicz et al., 2006) and allows to identify a non-protonated bidentate complex ($\equiv (FeO)_2AsO_2$) as the main species in the pH range of interest. No other species is allowed by the data to be dominantly present in this pH range if the CD value is not fitted but independently calculated. The adsorption reaction can be formulated as:

$$2\equiv FeOH^{-1/2} + 2H^{+} + AsO_4^{-3}(aq) \Leftrightarrow \equiv (FeO)_2^{-1+\Delta z_0} AsO_2^{\Delta z_1} + 2\,H_2O\,(l) \qquad [5]$$

with $\Delta z_0+\Delta z_1= -1$. Note that this sum of charge (-1) is equal to total charge added by the adsorption of one AsO_4^{-3} and two H^+ ions (eq.5).

A singly protonated monodentate surface complex ($\equiv FeOAsO_2OH$) has been found to play a role below pH ~7 at high loading, where also a protonated bidentate ($\equiv (FeO)_2AsOOH$) might be present (Stachowicz et al., 2006), leading to:

$$1\equiv FeOH^{-1/2} + 2H^{+} + AsO_4^{-3}(aq) \Leftrightarrow \equiv FeO^{-1/2+\Delta z_0} AsO_2OH^{\Delta z_1} + 1\,H_2O\,(l) \qquad [6]$$

$$2\equiv FeOH^{-1/2} + 3H^{+} + AsO_4^{-3}(aq) \Leftrightarrow \equiv (FeO)_2^{-1+\Delta z_0} AsOOH^{\Delta z_1} + 2\,H_2O\,(l) \qquad [7]$$

The above presented surface speciation, found by the analysis of the adsorption data (Stachowicz et al., 2006), can be in line with available spectroscopic results (Waychunas et al., 1993; Fendorf et al., 1997; Foster et al., 1998; Farquhar et al., 2002; Manning et al., 2002; Sherman and Randall, 2003). According to our MO/DFT calculations (Stachowicz et al., 2006), all above mentioned As(V) surface species have very similar As-Fe distances, close to the values observed with EXAFS. This indicates that a detailed differentiation with EAXFS between the various species used in this study is expected to be difficult. The CD values and log*K* values are given in Table 1.

4.5. Adsorption of CO_3

The adsorption of CO_3 on goethite has been measured for open and closed systems in $NaNO_3$ and NaCl by Villalobos and Leckie (2000). As shown by Hiemstra et al. (2004), analysis

of the adsorption data using the CD model, points to the formation of a bidentate surface complex, i.e. ≡ $(FeO)_2CO$. Recently, the formation of such a complex has been confirmed with a combination of ATR-FTIR spectroscopy and MO/DFT calculations (Bargar et al., 2005). The reaction can be formulated as:

$$2\equiv FeOH^{-1/2} + 2H^{+} + CO_3^{-2}(aq) \Leftrightarrow \equiv (FeO)_2^{-1+\Delta z_0} CO^{\Delta z_1} + 2\,H_2O\,(l) \qquad [8]$$

with $\Delta z_0+\Delta z_1=0$.

The geometry of a hydrated bidentate CO_3 complex has recently been optimized to obtain the interfacial CD coefficients (Hiemstra and van Riemsdijk, 2006). Only the affinity constant of this complex (Table 1) has to be derived by modeling for which we use the CO_3 adsorption data of (Villalobos and Leckie, 2000).

4.6. Predicting the HCO_3-As interaction

The parameters for describing the primary charge, arsenate, arsenite, and carbonate adsorption (Table 1) can now be used in combination to predict the (bi)carbonate-arsenic competition. The predicted competition is given in the Figs. 1 and 2 as dashed lines. Within the experimental error, the effect of competition is predicted very well.

In our systems, the largest interaction of bicarbonate occurs at the lowest pH values and is related to the pH dependency of the carbonate adsorption. In closed systems, the carbonate adsorption peaks around pH values of pH~6-7 (Villalobos and Leckie, 2000; Villalobos and Leckie, 2001). If such measurements are done in an open system, the interaction would be stronger at high pH values since the amount of carbonate in solution increases strongly with pH (Villalobos and Leckie, 2000; Villalobos and Leckie, 2001). With the model used, this effect can be quantified. The result is shown in the Appendix.

5. Environmental implications

The As concentrations in aquifers are reported to be correlated with bicarbonate (BGS and DPHE, 2001; Garcia-Sanchez et al., 2005). In Fig.3, we have predicted the effect of an increase

of the bicarbonate concentration on the As(V) binding at a pH value for groundwater (pH 7) and surface water (pH 8). In biologically active sediments, CO_2 is produced which may increase the HCO_3^- concentration to a typical value of a few hundred mg/L. Natural sediment samples generally have a reactive surface area of only a few m^2/g. In combination with a typical value for the solid : solution ratio of a porous medium (4 kg/l), this may lead to a reactive surface area of 10000 m^2/L, as used in Fig.3.

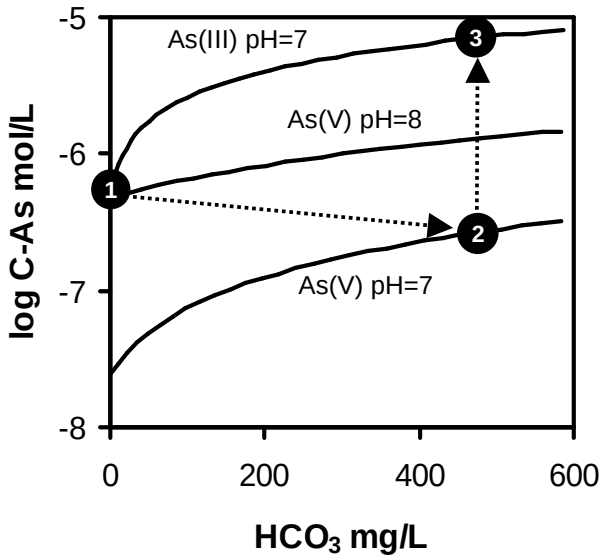

Fig.3. The predicted arsenic concentration in solution in a goethite system (10000 m^2/l, As-total = 750 mg/l, 0.01 M $NaNO_3$) as function of the bicarbonate concentration at different conditions. The two lower solid lines are for As(V) at pH 7 and 8, and the upper line is for As(III) at pH 7. The arrows suggest a reaction path between three hypothetical systems (black symbols), *i.e.* surface water (1), oxidized groundwater (2), and reduced groundwater (3). An increase of the partial CO_2 pressure and the corresponding decrease of pH diminish the As(V) concentration, while a subsequent change in redox state, from As(V) to As(III), increases the As concentration.

The As loading has been chosen (0.01 M) to result in an equilibrium As(V) concentration of about 5 10^{-7} M (35 μg/L) at pH 8. As shown in Fig.3 and expected from the experimental data (Figs.1 and 2), an increase of the As concentration is predicted at an increase of the HCO_3^- concentration at a constant pH. However, an increase of the bicarbonate concentration due to CO_2

production may also lead to a decrease in the pH of the sediment (Appelo et al., 2002). Our calculations show a clear decrease of the dissolved As(V) concentration in case of a pH decrease from pH 8 to 7, as illustrated in Fig.3 by an arrow between system 1 and 2.

A strong biogeochemical oxidation of organic mater will result in a reduction process changing As(V) to As(III). In such a case, the sediment will release a considerable amount of arsenic and the concentration may increase by a factor of 20 as indicated with the vertical arrow in Fig.3.

The above results are based on a model with predictive capabilities that have been verified. For As(V), our results are very different from the calculations made by Appelo et al.(Appelo et al., 2002), who used the generalized 2-p*K* DDL model of Dzombak and Morel (Dzombak and Morel, 1990). Appelo et al. (Appelo et al., 2002) predicted a strong release of As(V) in relation to a combination of an increase of HCO_3 and a decrease of pH. However, our data (Fig.1) as well as our modeling (Fig.3) show that for the As(V) solution concentration the positive competitive effect of (bi)carbonate is overshadowed by the suppressing effect of the change in pH.

In our calculations (Fig.3), the As loading of the solid phase is 1 μmol/m^2. In case of a reactive surface area of a few m^2 per gram of sediment (e.g. ~2.5 m^2/g), the corresponding loading is about 200 mg As/kg sediment. Such a value is extremely high compared to the experimental data for a series of Bangladesh sediments having typical values that are e.g. 100 times lower (BGS and DPHE, 2001). One of the main reasons for this discrepancy is the disregard of the presence of PO_4 in the calculations. This ion is known to be in competition with As (Hingston et al., 1971; Manning and Goldberg, 1996; Gao and Mucci, 2001; Dixit and Hering, 2003). Oxalate extractions of the Bangladesh sediments show a PO_4 loading that is often roughly 50-100 times higher than the As loading (BGS and DPHE, 2001). This dominance of PO_4 over As strongly suggests that the presence of PO_4 in the competition should not be ignored, if the aim is to asses the surface chemistry of sediments for field conditions, even in the simplest approach (Appelo et al., 2002). This will be a future challenge.

6. Appendix

The (bi)carbonate-arsenic interaction in closed systems differs from that of open systems. The As concentrations in the latter ones have been predicted with the parameterized CD model as shown below.

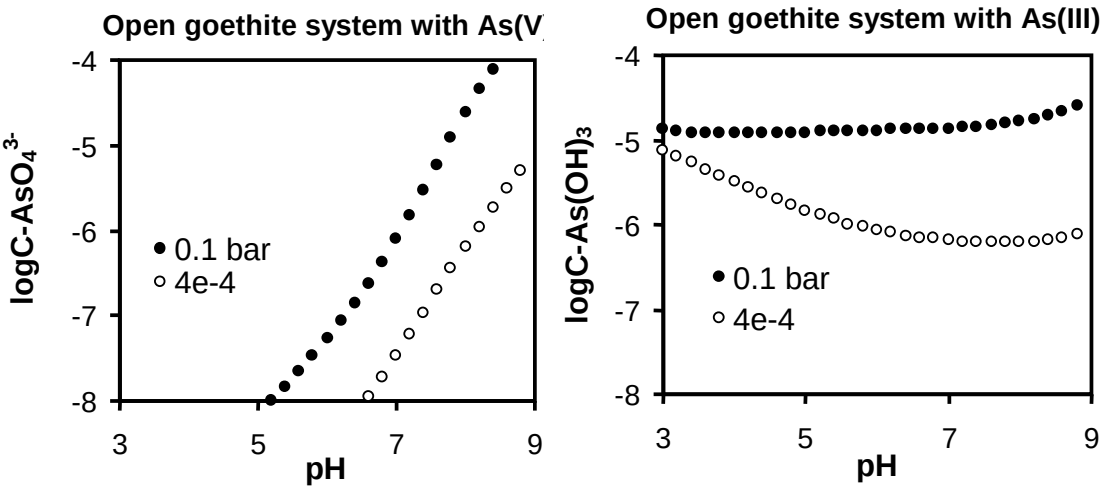

Fig. Predicted pH dependency of the equilibrium concentrations of As (V) and As (III) in open systems at two different partial CO_2 pressures ($4\ 10^{-4}$ and 0.1 bar), containing 0.5 mM As and 5 g/L goethite ($0.01 \leq I \leq 0.1$ M), using the parameters of Table 1 given in the main paper.

4

Multi-Competitive Interaction of As(III) and As(V) Oxy-anions with Ca^{2+}, Mg^{2+}, PO_4^{3-}, and CO_3^{2-} Ions on Goethite

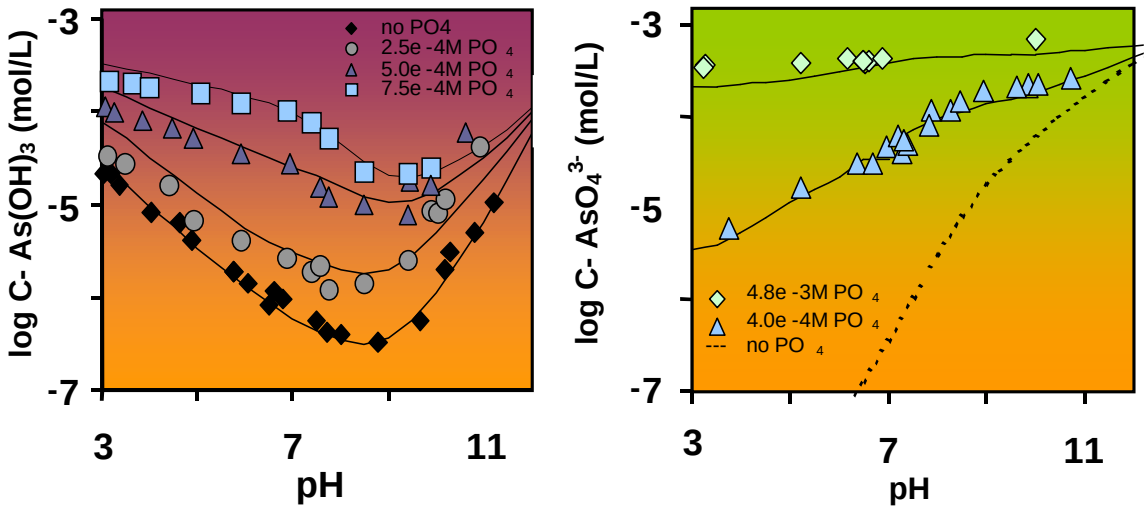

Stachowicz M., Hiemstra T., and van Riemsdijk W. H. (2007) "Multi-Competitive Interaction of As(III) and As(V) Oxy-anions with Ca^{2+}, Mg^{2+}, $PO_4^{3-}$and CO_3^{2-} Ions on Goethite" (*submitted*)

Abstract

Complex systems, simulating natural conditions like groundwater, have rarely been studied, since measuring and in particular, the modeling of such systems is very challenging. In this paper, the adsorption of the oxyanions of As(III) and As(V) on goethite has been studied in the presence of various inorganic macro-elements (Mg^{2+}, Ca^{2+}, PO_4^{3-}, CO_3^{2-}). We have used 'single-', 'dual-', and 'triple-ion' systems. The presence of Ca^{2+} and Mg^{2+} has no significant effect on As(III) oxyanion (arsenite) adsorption in the pH range relevant for natural groundwater (pH 5-9). In contrast, both Ca^{2+} and Mg^{2+} promote the adsorption of PO_4^{-3}. A similar effect is expected for the Ca^{2+} and Mg^{2+} interaction with As(V) oxyanions (arsenate). Phosphate is a major competitor for arsenate as well as arsenite. Although carbonate may act as competitor for both types of As oxyanions, the presence of significant concentrations of phosphate makes the interaction of (bi)carbonate insignificant. The data have been modeled with the charge distribution (CD) model in combination with the extended Stern model option. In the modeling, independently calculated CD values were used for the oxyanions. The CD values for these complexes have been obtained from a bond valence interpretation of MO/DFT (molecular orbital / density functional theory) optimized geometries. The affinity constants (log*K*) have been found by calibrating the model on data from 'single-ion' systems. The parameters are used to predict the ion adsorption behavior in the multi-component systems. This way calibrated model is able to predict successfully the ion concentrations in the mixed 2- and 3-component systems as a function of pH and loading. From a practical perspective, data as well as calculations show the dominance of phosphate in regulating the As concentrations. Arsenite ($As(OH)_3$) is often less strongly bound than arsenate (AsO_4^{3-}) for conditions relevant in nature and arsenite responses less strongly to changes in the phosphate concentration compared to arsenate, *i.e.* $\delta \log C_{As(III)} / \delta \log C_{PO4} \approx 0.4$ and $\delta \log C_{As(V)} / \delta \log C_{PO4} \approx 0.9$ at pH 7.

1. Introduction

Arsenic (As) in groundwater is a serious problem in many parts of the world. In Bangladesh, where millions of people suffer from arsenic-related illnesses (Chakraborti et al., 1999), the As contamination problem has been subject of several extensive studies (BGS and DPHE, 2001; Harvey et al., 2002; Smedley and Kinniburgh, 2002; Swartz et al., 2004; Harvey et al., 2005; Zheng et al., 2005). Mobility and bioavailability of arsenic in complex natural systems seems to be determined by a combination of factors such as the redox conditions, the presence of mineral surfaces and organic matter. Another factor is the co-occurrence of elements that may enhance or suppress the As concentration of groundwater. For instance, specifically adsorbed inorganic ions, such as Ca^{2+}, Mg^{2+}, PO_4^{3-}, CO_3^{2-} may be relevant for a release of arsenic (BGS and DPHE, 2001; Smedley and Kinniburgh, 2002). These ions are commonly present in natural waters and will interact with As when adsorbed on the sites of metal oxides surfaces, *i.e*. they may suppress or promote the binding of each other (Smedley and Kinniburgh, 2002).

Arsenic in groundwater originates from the natural iron oxides in aquifers. Inorganic arsenic is found in two oxidation forms, *i.e.* As(V) for arsenate and As(III) for arsenite. Both forms interact with iron (hydr)oxides as observed for hydrous ferric oxide (HFO) (Wilkie and Hering, 1996; Jain and Loeppert, 2000; Goldberg and Johnston, 2001; Dixit and Hering, 2003) and for goethite (Hingston et al., 1971; Smedley and Kinniburgh, 2002; Dixit and Hering, 2003; Antelo et al., 2005; Stachowicz et al., 2006). In addition, organic As compounds may adsorb (Smedley and Kinniburgh, 2002).

In natural waters, other cations and anions are present that may interact with arsenic adsorbed to metal (hydr)oxides. Abundantly present cations are Ca^{2+} and Mg^{2+}. Due to their positive charge, they may promote the adsorption of negatively charged ions like arsenate (AsO_4^{3-}) (Wilkie and Hering, 1996). Another important ion in groundwater is phosphate. Phosphate is known to have a strong affinity for iron oxides such as goethite (Dixit and Hering, 2003) and hydrous ferric oxide HFO (Dzombak and Morel, 1990; Dixit and Hering, 2003). Even at very low concentrations in solution, the ion is relatively important at the surface. Therefore, it will be a

competitor for arsenic (Hiemstra and van Riemsdijk, 1999; Jain and Loeppert, 2000; Dixit and Hering, 2003), resulting in a high P/As adsorption ratio. In groundwater, bicarbonate often is a major anion. Some authors have related the arsenic release from sediments to an increase of the HCO_3^- concentrations in groundwater and a decrease in pH (Appelo et al., 2002; Anawar et al., 2004). Conversely, this hypothesis is not supported by other authors who conducted experiments in iron oxide systems (Meng et al., 2002; Radu et al., 2005; Stachowicz et al., 2007) using arsenic and (bi)carbonate concentrations relevant for natural systems.

Complex systems, simulating natural conditions, have rarely been studied. Measuring, and in particular modeling of such systems is challenging. Modeling of the bioavailability or toxicity of elements like arsenic is only possible upon the comprehension of the complexity of the interactions between the co-occurring elements in the environment. In this paper, we will concentrate on the interactions between arsenic and some major elements often found in high-As-groundwater, as they could potentially be relevant for the arsenic concentration. We will analyze the As(III) and As(V) oxyanion adsorption in presence of Ca^{2+}, Mg^{2+}, CO_3^{2-} and/or PO_4^{3-}. Goethite has been chosen to represent the natural Fe(III) (hydr)oxide surfaces of aquifer material. We will study the ion interaction in a large series of 2- and 3-component systems. The data will be analyzed with the charge distribution (CD) model (Hiemstra and van Riemsdijk, 1996) The CD model is a surface complexation model in which the electrostatic energy contribution is calculated based on a distribution of the charge over two electrostatic potentials. For the model description, we refer to Hiemstra and van Riemsdijk (1996). Previously, the CD model has been used to describe adsorption behavior of the above mentioned ions in 'single-ion' ('pseudo-monocomponent') systems on goethite (Villalobos and Leckie, 2000; Rahnemaie et al., 2006; Stachowicz et al., 2006; Rahnemaie et al., 2007). An important parameter in the CD model is the charge distribution. In principle, the CD values can be found from an analysis of adsorption data as has been done for Ca^{2+} and Mg^{2+} (Rahnemaie et al., 2006). However, it may also be derived from the interpretation of the geometry of a surface complex (Hiemstra and van Riemsdijk, 2006) using the Brown bond valence concept (Brown and Altermatt, 1985). The geometry of a surface complex can be approximated using molecular orbital calculations applying density functional theory (MO/DFT). The resulting ionic CD values are corrected for the change in dipole orientation of interfacial water (Hiemstra and van Riemsdijk, 2006). The thus derived interfacial CD values are available for the relevant complexes of the oxyanions used in this study, *i.e.*

$As(OH)_{3+x}^{-x}$ (Stachowicz et al., 2006) The thus derived interfacial CD values are available for the relevant surface complexes of the oxyanions used in this study, *i.e.* $As(OH)_3$ (Stachowicz et al., 2006), AsO_4^{3-} (Stachowicz et al., 2006), PO_4^{3-} (Rahnemaie et al., 2007), and CO_3^{2-} (Hiemstra and van Riemsdijk, 2006). The use of calculated CD values has the practical advantage that the number of adjustable parameters is reduced. Only the formation constant of a surface complex has to be found from a data analysis. Moreover, from a theoretical perspective, independently derived CD values can be used to constrain the modeling and help to reveal the surface species when applied to adsorption data (Stachowicz et al., 2006; Hiemstra et al., 2007; Hiemstra and Riemsdijk, 2007; Rahnemaie et al., 2007).

It is important to note that we will use model parameters calibrated on 'single-ion' adsorption data and that all other interactions in the multi-component systems will be predicted, not fitted. These predictions will be compared with the data.

2. Experimental

2.1. Goethite material

The goethite material used in this study was prepared according to the preparation procedure of Hiemstra et al. (1989a) as described by Stachowicz et al. (2006). The material has been characterized in an acid-base titration experiment (Stachowicz et al., 2006). The PZC is 9.2. The specific BET-surface area of goethite, measured by N_2 gas adsorption, was 98 m^2/g. The particles are needle-shaped with an average diameter of about 10 nm and a length of about 100 nm (Hiemstra et al., 1989a; Weidler et al., 1998; Gaboriaud and Ehrhardt, 2003).

For the determination of adsorption edges, the stock of the goethite suspension was diluted with ultra-pure water to a concentration of approximately 20.0 g/L. The pH was adjusted to 5.5 and the suspension was purged overnight with moist, cleaned N_2 to remove CO_2.

2.2. Reagents solutions

We prepared stock solutions from 'analytical grade' chemicals (Merck) and pre-boiled ultra-pure water (≈0.018 dS/m) under N_2 atmosphere (except $NaHCO_3$) and stored them in polyethylene bottles, avoiding silica contamination. The concentrations of the stock solutions

were calibrated with ICP-AES using commercial available standard solutions. The solution of 0.100 M NaOH was prepared CO_2-free from Titrasol and stored in a plastic bottle to avoid silica contamination. CO_2 contamination was avoided by placing the bottle in a dessicator. The solution of 0.100 M HNO_3 was prepared from Titrasol and stored in a glass bottle to avoid contamination by organic material.

2.3. Adsorption experiments

Adsorption experiments were carried out in gas-tight 23.6 ml bottles of low-density polyethylene (Rietra et al., 2001). Fixed amounts of goethite, electrolyte solution, and stock solutions of calcium, magnesium, arsenite, or arsenate were added. Phosphate was always added to the suspension as the last solution in order to avoid irreversibility of phosphate adsorption due to change in the ionic strength and pH of suspension.

A pH range (3-11) was imposed with 0.0100 M or 0.100 M of HNO_3 or NaOH. The final total volume of the suspension in each individual bottle was 20.0 ml. All solutions were added to the bottles under a moist N_2 atmosphere to prevent CO_2 contamination. In the experiments with HCO_3^-, this solution was added at the end when the N_2 purging was stopped, and the bottles were immediately closed. A special procedure was followed (Rietra et al., 2001) in the adsorption experiments of PO_4^{3-} and Ca^{2+}, such that calcium-phosphate precipitation was avoided. Appropriate volumes of water and electrolyte were added to each bottle together with some acid (0.1 M HNO_3) or base (0.1 M NaOH), required to obtain later the final pH values in the experiment. The addition of the Ca^{2+} stock solution was followed by the addition of a goethite suspension, which was pre-equilibrated (> 2 hours) with PO_4^{3-} under N_2 atmosphere.

Series of competition experiments have been conducted using various combinations of ions and different initial concentrations but in all these experiments, we used 5 g goethite /L in 0.10 M $NaNO_3$. The bottles were equilibrated for 24 hours in a shaker in a constant temperature room (~22 ^oC). Next, the small reaction bottles were centrifuged and samples of the supernatant were taken for the ICP-MS (As) or ICP-AES (Ca, Mg, and P) analysis. The pH was measured in the bottles after re-suspension of the goethite. With respect to arsenite, we note that in principle, this ion is not stable in these systems. However, research has shown that arsenite is kinetically stable in the presence of goethite for reaction times well beyond the equilibrium time used in the present work, which is 24 hours. For example, Manning et al. (1998) found with spectroscopy

(XANES) no heterogeneous oxidation of arsenite to arsenate in goethite systems equilibrated for 3-5 days. The absence of oxidation has been confirmed recently in another study comprising several oxide minerals (Ona-Nguema et al., 2005). For HFO, no oxidation has been observed within hours (Voegelin and Hug, 2003). On the contrary, As(III) oxidation may occur rapidly in natural systems, but this has shown to be related to microbial interaction (Wilkie and Hering, 1998), which is unlikely in our synthetic goethite-water systems.

2.4. Calculations

The amount of carbonate present as CO_2 in the gas phase of the bottles (3.6 ml gas per 20 ml solution) was found from chemical equilibrium calculations and taken into account during modeling. All the model calculations have been done with a recent version of ECOSAT (Keizer and van Riemsdijk, 1998) and FIT (Kinniburgh, 1993).

3. Results

3.1. Primary charge and double layer model

At the crystal faces of goethite (Weidler et al., 1998; Gaboriaud and Ehrhardt, 2003), different types of surface groups are present, *i.e.* singly- (≡ FeOH(H)), doubly- (≡ Fe_2OH), and triply-coordinated (≡ $Fe_3O(H)$) surface groups (Hiemstra and van Riemsdijk, 1996). The primary charging behavior of goethite is supposed to be due to the protonation of the singly (≡ $FeOH^{-1/2}$) and triply (≡ $Fe_3O^{-1/2}$) coordinated surface oxygens, according to the following reactions (Hiemstra et al., 1996):

$$\equiv FeOH^{-0.5} + H^{+} \Leftrightarrow \equiv FeOH_2^{+0.5} \qquad [1]$$

$$\equiv Fe_3O^{-0.5} + H^{+} \Leftrightarrow \equiv Fe_3OH^{+0.5} \qquad [2]$$

The broken numbers in eqs.(1,2), referring to the average charge of the surface groups, stem from the application of the Pauling bond valence principle (Hiemstra et al., 1989b). The proton affinity

constants of both reactions have been set equal to the value of the PZC (9.2). The effective site densities of reactive surface groups are N_s(FeOH)=3.45/nm^2 and N_s(Fe_3O)=2.7/nm^2 (Hiemstra and van Riemsdijk, 1996; Hiemstra et al., 1996).

Rahnemaie et al. (2006) have studied the charging behavior of goethite for a series of electrolyte ions. For a simultaneous description of these data, it is essential to separate the head-end of the diffuse double layer (DDL) from the minimum distance of approach of electrolyte ions using a Stern layer with a capacitance of C_2 = 0.75 F/m^2 (Hiemstra and van Riemsdijk, 2006). According to Hiemstra and van Riemsdijk (2006), the existence of such a charge free layer is related to the interfacial structuring of water molecules.

Table 1. Table defining the formation of the basic surface species in terms of reactive surface groups; the charge allocation (Δz), solution stoichiometries of H^+, Na^+ and NO_3^- and affinity constants (log*K*). The capacitance of the first Stern layer C_1 = 0.85±0.01 F/m^2 is from Stachowicz et al. (2006). The capacitance of the second Stern layer (C_2= 0.75 F/m^2) is from Hiemstra and van Riemsdijk (2006). The site density of reactive surface groups (FeOH=3.45/nm^2 and Fe_3O=2.7/nm^2) is from Hiemstra and van Riemsdijk (1996).

Surface species	≡ FeOH	≡ Fe_3O	Δz_0	Δz_1	Δz_2	H^+	Na^+	NO_3^-	log*K*
≡ $FeOH^{-1/2}$	1	0	0	0	0	0	0	0	0.00
≡ $FeOH_2^{+1/2}$	1	0	1	0	0	1	0	0	9.20
≡ $FeOH^{-1/2}\cdots Na^+$	1	0	0	1	0	0	1	0	-0.60
≡ $FeOH_2^{+1/2}\cdots NO_3^{-1}$	1	0	1	-1	0	1	0	1	8.52
≡ $Fe_3O^{-1/2}$	0	1	0	0	0	0	0	0	0.00
≡ $Fe_3OH^{+1/2}$	0	1	1	0	0	1	0	0	9.20
≡ $Fe_3O^{-1/2}\cdots Na^+$	0	1	0	1	0	0	1	0	-0.60
≡ $Fe_3OH^{+1/2}\cdots NO_3^-$	0	1	1	-1	0	1	0	1	8.52

Electrolyte ions can only occupy stepwise positions between aligned layers of water molecules near the surface. This picture is supported by force measurements (Pashley and Israelachvili, 1984) and spectroscopic information showing a decaying ordering of water with distance from the surface (Toney et al., 1995; Fenter and Sturchio, 2004; Catalano et al., 2006), equivalent to about 3 layers of water (Hiemstra and van Riemsdijk, 2006). The proposed double layer model, including a Stern layer between the minimum distance of approach of electrolyte ions and the DDL, is known as an Extended Stern (ES) layer model (Westall and Hohl, 1980).

For the modeling, the ion pair formation constants and the capacitance value of the outer Stern layer have been taken from literature (Hiemstra and van Riemsdijk, 2006). The inner sphere capacitance value has been adapted to describe our experimental charging curves resulting in C_1=0.85±0.01 F/m^2. An overview of the parameters used is given in Table 1.

3.2. Ion adsorption

The ion adsorption experiments have been done for 'single', 'dual', and 'triple adsorbate' systems. The experimental data will be discussed in three different sections.

In the first section (3.2.1), we will focus on the interactions of phosphate, calcium, and magnesium ions. First, the CD model will be parameterized for 'single-ion' systems. This will be done for PO_4^{3-} using literature data (Rahnemaie et al., 2007) that refer to a very similar goethite preparation. However, the reported PZC is 0.2 units lower. To obtain a set of constants that is applicable in the present study, we will re-evaluate the PO_4^{3-} adsorption data of Rahnemaie et al. (2007b) assuming a value for the PZC and corresponding proton affinity constant (logK_H=9.2) as found for our goethite. For Ca^{2+} and Mg^{2+}, we will calibrate the CD model on acid-base titrations of goethite suspensions with calcium and magnesium nitrate as electrolyte solution (Rahnemaie et al., 2006).

In the next section (3.2.2), we will introduce arsenite, $As(OH)_3$. The monocomponent adsorption behavior of As(III) oxyanions on our goethite has been described elsewhere (Stachowicz et al., 2006). Starting point in the present study is the arsenite adsorption in a number of 2-component systems containing in addition to arsenite also calcium, magnesium or phosphate. This is followed by a test on systems that contain arsenite, phosphate and calcium or magnesium simultaneously (3-component systems).

In the last section (3.2.3), we will switch to arsenate, describing the monocomponent system (Stachowicz et al., 2006) and predicting the interaction with phosphate. In addition, we have added HCO_3^- ions to these systems, which will be described.

In our paper, the data will be presented and evaluated focusing on the concentration in solution for two reasons. In our experimental setup, a relatively large solid:solution ratio is used. It implies that a traditional scaling on the fraction adsorbed will result for many of our systems in almost complete adsorption, removing a wealth of valuable information. Scaling on the adsorption density results in similar problems that may easily lead to situations in which

modeling is less critical, because of the relatively low variation in adsorption density with changing conditions in comparison to the variation of the concentration in solution. Another reason is related to the application of our data to natural systems. Generally, natural systems have a very high solid:solution ratio (Stachowicz et al., 2007) and a high so-called K_d value, expressing that the vast majority of the ions is bound. Change in conditions will alter in particular the solution concentrations without any significant change of the surface loading. Predicting and understanding such changes is very relevant for *e.g.* groundwater systems that are used as drinking water source for instance in Bangladesh and elsewhere.

3.2.1. PO_4^{3-}, Ca^{2+}, and Mg^{2+}, and its interaction

Phosphate

Numerous authors have studied the adsorption of phosphate on goethite (Hingston et al., 1974; Barrow and Bowden, 1987; Hiemstra and van Riemsdijk, 1996; Geelhoed et al., 1997; Geelhoed et al., 1998; Hiemstra and van Riemsdijk, 1999; Gao and Mucci, 2001; Zhao and Stanforth, 2001; Tadanier and Eick, 2002; Ler and Stanforth, 2003; Antelo et al., 2005). Originally, the adsorption behavior of phosphate on goethite has been described with the CD model using 3 surface species, *i.e.* a monodentate ≡ $FeOPO_3$, a bidentate ≡ $(FeO)_2PO_2$, and a protonated bidentate ≡ $(FeO)_2POOH$ species (Hiemstra and van Riemsdijk, 1996; Geelhoed et al., 1997; Geelhoed et al., 1998; Rietra et al., 2001; Antelo et al., 2005). The corresponding CD values were calculated assuming for the non-protonated surface species a Pauling distribution of charge. For the protonated bidentate species, a shift of charge was required which was attributed to protonation of one of the outer ligands. Recently, Rahnemaie et al. (2007b) have reinterpreted the goethite-phosphate interaction. In their approach, the CD values were calculated based on the optimized geometry for a large series of possible PO_4 surface species. Application of the CD values in surface complexation modeling using a new, extensive data set for phosphate adsorption on goethite revealed that the adsorption could be described with two innersphere surface species, *i.e.* a protonated monodentate ≡ $FeOPO_2OH$ (MH), and a bidentate ≡ $(FeO)_2PO_2$ (B) surface complex. The bidentate species is found to be the major phosphate species at intermediate and

high pH. A contribution of MH is found in the lower pH range especially at high phosphate loading.

The reactions can be formulated as:

$$2 \equiv FeOH^{-1/2} + PO_4^{3-}(aq) + 2H^+(aq) \Leftrightarrow \equiv (FeO)_2^{-1+\Delta z_0} PO_2^{\Delta z_1} + 2\,H_2O(l) \qquad [3a]$$

$$1 \equiv FeOH^{-1/2} + PO_4^{3-}(aq) + 2H^+(aq) \Leftrightarrow \equiv FeO^{-1/2+\Delta z_0} PO_2OH^{\Delta z_1} + 1\,H_2O(l) \qquad [3b]$$

As described above, the data of Rahnemaie et al. (2007b) have been used to re-evaluate the PO_4 affinity constants for a PZC value ($\log K_H$=9.2) as found for our goethite. The $\log K$ values obtained for both PO_4 species are given in Table 2. This set of parameters can also describe the large data set of Rietra et al. (2001a), who reported a PZC of 9.25.

Table 2. Table defining the formation reactions of the surface species of phosphate. The interfacial charge distribution values (Δz_0, Δz_1) have been calculated from the geometry of hydrated iron-phosphate complexes optimized with MO/DFT with correction for water dipole orientation. The affinity constants ($\log K$) have been found by fitting the model to the adsorption data of Rahnemaie et al. (2007b) using a PZC value of 9.2 (N=197 data points, R^2=0.992).

Species	≡ FeOH	≡ Fe_3O	Δz_0	Δz_1	Δz_2	H^+	PO_4^{3-}	$\log K$
≡ $(FeO)_2\,PO_2$	2	0	0.46	-1.46	0	2	1	29.77 ± 0.02
≡ $FeOPO_2OH$	1	0	0.28	-1.28	0	2	1	27.65 ± 0.01

Calcium and Magnesium

The adsorption of Ca^{2+} on goethite has previously been studied by others (Ali and Dzombak, 1996; Rietra et al., 2001; Weng et al., 2005; Hiemstra and van Riemsdijk, 2006). In the present study, we will calibrate the adsorption behavior of Ca^{2+} using proton titration data. The result will be tested on Ca^{2+} adsorption data. This is also done for Mg^{2+}. We will try to develop a consistent molecular picture.

At present, no independent information is available with respect to the type(s) of surface species that these ions form. The relatively high affinity of magnesium for goethite may point to

the formation of innersphere complexes. Rahnemaie et al. (2006) could describe the data with this mechanism. The fitted CD value points to the formation of a bidentate complex. At high pH and loading, the complex hydrolyses. In the modeling,the outersphere complexation of Mg^{2+} could be ignored. Any outersphere complexation is minor and is probably hidden behind the dominating innersphere complexation, which results from the relatively high affinity of the Mg^{2+} ion for the surface. For Ca^{2+}, a much lower affinity for goethite is found. Rahnemaie et al. (2006) could describe the calcium adsorption on goethite with the CD model using a combination of inner and outer sphere complexation.

In the present modeling of the Ca^{2+} adsorption data, we allowed simultaneously outersphere complexation by the $\equiv FeOH^{-1/2}$ and $\equiv Fe_3O^{-1/2}$ surface groups. The reactions can be formulated as:

$$\equiv FeOH^{-1/2} + Ca^{2+}(aq) \Leftrightarrow \equiv FeOH^{-1/2} \cdots Ca^{\Delta z_1} \qquad [4a]$$

$$\equiv Fe_3O^{-1/2} + Ca^{2+}(aq) \Leftrightarrow \equiv Fe_3O^{-1/2} \cdots Ca^{\Delta z_1} \qquad [4b]$$

All charge of the Ca^{2+} ion is attributed to the 1-plane ($\Delta z_1 = 2$ v.u.).

Outersphere complexation alone cannot describe the titration data. Therefore, we included innersphere complexation with singly coordinated surface groups. Preliminary modeling resulted in a surface charge attribution of Ca^{2+} that is typical for monodentate innersphere complexation. The CD value is almost equal to the Pauling bond valence value if we allow this complex to be hydrolyzed. In this respect, the situation is comparable with Mg^{2+}. The monodentate Ca^{2+} complexation reactions can be formulated as:

$$\equiv FeOH^{-1/2} + Ca^{2+}(aq) \Leftrightarrow \equiv FeOH^{-1/2+\Delta z_0} Ca^{\Delta z_1} \qquad [5a]$$

$$\equiv FeOH^{-1/2} + Ca^{2+}(aq) + H_2O(l) \Leftrightarrow \equiv FeOH^{-1/2+\Delta z_0} CaOH^{\Delta z_1} + H^+(aq) \qquad [5b]$$

in which $\Delta z_0+\Delta z_1$ is respectively 2 and 1 v.u.

To reduce the number of adjustable parameters, we assume the same surface charge attribution (Δz_0) for both Ca(II) inner-sphere complexes (eq.(5)). The fitting results are given in Table 3. Although the fitted value of Δz_0 is uncertain (0.32 ± 0.19 v.u.), it is almost equal to the Pauling bond valence value (Δz_0=0.33 v.u.), suggesting one common ligand of the Ca^{2+} octahedron with the surface.

For Mg^{2+}, we have modeled the data allowing only innersphere complexation. The modeling points also to the formation of bidentate surface complexes. The formation reactions of $\equiv (FeOH)_2Mg$ and $\equiv (FeOH)_2MgOH$ are defined respectively as:

$$2 \equiv FeOH^{-1/2} + Mg^{2+}(aq) \Leftrightarrow \equiv (FeOH)_2^{-1+\Delta z_0} Mg^{\Delta z_1} \quad [6a]$$

$$2 \equiv FeOH^{-1/2} + Mg^{2+}(aq) + H_2O(l) \Leftrightarrow \equiv (FeOH)_2^{-1+\Delta z_0} MgOH^{\Delta z_1} + H^+(aq) \quad [6b]$$

As for Ca^{2+}, we assume for both Mg^{2+} complexes the same surface charge attribution (Δz_0). The fitted Δz_0 value of Mg^{2+} in Table 3 (0.71 v.u.) is close to the value expected (Δz_0=0.67 v.u.) based on a Pauling distribution model in which the Mg^{2+} ion attributes one-third of its charge to the surface (since a Mg^{2+} bidentate surface complex has one-third of its ligands common with the surface). The values of the fitted affinity constants log*K* (Table 3) illustrate that the bidentate binding of Mg^{2+} is considerably stronger than for Ca^{2+} (Δlog*K*~1.5). The low affinity of the Ca^{2+} innersphere complex and resulting lower contribution to the overall adsorption is also reflected in the larger uncertainties (±) in the fitted CD (Δz_0) and log*K* value compared to Mg^{2+}.

The log*K* values for the formation of $\equiv (FeOH)_2Mg$ and $\equiv (FeOH)_2MgOH$ can be used to obtain the proton affinity of the outer OH ligand of the MgOH surface complex, *i.e.* $\Delta \log K = \log K_H \approx 11.4 \pm 0.1$. This $\log K_H$ value is reasonable when compared with the proton affinity of the $Mg(OH)_2$ (aq) species in solution ($\log K_H$=11.6). The proton affinity constant of aqueous $Ca(OH)_2$ is about 1.3 log*K* units higher ($\log K_H$=12.7), illustrating the lower tendency of that ion to hydrolyze. The lower tendency of hydrolysis of Ca^{2+} is in agreement with our modeling showing a higher proton affinity for adsorbed $CaOH^+$ ($\log K_H$=12.9±0.1). The fitted set of constants are able to describe the acid-base titration data of Rahnemaie et al. (2006) very well (Fig.1a) and results in a good prediction of the previously published adsorption data for Ca^{2+}

(Weng et al., 2005; Rahnemaie et al., 2006) as shown in Fig.1b. Application of the parameters (Table 3) to our present data results in a rather good prediction of the adsorption behavior of Ca^{2+} and Mg^{2+} (Fig.2).

Table 3. Table defining the surface complexation of Ca^{2+} and Mg^{2+}.

Species	≡ FeOH	≡ Fe_3O	Δz_0	Δz_1	Δz_2	H^+	Ca^{2+}	Mg^{2+}	log*K*
≡ FeOH···Ca*[1]	1	0	0	2	0	0	1	0	3.00± 0.27*[2]
≡ Fe_3O···Ca*[1]	0	1	0	2	0	0	1	0	3.00± 0.27*[2]
≡ FeOHCa	1	0	0.32±0.19	1.6	0	-1	1	0	3.65± 0.06*[3]
≡ FeOHCaOH	1	0	0.32±0.19	0.6	0	-1	1	0	-9.25± 0.11*[3]
≡ $(FeOH)_2Mg$	2	0	0.71±0.01	1.2	0	0	0	1	4.90 ± 0.03*[3]
≡ $(FeOH)_2MgOH$	2	0	0.71±0.01	0.2	0	-1	0	1	-6.47 ±0.07*[3]

*[1] Outersphere complexes
*[2] One common log*K* value for outersphere complexation.
*[3] CD and log*K* value are fitted on the titration data of Rahnemaie et al. (2006). For each element, the surface charge attribution (Δz_0) of both complexes has been set equal.

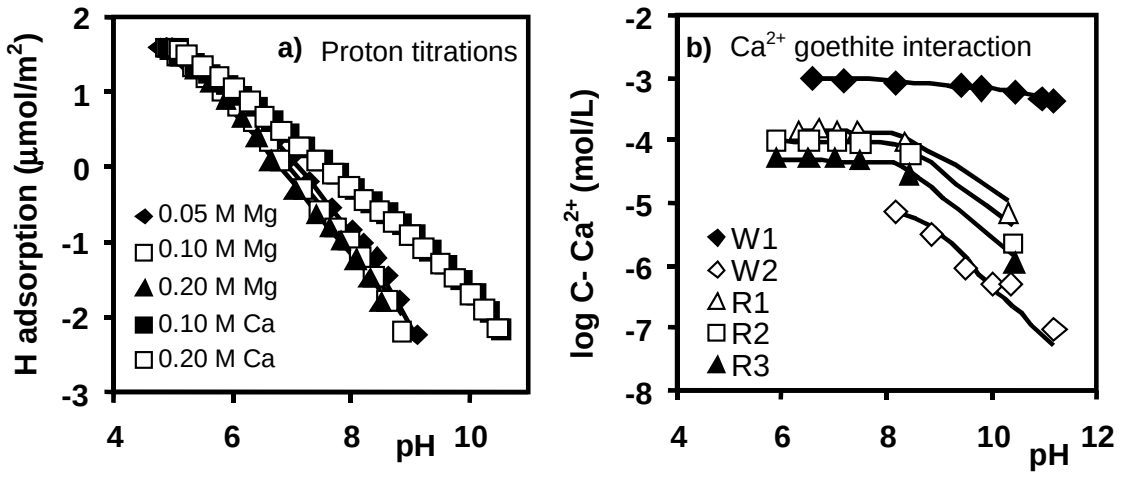

Fig.1a. Proton adsorption of goethite suspensions (16.52 g/L * 98.6 m^2/g =1630 m^2/L) with various initial concentrations of Ca^{2+} and Mg^{2+} (Rahnemaie et al. 2006), used to calibrate the CD model (Table 3). The proton adsorption is in excess to the proton adsorption in the PPZC. Fig.1b. Equilibrium concentrations of Ca^{2+} in the presence of goethite as a function of pH. Data of Rahnemaie et al. (2006) (986 m^2/L) are for initial Ca^{2+} concentrations of R1=0.15, R2=0.10 and R3=0.05 mM. Data of Weng et al. (Weng et al., 2005) are for W1=563m^2/L and W2=545 m^2/L with initial Ca^{2+} concentrations of W1= 1.02 mM and W2 =0.0096 mM. Lines give the predicted concentrations calculated with the CD model that has been calibrated on the acid-base titration data of Fig.1a.

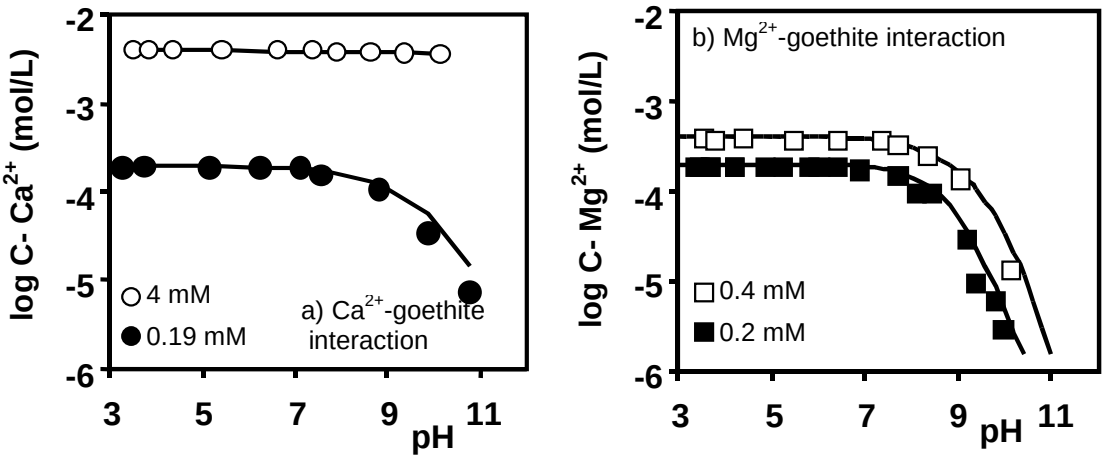

Fig.2. Equilibrium concentrations of Ca^{2+} (left panel) and Mg^{2+} (right panel) in the presence of goethite (490 m^2/L) as a function of pH in 0.1 M $NaNO_3$ for various initial concentrations indicated in the graphs. Lines are predicted with the CD model using the parameters of Tables 1 and 3.

In summary, the above model approach for the alkali earth ions leads to a rather consistent physical-chemical picture for the binding of both divalent ions. Magnesium has the highest affinity and may form two bonds with the surface. This ion has a tendency to hydrolyze easily. A combination of innersphere complexation and outersphere complexation is found for the weaker binding cation (Ca^{2+}). The weaker innersphere complex has one bond with the surface. The adsorbed ion hydrolyzes less easily. For both ions (Ca^{2+}, Mg^{2+}), the hydrolysis is in reasonable agreement with the behavior found in solution.

Interaction between Ca^{2+} and PO_4^{3-}

Interaction between calcium and phosphate ions is shown in Fig.3. As given in the left panel, the concentration of Ca^{2+} in solution decreases, (*i.e.* the adsorption of Ca^{2+} is higher) in the presence of phosphate. Based on the low Ca^{2+} and PO_4^{3-} concentrations precipitation of in soluble calcium-phosphate minerals can be excluded. A higher initial concentration of phosphate leads to a lower Ca^{2+} concentration in the solution. This behavior has also been observed by Rietra et al. (2001a) and can be explained by electrostatic interactions. The negative charge of the adsorbed PO_4^{3-} ions stimulates the binding of Ca^{2+}.

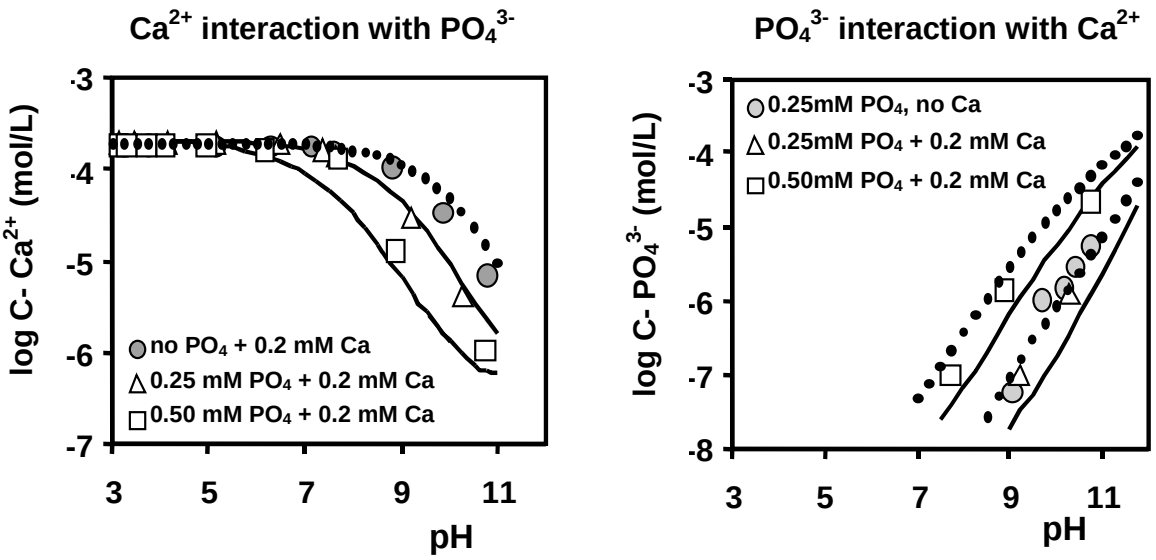

Fig.3. Interaction of Ca^{2+} and PO_4^{3-} in the presence of goethite (5 g/L) in 0.1M $NaNO_3$ as a function of pH. Open symbols refer to the measured equilibrium concentrations in the 'dual-ion' systems. One initial concentration of calcium was used, *i.e.* 0.2 mM and two initial concentrations of phosphate, *i.e.* 0.25 mM (triangles) and 0.50 mM (squares). Closed circles refer to the 'single-ion' systems. Note that there are no data for the 'single-ion' system with 0.5 mM phosphate. Full lines refer to the predicted equilibrium concentrations in competition experiments using the CD model with the parameters given in the Tables 1-3. Dotted lines refer to the concentrations calculated for the 'single-ion' systems.

The effects are successfully predicted with the CD model. According to the model, the phosphate adsorption should be enhanced by the presence of Ca^{2+}, leading to lower equilibrium concentrations as is shown in Fig.3 with lines (right panel). The effect can be explained by electrostatic interactions at the surface of goethite. Binding of PO_4^{3-} leads to more negative charge on the goethite particles, which is reflected by a strong decrease of the IEP(Tejedor-Tejedor and Anderson, 1990; Antelo et al., 2005). Increase of the negative charge will suppress a further binding of PO_4^{3-} and stimulate the binding of Ca^{2+}. In the experiment, the decrease of the PO_4^{3-} concentration is very small compared to the uncertainty and it is difficult to judge the predicted effect. Therefore, it is important to mention that our parameter set (Table 3) is able to describe the main features of the Ca^{2+}-PO_4^{3-} interaction of the data set of Rietra et al. (2001a), who found experimentally a clear synergy between the Ca^{2+} and PO_4^{3-} adsorption.

Interaction between Mg^{2+} and PO_4^{3-}

Interaction between magnesium and phosphate ions is also synergistic as shown in Fig.4.

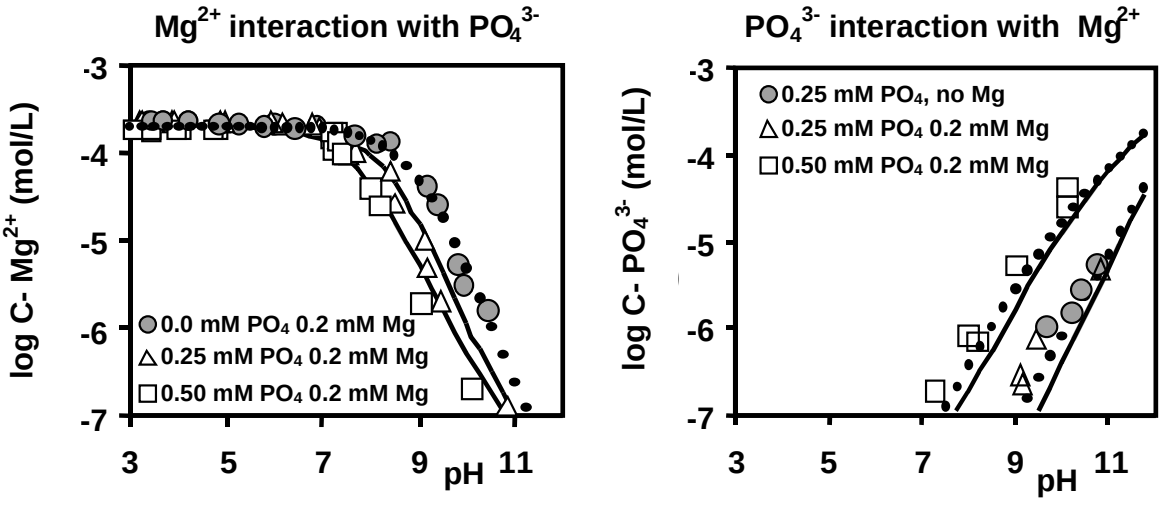

Fig.4. Interaction of Mg^{2+} and PO_4^{3-} in the presence of goethite (5 g/L) in 0.1M $NaNO_3$ as a function of pH. Open symbols refer to the measured equilibrium concentrations in the 'dual-ion' systems. One initial magnesium concentration was used, *i.e.* 0.2 mM Mg^{2+} and two initial concentrations of phosphate, i.e. 0.25 mM (triangles) and 0.50 mM (squares). The closed circles refer to the 'single-ion' systems. Full lines refer to the calculated equilibrium concentration in interaction experiments using the CD model with the parameters given in the Tables 1-3. Dotted lines refer to the concentrations calculated of the 'single-ion' systems for Mg^{2+} (left) and PO_4^{3-} (right).

In the presence of phosphate, the concentration of Mg^{2+} in solution decreases as result of an increased adsorption. As for Ca^{2+}, the observed effects are qualitatively explained by the interaction of the positive charge of Mg^{2+} with the negative charge of adsorbed phosphate ions.The predicted effect of Mg^{2+} on PO_4 and vice versa are smaller than for Ca^{2+} because Mg^{2+} adds less charge to the 1-plane where most of the interaction stems from (Hiemstra and van Riemsdijk, 1996).

3.2.2 Interactions with As(III) oxyanions

Arsenite

Recently, the adsorption behavior of arsenite and arsenate on goethite has been studied experimentally and interpreted using the CD model (Stachowicz et al., 2006). Two surface species have been used to describe the adsorption of arsenite, *i.e.* a bidentate (B) ≡ $(FeO)_2AsOH$ and a monodentate (M) ≡ $FeOAs(OH)_2$. Formation of these surface species has been confirmed by spectroscopic studies (Manning et al., 1998; Manning et al., 2002; Ona-Nguema et al., 2005). The bidentate species is found to be dominant over the whole pH range. The monodentate surface species is formed as minor species at low pH and high loading. Its contribution is growing for higher surface loadings of arsenite. The adsorption reactions can be defined as:

$$2 \equiv FeOH^{-1/2} + As(OH)_3(aq) \Leftrightarrow \equiv (FeO)_2^{-1+\Delta z_0} AsOH^{\Delta z_1} + 2\,H_2O\,(l) \qquad [7a]$$

$$1 \equiv FeOH^{-1/2} + As(OH)_3(aq) \Leftrightarrow \equiv FeO^{-1/2+\Delta z_0} As(OH)_2^{\Delta z_1} + 1\,H_2O\,(l) \qquad [7b]$$

with $\Delta z_0 + \Delta z_1 = 0$.

Stachowicz et al. (2006) derived the ionic CD value from MO/DFT optimized geometries and corrected them for dipole orientation of interfacial water, leading to the interfacial CD coefficients (Δz_0, Δz_1) given in Table 4. The log*K* values were fitted on adsorption data. In the present paper, the adsorption parameters derived (Stachowicz et al., 2006) (Table 4) will be used to predict the adsorption behavior of As(III) in the multicomponent experiments.

Table 4. Table defining the formation reaction of the surface species of arsenite ($As(OH)_3$) and arsenate (AsO_4^{3-}).

Species	≡ FeOH	≡ Fe_3O	Δz_0*	Δz_1*	Δz_2	H^+	$As(OH)_3$	AsO_4^{3}	log*K*
≡ $FeOAs(OH)_2$	1	0	0.16	-0.16	0	0	1	0	4.91[*1]
≡ $(FeO)_2\,AsOH$	2	0	0.34	-0.34	0	0	1	0	7.26[*1]
≡ $FeOAsO_2OH$	1	0	0.30	-1.30	0	2	0	1	26.60 ± 0.13[*2]
≡ $(FeO)_2\,AsO_2$	2	0	0.47	-1.47	0	2	0	1	29.27 ± 0.03[*2]
≡ $(FeO)_2\,AsOOH$	2	0	0.58	-0.58	0	3	0	1	33.00 ± 0.21[*2]

[*1] log*K* from Stachowicz et al. (2006).
[*2] log*K* values have been optimized in the present study by fitting all monocomponent adsorption data of Fig.11 (R^2=0.97 N=140 data points).
*[3]The given charge distribution values (Δz_0, Δz_1) are from Stachowicz et al. (2006).

Interaction of $As(OH)_3$ with Ca^{2+} or Mg^{2+}

The results of the experiments on the interaction of arsenite with Ca^{2+} and Mg^{2+} ions are shown in Fig.5. The effect of both divalent ions is very limited. It is difficult to establish any effect on the As(III) oxyanion adsorption precisely due to uncertainty of the data. From a practical perspective, we may state that in the natural pH range of soil and groundwater, no significant influence of Ca^{2+} and Mg^{2+} is to be expected based on this measured interaction in our 2-component systems.

The calculations predict a larger effect of Ca^{2+} compared to Mg^{2+}, which is related to the charge distribution. As will be discussed later in general, the ion-ion interaction in the model is mainly taking place via the charge and potential in the 1-plane. The negative charge on the outer ligand of arsenite (Δz_1=-0.34 v.u.) interacts with the positive charge introduced by the divalent cations. On average, Ca^{2+} introduces the highest amount of charge in the 1-plane. This leads in the prediction to more arsenite adsorption, i.e. a lower concentration in solution.

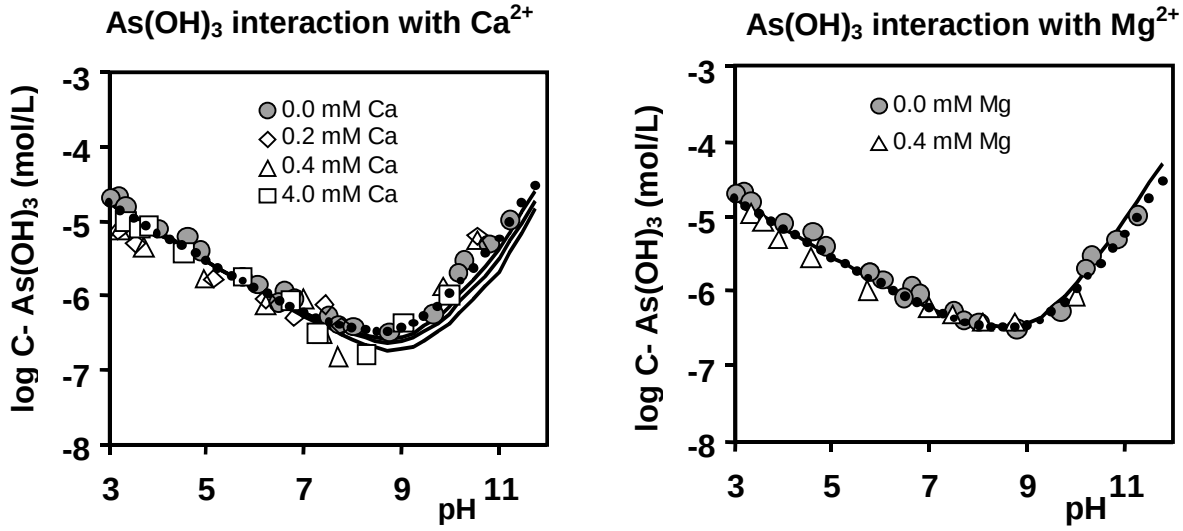

Fig.5. Interaction of $As(OH)_3$ with Ca^{2+} ions (left panel) and Mg^{2+} ions (right panel) in goethite suspensions (5 g/L) with 0.1 M $NaNO_3$. Open symbols refer to the measured equilibrium concentrations in the multi-component systems. For comparison, also the equilibrium concentrations in the "single ion" systems have been given (closed symbols). Full lines refer to the calculated equilibrium concentration in dual adsorbate systems using the CD model with the parameters of Stachowicz et al. (2006) for As(III) (Table 3) and the parameters for $Ca^{2+}$and Mg^{2+} derived in the present study (Table 4). Dotted lines refer to the "single ion" system and Mg^{2+} derived in the present study (Table 3). Dotted lines refer to the monocomponent system.

Competition of arsenite and phosphate

The predicted competition between arsenite and phosphate is given in Fig.6 together with the experimental data. In the left panel, the arsenite concentration is given for systems with different initial phosphate concentrations. In the other panel, the corresponding change of the phosphate concentration is given. For comparison, also the concentrations of the corresponding "single ion" systems have been given (closed circles). Our experiments show that the adsorption of arsenite depends strongly on the presence of phosphate and *vice versa*.

The effects are visible throughout the whole pH range. Arsenite, reaches a maximum adsorption around pH 8-9 (Dixit and Hering, 2003; Stachowicz et al., 2006), which results in a minimum solution concentration in that pH range. This minimum is shifted to a higher pH in the presence of phosphate, because of the larger competition of phosphate with arsenite in the lower pH range raising the arsenite concentrations in particular there.

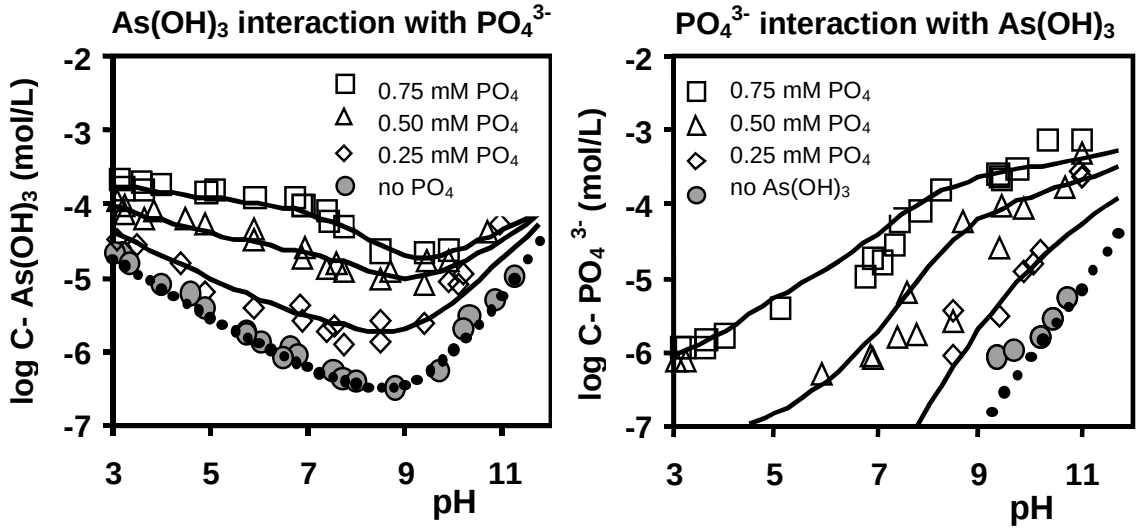

Fig.6. Competition between arsenite and phosphate on goethite (5 g/L) in 0.1 M $NaNO_3$. Open symbols refer to the measured equilibrium concentrations in the competition experiment. Closed symbols refer to the corresponding experimental data for the 'single-ion' systems. One initial concentration of arsenite was used (0.50 mM). Lines refer to the calculated equilibrium concentration using the CD model with parameters given in the Tables 1, 3, and 4. Both dotted lines refer to the prediction for the "single-ion" systems of arsenite (0.50 mM) and phosphate (0.25 mM).

Simultaneous interaction of arsenite, phosphate, and calcium ions

The effect of calcium ions on the adsorption of phosphate (Fig.3) and *vice versa* differs from the calcium effect on arsenite (Fig.4). Moreover, arsenite and phosphate are competitors. Therefore, we have designed an interaction experiment with 3-components, using as starting point some of the above arsenite-phosphate systems to which calcium ions have been added. The interaction of calcium with arsenite and phosphate is studied for two levels of phosphate (0.25 and 0.50 mM). Two levels of Ca^{2+} have been added, i.e. 0.2 and 0.4 mM. The results are shown in Fig.7 for the initial concentration of 0.2 mM Ca^{2+}. Full lines represent the predictions and the dotted lines show the concentrations in the corresponding 'single-ion' systems of calcium, arsenite, and phosphate. The arrows in the figure indicate the direction of the change at a given pH. The increase of the initial phosphate level, leads to an increase of the arsenite concentration, due to competition. For Ca^{2+}, the opposite is found. The observed changes in these systems are dictated by the competitive interaction of arsenite and phosphate, where PO_4^{3-} is a main regulator of the Ca^{2+} concentration.

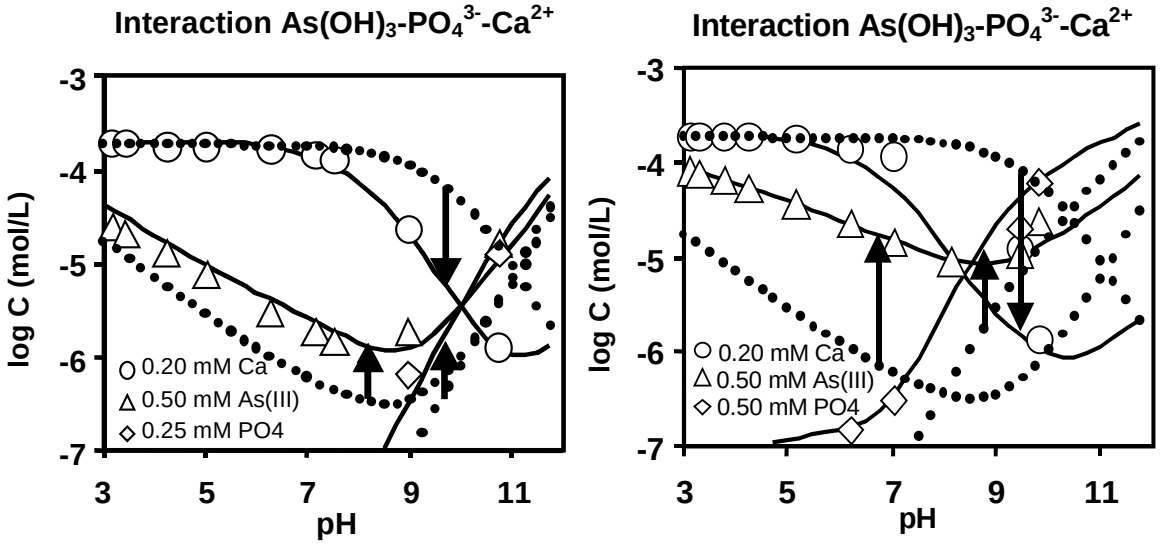

Fig.7. Equilibrium concentration of Ca^{2+} (circles), $As(OH)_3$ (triangles) and PO_4^{3-} (diamonds) in goethite suspensions (5 g/L) for two initial loadings with PO_4^{3-} (0.25 and 0.5 mM) in 0.1 M $NaNO_3$. The calcium and arsenite level is respectively 0.20 and 0.50 mM. Full lines refer to the calculated equilibrium concentration in the competition experiments using the CD model with the parameters given in the Tables 1-4. Dotted lines are the concentrations in the various monocomponent systems. Vertical lines indicate the shift that will occur when going from the 'single-ion' to the 'triple-ion' system.

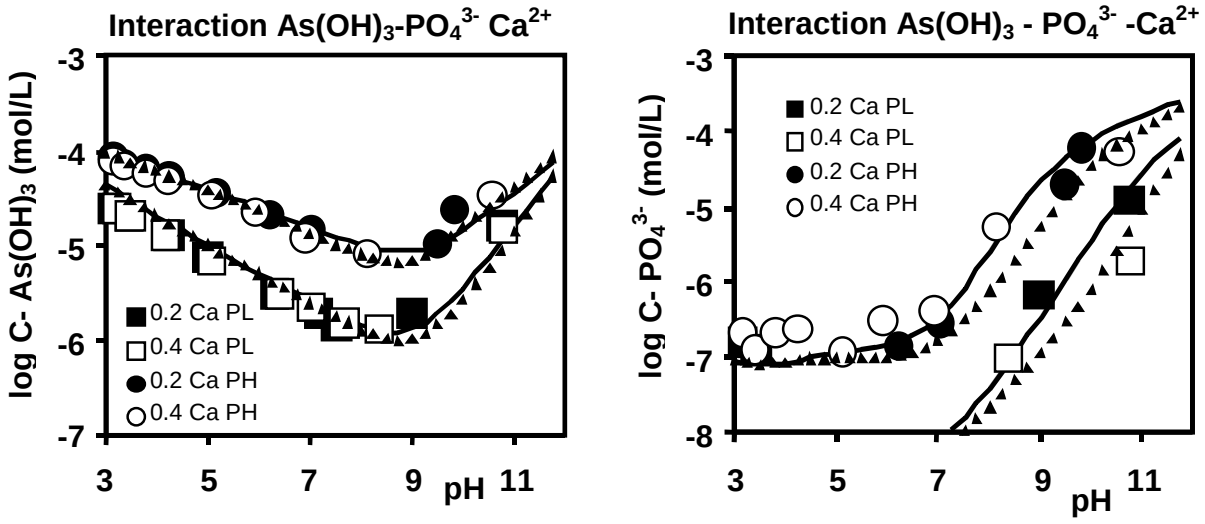

Fig.8. Equilibrium concentration of arsenite (left panel) and phosphate (right panel) as a function of pH in a 3-component Ca^{2+}-$As(OH)_3$-PO_4^{3-} goethite system (5 g/L) in 0.1 M $NaNO_3$, with 0.5 mM $As(OH)_3$ and 0.2 or 0.4 mM Ca^{2+} and a PO_4^{3-} loading of 0.25 mM (PL) and 0.50 mM (PH). Full (0.2 mM Ca^{2+}) and dotted (0.4 mM Ca^{2+}) lines are predictions using the parameters of Tables 1-4.

To judge the influence of Ca^{2+} on the arsenite concentration (triangles), the arsenite concentrations is given in the left panel Fig.8 as a function of pH for the systems with two levels of Ca^{2+}. The data show that the effect of Ca^{2+} is/remains insignificant. The effect of Ca^{2+} on the PO_4^{3-} concentration is larger (Fig.8 right panel). As discussed later in detail, an important reason for this is the larger charge attributed to the 1-plane by adsorbed ≡ $(FeO)_2PO_2$ (-1.46 v.u.) compared to the charge of ≡ $(FeO)_2AsOH$ (-0.34 v.u.). The CD model is able to predict the observed variation in the concentrations.

Simultaneous interaction of arsenite, phosphate, and magnesium ions

Interaction between $As(OH)_3$, PO_4^{3-}, and Mg^{2+} on goethite is shown in Fig.9. Two initial concentrations of phosphate were used (*i.e.* 0.25 mM and 0.5 mM), one concentration of arsenite (0.5 mM) and one concentration of magnesium (0.4 mM). Increase of the As(III) oxyanion adsorption (Fig.9a) is correctly predicted with the model. As for Ca^{2+}-$As(OH)_3$ -PO_4^{3-} systems,

the As(III) concentrations is mainly determined by the interactions with PO_4^{3-}, which are predicted well with the CD model.

3.2.3 Interactions with arsenate

Arsenate

In oxidized environments, arsenic is present as arsenate, (AsO_4^{3-}). The spectroscopic information with respect to surface complex formation on goethite (Waychunas et al., 1993; Fendorf et al., 1997; Foster et al., 1998; Manning et al., 1998; Farquhar et al., 2002; Sherman and Randall, 2003) has been discussed Stachowicz et al. (2006) who have used MO/DFT calculations to derive the geometry of the hydrated structures of the B, MH, and BH complexes. The calculated As-Fe distances for these three species were found to be very similar. This result complicates an unequivocal determination of the surface speciation with EXAFS.

The adsorption of arsenate has been described with three surface species, *i.e.* a non-protonated bidentate (B) ≡ $(FeO)_2AsO_2$, and a monodentate (MH) ≡ $FeOAsO_2OH$ surface species and a protonated bidentate (BH) ≡ $(FeO)_2AsOOH$) surface species (Stachowicz et al. 2006). The reactions can be defined as:

$$1 \equiv FeOH^{-1/2} + 2H^+(aq) + AsO_4^{3-}(aq) \Leftrightarrow \equiv FeO^{-1/2+\Delta z_0}AsO_2OH^{\Delta z_1} + 1\ H_2O(l) \qquad [8a]$$

$$2 \equiv FeOH^{-1/2} + 2H^+(aq) + AsO_4^{3-}(aq) \Leftrightarrow \equiv (FeO)_2^{-1+\Delta z_0}AsO_2^{\Delta z_1} + 2\ H_2O(l) \qquad [8b]$$

$$2 \equiv FeOH^{-1/2} + 3H^+(aq) + AsO_4^{3-}(aq) \Leftrightarrow \equiv (FeO)_2^{-1+\Delta z_0}AsOOH^{\Delta z_1} + 2\ H_2O(l) \qquad [8c]$$

in which $\Delta z_0+\Delta z_1$ is equal to the charge introduced by the adsorption of H^+ and AsO_4^{3-}.

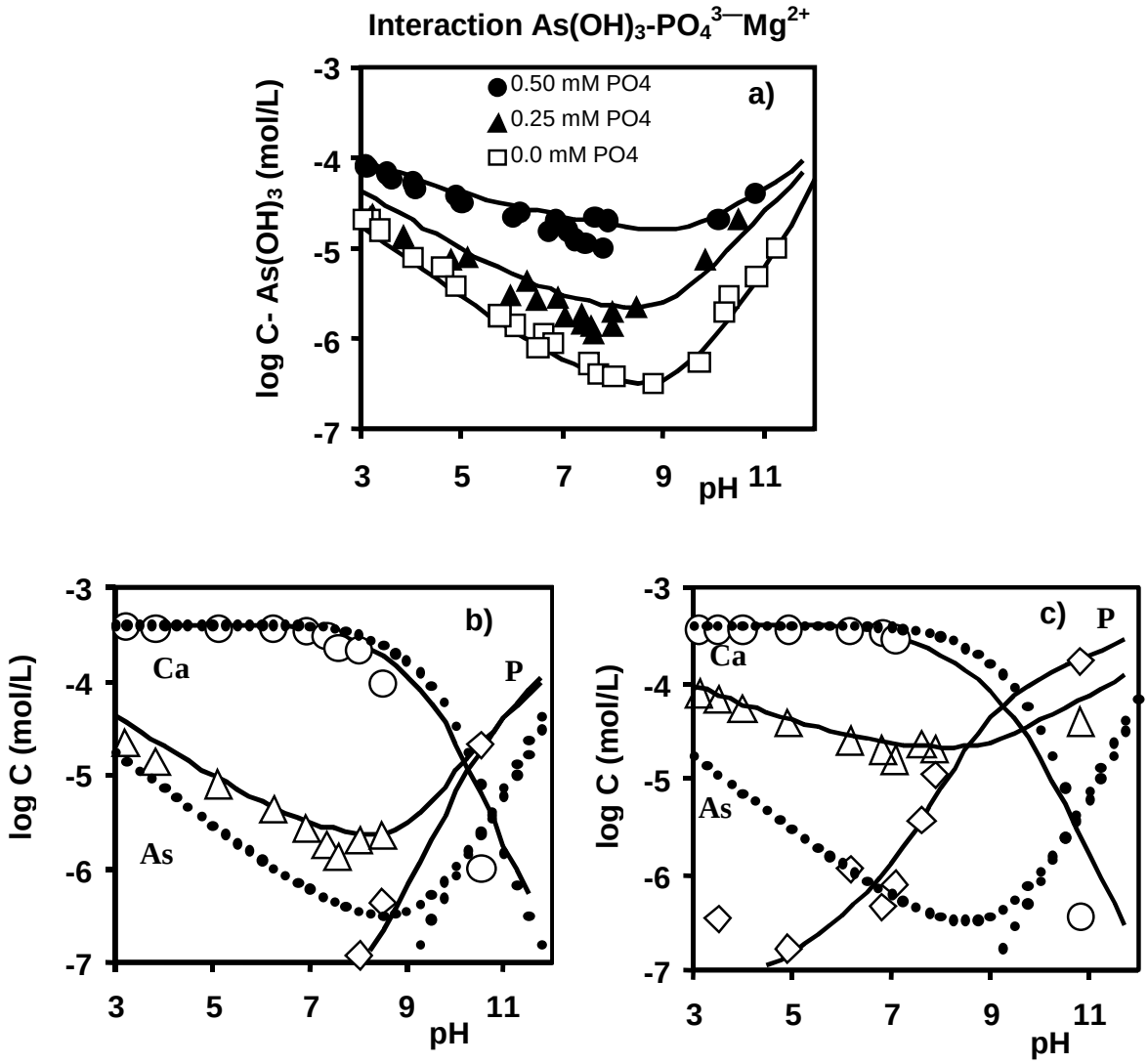

Fig.9a. Equilibrium concentration of arsenite as a function of pH at different phosphate loadings in a goethite system (5 g/L) containing 0.5 mM $As(OH)_3$, 0.4 mM Mg^{2+}, and 0.1 M $NaNO_3$. Fig9.b,c Equilibrium concentration of Mg^{2+} (circles), As(III) (triangles) and PO_4 (diamonds) as a function of pH at a PO_4^{3-} loading 0.25 (b) or 0.50 mM PO_4^{3-} (c) in goethite suspensions (5 g/L) with 0.5 mM $As(OH)_3$, 0.4 mM Mg^{2+}, and 0.1 M $NaNO_3$. Full lines in Fig.9 refer to the calculated equilibrium concentration in competition experiments using the CD model with the parameters given in the Tables 1-4. Dotted lines are the predicted concentrations in the various 'single-ion' systems.

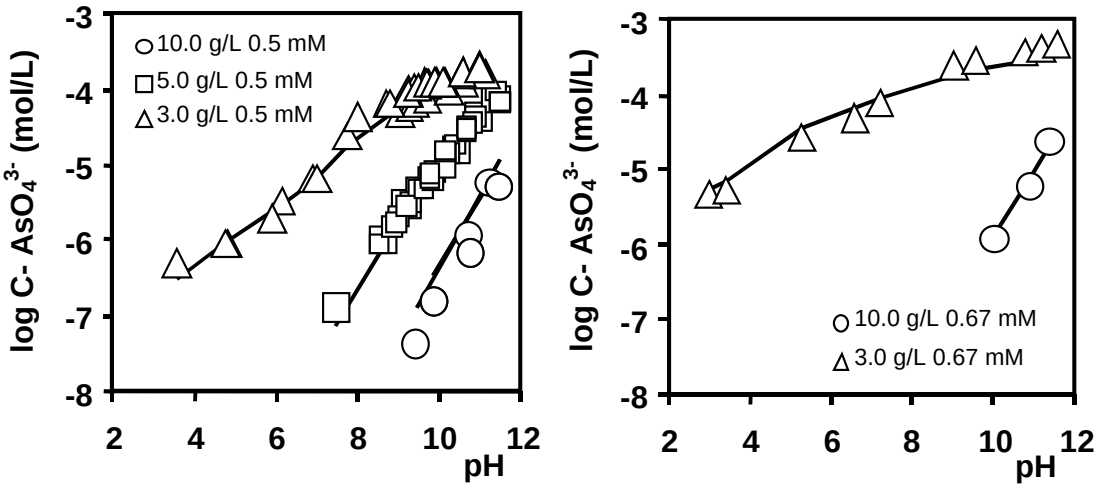

Fig.10. Equilibrium concentrations of arsenate as a function of pH in goethite systems (3, 5, or 10 g/L) containing 0.5 mM arsenate (left panel). Data are from Stachowicz et al. 2006. In the right panel, the present data are given for 3 and 10 g/L goethite and 0.67 mM arsenate. Lines are calculated with the affinity constants of Table 1,4.

The non-protonated bidentate (B) species is dominant, while the MH species becomes gradually more important at low pH and at a high surface loading. Any contribution of the BH species is minor and limited to low pH. The data of Stachowicz et al. (2006) could also be described reasonably well ignoring its contribution. According to Stachowicz et al. (2006), the contribution of BH will increase with loading. Therefore, we have done some additional 'single-ion' experiments with 3 and 10 g/L goethite at a higher AsO_4^{3-} loading (0.67 mM) than previously used. These data at a higher loading, enables a better determination of the log*K* value of the BH complex ($\equiv (FeO)_2AsOOH$). The complete set of data (Fig. 10) has been used to reevaluate the set of constants (Table 4). The log*K* values for the B and MH complex remained practically almost unchanged. The present log*K* value for BH is slightly higher (0.3 log*K* units). The CD values used in the evaluation have been calculated from the MO/DFT optimized geometry of hydrated iron-arsenate complexes found by Stachowicz et al. (2006).

Competition of arsenate and phosphate

Competition of arsenate with phosphate is given at Fig.11 for 2-component systems (open symbols). In the left panel, the arsenate concentrations are given for systems with a two different phosphate loadings.

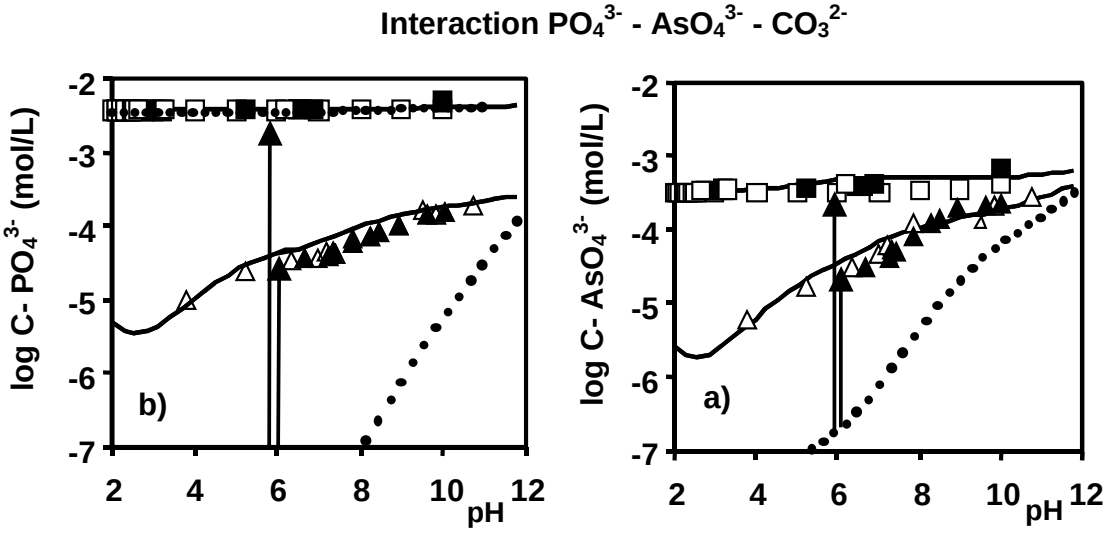

Fig.11. Equilibrium concentrations of arsenate (a) and phosphate (b) as a function of pH in goethite (5 g/L) in 0.1 M $NaNO_3$ with AsO_4^{3-}-PO_4^{3-} (open symbols) and AsO_4^{3-}-PO_4^{3-}-CO_3^{2-} (closed symbols). The systems contain 0.7 mM arsenate and 0.4 (triangles) or 4.8 (squares) mM phosphate. If present, the (bi)carbonate concentration is 0.01 M. Full lines show the predictions for the competition experiments. Dotted lines give the concentration in the 'single-ion' systems as predicted using the parameters of Tables 1-5. Vertical arrows indicate the change in concentration in case of competition in a 'dual-ion system'.

The corresponding phosphate equilibrium concentrations are given in the right panel. Arsenate is very sensitive to the presence of elevated concentrations of phosphate. This effect is most pronounced at a lower pH where both ions reach a maximum adsorption, yet, it is clearly visible throughout the whole pH range. The strong ability of phosphate to inhibit the arsenate adsorption on iron oxide has also been noticed by others (Manning et al., 1998; Gao and Mucci, 2001; Zhao and Stanforth, 2001; Dixit and Hering, 2003). As shown in Fig.11 with full lines, the competition between AsO_4^{3-} and PO_4^{3-} can be well predicted with the model.

Bicarbonate (HCO_3^-)

Adsorption of bicarbonate on goethite has been studied experimentally by (van Geen et al., 1994) and Villalobos and Leckie(2000 and 2001). The adsorption mechanism of carbonate has been studied with IR spectroscopy. The adsorption mechanism of carbonate has been studied with IR spectroscopy (Wijnja and Schulthess, 2000; Villalobos and Leckie, 2001). Initially, based on the low degree of band splitting, the data have been interpreted as the formation of a mononuclear monodentate complex. However, the CD value obtained from adsorption modeling (Villalobos and Leckie, 2001; Hiemstra et al., 2004) is typical for bidentate complex formation (≡ $(FeO)_2CO$). According to Hiemstra et al. (Hiemstra et al., 2004), the low band splitting is probably due to additional field effects for instance due to H bond formation. This has been recently confirmed by quantum chemical calculations (Bargar et al., 2005). The formation reaction can be formulated as:

$$2 \equiv FeOH^{-1/2} + 2H^+(aq) + CO_3^{2-}(aq) \Leftrightarrow \equiv (FeO)_2^{-1+\Delta z_0} CO^{\Delta z_1} + 2\ H_2O(l) \qquad [9]$$

Hiemstra and van Riemsdijk (2006) have calculated the ionic CD value of the carbonate bidentate complex from MO/DFT optimized geometries and corrected these for water dipole orientation, resulting in overall interfacial charge distribution coefficients (Δz_0,Δz_1). The affinity constant (log*K*) has been fitted on the adsorption data of Villalobos and Leckie (2000). The parameters are given in Table 5 and will be used in the present study. The parameter set of Table 5 has recently also been used by Stachowicz et al. (2007a) to predict the 2-component interaction between bicarbonate, and arsenite, and arsenate on goethite.

Table 5. Table defining the formation of the surface species of CO_3^{2-}.

Species	≡ FeOH	≡ Fe_3O	Δz_0*[1]	Δz_1*[1]	Δz_2	H^+	CO_3^{2-}	log*K**[2]
≡ $(FeO)_2$ CO	2	0	0.68	-0.68	0	2	1	22.33

*[1] The charge distribution values are from Hiemstra and van Riemsdijk (2006).

*[2] The log*K* is from fitting of the data of Villalobos and Leckie (2000) as given by Stachowicz et al. (2007a).

Simultaneous interaction of arsenate, phosphate, and carbonate

We have measured the effect of HCO_3^- on the interaction of PO_4^{3-} and AsO_4^{3-}. The arsenate and phosphate concentrations are given in Fig. 11 as closed symbols. The initial (bi)carbonate (0.01 M) concentration has been chosen to reflect an average concentration of groundwater. The lowest phosphate concentration level in our experiments is typically for eutrophic groundwater (BGS and DPHE, 2001) as can be found in Bangladesh. As follows from Fig.11, the presence of 0.01 M bicarbonate has no measurable influence on the PO_4^{3-} or AsO_4^{3-} concentrations. It illustrates the relatively low competitive power of HCO_3^- in the AsO_4^{3-}-PO_4^{3-} system. Previously, we have studied experimentally the AsO_4^{3-}-CO_3^{2-} competition in the absence of PO_4^{3-} (Stachowicz et al., 2007) for pH=6.5-10. In this system, ion competition is found reaching a maximum at the lowest pH studied. Presence of 0.01 M bicarbonate increased the arsenate concentration by a factor of about 10. In the present system, no effect is found due to the relatively strong binding of PO_4^{3-}, which suppresses the carbonate adsorption. In Fig.11, the calculated lines for the AsO_4^{3-}-PO_4^{3-} systems coincides with the lines for the AsO_4^{3-}-PO_4^{3-}-CO_3^{2-} systems, illustrating the insignificance of (bi)carbonate as a competitor.

3.2.4 General discussion

In the above, we have shown that based on "single-ion" systems, the CD model is able to predict the behavior of the elements in a multi-competitive environment, in which oxyanions and cations are interacting. We have not tried to improve the description by optimizing the affinity constants, but nevertheless a very good description is found in most cases.

The good predictability can be used to better understand differences in behavior of arsenite and arsenate. For instance, it has been speculated (Smedley and Kinniburgh, 2002) that the competition between PO_4^{3-} and $As(OH)_3$ is likely to be less important than the PO_4^{3-}-AsO_4^{3-} interactions. This statement can be tested with the calibrated CD modeling. Using a system with a high solid:solution ratio (10,000 m^2/L), as can be found in aquifers (Stachowicz et al., 2007), we have calculated the PO_4^{3-} dependency of $As(OH)_3$ and AsO_4^{3-} for conditions representative for average ground water, i.e. a pH 7 and I = 0.01 M (Fig.12).

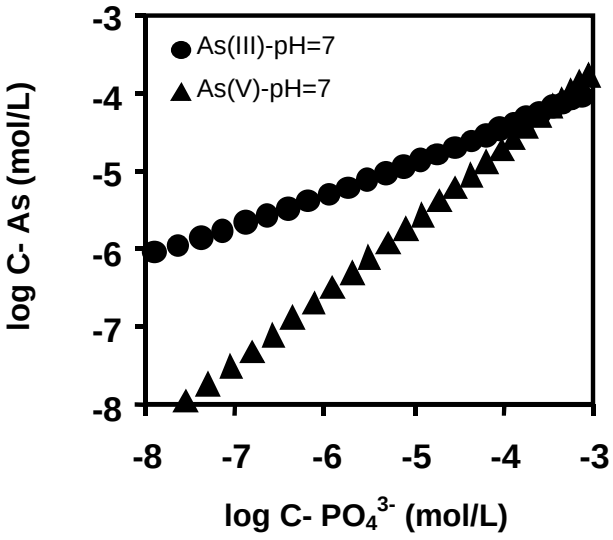

Fig.12. The predicted arsenate and arsenite concentration as a function of the phosphate solution concentration in a goethite system (10,000 m^2/L) in 0.01 M $NaNO_3$. The initial arsenic concentration is 5 mM.

The calculations show that at pH=7, arsenite is bound less strongly than arsenate in the major range of phosphate concentrations. If the same calculations are done at pH=8 the lines for arsenite and arsenate cross at about 2 10^{-5} M phosphate, which is mainly due to the higher binding of $As(OH)_3$ at pH 8, giving lower concentrations of arsenite.

A second feature illustrated in the figure is the larger PO_4^{3-} dependency of AsO_4^{3-} in comparison to $As(OH)_3$. The difference in sensitivity of both As species for the presence of phosphate is due to a different electrostatic interaction. The electrostatic energy of the binding is, according to the CD model, determined by the potential at the surface (ψ_0) and the potential in the 1-plane (ψ_1). Iron oxide surfaces have a near-Nernstian character. It means that the value of surface potential is strongly dominated by the pH. For a given pH, the surface potential ψ_0 is relatively constant upon ion adsorption, due to the high proton buffering. In contrast, the potential in the 1-plane (ψ_1) will strongly change with the amount of charge that is introduced in the 1-plane by adsorbing ions. The variable potential of the 1-plane is responsible for the main

variation in the electrostatic energy as a function of loading. This variation is relevant for the shape of the adsorption isotherm ('electrostatic bending') at a given pH and will cause synergy or competition. As follows from Table 4, the main surface complex of $As(OH)_3$ has a relatively small charge attribution to the 1-plane (Δz_1= -0.34 v.u.) in comparison with the two main surface species of AsO_4^{3-} that are active at pH 7 (Δz_1=-1.47 and -1.30 v.u.). The difference in charge attribution is about 1 v.u. The charge attribution to the 1-plane of the relevant PO_4^{3-} species (Δz_1=-1.46 and -1.28 v.u.) is very comparable with AsO_4^{3-} (Table 1). Adsorption of PO_4^{3-} will change the potential of the 1 plane substantially. Since the AsO_4^{3-} species introduces more charge in the 1-plane, this ion will be more (negatively) affected by the presence of the charge of the adsorbed PO_4^{3-} species than $As(OH)_3$. This leads to a larger sensitivity of AsO_4^{3-} for PO_4^{3-} in comparison to $As(OH)_3$, as is demonstrated in Fig.12 focusing on the slope of the lines, *i.e.* $\delta \log C_{As(III)} / \delta \log C_{PO4} \approx 0.4$ while $\delta \log C_{As(V)} / \delta \log C_{PO4} \approx 0.9$ at pH 7.

4. Conclusions

The above can be summarized in a series of conclusions.

- Both Ca^{2+} and Mg^{2+} ions promote the adsorption of PO_4^{3-}. This promotion is of an electrostatic nature. Since AsO_4^{3-} is chemically comparable with PO_4^{3-} and has a very similar interfacial charge distribution, the same type of electrostatic effect is expected for the interaction of Ca^{2+} and Mg^{2+} with AsO_4^{3-}.
- The presence of Ca^{2+} ions has a minor effect on the As(III) oxyanion adsorption in Ca-As(III) systems, only occurring at very high pH. In the pH range, relevant for natural groundwater (pH 6-9), no significant effect is observed.
- Mg^{2+} ions have no significant effect on the As(III) oxyanion binding over a very large pH range.
- Interaction between PO_4^{3-} and AsO_4^{3-} is stronger than the interaction of PO_4^{3-} and $As(OH)_3$.
- Phosphate adsorption has a strong interaction with both $As(OH)_3$ and AsO_4^{3-} and therefore it is of critical importance in groundwater systems.

- The sensitivity of As(III) oxyanions for changes in the phosphate concentrations is smaller than the sensitivity of As(V) oxyanions for phosphate, *i.e.* $\delta \log C_{As(III)} / \delta \log C_{PO4} \approx 0.4$ while $\delta \log C_{As(V)} / \delta \log C_{PO4} \approx 0.9$ at pH 7.
- In 3-component experiments with $As(OH)_3$-PO_4^{3-}, and divalent cations, the arsenite concentration is dominantly regulated by phosphate. The phosphate concentration is regulated by arsenite with some influence of Ca^{2+} and Mg^{2+}. The Ca^{2+} and Mg^{2+} concentrations are mainly regulated by the adsorption of the PO_4^{3-} ions.
- Bicarbonate is a very weak competitor in a 3-component goethite system with AsO_4^{3-}-PO_4^{3-}-CO_3^{2-}.

5

Linking the Arsenic Binding to Goethite with the Binding to Amorphous Iron (Hydr)oxide

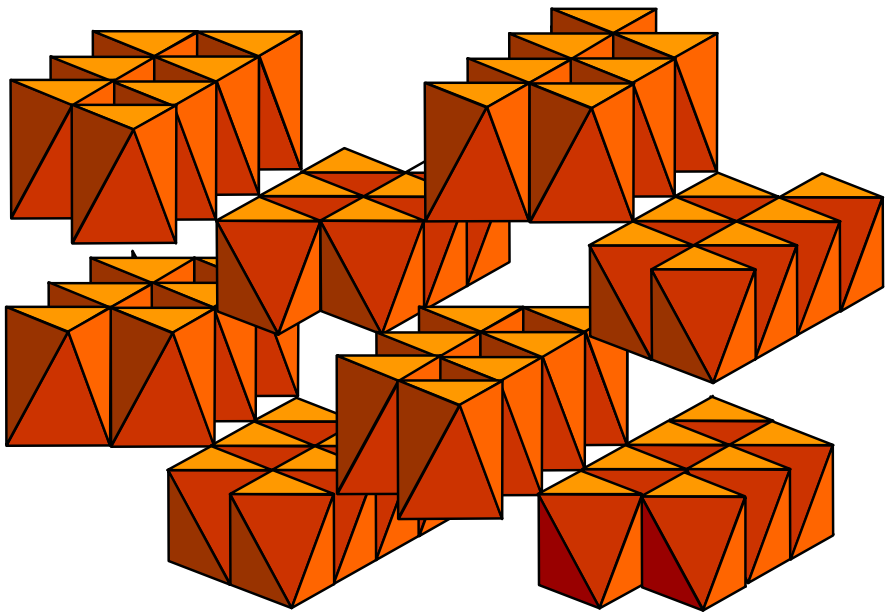

Abstract

Iron oxides are a primary source of arsenic in Bangladesh groundwater. Ion binding of iron oxides is strongly determined by the structure of the surface and the type of surface complexes formed. The primary structures of HFO and goethite have similarities. Our objective is to model the multi-component interaction of arsenic adsorption and the primary charging behavior for goethite and hydrous ferric oxide (HFO) simultaneously in a coherent manner using the charge distribution (CD) model approach assuming a common set of different types of surface groups with different site densities and affinities of protons and the oxyanions of As(III) and A(V). For goethite the apparent fraction of top-end faces at the crystals was assumed to be 5%, while for HFO, a 50% contribution of similar faces was used. As a result, the primary charging behavior of goethite and HFO has been modeled in a coherent manner using the MUSIC model approach. The adsorption parameters for As(III) and for As(V) were optimized using adsorption data for "single-ion" systems as presented in literature. The CD values of the different type of As(III) and As(V) complexes were found independently from the MO/DFT optimized geometries of hydrated complexes. The affinity constants were fitted iteratively on adsorption data of goethite and HFO. Theses parameters were used to predict As(III) and As(V) competition on goethite as well as on HFO. The modeling results have been tested on data from competition experiments. The model successfully predicted the competition between arsenic species, As(III) and As(V), on both minerals. For the highest surface loading discrepancies between the data and model predictions were observed for adsorption on HFO. However, it is possible that for such an extreme surface loadings a surface precipitation occurs.

The above suggests that despite the differences in the reactivity of goethite and HFO a link exists between the adsorption behavior of both minerals. Since both HFO and nano-goethite have been considered dominant reactive surfaces for 'field' conditions this is of important practical relevance. In future the CD model can be used to predict adsorption in complex systems simulating natural conditions.

1. Introduction

Elevated concentrations of arsenic in groundwater have been found in many aquifers around the world (BGS and DPHE, 2001; Mandal and Suzuki, 2002; Smedley and Kinniburgh, 2002). While arsenic ingestion is related to serious health risks, in Bangladesh alone tens of millions of people have been exposed to arsenic in drinking water. Therefore, since the discovery of the arsenic problem, a lot of attention has been given to the subject. So far, the characterization of the fate of arsenic in the environment has been a challenge.

Natural systems are complex and thus the mobility and bioavailability of arsenic is affected by the presence of various mineral surfaces as well as other co-occurring elements. One of the common mineral surfaces in soils and sediments are iron oxides such as goethite, hematite and hydrous ferric oxide (HFO) (Buffle, 1990; Schwertmann and Cornell, 1991). The data obtained in the BGS study (BGS and DPHE, 2001) support the hypothesis that As bound by iron oxides is a primary source of arsenic in Bangladesh groundwater. Iron oxides present in those sediments include Fe(III)-oxides such as HFO, goethite or hematite, and possibly various mixed valence oxides such as magnetite and green rust (Smedley and Kinniburgh, 2002). The amount of mobile arsenic under field conditions is often linked to the amount of iron found by oxalate extraction (BGS and DPHE, 2001). It is believed that the oxalate-extracted Fe is related to oxide material with a high reactive surface area (Roden and Zachara, 1996). HFO is seen as an important representative and for this reason it has been considered a useful proxy for the natural Fe (hydr)oxide fraction.

Ion binding to Fe (hydr)oxides is strongly determined by the structure of the surface and the type of surface complexes formed. The variation in adsorption as a function of the solution conditions like pH and ion concentrations is strongly regulated by the electrostatic properties of the interface. On a molecular scale, arsenic adsorption is due to interaction of the oxyanions with singly coordinated surface groups. Singly coordinated surface groups can be found at the main

crystal faces of goethite, i.e. the 110 and 100 face (Weidler et al., 1996; Prelot et al., 2003), and on top-end crystal faces like the 021 and 001 face. The type of surface groups present on the goethite faces are assumed to contribute also to the reactivity of HFO (Spadini et al., 1994; Venema et al., 1996; Spadini et al., 2003; Ponthieu et al., 2006). Little is known about the crystal structure of HFO (Jambor and Dutrizac, 1998). It has been suggested that it contains linked rows of octahedra as found in goethite, but that the structure is defect (Manceau and Combes, 1988). The particles are very small (~2 nm) and spherical-like. These small HFO particles are probably anisotropic with respect to surface properties, since these nano-sized particles thread together in lines upon aging, finally forming goethite (Murphy et al., 1974). The same process of alignment can be observed for nanogoethite particles (Waychunas et al., 2005).

In contrast to HFO, goethite is a well-crystallized iron oxy-hydroxide with a relatively well-known surface structure. It has been widely studied with respect to the formation, morphology and reactive sites (Sun and Doner, 1996; Weidler et al., 1998; Hiemstra and van Riemsdijk, 2000; Blakey and James, 2003; Gaboriaud and Ehrhardt, 2003; Kosmulski et al., 2003; Betancur et al., 2004; Kosmulski et al., 2004; Rustad and Felmy, 2005; Burleson and Penn, 2006). Ion adsorption on goethite can be described with a surface complexation model, like the Charge Distribution (CD) model (Hiemstra and van Riemsdijk, 1996). In the CD model the electrostatic energy contribution of the overall adsorption energy is calculated based on two electrostatic potentials at the solid-liquid interface. The CD model has been successfully used to describe arsenic adsorption on goethite (Hiemstra and van Riemsdijk, 1999; Antelo et al., 2005; Stachowicz et al., 2006). Although the adsorption of arsenic on HFO has frequently been studied (Pierce and Moore, 1982; Hsia et al., 1992; Wilkie and Hering, 1996; Raven et al., 1998; Jain et al., 1999; Jain and Loeppert, 2000; Goldberg and Johnston, 2001; Holm, 2002; Dixit and Hering, 2003), so far, it has not been described with the CD model approach.

If the primary structure of HFO and goethite have large similarities, it is possible that the notable differences in reactivity for goethite and HFO may be caused by differences in the relative number of the various types of reactive surface groups (Ponthieu et al., 2006). Our objective is to model the arsenic adsorption and the primary charging behavior of goethite and HFO in a coherent manner using the CD model approach. This exploration may result in one set of parameters, common for both materials. The adsorption parameters for As(III) and As(V) oxyanions will be optimized using the pseudo-monocomponent adsorption data presented in

literature. We will critically select the adsorption data for arsenic on HFO as some inconsistency is present between the various data sets. Next, the adsorption parameters, optimized for monocomponent data, will be used to predict As(III) and As(V) oxyanion competition on goethite as well as on HFO. The prediction will be compared with new experimental data for As(III) and As(V) oxyanion competition on goethite, and with some experimental literature data for the competition between arsenic species on HFO (Jain and Loeppert, 2000).

2. Materials and Methods

2.1. Goethite material

Goethite material used in this study has been described previously by Stachowicz et al (Stachowicz et al., 2006). The specific BET-surface area of goethite measured by N_2 gas adsorption was 98 m^2/g. The material was characterized in an acid-base titration experiment for three background electrolyte levels: 0.003, 0.012, and 0.1 M $NaNO_3$ by means of a computer-controlled titrator. The initial goethite concentration used in the titration experiment was 16.5 g/L.

For adsorption experiments, the stock of the goethite suspension was diluted with ultra pure water to a concentration of approximately 20.0 g/L. After pH adjustment to pH 5.5, the suspension was purged overnight with moist N_2 (cleaned) to remove CO_2.

2.2. Reagents solutions

Stock solutions ($NaAsO_2$, $NaHAsO_4$ and $NaNO_3$) were prepared from 'analytical grade' chemicals (Merck) by dilution with ultra pure water (≈ 0.018 dS/m). Stocks were stored in polyethylene bottles to avoid silica contamination. All solutions were prepared with pre-boiled water and under N_2 atmosphere to avoid CO_2 contamination. The ICP-AES was used to verify stock concentrations. The solution of 0.100 M NaOH was prepared CO_2-free from Titrasol. Preventive measures were undertaken to avoid silica and CO_2 contamination, i.e., the base solution was stored in a plastic bottle in a dessicator. The solution of 0.100 M HNO_3 was prepared from Titrasol and stored in a glass bottle (to avoid contamination by organic material).

2.3. Adsorption experiments

Adsorption experiments were performed according to the procedure described by Stachowicz et al. (Stachowicz et al., 2006). Tests were carried out in gas-tight 23.6 ml bottles of low-density polyethylene (Rietra et al., 2001) with fixed amounts of salt, arsenite and arsenate solution and goethite suspension at different pH values. The pH was adjusted with 0.0100 M or 0.100 M HNO_3 (or NaOH). The experiments were done in the pH range 3-12. All solutions were added to the bottles under N_2 atmosphere to prevent CO_2 contamination. The bottles were equilibrated for 24 hours in a shaker in a constant temperature room (~22 ^oC). Subsequently, the bottles were centrifuged and the samples of the supernatant were collected for analysis. Equilibrium concentrations of As(III) and As(V) oxyanions in competition experiments were measured by means of atomic fluorescence spectrometer (AFS Millenium Excalibur by PS Analytical Ltd) using the HPLC-AFS method (Gomez-Ariza et al., 1998; Moreno et al., 2000) as described in Millenium Excalibur Users Manual (Appendix I, Speciation System).

The pH was measured in the bottles after re-suspension of goethite. The total concentrations of components in each bottle, representing one data point, were calculated based on the amounts and concentrations of the solutions added. Three initial concentrations of arsenite (0.25, 0.50 and 0.75 mM) and three concentrations of arsenate (0.25, 0.50 and 0.75 mM) were used. In all adsorption experiments, the final goethite concentration was 5.0 g/L. Competition experiments were done for five As(III):As(V) ratios, i.e., 0.50 : 0.25 mM; 0.50 : 0.50 mM; 0.75 : 0.50 mM; 0.25 : 0.50 mM; and 0.75: 0.50 mM respectively. The background electrolyte concentration was in each case 0.10 M $NaNO_3$. The total volume of the suspension in each individual bottle was 20.0 ml. The amount of adsorbed arsenite and arsenate was calculated as the difference between the total initial arsenite or arsenate concentration and the measured equilibrium concentration.

2.4. Surface complexation modeling

The surface complexation modeling was done with ECOSAT (Keizer and van Riemsdijk, 1998) and FIT (Kinniburgh, 1993). The CD model (Hiemstra and van Riemsdijk, 1996) has been used for modeling the ion adsorption behavior on goethite and HFO.

In the next sections, all the assumptions made for modeling of the adsorption data for goethite and HFO are discussed. These assumptions refer to the structure, the ratio of the

crystallographic faces and other parameters such as proton affinities, capacitance of the different layers, and ion pair formation constants. At the end, the formation of the arsenic surface complexes is discussed and the relation to the charge distribution parameter.

2.4.1. Morphology, crystal structure and surface groups

Goethite is a well-crystallized iron oxide with needle-shaped or lath-shaped crystals (Fig.1a) (Hiemstra et al., 1989a; Schwertmann and Cornell, 1991; Weidler et al., 1996; Weidler et al., 1998; Gaboriaud and Ehrhardt, 2003; Prelot et al., 2003). The specific surface area of the material depends on the preparation procedure (Kosmulski et al., 2004) and varies between about 20-200 m^2/g. The main crystal surfaces of needles or laths of synthesized goethite are the 110 and 100 face. The relative importance of the 100 face (70-30%) is a function of the BET surface area (Gaboriaud and Ehrhardt, 2003). Increase of the surface area is accompanied by a decrease of the contribution of the 100 face in favor of the 110 face (Gaboriaud and Ehrhardt, 2003). The fraction of the total surface area that is contributed by the faces at the top-ends of the crystals is determined by the length of the crystals (Hiemstra et al., 1989a). Various faces may be present like the 001, 021 and/or 112 face (Prelot et al., 2003; Spadini et al., 2003). The relative length and corresponding importance (3-13 %) of these crystal faces also vary with the total surface area (Cornell et al., 1974; Kosmulski et al., 2004). One may conclude that increase of the surface area will lead to a higher contribution of the 110 faces, relative to the 100 face, and of the top-end crystals faces like the 021 face, relatively to the 110 and 100 faces. We note that the crystal indexes for the various faces depend on the definition of the orientation of the axis in the crystal. The above faces refer to the Pbma space group as used in the Inorganic Crystal Structure Database.

At the main crystal faces, three types of surface groups are present, each with a different metal coordination, i.e. singly coordinated ≡ FeOH(H), doubly coordinated ≡ Fe_2OH, and triply coordinated ≡ $Fe_3O(H)$ (Hiemstra and van Riemsdijk, 1996). Variation in the relative presence of the 110 and 100 faces on goethite crystals does not have a particular influence on the PZC of the particle (Gaboriaud and Ehrhardt, 2003), suggesting a large similarity in the type of reactive surface groups, which also follows from an analysis of the surface structure (Weidler et al., 1996; Weidler et al., 1998). At the top-end faces of goethite, only singly ≡ FeOH(H) and doubly ≡ Fe_2OH coordinated surface groups exist (Venema et al., 1998; Spadini et al., 2003).

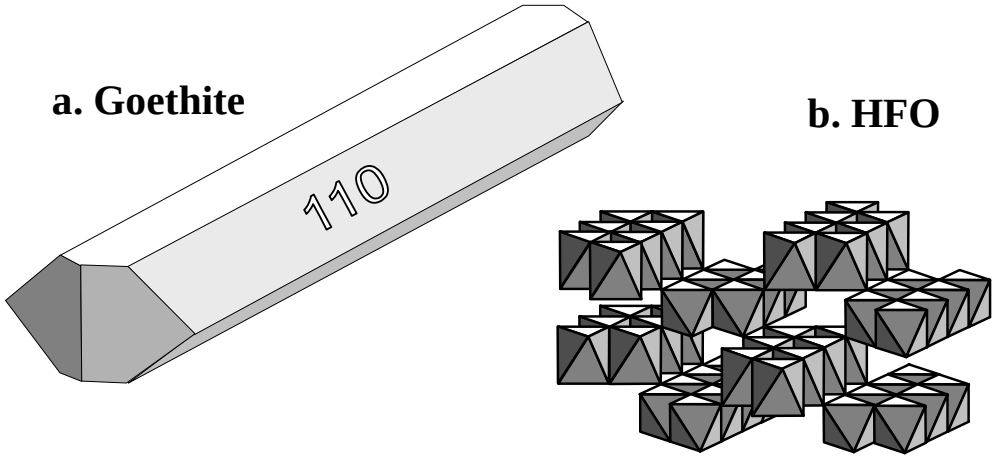

Fig.1a (left). The idealized crystal morphology of needle shaped goethite. The main faces of needle- or lath-shaped goethite are the 110 and 100 faces (Weidler et al., 1998). The 110 face is dominant in high surface area goethite preparations. The top-end crystal faces, like the 021 (shown) and 001 (not shown) faces, represent about 5-15 % of the surface area (Cornell et al., 1974), which depends on the relative length of the crystals (Hiemstra et al., 1989a).
Fig.1b (right). The hypothetical mineral structure of small HFO particles. The structure has some resemblance with goethite. The basic unit is thought to be a short double-chain of several Fe octahedra with two Fe-O distances characteristic for goethite (Waychunas et al., 1993). These chains are cross-linked, but the average number of inter-chain linkages is lower than in goethite and may be irregular.

Freshly prepared HFO particles are apparently spherical with a diameter of 1.5-3.0 nm (Murphy et al., 1974). Because of the small size, a determination of the surface area using the BET approach is questionable. Typical values of the BET surface area are 200-350 m^2/g (Dzombak and Morel, 1990). This number is lower than expected based on the size of the spherical particles, for which one calculates a reactive surface area of about 1000-500 m^2/g using the above given diameters.

Freshly prepared iron oxides are almost X-ray amorphous and are known as 2-line ferrihydrite. Aging, dehydration and drying may produce a 6-line ferrihydrite (Jambor and Dutrizac, 1998). It has been suggested that the local structure of freshly prepared HFO may partly resemble that of goethite (Manceau and Combes, 1988; Waychunas et al., 1993; Manceau and Charlet, 1994; Spadini et al., 1994; Spadini et al., 2003). Similar as in goethite, two characteristic

Fe-O bond lengths are found (Combes et al., 1989; Waychunas et al., 1993), i.e. $d_{FeO} \approx 195 \pm 1$ pm and $d_{FeOH} = 209 \pm 1$ pm. These two different Fe-O(H) distances are very similar to the distances found in goethite. The fundamental unit of a synthetic 2-line ferrihydrite is the $Fe(O,OH)_6$ octahedron. The octahedrons are linked together in short double chains (Fig.1b) which are cross-linked. The inter-chain linkage is probably disordered which may result in smaller Fe-Fe distances (Manceau and Combes, 1988; Waychunas et al., 1993). Similar as for goethite, the structure of HFO (Fig.1b) gives rise to the presence of singly, doubly and triply coordinated surface groups. The relative short chain length of the crystals will enhance the number of singly coordinated surface groups at the expense of triply coordinated surface groups. In case of an equal fraction of "110- and 021-like" faces, three-quarters of the apparent reactive surface sites might be singly coordinated surface groups. As will be discussed later on, the singly coordinated groups at the reactive faces may have a proton affinity that is lower than that of the reactive triply coordinated surface groups. This is predicted with the MUSIC model (Venema et al., 1998; Gaboriaud and Ehrhardt, 2003). The relatively large number of the singly coordinated surface groups may explain the lower PZC value of HFO (PZC=7.9-8.3) in comparison to the values reported for goethite (PZC=8.9-9.3).

2.4.2. Proton affinities and site densities

The main proton reactive surface groups at the surface of goethite are singly (≡ FeOH) and triply coordinated surface groups (≡ Fe_3O). The proton affinity is related to the charge neutralization of the oxygen by Fe^{3+} ions and protons. Two types of oxygens (O_I and O_{II}) can be found in the mineral structure and at the surface. These oxygens differ in the Fe-O bond length (d(Fe-O_I)~210pm, d(Fe-O_{II})~196pm), which implies another bond valence (Brown and Altermatt, 1985), neutralization, and proton affinity (Hiemstra and van Riemsdijk, 1996). Venema et al. (Venema et al., 1998) and Gabrioaud and Ehrhard (Gaboriaud and Ehrhardt, 2003) have calculated the proton affinities of individual surface groups of goethite for representative crystal faces using the MUSIC model. In a simplified picture, the charging behavior of the main crystal faces is apparently only determined by the presence of one row of ≡ $FeO_{II}H(H)$ surface groups and an equivalent row of triply ≡ $Fe_3O_I(H)$ (Hiemstra and van Riemsdijk, 1996; Hiemstra et al., 1996). The reactions may be formulated as:

$$\equiv FeOH^{-0.5} + H^{+} \Leftrightarrow \equiv FeOH_2^{+0.5} \quad [1a]$$

$$\equiv Fe_3O^{-0.5} + H^{+} \Leftrightarrow \equiv Fe_3OH^{+0.5} \quad [1b]$$

The relevant proton affinity constants are given in Table 1.These values are estimated with the MUSIC model. It is noted that the estimated value of the affinity constant depends on an arbitrary choice of the number H bonds that are formed with the surface group. The proton affinity constant may change in steps of about 4 logK_H units per H bond (Hiemstra and van Riemsdijk, 1996).

Table 1. The proton affinity ($logK_H$) and site density (Ns) of the reactive surface groups present of various representative crystal faces of goethite.

Surface group	**Face**[a]	**Ns**	**$logK_H$**
$\equiv FeO_{II}H$	110[b]	3.03	7.7
$\equiv Fe_3O_I$	110	3.03[d]	11.7
$\equiv FeO_{II}H$	100[c]	3.34	8.0
$\equiv Fe_3O_I$	100	3.34[d]	11.7
$\equiv FeO_{II}H$	021[b]	3.75[e]	8.1
$\equiv FeO_IH$	021	3.75[e]	7.9

(a) Depending of the axis chosen, the 110, 100, 021 and 001 faces can also be named respectively 101, 001, 210 and 100 faces (Gaboriaud and Ehrhardt, 2003).
(b) Venema et al. (Venema et al., 1998)
(c) Hiemstra et al. (1989b), Gabriaud and Ehrhardt (2003)
(d) Apparent site density, assuming that the charge of a combination of one $\equiv Fe_3O_I^{-1/2}$ and one $\equiv Fe_3O_{II}H^{+1/2}$ cancels (Hiemstra and van Riemsdijk, 1996; Hiemstra et al., 1996)
(e) The site density of the 001 face is slightly higher, i.e. 4 nm^{-2}

The PZC of a particle depends on the relative presence of the reactive groups and corresponding affinity constants if it is assumed that all surface groups experience the same average surface potential, instead of a potential that is specific for a certain crystal plane. In our treatment we will use this simplifying assumption. As shown in Table 1, the singly coordinated surface groups at the various faces of goethite have the same logK_H value within the expected uncertainties. Therefore, one may reduce, in a simplification, the type of reactive sites with respect to proton binding. In case of two types of reactive groups, $\equiv FeOH^{-1/2}$ and $\equiv Fe_3O^{-1/2}$, the

relation between the fraction of reactive sites ≡ FeOH (f_{FeOH}) and the proton activity in the PZC, $(H)_{PZC}$, can be derived from (Venema et al., 1998):

$$f_{FeOH} = \left\{ \frac{(H)_{PZC} K_{Fe3O}}{1+(H)_{PZC} K_{Fe3O}} - 1/2 \right\} \Big/ \left\{ \frac{(H)_{PZC} K_{Fe3O}}{1+(H)_{PZC} K_{Fe3O}} - \frac{(H)_{PZC} K_{FeOH}}{1+(H)_{PZC} K_{FeOH}} \right\} \qquad [2]$$

where K_{FeOH} and K_{Fe3O} refer to protonation constants of two reactive sites. This relationship is shown in Fig.2, using $\log K_{FeOH}$=7.8 and $\log K_{Fe3O}$=11.7. These values will be used in our simplified treatment of the proton reactivity of goethite and HFO.

The calculated curve (Fig.2) can be compared with the experimental PZC value of goethite and HFO using the fractions of singly coordinated surface groups as estimated for these surfaces. For goethite, estimation is based on the relative presence of the 110 +100 and 021 faces. As discussed above, the relative contribution of the top end crystal faces often is about 5-10 % for goethite (Cornell et al., 1974; Hiemstra et al., 1989a). Using the apparent site densities of the faces (Table 1), the relative contribution of crystals faces can be transformed to a fraction of singly coordinated surface groups, which is approximately f = 0.53-0.56. For HFO, the fraction of singly coordinated surface groups is higher, due to the relatively short elongation of the double chain of Fe octahedrons, which may lead to a relative fraction of $f = 0.78 \pm 0.1$ in case of an equal contribution of the two types of representative faces. These numbers are plotted in Fig.2 in combination with the mean PZC values. Within the limitations and uncertainties of the approach, the data are sufficiently close to the model line that is calculated with eq.(2).

In the surface complexation modeling, we will use the $\log K_H$ values used in Fig.2. The site densities are based on the mean apparent fraction of top-end crystals which is set at 5 % for our goethite (Hiemstra et al., 1989b), leading to respectively $N_s(FeOH)$= 3.23 nm^{-2} and $N_s(Fe_3O)$= 2.85 nm^{-2}. For HFO, a 50 % contribution of a similar crystal faces is used, leading to N_s (FeOH) = 5.25 nm^{-2} and $N_s(Fe_3O)$ = 1.5 nm^{-2}. The ion pair formation constants are based on the data of Rahnemaie et al. (2006) as presented in ref. (Hiemstra and van Riemsdijk, 2006). The parameters are given in Table 2. The capacitance used for the description of the charging behavior of goethite and HFO is discussed in the next section.

2.5. Quantum chemical calculations

The geometry of two types of hydrated surface complexes of arsenite has been given by (Stachowicz et al., 2006). In the present study, we have optimized with molecular modeling (MO) the geometry of a bidentate edge complex, applying density functional theory (DFT) using software of Wavefunction (Spartan'04). The calculated geometry has been interpreted with the Brown bond valence approach (Brown and Altermatt, 1985), in order to obtain the charge distribution value of the complexes. All calculations were done for a hydrated structure.

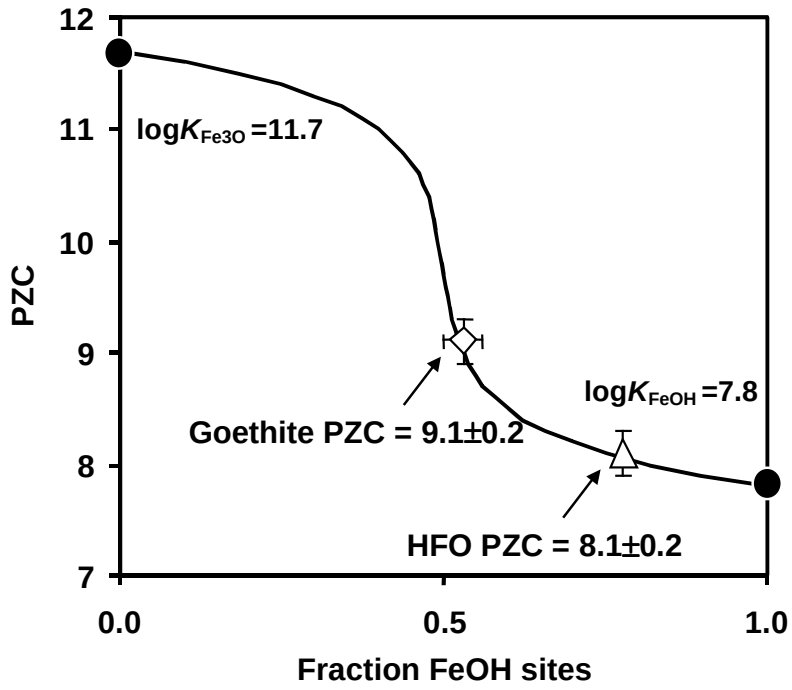

Fig.2. Relationship (Venema et al., 1998) between the fraction of singly coordinated FeOH surface groups and the predicted PZC, using the given affinity constants for the proton adsorption of the two main reactive surface groups of goethite and HFO, estimated with the MUSIC model. Open symbols show the estimated fraction of FeOH and experimental PZC of goethite, 9.1 (diamonds) and of HFO, 8.1 (triangle). The black spheres represent a calculated PZC at a surface with only one type of reactive sites having a log*K* as indicated.

3. Results and Discussion

3.1. Primary charge

3.1.1. Goethite

The charging behavior of our goethite material has been measured and described earlier (Stachowicz et al., 2006). Here, it is re-evaluated with the present approach, using the logK_H values and site densities of Table 2. The Extended Stern (ES) model (Westall and Hohl, 1980) has been used for data analysis, in which two Stern layers are present. For the description of the charging curves, the capacitance of the outer layer (C_2=0.75±0.11 F/m^2) is taken from literature (Hiemstra and van Riemsdijk, 2006) and the capacitance of the inner layer has been fitted on our experimental data, giving C_1=1.1±0.02 F/m^2. For the present goethite, the fraction of 021 face is set at 5%, slightly lower than previously used (Hiemstra and van Riemsdijk, 1996). This choice leads to $FeOH_{tot}$=3.23 sites/nm^2, Fe_3O_{tot}=2.85 sites/nm^2.

Table 2. Table of surface species of H^+, Na^+ and NO_3^{-1}.. The capacitance of the first Stern layer of the extended Stern model , C_1 = 1.1±0.02, was fitted (R^2=0.978). The capacitance of the second Stern layer (C_2= 0.74±0.10 F/m^2) is from ref. (Hiemstra and van Riemsdijk, 2006). These capacitance values were also used to describe the charging of HFO, only adjusting the specific surface area.

Surface species	**logK_H**
≡ $FeOH^{-1/2}$	0
≡ $FeOH_2^{+1/2}$	7.8[a]
≡ $FeOH^{-1/2}\cdots Na^+$	-0.60[b]
≡ $FeOH_2^{+1/2}\cdots NO_3^{-1}$	7.8-0.68=7.12
≡ $FeOH_2^{+1/2}\cdots Cl^{-1}$	7.8-0.45=7.35
≡ $FeOH_2^{+1/2}\cdots ClO_4^{-1}$	7.8-1.29[c]=6.58
≡ Fe_2OH^0	0
≡ $Fe_3O^{-1/2}$	0
≡ $Fe_3OH^{+1/2}$	11.7[a]
≡ $Fe_3O^{-1/2}\cdots Na^+$	-0.60[b]
≡ $Fe_3OH^{+1/2}\cdots NO_3^{-1}$	11.7-0.68[b]=11.02
≡ $Fe_3OH^{+1/2}\cdots Cl^{-1}$	11.7-0.45[b]=11.25
≡ $Fe_3OH^{+1/2}\cdots ClO_4^{-1}$	11.7-1.29[c]=10.41

(a) From Fig.2, based on Table 1
(b) Based on interpretation of data of Rahnemaie et al. (2006) as given by Hiemstra and van Riemsdijk (2006).
(c) The affinity values for ClO_4^{-1} were optimized on the goethite titration data of Rietra et al. (2000)

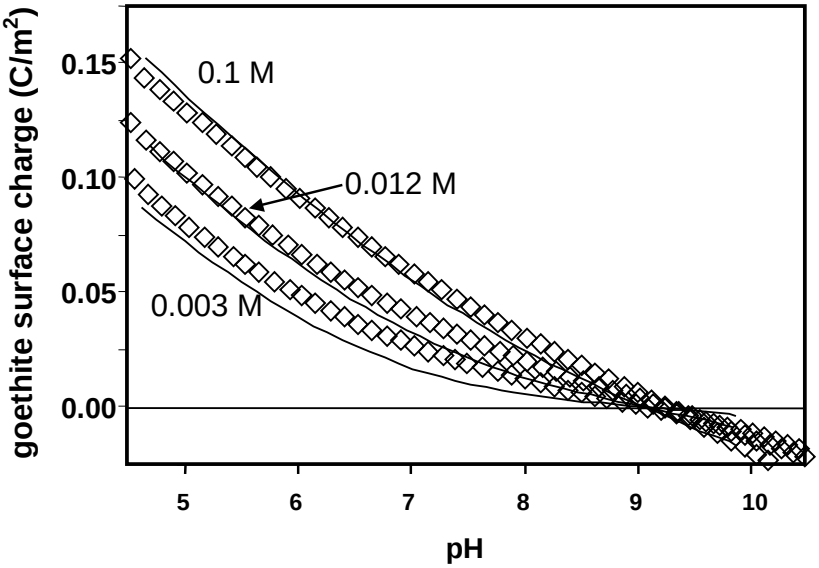

Fig.3. Surface charge as a function of pH for goethite. Symbols show experimental data of Stachowicz et al. (Stachowicz et al., 2006) for three electrolyte levels (0.003 M, 0.012 M and 0.1 M $NaNO_3$). The experimental PZC is about 9.2±0.1. The lines are calculated with the CD model (using site densities: $FeOH_{tot}$=3.23 sites/nm^2, Fe_3O_{tot}=2.85 sites/nm^2). The affinity constants are given in Table 2.

3.1.2. HFO

The charging characteristics of HFO have been studied by Davis et al. (Davis, 1977), Davis and Leckie (Davis and Leckie, 1978), Hsi and Langmuir (Hsi and Langmuir, 1985), Jain et al. (Jain et al., 1999). The experimental point of zero charge (PZC) was found to be around PZC= 7.9-8.2. The charging behavior of HFO can be predicted, using the above estimated parameter values for the affinities and estimated relative fraction of reactive surface groups (Fig.2), and a set of capacitance values derived for goethite (Fig.3). The predicted PZC value is 8.1, which is in agreement with experimental values (8.1±0.1) reported in the literature for HFO. For the description of the data in mC/kg, we have only adjusted the reactive surface area of HFO. The reactive surface area of the preparations varied between about 600-700 m^2/g (Fig.4). Gustafsson 2001 assumed 750 m^2/g as the reactive surface area of 2-line ferrihydrite in the CD model to model competitive anion adsorption on oxide minerals.

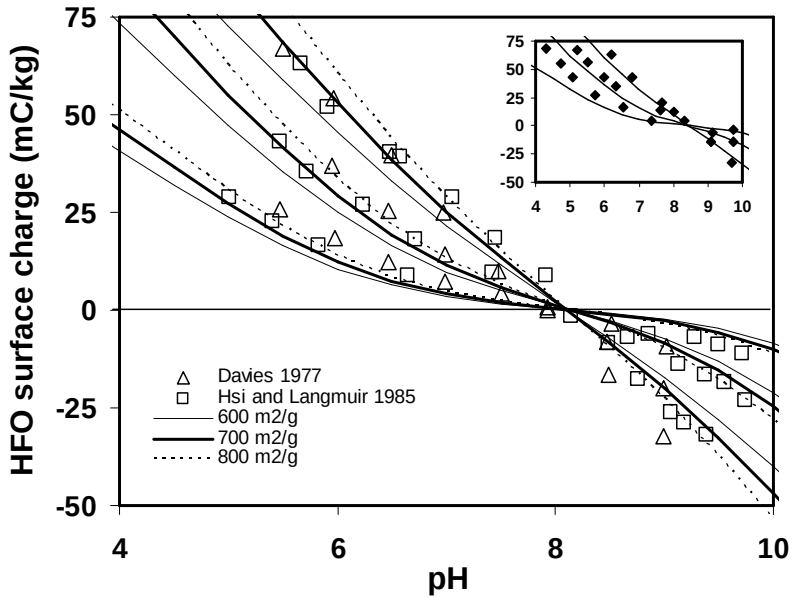

Fig.4. Surface charge per unit mass (mC/kg) as a function of pH for HFO in 0.1, 0.01 and 0.001 M $NaNO_3$ (Davis, 1977; Hsi and Langmuir, 1985) or NaCl (Jain et al., 1999). Symbols show experimental data of ref. (Davis, 1977; Hsi and Langmuir, 1985). The lines show prediction with the CD model ($FeOH_{tot}$= 5.25 sites/nm^2, Fe_3O_{tot}=1.5 sites/nm^2) using three different specific surface areas (600, 700 and 800 m^2/g). A value of 700 m^2/g is used in this paper for HFO in the description of arsenic adsorption. Small graph- Closed symbols refer to data of Jain et al. 1999 (reported PZC=8.5) and the lines show predicted charging behavior calculated for HFO (A=700 m^2/g) for site densities of surface groups corresponding with a PZC=8.5 (for a PZC=8.5: 021 fraction= 0.22 => $FeOH_{tot}$=3.99 sites/nm^2, Fe_3O_{tot}=2.34 sites/nm^2, Fe_2OH_{tot}=1.65 sites/nm^2).

Our approach is different from Ponthieu et al. 2006 who used the CD model to describe metal ion binding simultaneously on HFO and goethite. A main difference is related to the treatment of the electrostatics. In the present study, the charge is fully smeared-out, while in treatment of Ponthieu et al. 2006 each representative crystal face has its own surface potential. In addition, the ion pair formation constants for the surface groups at the 021 face were adjusted. As a result, the calculated PZC for HFO (8.5-8.8) was higher than measured and the prediction of the charging behavior above PZC was relatively poor.

3.2. Data acquisition

Before modeling the arsenic adsorption, we will evaluate the consistency of the various data sets. This is particularly important for the data on HFO, where inconsistency may be found due to variation in the preparation of the HFO material.

3.2.1. Goethite

For the modeling of goethite, we used our own experimental data reported previously by Stachowicz et al. (Stachowicz et al., 2006). Five different surface loadings of As(III) and three surface loadings for As(V) on goethite in 0.1M $NaNO_3$ have been used. Our data are reasonably consistent with adsorption data reported earlier by other authors (see Fig.5 and 6).

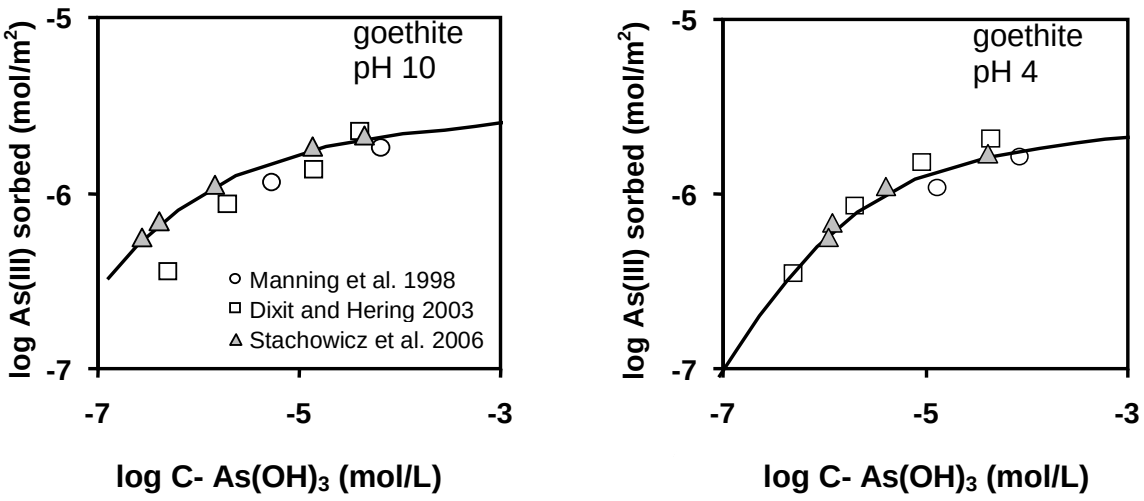

Fig. 5. Arsenite adsorption isotherms on goethite for pH 4 (left) and pH=10 (right). Closed symbols refer to the 0.1M $NaNO_3$ background electrolyte level. The open symbols are for the 0.01M $NaClO_4$ (Dixit and Hering 2003) or NaCl (Manning et al. 1998) background electrolyte level. Lines refer to the final modeling (Table 5) and were calculated for 0.1M $NaNO_3$ background.

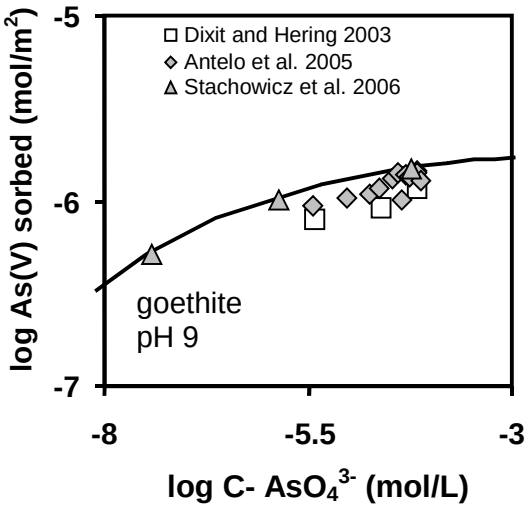

Fig. 6. Arsenate adsorption isotherm of goethite for pH 9. Closed symbols refer to the 0.1M $NaNO_3$ (Stachowicz et al. 2006) and KNO_3 (Antelo et al. 2005) background electrolyte level. The open symbols are for the 0.01M $NaClO_4$ (Dixit and Hering 2003) background electrolyte level. Lines refer to the final modeling (Table 6) and were calculated for 0.1M $NaNO_3$ background.

3.2.2. HFO-As(III)

For the arsenic adsorption on amorphous iron oxides, a number of data sets have been reported in the literature (Table 3). We encountered different names for the synthesized products, such as HFO, ferrihydrite and amorphous iron oxide. Some authors use those names interchangeably. It is not exactly clear what the differences are between the materials referred to by different authors. The literature data are available for different background salt levels (0.01 M, 0.1 M and 1M). A major difference might be the reactive surface area, which, however, cannot be measured with certainty. In most cases, the surface area is assumed to be 600 m^2/g. However, procedures like aging (Waychunas et al., 2005) and (freeze) drying may change the structure and the surface area of materials involved.

Table 3. Inventory of available literature data on As(III) and As(V) adsorption on iron oxides.

Source	PZC	Material name	Treatment	Ionic strength
Pierce and Moore 1982[a]	NR[b]	am. Fe oxide	fresh	0.01M $NaNO_3$
Hsia et al. 1992[c]	NR[b]	am. Fe oxide	fresh	0.01M $NaNO_3$
Wilkie and Hering 1996	NR[b]	HFO	fresh	0.01M $NaNO_3$
Raven et al. 1998[d]	8.5	2-line ferrihydrite	stored	0.10 M NaCl
Jain and Loeppert 2000	8.5	2-line ferrihydrite	stored	0.10 M NaCl
Goldberg 2001[e]	8.5	am. Fe oxide	fresh	0.01-1.0M NaCl
Dixit and Hering 2003	NR[b]	am. Fe oxide (HFO)	fresh	0.01M $NaClO_4$

(a) As (V) data set excluded from the modeling (see Fig.8)
(b) NR (not reported)
(c) only As(V) adsorption data available
(d) Two highest As(III) loadings excluded from the modeling (see text)
(e) As(III) and As(V) data excluded from the modeling (see Fig.8)

The adsorption data are usually reported as adsorption edge showing the fraction of the amount adsorbed as a function of pH. At a low relative adsorption, only the equilibrium concentration is accurately known. At a high relative adsorption, the adsorption can be read accurately from the graph. Unfortunately, in that case it is quite difficult to obtain the corresponding equilibrium concentration accurately. This limits the pH range from which an adsorption isotherm can be constructed for a direct comparison of data.

Despite some differences in the material characteristics and background salt levels used in the experiments, the reported As(III) data give a consistent trend (Fig. 7). However, we have excluded some adsorption data from modeling. We did not consider any data referring to a loading >5 $\mu mol/m^2$; i.e. the highest surface loading of Raven et al. 1998. At such an extreme loading, surface precipitation or solid-solution formation may occur.

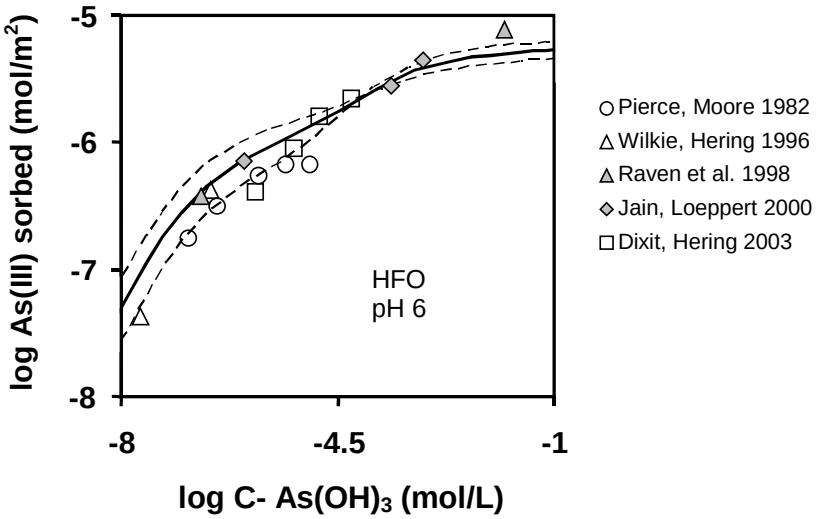

Fig.7 Adsorption isotherm for As(III) adsorption on HFO at pH 6. Symbols show the experimental data reported in the literature. Open symbols represent experimental data in 0.01M $NaNO_3$ (Pierce and Moore 1982 and Wilkie and Hering 1996) or $NaClO_4$ (Dixit and Hering 2003), gray symbols 0.1 M NaCl. Some data were obtained from extrapolation to pH 6. All data refer to a surface area of 700 m^2/g. Lines refer to the final modeling (Table 5) and were calculated for 0.1M $NaNO_3$ background. The full line was calculated assuming 50% of FeOHa site. The dotted lines show a variation related to different $FeOH_a$: $FeOH_b$ ratio; i.e. 30:70 respectively (the upper dotted line) and 70:30 (the lower dotted line).

3.2.3. HFO-As(V)

In case of As(V), we found that a considerable number of data gave a consistent trend (Fig. 8) with the exception of the data by Pierce and Moore (1982) and Goldberg and Johnston (2001) showing a lower adsorption. The irregularity of the data by Goldberg and Johnston (2001) could be caused for example by a lower reactive surface area of the material used. However, the same reasoning cannot be used to explain the lower As(V) adsorption of Pierce and Moore (1982) as their adsorption data for As(III) seem to be consistent with other available data (Fig.7). The observed discrepancy cannot be explained by possible differences in the ratio of the crystal phases between different materials either. The variation in adsorption isotherm related to different

ratios of the crystal planes is illustrated in Fig.8 (dotted lines). The dataset of Pierce and Moore 1982 as well as of Goldberg and Johnston 2001 were not considered in the modeling.

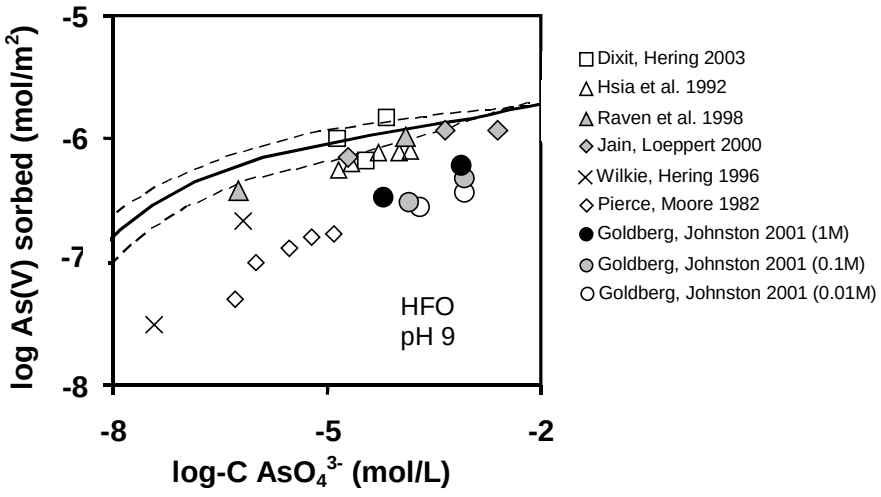

Fig.8 Adsorption edge for As(V) adsorption on HFO at pH 9.0. Symbols show the experimental data reported in the literature. Open symbols represent experimental data measured in 0.01M $NaNO_3$ (Pierce and Moore 1982, Wilkie and Hering 1996, Hsia et al. 1992) or NaCl (Goldberg and Johnston 2001), gray symbols in 0.1M NaCl and black symbols in 1M NaCl. Some data were obtained from extrapolation to pH 9. Lines refer to final modeling (Table 6) and were calculated for 0.1M $NaNO_3$ background. The full line was calculated assuming for 50% of $FeOH_a$ sites. The dotted lines show a variation related to different $FeOH_a$: $FeOH_b$ ratio; i.e. 70:30 respectively (the upper dotted line) and 30:70 (the lower dotted line

3.3. Adsorption of As(III)

3.3.1. Surface species

For goethite, the surface complexation of As (III) has been studied with EXAFS by a number of authors (Manning et al., 1998; Farquhar et al., 2002; Manning et al., 2002; Ona-Nguema et al., 2005). The surface speciation has recently been evaluated by Stachowicz et al. (Stachowicz et al., 2006). Arsenite coordinates to singly coordinated surface groups, mainly forming a bidentate complex ≡ Fe_2O_2AsOH. At high loading and low pH (Stachowicz et al.,

2006), also a monodentate complex may be found ≡ $FeOAs(OH)_2$. For HFO, the information is limited to one study for As(III) (Ona-Nguema et al., 2005). The EXAFS data point to the presence of two shells with a Fe-As distance of 292 ± 3 and 340 ± 4 pm. These distances are representative for the formation of bidentate edge ^{2}E and double corner ^{2}C complexes. The ^{2}E complexes will be formed by the "top-end" crystal faces of HFO. No formation of monodentate complexes has been reported, which may imply that these complexes are only found on the 110 face of goethite and on its equivalent of HFO. However, Stachowicz et al. (2006) showed that monodentate complexes may have very similar Fe-As distances. Therefore these complexes cannot be excluded beforehand.

3.3.2. Quantum chemical geometry calculations

The geometry optimization has previously been described for As monodentate and double corner complexes. (Stachowicz et al., 2006). In these calculations, a starting point was a cluster with two Fe oxide octahedrons having the Fe-O distances and bond angles as in goethite. This cluster has been used to calculate the formation of an As(III) edge complex. The bidentate edge As(III) complex was defined by exchanging one H_2O ligand and 1 OH^- ligand from the $Fe_2(OH)_4(OH_2)_6^{2+}$ cluster to enable the binding of an AsO_2OH^{-2} moiety. The exchanged OH_2 ligand on top of the octahedron (Fig.9) represents a protonated singly coordinated surface group at the 110- and/or 021/001-face of goethite. The exchanged OH ligand on the side of the octahedron represents a protonated doubly coordinated surface group at the 021/001 face of goethite.

To mimic the influence of hydration, the free OH ligand in the coordination sphere of the adsorbed As(III) was allowed to interact with two water molecules via H bridges (O-H···O). In addition, we defined a hydrogen bond between each common O ligand in the Fe-O-As(III) bond and an additional water molecule. During the optimization, all positions were fixed except those of AsO_2OH, the water molecules for hydration and the coordinated OH_2 ligand on top of the other octahedron in Fig. 9. Finally, the geometry was optimized using the BP86 model. The result is shown in Fig.9. The calculated distances have been given in Table 4. It is interesting to note that the both Fe-As distances calculated are equal to the ones observed for HFO with EXAFS, i.e.292 and 341 pm (Ona-Nguema et al., 2005).

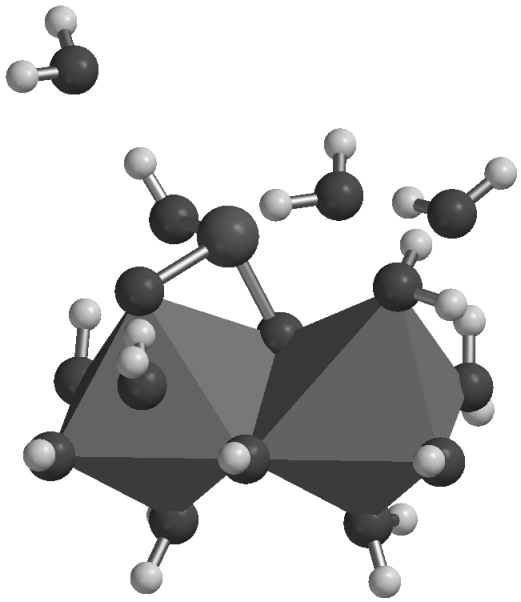

Fig.9. Two Fe(III)-O(H) octahedra with a bidentate edge arsenite complex that is hydrated, have the composition $Fe_2(OH)_3(OH_2)_5O_2AsOH.(H_2O)_4^+$. The geometry has been optimized with the BP86 model.

Table 4. The calculated distances (pm) in the geometry of a hydrated bidentate edge arsenite complex optimized with the BP86 model and the ionic charge allocation.

Distance	**BP86**
Fe-As	340.9
Fe-As	291.6
Fe-O-	237.4
Fe-O-	196.2
O-As	177.6
O-As	181.3
As-OH	191.2
R_0	183.0
n_0+n_{H0}	+0.18+0
n_1+n_{H1}	-0.18+0

3.3.3. The charge distributions

The geometries of Table 4 can be interpreted in terms of charge distribution using the Brown bond valence concept. According to Brown (Brown and Altermatt, 1985), the bond valence *s* is related to the distance *R* as:

$$s = e^{-(R-R_0)/b} \quad [3]$$

in which b is a constant (b=37 pm) and R_0 is the element specific parameter. The value of R_0 is chosen such that the sum of the bond valences around the As(III) ion corresponds to the formal valence (z=+3). The above derived ionic charge distribution coefficients (n_0+n_{H0} and n_1+n_{H1}) can be corrected for the electrostatic dipole effect that is induced by the introduction of charge in the interface. This correction results in the overall charge distribution coefficients (Δz_0, Δz_1), which is calculated according to Hiemstra and van Riemsdijk (Hiemstra and van Riemsdijk, 2006) as:

$$\Delta z_0 = n_0 + n_{H0} - \phi(n_0 + n_{H0} + \Sigma n_{ref} z_{ref}) = +0.18 - 0.17 * (0.18 - 0.5) = +0.24 \quad [4]$$

and

$$\Delta z_1 = n_1 + n_{H1} - \phi(n_0 + n_{H0} + \Sigma n_{ref} z_{ref}) = -0.18 + 0.17 * (0.18 - 0.5) = -0.24 \quad [5]$$

in which n_0 and n_1 are the charge attributions to respectively the 0 and 1-plane of the ion species defined in the reaction equation and n_{H0} and n_{H1} is the charge attributed to the 0- and 1-plane of any additional protons formulated in the reaction equation. The factor ϕ is a proportionality constant ($\phi \sim 0.17$) and n_{ref} is the number of reference groups used in the reaction and z_{ref} is the charge of these reference group(s) (Hiemstra and van Riemsdijk, 2006).

3.3.4. Modeling adsorption of As(III)

In a previous modeling attempt of the adsorption of As(III) on goethite (Stachowicz et al., 2006), all singly coordinated surface groups have been treated equally with respect to the binding of As(III). Any possible differences between different crystal faces have been disregarded as the

goethite surface is mainly represented by the 110+100 faces. It is possible that other complexes (with different corresponding affinities) are formed at the minor crystal faces at the top-end of the crystals. Formation of such complexes would become relatively very important in case of the adsorption As(III) on HFO. We therefore have differentiated between the sites representative for the 110+100 face (≡ $FeOH_a$) and those that are representative for the 021+001 faces (≡ $FeOH_b$). The corresponding site densities are given in Table 5. It is assumed that for goethite 5 % are 021+001 faces and for HFO 50%

Table 5. Table of site densities (nm^{-2}) of reactive surface groups on HFO and goethite

Representative face	**Surface species**	N_s **goethite**	N_s **HFO**
110+100	≡ $FeOH_a$	2.85	1.50
110+100	≡ Fe_3O	2.85	1.50
021+001	≡ $FeOH_b$	0.38	3.75
021+001	≡ Fe_2OH	0.38	3.75

For goethite, the spectroscopy identified the bidentate double corner ^2C as the main species with only a minor contribution of a monodentate. For reasons of simplicity, the formation of this monodentate species has been neglected. For HFO, a bidentate edge ^2E has been found. In the process of modeling, it was found that the data was not sensitive to the presence of a bidentate species at the 021+001 faces. Bidentate edge (^2E) complexes are formed by interaction with one singly coordinated surface group (≡ $FeOH_b$ sites) and one doubly coordinated surface group (≡ Fe_2OH) at the top-end crystal faces (Table 5), resulting in ≡ $(FeO)(Fe_2O)AsOH$ (BE_b). The double corner complex at the 110 face is formed by exchange with two OH ligand from singly coordinated surface group (≡ $FeOH_a$ sites). Double corner and edge formation can be described by respectively:

$$2 \equiv FeOH^{-1/2} + As(OH)_3(aq) \Leftrightarrow \equiv (FeO)_2^{-1+\Delta z_0} AsOH^{\Delta z_1} + 2\,H_2O\,(l) \quad [6]$$

$$1 \equiv FeOH^{-1/2} + 1 \equiv Fe_2OH^0 + As(OH)_3(aq) \Leftrightarrow \equiv (FeO)(Fe_2O)^{-1/2+\Delta z_0} AsOH^{\Delta z_1} + 2\,H_2O\,(l) \quad [7]$$

Table 6. Table of surface species for As(III) with the charge distribution and the affinity constants (log*K*) for goethite and HFO adsorption. The log*K* for surface species adsorbed on the 110 face were fitted based mainly on the goethite data (R^2=0.969), and the surface species on the top-end crystal faces were fitted based mostly on HFO data (R^2=0.868). The fitting was an iterative process using data for both minerals, see text.

	Species	≡ $FeOH_a$	≡ $FeOH_b$	≡ Fe_2OH	Δz_0	Δz_1	Δz_2	log*K*[3]
B_a	≡ $(FeO)_2$ AsOH	2	0	0	0.34[1]	-0.34[1]	0	6.81 ± 0.01
BE_b	≡ (FeO)(Fe_3O) AsOH	0	1	1	0.24± 0.05[2]	-0.24±0.05[2]	0	3.79 ± 0.08

(1) values taken from Stachowicz et al. (2006)
(2) values calculated from the MO/DFT optimized geometry of this study The uncertainly is estimated.
(3) values optimized in this study by fitting

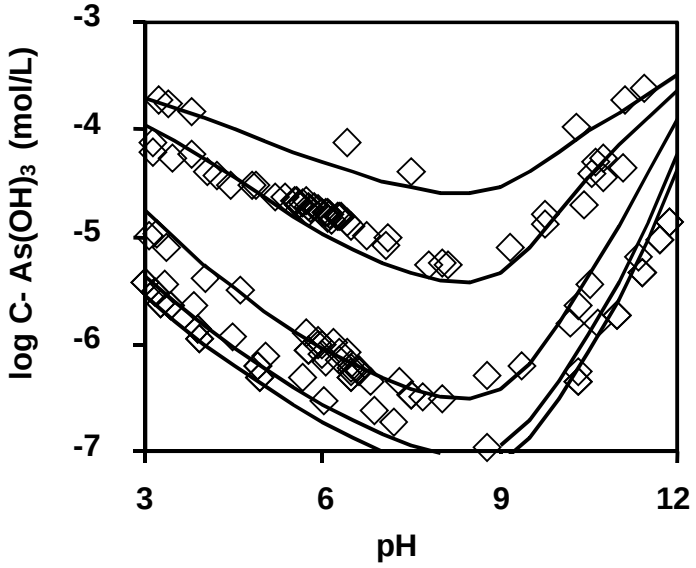

Fig.10. Equilibrium concentrations of As(III) as a function of pH for adsorption on goethite. Symbols represent experimental data of Stachowicz et al. (2006). The lines show the simulation for experimental conditions with the parameters given in Table 6.

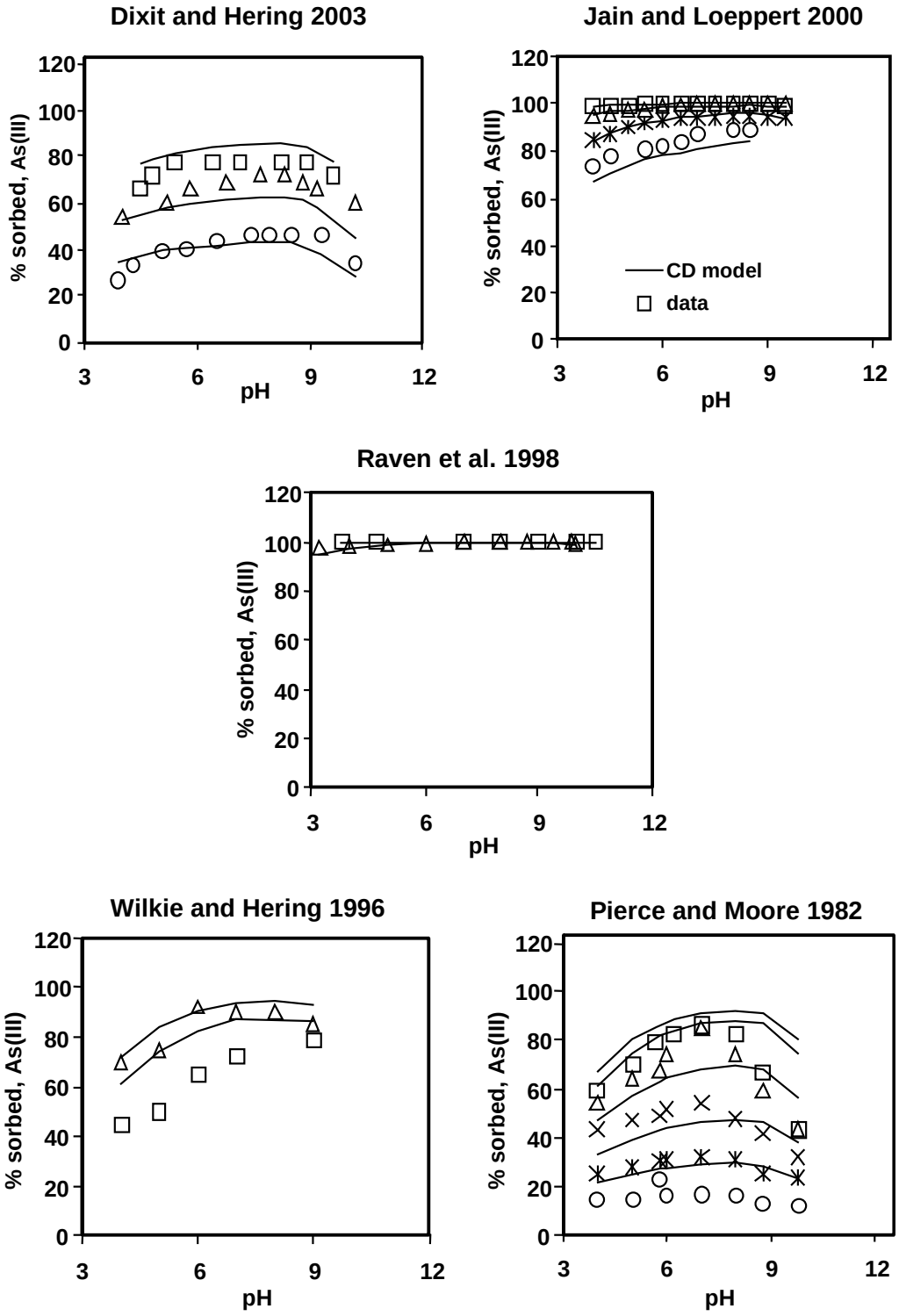

Fig. 11. As(III) adsorbed on HFO as a function of pH. Symbols show experimental data taken from the literature. The lines show simulation for the experimental conditions given in Table2.

For our bidentate edge linkage ^{2}E, we used the above CD values found from the MO/DFT optimized geometry of the adsorbed arsenic ions. The CD values of the bidentate double corner species are from Stachowicz et al. (2006). The CD values used here are given in Table 6. The adsorption data of goethite and HFO have been fitted iteratively using the same two types of surface complexes for the different minerals. The affinity constant for the species B_a, representative for the dominant planes of goethite have been fitted using the goethite data set of As(III). The affinity constant for the BE_b surface species is found from the selected As(III)-HFO data sets. The fitted log*K* values are given in Table 6. The description of the goethite and HFO data has been shown in Fig.11 and Fig.12.

3.5. Adsorption of As(V)

3.5.1. Surface species

For goethite, the surface complexation of As (V) has been measured with EXAFS by a number of authors (Waychunas et al., 1993; Fendorf et al., 1997; Foster et al., 1998; Farquhar et al., 2002; Manning et al., 2002; Sherman and Randall, 2003). The surface speciation has recently been evaluated by Stachowicz et al. (Stachowicz et al., 2006). Arsenate mainly binds as a bidentate complex to singly coordinated surface groups, forming ≡ $Fe_2O_2AsO_2$ (B), which may protonate at high loading and low pH (≡ Fe_2O_2AsOOH). The presence of a particular type of surface complex is mainly based on the As-Fe distance observed. However, it has been pointed out (Stachowicz et al., 2006) that mono and bidentate complexes may have a very similar Fe-As distance as derived form MO/DFT optimized geometries. The presence of a protonated monodentate complex (≡ $FeOAsO_2OH$) has been suggested based on fitted experimental data while constraining the CD values to the values found from MO/DFT optimized geometries. Using the same approach, a monodentate surface species has also been suggested by Rahnemaie et al. (2007) and was recently been proposed for PO_4 adsorbed on hematite (Elzinga and Sparks, 2007). The presence of a monodentate As(V) species might also be in line with quantum chemical calculations of Kubicki (Kubicki, 2005). In the present analysis, we will use the CD values calculated for mono and bidentate complexes (Stachowicz et al., 2006). The formation of the

surface species has been previously described (Stachowicz et al., 2006) with the following set of reactions:

$$1 \equiv FeOH^{-1/2} + 2H^{+}(aq) + AsO_4^{-3}(aq) \Leftrightarrow \equiv FeO^{\Delta z_0} AsO_2OH^{\Delta z_1} + 1\ H_2O(l) \quad [8]$$

$$2 \equiv FeOH^{-1/2} + 2H^{+}(aq) + AsO_4^{-3}(aq) \Leftrightarrow \equiv (FeO)_2^{\Delta z_0} AsO_2^{\Delta z_1} + 2\ H_2O(l) \quad [9]$$

$$2 \equiv FeOH^{-1/2} + 3H^{+}(aq) + AsO_4^{-3}(aq) \Leftrightarrow \equiv (FeO)_2^{\Delta z_0} AsOOH^{\Delta z_1} + 2\ H_2O(l) \quad [10]$$

The surface complexation of As(V) on ferrihydrite has been studied by Waychunas et al. 1993, Waychunas et al. 1995 and Sherman et al. 2003. At first, three possible surface complexes were suggested, i.e. a bidentate corner-sharing (^{2}C), a bidentate edge-sharing (^{2}E) and a monodentate corner-sharing (^{1}V) (Waychunas et al. 1993). However, Sherman et al. 2003 argued that peaks (2.85 Å) previously attributed to the presence of ^{2}E complexes are a result of As-O-O-As multiple scattering rather than a surface species. Moreover, these authors concluded that the observed 3.26 Å As-Fe distance agrees with that predicted for the bidentate corner-sharing surface (^{2}C) complex and found no evidence for monodentate (^{1}V) complexes. However, as mentioned before, monodentate and bidentate of arsenate may have a very similar Fe-As distance.

Table 7. Table of surface species for As(V) adsorption on goethite and HFO. The affinity constants (log*K*) were fitted on adsorption data for goethite and HFO (goethite R^2=0.933; HFO R^2= 0.847) and the charge distribution (CD) values were taken from Stachowicz et al., 2006.

Species		≡ $FeOH_a$	≡ $FeOH_b$	Δz_0	Δz_1	Δz_2	log*K*
MH_a	≡ $FeOAsO_2OH$	1	0	0.30	-1.30	0	26.24 ± 0.22
B_a	≡ $Fe_2O_2AsO_2$	2	0	0.47	-1.47	0	28.76 ± 0.03
BH_a	≡ Fe_2O_2AsOOH	2	0	0.58	-0.58	0	32.19 ± 0.35
MH_b	≡ $FeOAsO_2OH$	0	1	0.30	-1.30	0	24.72 ± 0.25

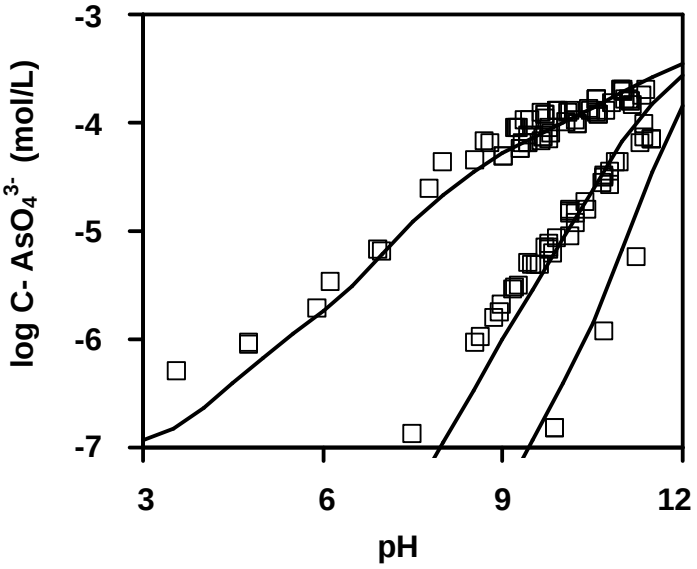

Fig.12. Equilibrium concentrations of As(V) as a function of pH for adsorption on goethite. Symbols show experimental data of Stachowicz et al. (2006). The lines show the simulation for experimental conditions with the parameters given in Table 7.

For modeling of As(V) of HFO, we used data of Hsia et al. (Hsia et al., 1992), Wilkie and Hering (Wilkie and Hering, 1996), Raven et al. (Raven et al., 1998), Jain and Loeppert (Jain and Loeppert, 2000) and Dixit and Hering (Dixit and Hering, 2003). However, within these sets, we excluded any data referring to a loading >5 μmol/m^2, i.e. the highest surface loading of Raven et al. 1998.

We have fitted iteratively the model to the adsorption data of goethite and HFO, using the same procedure as for the As(III) oxyanion adsorption. We tried to minimize the number of adjustable parameters. However, it is not possible to get a unique fit. In a first approach, we assumed the presence of 3 species reacting with $FeOH_a$, i.e. MH_a, B_a and BH_a and allowed the presence of 3 surface species reacting with the $FeOH_b$ site (MH_b, B_b and BH_b). The best fit found was with only one As species interacting with the $FeOH_b$ site i.e. BH_b (R^2=0.865). However, an almost equally good fit (R^2=0.861) is possible when using only MH_b.

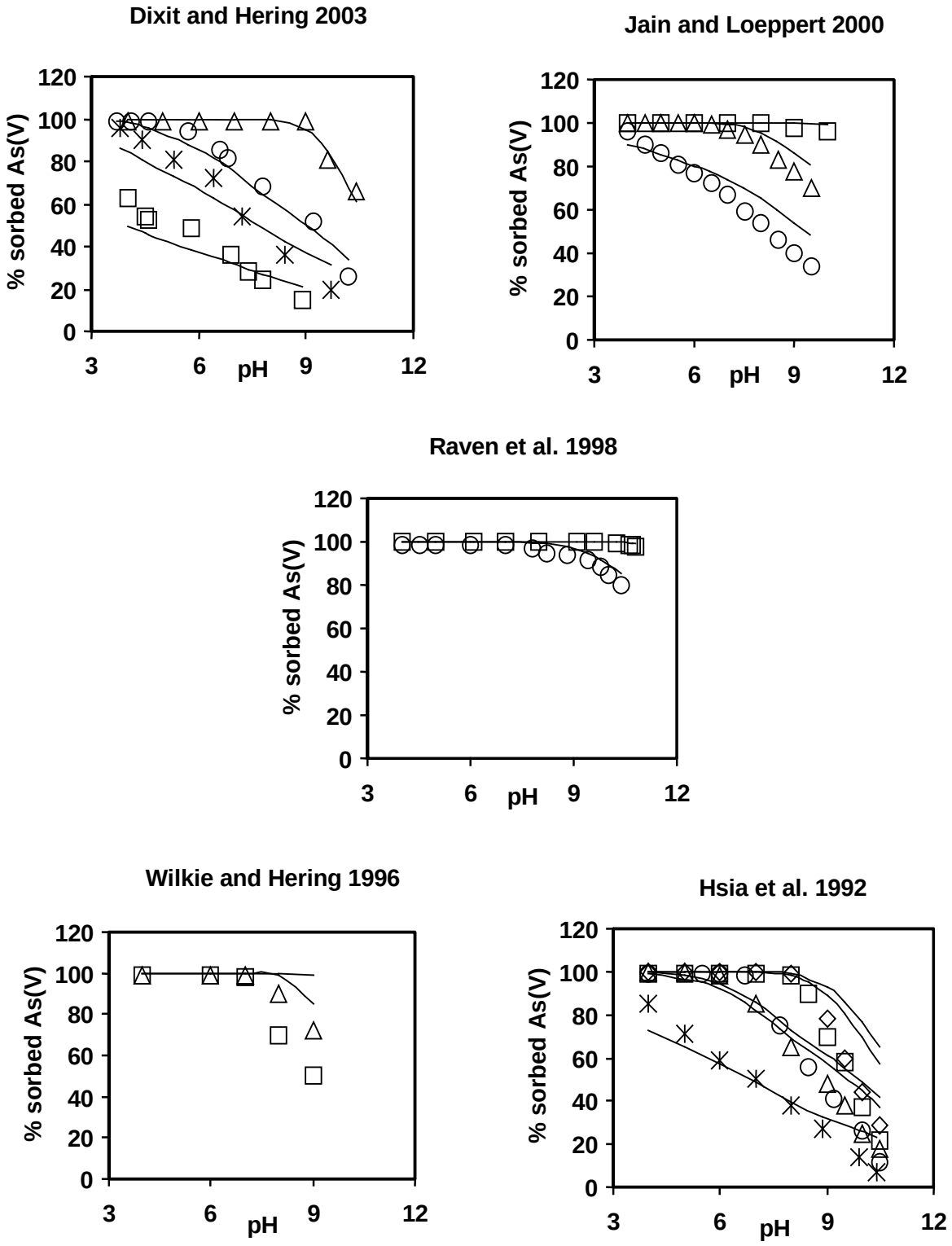

Fig. 13. As(V) adsorbed on HFO as a function of pH. Symbols show experimental data taken from the literature. The lines show simulation for the experimental conditions given in Table 7.

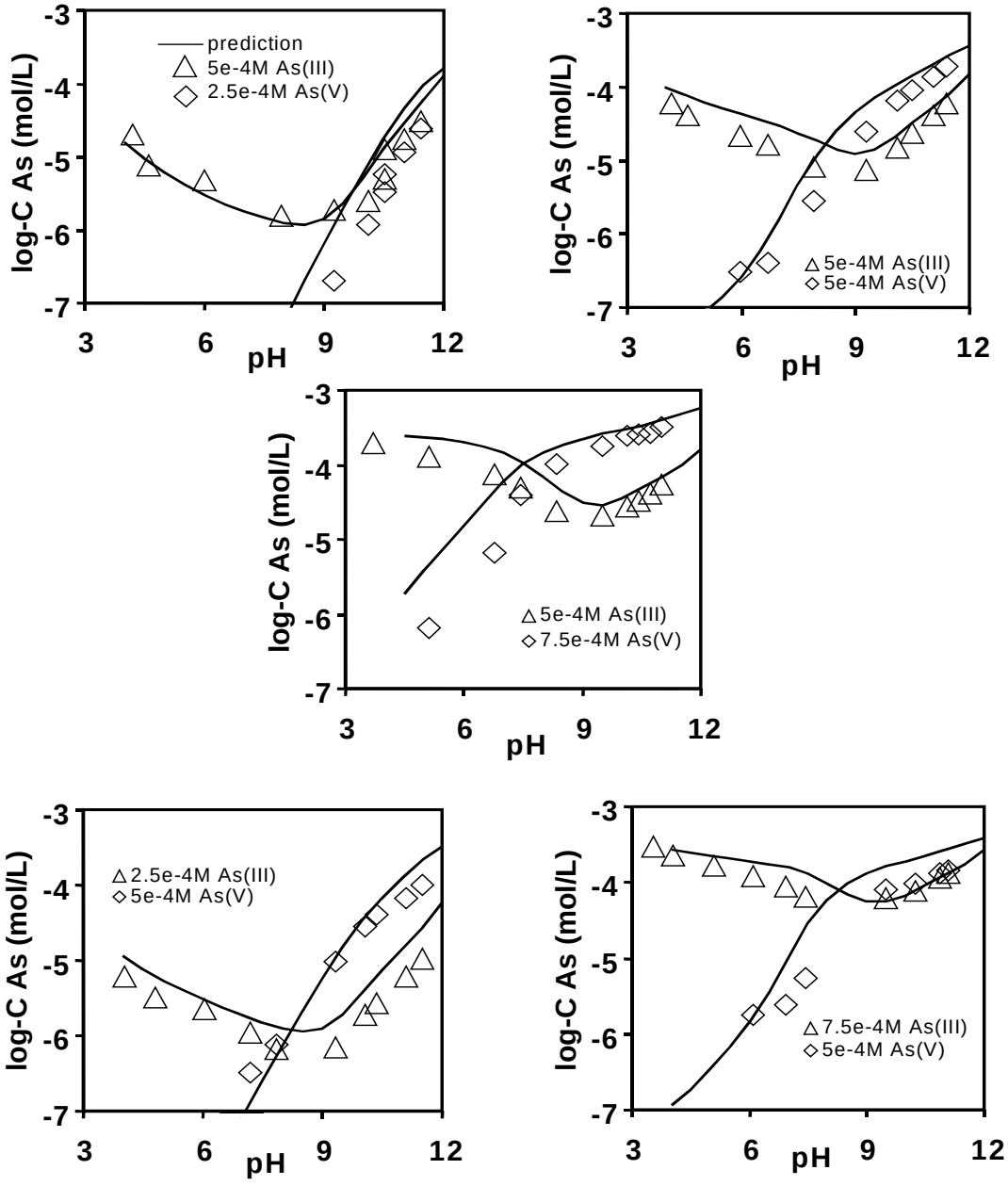

Fig. 14. Competition between As(III) and As(V) on goethite. Symbols show the experimental data. Lines show the prediction with the CD model (parameters from Table 6 and 7). The experiments were done for different concentrations of As(III) and As(V) and one goethite concentration (5 g/L) at the background salt level 0.1M $NaNO_3$.

We consider the formation of a protonated double corner bidentate complex less likely on the 021+001 faces when considering the modeling of the As(III) data, where no double corner complex is found for these faces. The arbitrary use of the MH_b, leads to more consistency with the description of the As(III) adsorption data.

To summarize, based on the analysis of the adsorption data for the "single-ion" systems of goethite and HFO, it is not clear which set of surface species should be used. Lack of consistent EXAFS results does not allow discriminating between available options. The changing ratio of sites depending on the material, 0-100% $FeOH_a$ and 100-0% $FeOH_b$, does not allow elimination of one of the parameter sets. Moreover, if the competition data (next section) are included in the test to discriminate between the various options, the differences in the quality of the description depending on the various As(V) parameter sets are small. Therefore, we make here an arbitrary choice for As(V) surface speciation. Table 7 presents the common set of adsorption parameters for the surface speciation chosen here to describe As(V) adsorption on goethite (Fig.12) and HFO (Fig.13); i.e. MH_a, B_a, BH_a, and MH_b.

3.6. Competition As(III) and As(V).

3.6.1. Prediction of As(III)-As(V) competition on goethite

Information on the primary proton charge (Table.2) together with arsenic surface speciation and adsorption parameters (Tables 5-7) were used as an input for our calculations. Fig. 14 shows for our goethite the experimental adsorption data (symbols) and our predictions (lines). Our set of adsorption parameters for As(III) and As(V) gives a rather good prediction of the competition effects for all experimental ratios (Fig.14).

In each case, the model was able to correctly predict the trend. For As(III), the predicted equilibrium concentrations seems to be slightly under predicted mainly in the lower pH range. For As(V), only in one case (As(III) = 0.5 mM; As(V) = 0.75 mM), the adsorption is somewhat under predicted in the lower pH range.

3.6.2. *Prediction of As(III)-As(V) competition on HFO*

The competition between As(III) and As(V) on HFO can be compared with the adsorption data of Jain and Loeppert (Jain and Loeppert, 2000). Fig.15 shows the result of our predictions. Unfortunately, the data partly refer to surface loadings that are extremely high, i.e. 6.9 and 11.6 μmol As/m^2 in the last two panels of Fig.15. The latter value can only be reached if all sites are occupied with a monodentate surface species. In case of the highest surface loading the prediction is reasonable for As(V), but the As(III) adsorption becomes increasingly under estimated, in particular in the lower pH range. The observed discrepancy between the data and model predictions can be due to a number of reasons. For instance, it is possible that for such extreme surface loadings a surface precipitation occurs.

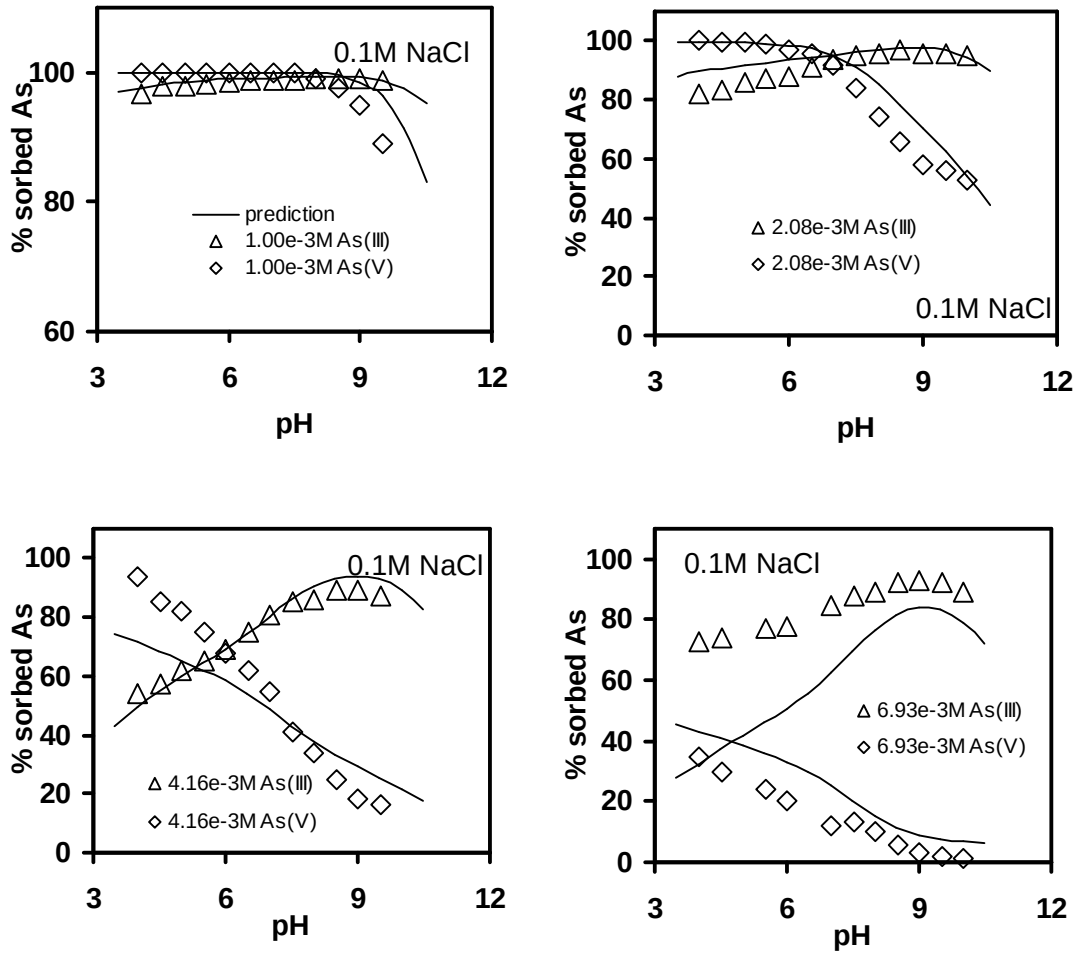

Fig.15. Competition between As(III) and As(V) on HFO. Symbols show the experimental data of Jain and Loeppert 2000. Lines show the prediction with the CD model (parameters from Table 6 and 7). The experiments were done for different concentrations of As(III) and As(V) in 1:1 ratio at the background salt level 0.1M NaCl.

4. Conclusions

Ion binding of iron oxides is strongly determined by the structure of the surface, and the type of surface complexes formed. The primary structure of HFO and goethite has similarities, that have been used here as a common basis in the modeling of the proton and arsenic adsorption behavior on both materials.

If the local structure of HFO resembles that of goethite, than, as for goethite, the structure of HFO gives rise to the presence of ≡ FeOH and ≡ Fe_3O as reactive groups. The relatively short chain length in HFO suggests a higher number of singly coordinated surface groups at an expense of triply coordinated surface groups. This relatively large number of singly coordinated groups may explain the lower PZC value of HFO compared to goethite. For HFO and goethite, we differentiated between a relative number of the various reactive surface groups. For goethite the apparent fraction of top-end faces at the crystals was assumed to be 5%, while for HFO, a 50% contribution of similar faces was used. As a result, the primary charging behavior of goethite and HFO has been modeled in a coherent manner using the MUSIC model approach. This way a basis to model the arsenic adsorption has been established.

Adsorption of As(III) on HFO and goethite has been described assuming the formation of 2 species; a bidentate double corner (^{2}C) and a bidentate edge (^{2}E), as found by spectroscopy. Bidentate double corner complex formation occurs on the 110+100 face, while the bidentate edge complexes are formed at the 021+001 face. In case of the adsorption of As(V) we were not able to identify the surface speciation unambiguously for the different crystal phases. We found a number of possible options. We arbitrarily chose the following As(V) surface speciation: three species on the 110+100 face; i.e. a bidentate, a protonated bidentate and a protonated monodentate; and one type of species on the 021+001 face; i.e. a protonated monodentate. The CD values of the different types of As(III) and As(V) complexes were found independently from the MO/DFT optimized geometries of hydrated complexes. The affinity constants were fitted iteratively on adsorption data of goethite and HFO.

The modeling results have been tested on data from competition experiments. The model successfully predicted the competition between arsenic species, As(III) and As(V), on both minerals. For the highest surface loading discrepancies between the data and model predictions

were observed for adsorption on HFO. However, it is possible that for such an extreme surface loadings a surface precipitation occurs.

The above suggests that despite the differences in the reactivity of goethite and HFO a link exists between the adsorption behavior of both minerals. Since HFO has been considered representative for 'field' conditions this is of important practical relevance. However, recently the importance of the presence nano size goethite has been stressed as well (van der Zee et al., 2003). In the future the CD model can be used to predict adsorption in complex systems simulating natural conditions.

6

Biogeochemical Key Factors Controlling Arsenic in Groundwater

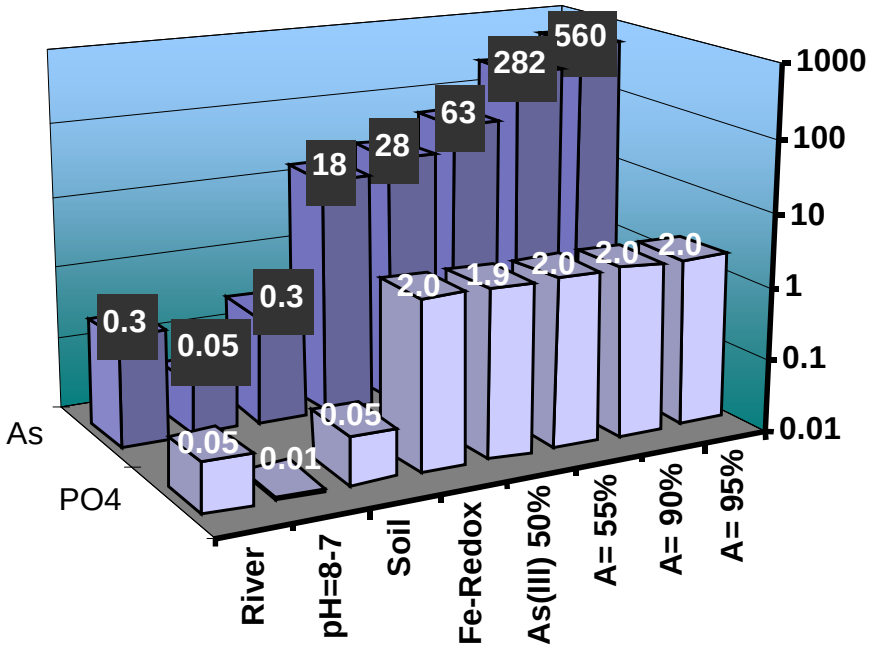

Abstract

The large number of different explanations for the occurrence of high arsenic concentrations in some groundwater systems that have been suggested in recent years points to the complex nature of the arsenic problem and proves that our understanding of the problem is still limited. The identification of processes is often based on speculations using correlations and observed trends. Relevant data, related to the solid phase composition are unfortunately almost always lacking. The aim of this study is to discuss quantitatively varies biogeochemical processes that may be involved in the release of As; i.e. the effect of pH and an equilibration with calcite, the release of PO_4^{3-} due to mineralization and reductive dissolution of Fe (hydr)oxides, the reduction of As(V) to As(III), and the effect of additional diagenetic processes that change the reactive surface area of the sediment. Eventually, a scenario has been used to predict the impact of changing conditions on the arsenic concentration in pore waters. In the scenario analysis for average sediments the reductive dissolution with a release of PO_4^{3-} was identified as the first factor that may increase very low As concentrations to levels that are beyond the WHO standards for drinking water. Reduction of As(V) to As(III) may approximately double these values and further doubling may occur each time that the surface area decreases by a factor of 2. The average concentration of 55 µg As/L may result from a transformation of about 50 % of the iron (hydr)oxides and 50 % reduction of the As(V) to As(III) assuming limitation of the phosphate and ferrous ion concentration due to (co) precipitation reactions. The CD model has been used in the calculations as it has been tested for a large number of ion-ion interactions relevant in the As binding process and it can successfully predict competitive effects in 2- and 3- component systems containing As.

1. Introduction

Arsenic in groundwater is a major problem in many parts of the world (Smedley and Kinniburgh 2002). For Bangladesh, the As distribution in groundwater has been widely studied (Chowdhury, Basu et al. 1999; BGS and DPHE 2001; Harvey, Swartz et al. 2002; Smedley and Kinniburgh 2002; Swartz, Blute et al. 2004; Harvey, Swartz et al. 2005; Zheng, van Geen et al. 2005). Based on the results, a number of hypotheses have been formulated to explain the origin of elevated As concentrations, such as: (1) pyrite oxidation (Das, Samanta et al. 1996; Mandal, Chowdhury et al. 1996); (2) reductive dissolution of iron oxides in conjunction with mineralization of organic matter (Chowdhury, Basu et al. 1999; BGS and DPHE 2001; Harvey, Swartz et al. 2002; Smedley and Kinniburgh 2002; Islam, Gault et al. 2004; Swartz, Blute et al. 2004; Zheng, van Geen et al. 2005); (3) reduction of arsenate (AsO_4^{3-}) to arsenite ($As(OH)_3$) and corresponding change in bond strength (Ahmann, Krumholz et al. 1997; BGS and DPHE 2001); (4) displacement of arsenic by dissolved carbonate (Appelo, Weiden et al. 2002; Anawar, Akai et al. 2004) and (5) arsenic mobilization by DOC (dissolved organic carbon) (Harvey, Swartz et al. 2002).

The large number of different explanations that have been suggested in recent years points to the complex nature of the arsenic problem and proves that our understanding of the problem is still limited. Some of the theories have already been questioned. For instance, a negative correlation has been found between dissolved arsenic and dissolved sulphate (BGS and DPHE 2001), suggesting that sulphate reduction is associated with arsenic release. This observation contradicts the pyrite oxidation theory. Another hypothesis, i.e. the carbonate displacement, does not seem to be supported by experimental results (Meng, Korfiatis et al. 2002; Arai, Sparks et al. 2004; Radu, Subacz et al. 2005; Stachowicz, Hiemstra et al. 2007). Interestingly, most of the explanations mentioned here have their roots in a set of the same or similar observations recognized in numerous field studies.

The arsenic content of the sediment is associated with the presence of sediments rich in iron oxides, such as HFO, hematite, goethite, and magnetite. Only a relatively small fraction

needs to be released to create elevated As concentrations in the pore water. Arsenic contamination of groundwater in Bangladesh has been found primarily in shallow aquifers (BGS and DPHE 2001; Swartz, Blute et al. 2004; Zheng, van Geen et al. 2005). A frequency distribution of the As concentration with depth shows that the As concentrations peak in the upper part (about 20-40 m) of the Holocene aquifer (BGS and DPHE 2001). The average measured concentration of As is about 55 μg/L (~0.7 μM). The As concentrations vary enormously; from less than 1μg/L (~0.01 μM) up to even 5000 μg/L (~70 μM) (Smedley and Kinniburgh 2002). However, the majority (90%) of all samples collected in the BGS and DPHE study (2001) contained less than 200 μg/L As (2.7 μM). The value of 200 μg/L is still 4 times higher than the drinking water standard in Bangladesh (50 μg/L) and 20 times higher than the limit set by World Health Organisation (10 μg/L).

Arsenic in groundwater has been found in two oxidation forms, i.e. As(V) and As(III), respectively present as arsenate (AsO_4^{3-}) and arsenite ($As(OH)_3$). The fraction of As(III) varies strongly. Both forms of arsenic are known to have high binding affinity for iron oxides such as HFO (Jain and Loeppert 2000; Dixit and Hering 2003) and goethite (Dixit and Hering 2003; Stachowicz, Hiemstra et al. 2006), but the binding characteristics and affinities differ.

Elements commonly present in natural waters may interact directly or indirectly with arsenic. The shallow aquifers are generally rich in Mg^{2+}, Ca^{2+}, and HCO_3^-, with an average concentration of respectively 35 mg Mg^{2+}/L (~1.5 mM), 90 mg Ca^{2+}/L (~2 mM) and about 500 mg HCO_3^-/L (~8 mM). These macro-elements will interact with iron oxide surfaces, at which the As oxyanions reside too. We have mentioned above the influence of SO_4, which forms pyrite at the expense of Fe (hydr) oxides. Such a transformation decreases the reactive surface area of iron oxides releasing As bound at these surfaces. The iron oxide surfaces may also interact with PO_4^{3-}, $H_4SiO_4^o$, and Fe^{2+} (BGS and DPHE 2001; Smedley and Kinniburgh 2002). For the shallow aquifers, positive correlations have been found in pore water between dissolved As and Fe, as well as As and P. Phosphate is most likely one of the key-competitors for arsenic in the adsorption process on iron oxides (Hiemstra and van Riemsdijk 1996; Hiemstra and van Riemsdijk 1999; Dixit and Hering 2003; Stachowicz, Hiemstra et al. 2007). The median concentration of phosphate in As-contaminated sediments is >50 μg/L.

In general, many data are available in relation to the groundwater quality at different locations and depths, but the relevant data related to the solid phase composition, are

unfortunately almost completely absent. Therefore, the identification of processes is often based on speculations using correlations and observed trends. In the view of the field observations, it is unlikely that the arsenic problem is caused by a single phenomenon. The aim of this study is to identify the main processes that cause high As concentrations in groundwater. We will use a quantitative approach. First, we will focus on the relation between the average river water composition and the average As loading of the sediment. This is followed by a quantitative discussion of varies biogeochemical processes that may be involved in the release of As once sediments are deposited. We will evaluate the effect of pH and an equilibration with calcite, the release of PO_4^{3-} due to mineralization and reductive dissolution of Fe (hydr)oxides, the reduction of As(V) to As(III), and the effect of additional diagenetic processes that change the reactive surface area of the sediment. Eventually, a scenario analysis will be used to predict the impact of changing conditions on the arsenic concentration in pore waters. A similar analysis has been done previously by BGS and DPHE (2001). However, the authors used the generalized two layer (GTL) model (Dzombak and Morel 1990) that is known to have limitations (Dixit and Hering 2003; Dixit and Hering 2006) when it comes to predicting multi-component interactions. In the present approach, we will use the CD model that has been tested for a large number of ion-ion interactions relevant in the As binding process. We have shown that the CD model, calibrated on 'single component' systems, can successfully predict competitive effects in 2- and 3- component systems containing As (Stachowicz, Hiemstra et al. 2007). The relevant reactions and parameters used in the CD model are described in the Appendix.

We will start with a brief overview of relevant processes that may be involved in the process of As release in groundwater systems.

2. Concept

Many processes may lead to changes in the groundwater composition. A conceptual picture is given Fig.1. Arsenic in river water will be adsorbed by suspended particles that may settle. For a while, the particles will be part of a soil system. This may change the chemical conditions, such as the pH value. Some additional organic matter may also be introduced.

If the soil/sediment becomes buried below the groundwater table, the microbial activity, decomposing natural organic matter, will still release HCO_3^-/H_2CO_3, some DOC, and nutrients like NH_4^+ and PO_4^{3-}. In the absence of oxygen, Mn(IV) and Fe(III) may be used by the microbes as electron acceptor, leading to chemical reduction. In this process, the release of Fe(II) is in principle linked to changes in HCO_3/H_2CO_3, NH_4^+, and PO_4^{3-}. However, secondary adsorption and precipitation reactions may complicate the interpretation.

The phosphate that is released in the redox process may re-adsorb to oxide surfaces. Under anaerobic conditions, NH_4^+ is relatively stable. Part of it may bind to the solid phase (CEC) by ion exchange, competing with Ca^{2+} and Mg^{2+} (Fig.1). The ferrous ion (Fe^{2+}) may adsorb too. In addition, some Fe^{2+} may adsorb to oxide surfaces, including Fe-(hydr)oxides (Zhang, Charlet et al. 1992; Williams and Scherer 2004; Dixit and Hering 2006; Hiemstra 2007).

At a sufficiently high concentration, Fe(II) may also precipitate, forming minerals like magnetite (Fe_3O_4) and siderite ($FeCO_3$). In the presence of sufficient sulphur (originating from sulphate in river water or intruded seawater), also some pyrite (FeS_2) can be formed. At a high PO_4^{3-} concentration, vivianite ($Fe_3(PO_4)_2 \cdot 8H_2O$) may precipitate. In case of adsorption or precipitation, no simple balance exists between the elements C, N, P, and Fe(II) in the groundwater. This complicates the interpretation of groundwater quality in terms of a quantification of the processes that take place.

The surfaces of iron oxides (circle in Fig.1) are carrying adsorbed ions. As will be illustrated later, the adsorption phase is dominated by Ca^{2+} and PO_4^{3-} in many cases. Upon reduction, Fe(II) may bind in a considerable amount too. The amount of adsorbed AsO_4^{3-} is minor due to the relatively low As concentration in the river water in comparison to PO_4^{3-} (to be discussed later). In case of the dissolution of Fe-(hydr)oxide in a reduction process, the adsorbed ions are released. Since PO_4^{3-} is the dominant anion adsorbed, its contribution in the release will be most prominent. Phosphate will be partially re-adsorbed and this process will intensify the competition with As oxyanions, resulting in an increase of arsenic release. Reduction will have also an effect on the valence of arsenic, changing As(V) to As(III) at low pe (Fig.1). This transformation process may lead to desorption of arsenic and is directly related to a change in the redox status.

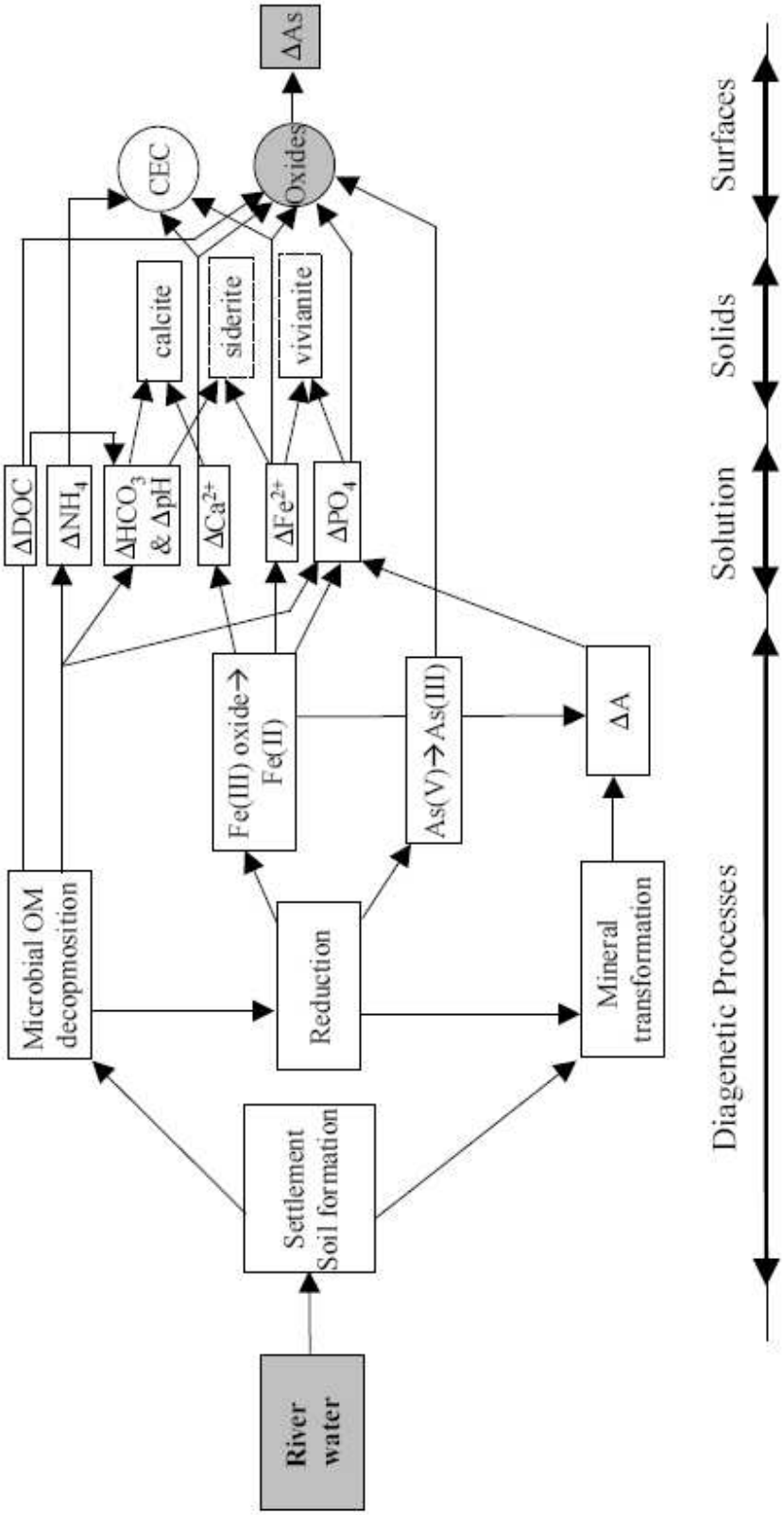

Fig.1. Conceptual picture of interrelated geochemical processes that may potentially contribute to elevated concentrations of As in aquifers.

During diagenesis, the reactive surface area (ΔA m^2/kg sediment) may change (Fig.1). In case of Oswald ripening, the average size of the oxide particles may increase, leading to a decrease of the specific surface area (SSA) of the oxides particles (m^2/kg oxide). Less reactive surface area (ΔA) will be available in the sediment to bind the As oxyanions. The reactivity of a sediment may also be affected by the transformation of Fe(III) (hydr)oxides to other mineral structures like Fe_3O_4, $FeCO_3$, FeS_2, etc. If these minerals have a lower affinity for the As oxyanions, phosphate, and other relevant ions, the effective reactive surface area of the sediment (ΔA m^2/kg sediment) will decrease.

3. Results

3.1. Surface water chemistry and As-loading of a sediment

3.1.1. As loading of the sediment

The first interpretation of the relation between the chemistry of surface water and the As loading of sediments of Bangladesh has been given by BGS and DPHE (2001). The focus was on a large number (n=227) of aquifer materials, originating from 13 different areas across Bangladesh. That study showed that the average As loading is related to the presence of Fe (hydr)oxides (Fig.2a). A clear correlation was found for the average amount of As and Fe extracted with oxalate. A multiple linear regression showed that about ¾ of the oxalate-extractable As fraction is related to the amount of extracted iron. The remaining part is related to extractable magnesium, for instance released by the clay mineral fraction. The correlation found for the elements is As(mg/kg) = 39 Fe(g/kg) + 0.45 Mg(μg/kg) (R^2=0.99). Oxalate-extractable iron can be considered to represent the most reactive iron (hydr)oxide fraction. It has been shown (Roden and Zachara, 1996) that the dissolution rate of iron oxides in the presence of oxalate increases exponentially with the reactive surface area of iron oxides, implying that the finest fractions contribute the most. Oxalate-extractable iron has been attributed to the presence of ferrihydrite but it can also be due to the presence of other Fe (hydr)oxides like magnetite (Kostka and Luther, 1994) and nano-goethite (Thompson et al., 2006). In case of HFO and nanogoethite, the SSA is expected to be between respectively about 600 m^2g^{-1} (Davis and Leckie, 1978) and for instance 200 m^2g^{-1} (Waychunas et al., 2005).

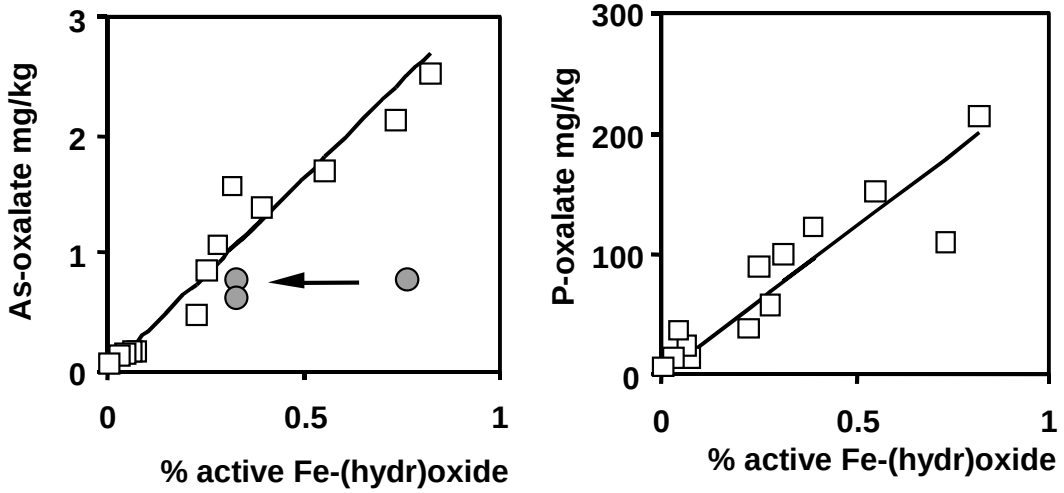

Fig.2. Relation between the averaged amount of iron oxide extractable in ammonium oxalate and the associated amount of arsenic (left hand side) and phosphate (right hand side), for a series of sediments from across Bangladesh (open squares). The lines are calculated with the CD model, accounting for the interaction of AsO_4^{3-} with Na^+, K^+, Ca^{2+}, Mg^{2+}, H_4SiO_4, HCO_3, and PO_4^{3-} on goethite, assuming a surface area of 350 m^2/g Fe (hydr)oxide and using the river water composition given in Table 1 for pH=7 (see text). Data are from BGS and DPHE (2001). The colored spheres refer to the amount of Fe and As extracted by Swartz et al. (2004) in a sequential extraction comprising of an extraction with 1 M HCl before extraction with oxalate. If the amount of Fe or Fe and As, found in the extraction preceding the "1M HCl" treatment is excluded, the As/Fe ratio is close to the average value found by BGS and DPHE (2001).

Swartz et al. (2004) have carried out a series of sequential extractions for Bangladesh sediments to characterize the release of As and Fe. Magnesium and phosphate solutions were used to remove weakly bound ions. Then the first 1 M HCl extraction and next an oxalate extraction followed. The amount of Fe extracted with 1 M HCl was on average slightly more than half (55 ± 8 %) of the cumulative amount that was extracted in the given sequence. This Fe was mainly Fe(II). The average total amount of Fe (0.76 ± 0.72 % Fe (hydr)oxide) extracted in oxalate and corresponding total amount of As (0.77 ± 0.44 mg/kg) can be compared with the oxalate extraction data of BGS and DPHE (2001) given in Fig.2a. When plotted, the data point is an outliner. However, if the amount of Fe, or Fe and As, extracted with 1 M HCl is excluded, the data point comes in line with the data of BGS and DPHE (2001) (Fig.2a). It might suggest that

the Fe(II) fraction extractable with 1 M HCl does not contribute significantly to the amount of Fe extractable in a regular oxalate extraction. The amount of As associated with this fraction, if any, is relatively small. Nevertheless, this "1M HCl" Fe-fraction may be very important in determining the fate of As in the sediments. When formed, it probably will be at the expense of the original Fe (hydr)oxides, which may lead to some As-release as discussed above.

The chemical loading of iron (hydr)oxide particles in contact with average river water of Bangladesh can be estimated assuming that the reactivity of the natural iron particles can be represented by a synthetic Fe (hydr)oxide. In this study, we will use goethite as proxy because for this mineral the relevant ion-ion interactions have been well tested with the CD model (Stachowicz et al., 2007b). If iron (hydr)oxide particles settle and become buried, it will lead to a certain arsenic loading of the sediment that depends on the amount and type of Fe-(hydr)oxides present, their specific surface areas and the field conditions during sedimentation. Such a process may result in a linear relation between As and Fe extractable in oxalate. Such a relationship is found for the Bangladesh sediments as illustrated in Fig.2a.

Comparison of the total amount of As and the amount of As extractable with oxalate (BGS and DPHE, 2001) shows that for 2/3 of the samples the As-oxalate content is close to the As-total, while in the other samples, As-oxalate is only 30 % of the total As. In the latter samples, As might be associated with other metal oxides or silicates, and sulfides that resist dissolution in oxalate and do not desorb As. Swartz et al. (2004) found that a considerable amount of As in their sediments samples can be only extracted with HF and concentrated hot nitric acid.

3.1.2. Surface complexation modeling

Inspired by the idea of a relation between river water chemistry and As loading of aquifer materials (Fig.1), the survey of BGS and DPHE (2001) used surface complexation modeling to estimate the average As loading, assuming that the reactive oxide fraction during sediment formation can be represented by hydrous ferric oxide (HFO). The generalized two layer model (GTM), parameterized for 'single ion' systems with HFO (Dzombak and Morel, 1990), was applied to predict the As loading assuming interaction of AsO_4^{3-} and PO_4^{3-} at an equilibrium concentration of 1 μg As /L and 0.03 mg P/L. The interactions of silicic acid and bicarbonate were omitted, so was the interaction of Ca^{2+} and Mg^{2+}. The calculated As(V) loading was almost an order of magnitude smaller than the measured average As loading of the sediments. To match the relation between As(V) and extractable iron (hydr)oxide (Fig.2a), one has to assume that the

reactive surface area of the oxalate extractable iron is about 75 m^2/g Fe-(hydr)oxide, which is substantially lower than the value expected for HFO (600 m^2/g).

The same type of calculations can also be done with the CD model. The model has been tested for a large number of ion-ion interactions on goethite like the Ca-PO_4 (Rietra et al., 2001), Mg-PO_4, AsO_4-PO_4, $As(OH)_3$-PO_4 (Stachowicz et al., 2007b), $As(OH)_3$-CO_3 (Stachowicz et al., 2007a), PO_4-CO_3 (Rahnemaie et al., 2007a), and H_4SiO_4-PO_4 interaction (to be published). In the present calculations, we account for the simultaneous interaction of the major cations and anions of the river water that might be involved, i.e. AsO_4^{3-}, PO_4^{3-}, H_4SiO_4, Ca^{2+}, Mg^{2+}, and HCO_3^-. Assuming the AsO_4^{-3} and PO_4^{-3} concentrations of 1 μg As/L and 0.03 mg P/L and for the other ions the concentrations average for river water, we calculate the As and P loading of respectively 0.06 μmol As/m^2 and 2.1 μmol P/m^2. To match the As-loading of the sediment with the experimental relation between oxalate extractable As and Fe, we have to assume a reactive surface area of about 70 m^2/g. This number is close to the above value estimated with the GTM that assumed only the AsO_4^{3-}-PO_4^{3-} interaction.

For the same sediments, also the average oxalate extractable P loading has been measured (Fig.2b). To explain these data with the P loading calculated applying the CD model (2.1 μmol P /m^2), we have to assume a reactive surface of about 380 m^2/g. Comparison of both calculated specific surface areas (70 and 380 m^2/g) shows a large inconsistency. The low reactive surface area, found for As(V), is due to a calculated As loading that is far too high, while the calculated PO_4^{3-} loading is too low to be explained by a common reactive surface area. Therefore, equilibration of the sediment with the above combination of the As and P concentration (1 μg As /L and 0.03 mg P/L) can be questioned. To explain the oxalate extraction data, one may assume equilibration with another As/P ratio during the time of sediment formation.

3.1.3. River water composition

The experimental arsenic concentrations reported for several rivers of Bangladesh (BGS and DPHE, 2001) vary. The numbers range from <0.5 to 2.7 μg As/L, with an exception near an As-hotspot where the values differed by a factor 10 between two sampling times (2.7-27 μg As/L). This variation at the As-hotspot suggests that the actual As value in the Bangladesh river waters could have been influenced by drained groundwater that contain elevated arsenic concentrations.

The measured P concentrations were low and reported as '<0.2 mg/L' because of the uncertainty of the measurement. The actual (unpublished) average value found was 0.05±0.02 mg/L. In Fig.3, we have plotted the experimental As and P concentrations excluding the exceptionally high As concentration of 27 μg As/L. The graph shows that the concentrations of As and P are strongly correlated (R^2=0.80). Remarkably, all Bangladesh river waters sampled have approximately the same As/P ratio. This correlation can be explained as due to the competitive interaction of the PO_4^{3-} and AsO_4^{3-} ions with the particles suspended in the river water. Such an idea is supported by the observed diurnal rhythm of the As concentrations in the Madison River, Montana, USA (McNeill et al., 2002). An increase of the pH at daytime due to photosynthesis leads to desorption of As from the particles, increasing the experimental As concentration of the water. The opposite occurs at night.

The experimental average As/P ratio in the Bangladesh river waters is 1/27 g/g or 1/64 mole/mole (slope of the line in Fig.3). Using the average river water composition with 1.7 μg As /L and 0.046 mg P/L leads to a calculated As/P value for the sediment of about 1/14 g/g or 1/32 mole/mole. This number can be compared with the average As/P ratio that is found in the oxalate extract, which is 1/85 g/g or 1/207 mole/mole. The average As/P ratio calculated for the sediment in equilibrium with the river is more than 6 times lower than that found in the aquifer sediment. The lower As/P ratio in the sediment suggests that the sediment formation has taken place at a higher As/P than suggested from the actual present experimental river water data. Both a lower As concentration or higher P concentration can explain the data. A higher P concentration might be due to in-situ soil formation.

However, this process will lead to a large increase of the As concentration in the pore water of the average sediment (resulting from desorption) leading on average to about 10 μg As /L. Another possibility is that the present As concentrations in the various river waters differ from the ancient concentrations present during the Holocene period of sediment formation. In case of groundwater drainage, the present average As concentrations in the river water are elevated in comparison to the ancient values that may have determined the As loading of the sediments. An average As concentration of about 0.3 μg/L in ancient Bangladesh river water at an average P concentration of 1.5 μM (~0.05 mg/L) can explain the above discussed discrepancy in the oxalate extract. The water composition is given in Fig.3 as a colored sphere. We note, what counts is the As/P ratio, which is the same in both hypotheses.

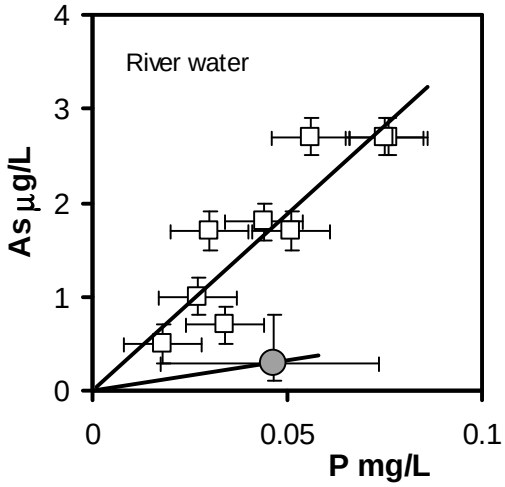

Fig.3. Relation between the experimental As and P concentration in a number of Bangladesh river waters (open squares and regression line R^2=0.80). The error in the P concentration is ±0.01 mg/L, which is based on measurements in duplicate. The vertical error bar is estimated as ±0.2 µg/L. The average As loading in the sediment can be explained with an As concentration of 0.3 µg/L at an average P concentration of 1.5 µM. This is indicated as the colored sphere. The variation in the As/P ratio can be estimated (see text) and is indicated with bars around the sphere.

For the As and P concentration chosen in Fig.3, we have calculated with the CD model the expected loading of the Fe (hydr)oxide particles in equilibrium with average river water at pH=8, and at pH=7. The latter pH value is considered as representative for soil conditions. The results have been given in Table 1 (Case 1 and 2). The loading of AsO_4^{3-} and PO_4^{3-} is slightly lower at pH=7. It implies that after sedimentation, particles may act in the soil environment as a sink, filtering additional P and As out of the infiltrating river water during flooding. Therefore, we have used river water at pH=7 as determinative for the sediment loading.

3.1.4. Average surface area and composition

The Fe-(hydr)oxide surface in equilibrium with average river water of Bangladesh at a pH of 7 (Table1, case 2), is dominated by adsorbed Ca^{2+} (~1.2 µmol/m^2) and PO_4^{3-} (~2.3 µmol/m^2) with some contribution of Si (~0.2 µmol/m^2) and HCO_3^- (~0.02 µmol/m^2). The As loading is very low (~0.01 µmol/m^2) and the binding of the other ions negligible. To explain simultaneously the

oxalate extractable fractions of arsenic, phosphate, and iron, we used the above chosen combination of concentrations for As (0.04 μM) and P (1.5 μM).

Table 1. Average river water and groundwater composition of Bangladesh and corresponding loading of the iron (hydr)oxide particles. The average As and P concentrations in the river water river are uncertain (see text).

Case 1 River Water Composition and surface loading*[1]											
Na^+	K^+	Mg^{2+}	Ca^{2+}	Cl^{-} *[2]	HCO_3^{-}*[2]	SO_4^{2-}	Fe^{2+}	Si	P*[3]	As(V)*[4]	pH=8*[5]
10.7	4.1	9.8	17	-	<122	12.2	-	8.7	0.05	$0.30\ 10^{-3}$	mg/L
0.47	0.10	0.42	0.42	-	2.0	0.13	-	0.31	$1.5\ 10^{-3}$ 10	$0.004\ 10^{-3}$	mM
*[6]	*[6]	0.09	1.21	-	0.02	*[6]	-	0.42	1.85	0.0097	μmol/m^2
Case 2 Soil Water Composition and surface loading A=350 m^2/g*[1]											
Na^+	K^+	Mg^{2+}	Ca^{2+}	Cl^{-}	HCO_3^{-}	SO_4^{2-}	Fe^{2+}	Si	P*[2]	As(V)*[3]	pH≡7*[7]
10.7	4.1	9.8	17	-	<122	12.2	-	8.7	0.05	$0.30\ 10^{-3}$	mg/L
0.47	0.10	0.42	0.42	-	2.0	0.13	-	0.31	$1.5\ 10^{-3}$ 10	$0.004\ 10^{-3}$	mM
*[6]	*[6]	0.02	1.21	-	0.02	*[6]	-	0.18	2.26	0.0125	μmol/m^2
Case 3 Groundwater Water Composition and surface loading*[8]											
Na^+	K^+	Mg^{2+}	Ca^{2+}	Cl^{-}	HCO_3^{-}	SO_4^{2-}	Fe^{2+}	Si	P	As_{tot}*[9]	pH=7*[10]
76	7	36	90	81	502	13	3	16	0.6	$120\ 10^{-3}$	mg/L
3.3	0.18	1.5	2.3	2.3	7.8	0.14	0.06	0.56	$20\ 10^{-3}$	$1.6\ 10^{-3}$	mM
*[6]	*[6]	*[6]	1.33	*[6]	*[6]	*[6]	0.58	*[6]	2.79	0.190	μmol/m^2

*[1] The average river water composition is from BGS and DPHE (2001) (n=7).
*[2] The Cl^- concentration is not reported, but probably low. The HCO_3^- concentration is calculated based on the charge balance assuming a zero chloride concentration. If $Cl^- > 0$, $HCO_3^- < 122$ mg/L
*[3] The experimental P concentration has been reported as <0.2 mg P/L, However, it is 0.05±0.02 mgP/L See text.
*[4] The experimental arsenic concentration is variable. The lowest reported concentration is <0.5 μg As/L. See Fig.3
*[5] The calculated pH value of this average water is pH=8.05. See text.
*[6] The calculated number is (much) smaller than 0.01 μmol/m^2.
*[7] The pH value corresponds to a partial pressure of ~10-40 mbar. See text
*[8] The average groundwater composition is from samples (n=187) of the special survey areas of BGS and DPHE (2001).
*[9] The average relative As(III) amount in the groundwater is As(III)/As_{tot} = 56 %, which is used in the calculation of the As loading. The loading given as adsorbed As_{tot}.
*[10] The average pH of the groundwater in the special survey areas of BGS and DPHE (2001).

The effective specific surface area (SSA) for the iron (hydr)oxide fraction, extractable with oxalate, was found to be ~350 m^2/g, resulting in the calculated lines of Fig.2a,b. We note that the actual average value of SSA of the iron (hydr)oxide fraction can be lower, since only about ¾ of the As is associated with Fe. In that case, the average SSA of the iron (hydr)oxide fraction might be ~250 m^2/g Fe-(hydr)oxide. It is very important to note that the actual Fe-oxalate fraction may differ from the initial Fe-oxalate fraction present at the time of formation of the sediment. If for instance due to diagenesis, part of the Fe (hydr)oxide is transformed into a mineral fraction, that is not extractable with oxalate, the initial surface area of the natural Fe (hydr)oxide would be lower than calculated. According to our scenario calculation (section 3), this might be 25% or less in 60 % of all samples. Fortunately, the initial SSA is not a controlling key factor for As, as will be discussed later (section 3). Although it is difficult to pinpoint the average initial SSA precisely, the various calculated values of the average SSA are reasonable, typically for rather fine (hydr)oxide particles of e.g. aged ferrihydrite or nanogoethite (Waychunas et al., 2005).

3.1.5. Natural variation in loading

It is important to note that in the above analysis, the average value is considered. The individual sediment samples may strongly deviate. But, where is this variation coming from? Can it be due to differences in local conditions during sedimentation or for instance variation in the specific surface area of the particles at settlement or both? Fig.4c shows the variation in the As and P loading of the sediments. The As/P ratio differs and can be explained assuming a variation in the As concentration (0.15-0.6 μg/L) at the given average P concentration (1.5 μM or 0.03 mg/L) or assuming a variation in the P concentration (0.02-0.08 mg/L) at the given average As concentration (0.3 μg/L). The latter combination is used to calculate the upper and lower line in Fig.4c. The variation in PO_4^{3-} used corresponds to the experimental P range of the Bangladesh river waters (Fig.3), but note that the absolute concentration level is not relevant. What counts is the As/P ratio, which is variable.

The variable As/P concentration can also explain a considerable part of the variation in the As loading expressed per unit Fe (hydr)oxide. However, it cannot explain the different P loadings of Fig.4b. As will be illustrated later in detail, this is due to the different slopes of the adsorption isotherm for PO_4^{3-} and AsO_4^{3-} in an As-P system in which phosphate dominates. In that case, the adsorption isotherm of AsO_4^{3-} on goethite will be linear, while the adsorption isotherm of PO_4^{3-} is

highly nonlinear. This means that the AsO_4^{3-} adsorption will change almost proportionally with the AsO_4^{3-} concentration while a change in the adsorption of PO_4^{3-}, related to the variation of the PO_4^{-3} concentration in solution, is very small.

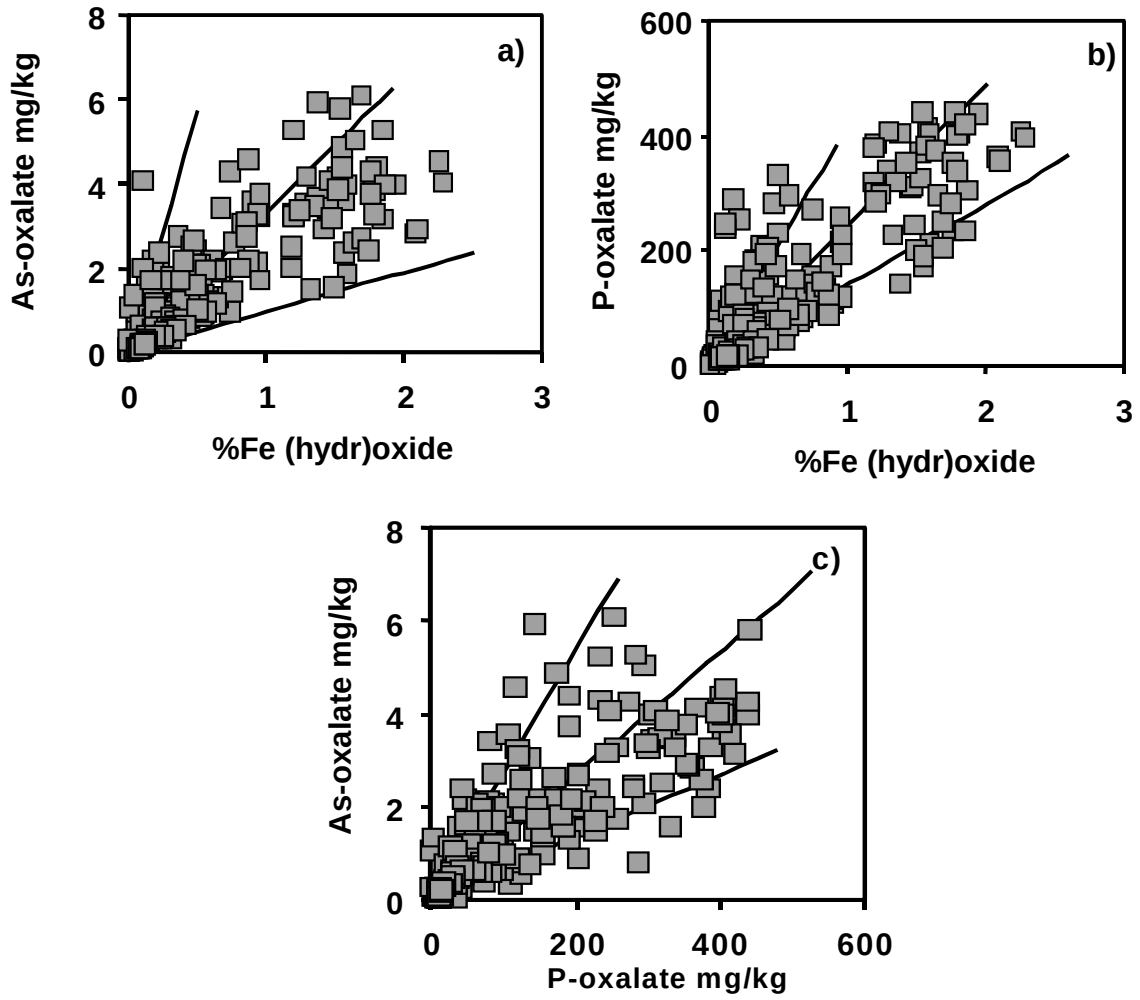

Fig.4. The variation in arsenic (a) and phosphorous (b) extractable in ammonium oxalate extractable as a function of the amount of extractable Fe (hydr)oxide for the individual sediment samples from across Bangladesh (BGS and DPHE, 2001). The P data are unpublished results of BGS and DPHE (2001). In addition, the relation between oxalate extractable As and P is given (c). The lines are calculated assuming a deviation in the As/P ratio of a factor 2 and a variation in the SSA between 600 and 200 m^2/g. The average situation is described by SSA=350 m^2/g, P=1.5 μM and As=0.3 μg/L.

Therefore, a range of AsO_4^{3-} and PO_4^{3-} levels cannot be explained simultaneously with a variation in the P and As concentration during sediment formation only. Nevertheless, a large span in the extractable amount exists for phosphate (Fig.4b). It can be explained by differences in the SSA of the (hydr)oxide particles. Increase of the SSA will linearly increase the loading of the sediment with adsorbed PO_4^{3-} as well as adsorbed AsO_4^{3-}. The average SSA found above is 350 m^2/g (Fig.2). In Fig.4a,b, we have given the calculated range of loadings related to the diverse As/P ratios found and combined it with the SSA of 600, 350, and 200 m^2/g (Fig.4c). With these values, the large proportion of the observed variations can be explained. We note that part of the range in Fig.4a,b might be due to transformation of Fe oxide particles during the diagenesis of the sediment.

3.1.6. Buffering of As concentration by the sediment

The effective average SSA of the natural Fe hydroxide fraction is about 350 m^2/g using goethite as reference in the interpretation of the amount of As, P, and Fe extractable with oxalate. The average amount of Fe (hydr)oxides extracted with oxalate for the 227 sediment samples is 0.56±0.56 % (w/w). In combination, this is an equivalent of an effective surface area of about 2000 m^2/kg sediment. In case of a pore volume fraction of θ=0.4 and a mineral mass density of 2650 kg/m^3, the solid : solution ratio in the aquifer will be about 4 kg/L, which results in an average reactive surface area of about 8000 m^2/L. This number is very high compared to values used in ordinary experimental adsorption studies. In case of equilibration of the iron (hydr)oxide with average river water of 0.04 μM (0.3 μg As /L) and 1.5 μM PO_4^{3-} at pH=7, we calculate a loading of 0.0125 μmol As /m^2 goethite (Table 1). If the distribution ratio (R_d) is defined as the ratio of the amount adsorbed (mole/L) and the amount in solution as (mole/L), then $R_d \approx 2500$. The number expresses that 2500 times more As is bound by the solid phase in comparison to the amount present in the pore water. This illustrates that the average As storage at the solid surface is very large. It implies that the As and P loading of the sediment, once formed, is not easily changed by desorption and leaching.

In contrast to the near constant amount of As bound by the solid phase particles, the solution composition can change drastically upon changes in the system conditions like pH, redox, and release of P and Fe by mineralization or reductive dissolution *etc*. These issues will be discussed next.

3.2. The conditional change of the arsenic concentration in pore water

In the following part, we will focus on the factors that may change the composition of the pore water chemistry once the sediment is loaded with As. The processes related to the conceptual framework of Fig.1 will be discussed in detail. This will be followed later in part 3 by some scenario calculations in which we will quantify the key factors causing elevated As levels in the Holocene sediments of Bangladesh and elsewhere.

3.2.1. pH change at sedimentation

Solid particles suspended in the river water may ultimately deposit on the riverbed in tiny layers at flooding. In biologically active soils and in particular in sediments, the partial pressure of CO_2 (P-CO_2) will increase. This will lead to a decrease of pH. Bangladesh river water contains on average bicarbonate concentrations close to ≤ 120 mg HCO_3^- /L, but in the groundwater, the bicarbonate levels may raise to values of 500 mg/L (Table 1). The increase may be due to microbial respiration and due to equilibration with calcite, $CaCO_3$ (Swartz et al., 2004). Ca^{2+} may be released by weathering and additionally due to reductive dissolution of iron (hydr)oxides that bind Ca^{2+} (Table 1).

The following calculations are done stepwise. Starting point is the average composition of Bangladesh river water (Table 1). Note that this average water considerably differs from the composition given by Appelo et al. (2002). The average river water of Table 1 has a calculated pH of 8.05 and the corresponding P-CO_2 is 1 mbar. The water is close to or at equilibrium with calcite (the saturation index SI is –0.1), as given in Table 2. In Step 1, the water enters the soil and meets a higher CO_2 pressure, for instance 1 10^{-2} bar, a typical value for aerated, biologically active (sub)soils. The pH drops from about pH~8 to pH~7 without much change of the bicarbonate concentrations. The water in the soil becomes under saturated with respect to calcite (SI=-1), which is in agreement with data of Swartz et al.(2004), showing only an equilibration with respect to calcite in the deeper parts of the sediment profile that was studied. Next (Step 2), the groundwater is formed and brought in an equilibrium with calcite at a (chosen) higher CO_2 pressure (4 10^{-2} bar) resulting in pH ~7. The calculated HCO_3^- concentration (470 mg/L) is much higher than in the river water. The calcium concentration (103 mg/L) is also strongly increased. Both values agree with the typical values found for average groundwater of Bangladesh as given in Table 1, showing the consistency of the approach.

Table2. Change in water composition (pH, ionic strength I, Ca^{2+} and HCO_3^- concentration) calculated for a 2-step scenario as described in the text, starting with an average river water composition (given in Table 1), that changes when in contact with soil at a higher CO_2 pressure (Step 1). In Step 2, soil water becomes groundwater, that calibrates with $CaCO_3$ at a higher P-CO_2 at pH=7. In the last column, the saturation index Si with respect to calcite is given (solubility constant =-8.4).

	pH	**I** M	**Ca^{2+}** mg/L	**HCO_3** mg/L	**P-CO_2** mbar	**SI** $CaCO_3$
Start	8.05	0.003	17	122	1	-0.1
Step1	7.09	0.003	17	143	10	-1.1
Step2	6.96	0.009	103	470	40	0

The above-illustrated change in pH and water composition may affect the ion loading of the sediment. According to Table 1, an increase of about 25% in the As and P loading is calculated. As mentioned above, the soil becomes a sink filtering additional As and P out of the river water.

3.2.2. Effect of PO_4^{3-} on As(V) binding

Phosphate is a known competitor for arsenic species. For instance, Dixit and Hering (2003) have shown that phosphate inhibits strongly the adsorption of AsO_4^{3-} on iron oxides such as HFO, goethite and magnetite. Fig.5 shows the pH dependency for the mono-component As(V) and the 2-component As(V)-P(V) system. Several features are of interest. First of all, in the absence of PO_4^{3-}, the AsO_4^{3-} adsorption strongly depends on the pH value (Fig.5a). The arrow in Fig.5a shows the variation in the AsO_4^{3-} equilibrium concentration at pH between 8 to 7 in the absence of phosphate. In the presence of PO_4^{3-} (Fig.5b), the variation in the As concentration also depends on the presence of PO_4^{3-}. As a result, a much smaller pH dependency is observed for the same concentration range, but at a different loading, than in a 'single-ion' system (compare Fig.5a and 5b).

A second important feature of Fig. 5 is the striking difference in the shape of the adsorption isotherm in the absence and presence of PO_4^{3-}. In the concentration range of interest, As(V) in the mono-component system is typically a high affinity adsorption isotherm that is strongly non-linear. This results in a slope (S) in the log-log plot that is considerably smaller than 1 (typical value of S ~0.1). In case of the dominant presence of PO_4^{3-}, the slope changes dramatically to S=1. The isotherm becomes linear. It implies that the loading is directly

proportional to the concentration in solution and vice versa. This behavior is caused by the dominance of PO_4, which fixes the electrostatic potentials of the interface for a certain pH and PO_4 concentration.

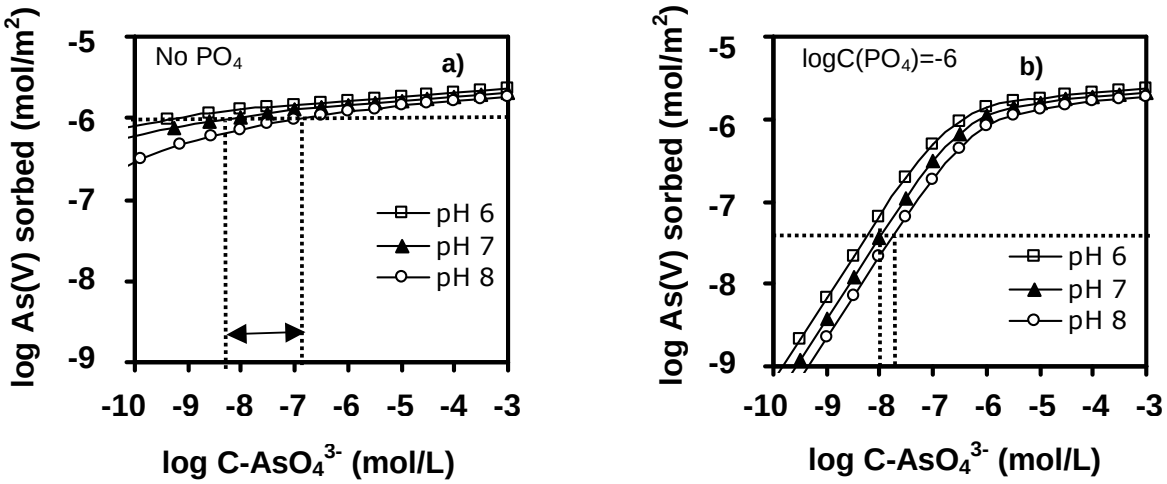

Fig. 5. Adsorption isotherms for As(V) adsorption on goethite calculated using the CD model and the parameters of Stachowicz et al.(2007a). The electrolyte background is 0.01M NaCl. The lines in the graphs show how the pH change impacts the As(V) adsorption in a 'single-ion' system (a) and in a system with 10^{-6} M PO_4^{3-} (b).

It is important to note that the behavior of PO_4^{3-} in the AsO_4^{3-}-PO_4^{3-} system is very comparable with the AsO_4^{3-} behavior in the 'single ion' system (Fig.5a), i.e. the variation in the concentration only slightly affects the loading (see also Table 1). For this reason, the large variation in the P loading of sediments (Fig.4b) cannot be explained by the large natural variation in the PO_4^{3-} concentration. In contrast, the linearity of the As adsorption isotherm implies that the As loading is relatively easily changed. This factor is mainly responsible for the variation in the As/P ratio as shown in Fig.4c.

3.2.3. Mineralization of OM

In natural situations, the phosphate concentration in Bangladesh river water will be low (0.02-0.08 mg/L in Fig 3). The PO_4 concentration in groundwater (Table 1) is much higher, on average close to 20 μM (0.6 mg P/L), but higher concentrations are also frequently found (Fig. 6). Higher PO_4 concentrations can be due to the decomposition of the organic matter by microorganisms. Mineralization of organic matter will lead to a release of P and N in a ratio of

about 7 ± 1 g/g or 16 mole/mole. In Bangladesh groundwater, ammonium is correlated with the amount of phosphate (Fig.6a) (BGS and DPHE, 2001). In case of absence of buffering of the N and P concentration by the solid phase, a release of 10 mg N-NH_4/L will lead to a concentration of about 1.5 mg P/L.

In case of anaerobic mineralization, Fe-(hydr)oxide may act as oxidator for organic matter, leading to the dissolution of the Fe (hydr)oxides with corresponding release of adsorbed P. Therefore, in case of reductive dissolution, P will originate from two different sources, i.e. the organic matter and Fe (hydr) oxides. The relative contribution of both processes, based on only the water composition, is uncertain due to the variation in the buffering of NH_4 by the CEC and in particular the buffering of P by the reactive (hydr)oxide surfaces and/or the formation of phosphate minerals like vivianite $(Fe_3(PO_4)_2)\cdot 8H_2O$ (Fig.1). These processes will be quantified in the next section.

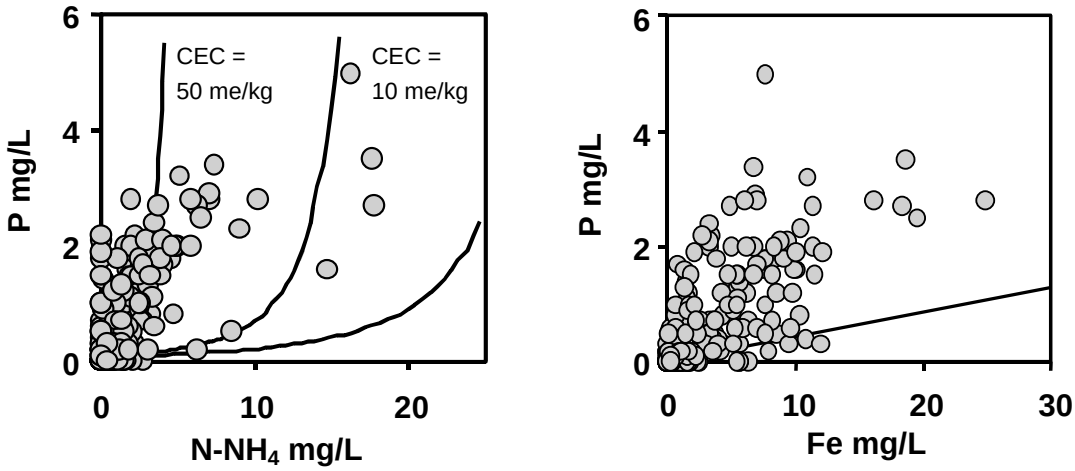

Fig. 6a. Relation between the ammonium and phosphorus concentrations in Bangladesh groundwaters (BGS and DPHE, 2001). The lines have been calculated assuming 1) P release by reductive dissolution of iron (hydr)oxide, which is buffered by the remaining (hydr)oxide fraction, and 2) NH_4^+ release (eq.[2]) with buffering via Gaines-Thomas ion exchange using CEC values of 0, 10, and 50 meq/kg. Average groundwater saturated with $CaCO_3$ at pH=7 was used. For reasons of simplicity, some concentrations were fixed, i.e. Mg^{2+} = 0.14 mM, Fe^{2+}=0.1 mM, H_4SiO_4=0.56 mM. In Fig.6b, the relation between dissolved Fe(II) and phosphorus is given. The line refers to the stoichiometry of the reductive dissolution of FeOOH releasing Fe^{2+} ions and adsorbed PO_4^{3-} eq. [2a] without any buffering (see text).

3.2.4. Reduction

Biogeochemical oxidation of organic mater in a closed system will result in a chemical reduction process. The Fe(III), present in iron oxides, can be transformed into Fe(II) under reducing conditions. This transformation can be catalyzed by Fe^{2+} (Pedersen et al., 2005). Reduction may also transform As(V) into As(III). Both processes will affect the As levels in groundwater in a number of ways.

3.2.4.1.Reductive dissolution of iron (hydr)oxides

The release of PO_4, due to reductive dissolution of iron (hydr)oxides, will depend on the P loading per mole of Fe that is part of the Fe (hydr)oxide. The moles of Fe per unit surface area (Γ_{Fe}) can be given as:

$$\Gamma_{Fe} = \frac{1}{A\mathrm{M}} \qquad [1]$$

in which M is the molar mass of the Fe(hydr)oxide and *A* is the specific surface area (SSA). In case of A = 350 m^2/g and M=89 g/mole, equation [1] gives Γ_{Fe} = 32 μmol/m^2. Combination with a P loading of Γ_P = 2.8 μmol/m^2 (Table 1, groundwater), the P/Fe stoichiometry of the reaction can be calculated as 2.8/32 = 0.09 ≈ 1/12. Note that the precise number will depend on the P loading and the SSA (*A*).

In case we assume that the ratio Γ_{Fe}/Γ_p is preserved, i.e. no significant change of the surface area (A) and no (partial) re-adsorption of the PO_4^{3-} and Fe^{2+} ions that have been released, the overall stoichiometry can be written as:

$$CH_2O\text{-}N_{1/15}P_{1/240} + 4\ FeOOH\text{-}P_{1/12} + 7\ H_2CO_3 \Rightarrow$$
$$\Rightarrow 4\ Fe^{2+} + 8\ HCO_3^{-1} + 1/15\ N + 1/3\ P + 6\ H_2O \qquad [2a]$$

$$CH_2O\text{-}N_{1/15}P_{1/240} + 4\ FeOOH\text{-}P_{1/12} + 3\ H_2CO_3 \Rightarrow 4\ FeCO_3 + 1/15\ N + 1/3\ P + 6\ H_2O \qquad [2b]$$

The molar N/P ratio in both reactions is ~ 1:5 (mole/mole). This number is very different from what is found at aerobic oxidation of organic matter, i.e. 16 : 1 mole/mole. If the N/P ratio 1 : 5

would be plotted in Fig. 6a, a very steep slope would result. However, when P is released, a considerable part may re-adsorb. According to the calculated P adsorption in Table 1, the original P loading increases with $\Delta P \approx 0.5$ μmol/m^2 when groundwater is formed. In combination with the average surface area of 8000 m^2/L, this is equivalent with about $\Delta P = 4$ mM. The number can be compared with the change in the solution concentration of ~0.02 mM. It illustrates the large buffering of P by oxide surfaces. Almost 200 times more P is (re)adsorbed than brought into solution, i.e. > 99 % of the P-release is re-adsorbed. It implies that the actual situation is very far from a simple interpretation of the overall stoichiometry of eq.[2].

The lower line in Fig.6a, is the predicted relationship between the NH_4^+ and PO_4^{3-} concentration in solution, assuming P-buffering by the iron (hydr)oxide surface. We assumed reductive dissolution of Fe in the average sediment having 0.56 % Fe oxides, a SSA of 350 m^2/g, and a solid :solution ratio of ρ =4 kg/L. The line has been calculated by a stepwise decrease of the reactive surface area of the iron (hydr) oxide in the system, in total about 25 %. According to the data, a too high NH_4 concentration is predicted. This might be due to anaerobic ammonium oxidation, nitrification, or it is due to ion exchange buffering. In the next calculation, the latter contribution is quantified, assuming ion exchange using a CEC of 20 or 50 meq/kg sediment, which is representative for a sandy material having 2-10 % clay in case of a CEC of 500 meq/kg clay. The calculations show that in principle the behavior of N and P can be quantitatively understood based on the reductive dissolution of Fe-(hydr)oxide in combination with a N and P buffering by the solid phase (see also Fig.1). In addition, the biological N transformations may contribute.

The above process of the reductive dissolution can also be judged from the point of view of the Fe/P ratio. The above reactions (eq.[2]) show that Fe(III) (hydr)oxide is the main P source. The Fe/P ratio is about 12/1. This ratio has been given as line in Fig.6b. This reaction path will only be followed if the PO_4^{3-} and Fe(II) ions released are not buffered by the solid phase. However, application of the same approach as for NH_4^+ with ion exchange shows that the release of Fe^{2+} is tremendous and the much lower experimental values of the Fe^{2+} concentration can only be understood assuming Fe(II) precipitation. Swartz et al. (2004) have shown that pore water can be supersaturated with respect to siderite ($FeCO_3$). This may be in line with their sequential extraction pointing to the presence of Fe(II) that is extractable in 1M HCl (see discussion at

Fig.2). We note that also the formation of vivianite is possible since the pore waters can also be oversaturated with respect to this mineral (Swartz et al., 2004).

3.2.4.2. Reduction of As(V) to As(III)

Reduction of As(V) to As(III) will change the binding of arsenic, affecting the As levels of the groundwater. This effect is illustrated in Fig.7 showing the competitive adsorption isotherms of As(V) and As(III) in the absence and presence of PO_4^{3-} for different phosphate concentrations, i.e. 10^{-8} M, 10^{-6} M, and 10^{-4} M. Comparison of the equilibrium concentrations of As(V) and As(III) for a chosen As loading and PO_4^{3-} concentration shows that As (III) is less strongly bound than As(V). For a loading of 0.01 μmol/m^2 and a phosphate concentration of 1 μM, the concentration of As(V) is ~0.002 μM, while for As(III) it is 50 times higher (~0.1 μM). This means that reduction of As(V) to As(III) may lead to a considerable release of As.

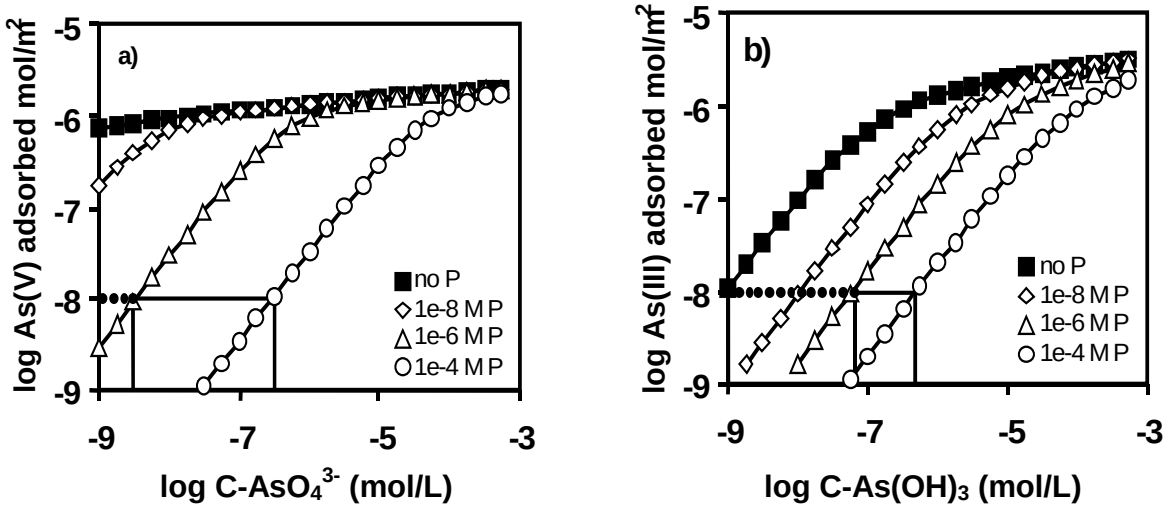

Fig. 7. Calculated adsorption isotherms of As(V) (a) and As(III) (b) at pH 7 (0.01M NaCl) as a function three dissolved PO_4^{3-} concentrations, i.e. 10^{-8}, 10^{-6}, and 10^{-4} M. Figures illustrate that As(V) is more sensitive to the PO_4^{3-} concentration than As(III) and that As(III) is less strongly bound than As(V).

It is important to note that the difference between As(III) and As(V) becomes much smaller at a high P concentration of e.g. 10^{-4} M. In that case, the As(III) concentration is only 1.6 times higher. This phenomenon is related to the difference in the sensitivity of the isotherms of

both As-oxyanions to phosphate. Adsorbed As(V) is more sensitive to changes in P concentration than As(III). Change of the PO_4^{3-} concentration from e.g. 10^{-6} to 10^{-4} M at a chosen As loading of 0.01 μmol/m^2 leads to a shift of ΔlogC-As ≈ 2 for As(V), while it is only ΔlogC-As ≈ 0.9 for As(III). This indicates that isotherms of As(V) as well as As(III) are both linear in case of dominance of PO_4^{3-}.

In many cases, arsenic in groundwater is a mixture of arsenite and arsenate. Measurements in Bangladesh show (BGS and DPHE, 2001) that the ratios between As(III) and As(V) may vary between 0-100%. Swartz et al. (2004) reported As(III) fractions between about 35-95 % for As(III) in solution. We have calculated the expected relative binding of As(III), using their pore water composition. The results (Fig.8) show that in case of 50% As(III) in solution, the majority of As bound to the sediment is still As(V). At a low P concentration, this effect is most strong because then AsO_4^{3-} can better compete with PO_4^{3-}. This preference is further stimulated by a lower pH value. The full line in Fig.8 represents the predicted relationship for average groundwater (Table 1). The dotted line is for the same composition and As/P ratio, but at a 10 times lower concentration of As and P.

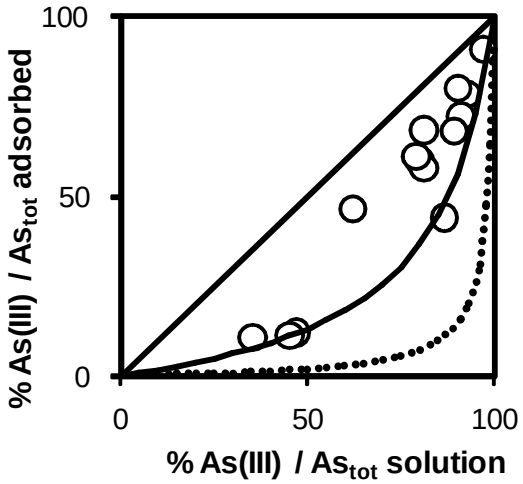

Fig. 8. The fraction of As(III) adsorbed (As(III) / As_{tot}) by goethite in relation to the relative presence of As(III) in solution. The relative presence is calculated using the reported solution chemistry of an aquifer profile studied by Swartz et al. (2004), having pH values between 6.6-7.1, P concentrations around 2 mg/L and As concentrations ranging between about 5-500 μg/L. The surface interactions considered are for K^+, Na^+, Cl^-, Ca^{2+}, Mg^{2+}, Fe^{2+}, PO_4^{3-}, As(III), As(V), and H_4SiO_4. The lines are calculated for average groundwater conditions (full line) and with a 10 times lower As and P concentration (dotted line).

3.2.5. Additional diagenesis

The surface area of sediments may change in several ways. Freshly formed iron oxides may have a high SSA. These particles may be thermodynamically less stable than the corresponding bigger particles. Over time, oxides tend to re-crystallize, which may increase the size of the particles, decreasing the SSA of the iron (hydr)oxide particles. The SSA may also decrease in case of a preferential dissolution of the finest oxide fraction. In both cases, the reactive surface of the sediment and the number of sorption sites per unit mass decrease. Another process that may change the surface area is the transformation of Fe(III) (hydr)oxide to other minerals like mixed valence oxides minerals (magnetite Fe_3O_4 and green rust) and siderite ($FeCO_3$). If these minerals have a larger particle size or if they are less reactive than the original Fe (hydr)oxide, the effective reactive surface area of the sediment will decrease.

The effect of any change in the reactive surface area can be illustrated by comparing the isotherms of As(III) and As(V) at pH=7 in the presence of a dominant amount of PO_4^{3-} (Fig.9a). As mentioned above, both isotherms are linear. In that case, the change of the reactive surface area A_{sed} may lead to a relatively small change of the As concentration in the pore water if the system is dominated by phosphate. This phenomenon can be mathematically described.

In case of a change in A_{sed} without leaching, the total amount of ions in an aquifer is preserved. The total amount of arsenic T (mol/L) is the sum of the amount adsorbed (expressed in mol/L) and the As concentration in solution (C), according to:

$$T = \rho A_{sed} \Gamma + C \qquad [4a]$$

in which ρ is the solid: solution ratio (kg/L) and Γ the As adsorption per unit surface area (mol/m^2). In case of dominance of PO_4, the adsorption of the minor ion will be linearly related to the concentration, which can be expressed as:

$$\Gamma = K C \qquad [4b]$$

in which K is a conditional constant. Its value will depend on the concentration of the potential determining ions, like for instance H^+, PO_4^{3-}, and cations like Ca^{2+} and Fe^{2+}. Combining both equations leads to:

$$T = \rho A_{sed} KC + C \approx \rho K A_{sed} C \qquad [4c]$$

The last simplification is allowed as long as the R_d value ($\equiv \rho A_{sed}\Gamma/C$) is high (see section 3.1.6.).

In case of preservation of the total amount T at constant conditions (pH, PO_4^{3-}, etceteras), the product A_{sed}.C is a constant, which implies that a decrease of the surface area is inversely related to the concentration in solution. For instance, if the reactive surface area decreases with 50 %, the concentration is solution will increase with a factor of (only) 2, provided that the pH and PO_4^{-3} concentration are constant (constant *K*). This effect is illustrated in Fig.9a.

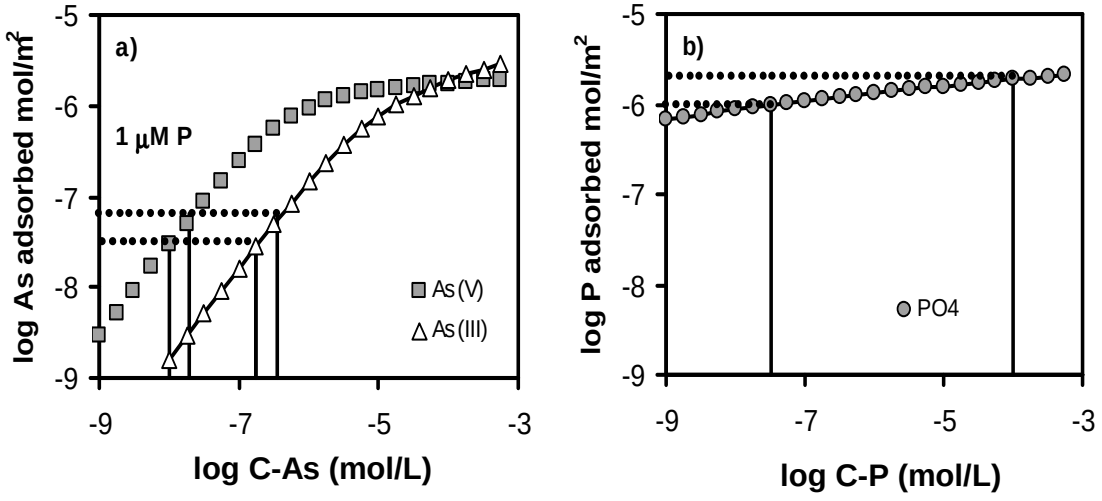

Fig.9a. Adsorption isotherm of As(III) and As(V) at pH 7 in the presence of 1 µM P, in 0.01M NaCl. Fig.9b Adsorption isotherm of PO_4^{3-} in 0.01 M NaCl at pH=7. A change in the amount of reactive surface area with a factor of 2 leads to a small change in surface loading (+0.3 units) if the pH and PO_4^{3-} concentration remain constant, whereas the same change in SSA has a dramatic effect on the P concentration.

However, a decrease of the reactive surface area may have a very large impact on the surface loading of phosphate, which may lead to a large increase of the PO_4^{3-} concentration in solution. In contrast to the isotherms of As(V) and As(III) oxyanions, the isotherm of PO_4 ion in the As-PO_4^{3-} system is very non-linear (Fig. 9b). The non-linear character of the isotherm of P implies that a small change of surface area A (m^2/kg) will have a dramatic effect on the PO_4^{3-}

concentration (Fig.9b). This will occur in the early stages of reduction. An increase of the loading with a factor of two will lead to a PO_4^{3-} concentration from e.g. 3.10^{-8} M to 10^{-4} M. Therefore, diagenesis can be an important source of P (see also 2.4.1), and may indirectly affect the adsorption of As(V) and As(III). However, note that P concentrations are limited in the groundwater in Bangladesh to values around 2 mg/L (Fig.6b). This might be due to the formation of a phosphate mineral that can control the P concentration, for instance vivianite $Fe_3(PO_4)_2.8H_2O$.

3. Scenario analysis

The effect of the various processes discussed above can be quantified using a scenario calculation. In the scenario, the sediment with a chosen reactive surface area will be subject to a number of changes. The effect on the As and P concentration will be given. In the scenario, the surface interaction will be quantified using the interactions of the oxyanions of As(V) and As(III) with PO_4^{3-}, H_4SiO_4, HCO_3^-, Na^+, K^+, Ca^{2+}, Mg^{2+}, and Fe^{2+}.

After sedimentation, equilibration with $CaCO_3$ occurs and the total loading of the system will be kept constant while the change of the concentrations will be predicted. We assume that the mean sediment has initially an effective surface area of 8000 m^2/L pore water (section 3.1.6.). The increase of the PO_4^{3-} concentration in the reductive dissolution step is supposed to be due to the decrease of the reactive surface area A_{sed}. The ions released are allowed to re-adsorb.

Step 1- From river to sediment

The release of As during sediment formation has been calculated starting with the river water composition. This is shown in Fig.10 for the As concentration (in μg/L) in the pore water together with the development of the PO_4^{3-} concentration (in mg/L). The suspended particles in the river are assumed to be in an equilibrium with the river water at pH 8. At settlement, the pH will decrease due to a higher CO_2 pressure (Table 2). In case of pH=7, the As(V) concentration decreases from 0.3 μg/L to 0.05 μg/L. If the settled particles remain part of a soil that is regularly flooded, the As concentration may reach again the 0.3 μg/L level. However, as noted above, the increase of the As(III) loading requires much water. We assume that the particles will come again

in equilibrium with 0.3 μg As/L and 1.5 μM PO_4^{3-} at pH=7. The total amount of As is assumed not to change in the next steps, i.e. no significant leaching or precipitation of As is assumed to occur when the particles become part of the groundwater system.

Step 2- Reductive dissolution of Fe-(hydr)oxide

After soil formation, we assume that the sediment comes in an equilibrium with $CaCO_3$ with P-CO_2 = 40 mbar at pH 7 (Table 2). The concentrations Na^+, K^+, Mg^{2+}, and H_4SiO_4 have been fixed to the values given in Table 1 (groundwater). The sediment becomes chemically reduced due to the microbial activity. This will decrease the effective total surface area A_{sed}, releasing Fe^{2+} and adsorbed PO_4^{3-}. In the calculation, A_{sed} is changed to reach a P concentration of 6.5 10^{-5} M (2 mgP/L). The corresponding concentration of Fe^{2+} is set at 1 10^{-4} M (~6 mg /L). This choice is based on Fig.6b. The reductive dissolution results in a decrease of the reactive surface area to 5830 m^2/L, i.e. a decrease of about 25 %. The As concentration increases tremendously, about 50 times (Fig.10). This is predominantly due to the large increase of the P concentration in solution, while the effect of the decrease in the reactive surface area is relatively small (see Fig.9b).

Step3- Reduction of As(V) to As(III)

At low redox potentials, As(V) will change into As(III). The reactive surface area is assumed to remain constant. We calculated the As release assuming a reduction of 50 % of the total As fraction in the sediment. The calculation shows that in that case 70 % of the As in solution is As(III). Such a number is reasonable in case of the reduction (BGS and DPHE, 2001; Swartz et al., 2004), see also Fig.8. The relatively moderate reduction of As(V) leads to a relatively small increase of the total As concentration by less than a factor 2 (Fig.10). The effect of reduction is relatively small because of a high PO_4^{3-} concentration in solution (Fig 7). In that case, the affinity of A(V) and As(III) oxyanions is not very differently anymore. At a low P concentration, the effects are more pronounced (see the discussion at Figs.7, 8). The PO_4^{3-} concentration is only slightly lowered as a result of the As(V) reduction and a desorption of As(III).

Step 4- Additional Diagenesis

Diagenesis may be accompanied by a change of particle size and mineral transformation (Fig.1). In both processes, the effective reactive surface of the sediment may decrease. Actually, the process would start already with the above reductive dissolution process (step 2). The results of the sequential extraction of Swartz et al. (2004) suggest that about 55 % of the iron may have been transformed into Fe(II) minerals like siderite $FeCO_3$ (see Fig. 2). In our calculated reductive dissolution step (2), the surface area has decreased with about 25 %. It implies that additional transformation may occur in the sediment (about another 30 %). Such a severe transformation would release again a lot of PO_4^{3-}, which cannot be stored at the surface of the Fe-(hydr)oxide fraction and therefore, the P concentration would become very high. However, the P concentration levels are usually restricted to about 2 mg/P/L (Fig. 6), which might be due to (co)precipitation mechanisms (the formation of e.g. vivianite). We have limited the phosphate concentration during the additional diagenesis steps to 2 mg P/L. The maximum concentration of Fe^{2+} is set at 0.1 mM (~6 mg Fe/L) and all arsenic is assumed to be reduced to As(III) in this step. In our calculation, the total transformation of 55 % of the original iron (hydr)oxide fraction, equivalent with a decrease to 3600 m^2/L, leads to an As concentration of 65 μg/L.

The average increase of the As concentration due to biogeochemical changes in the sediment can be compared with the average situation in the Bangladesh sediments. As mentioned in the introduction, the large data set of the survey of BGS and DPHE (2001) shows that 58 % of all samples is below the WHO standard for drinking water of 10 μg/L and 75 % below 50 μg/L (Bangladesh standard). The value of 50 μg/L is rather close to the concentration in our system with 55% reduction of the surface area (transformation of the Fe (hydr)oxide fraction and 100% As(V) reduction, i.e. 63 μg/L). In case of reduction to 50% As(III), the final concentrations is 46 μg/L. It implies that the As concentration in about 60% of all Bangladesh sediments can be described with reductive dissolution. In the next 15 % of the samples, the reduction of the surface area is restricted to about 50 %.

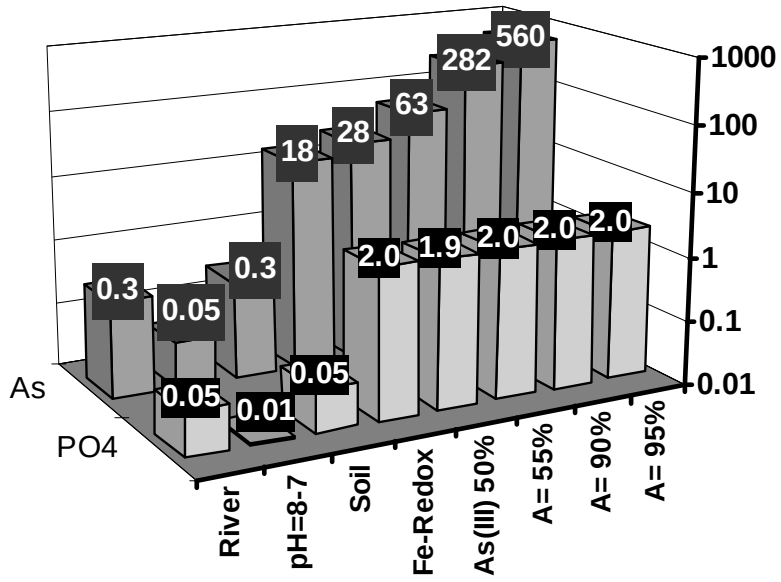

Fig.10. Change of the As concentration in a series of steps, starting with 1) river, 2) a pH change 3) soil formation. Step 4) is the reductive dissolution of Fe (hydr)oxide and adsorbed PO_4^{3-} resulting in a change of the surface area from 8000 m^2/L to 5830 m^2/L, which is corresponding with a transformation of about 25 % of the Fe (hydr)oxide fraction. Next, 5) a reduction of 50 % of As(V) to As(III) leading to 67 % As(III) in solution, and 6) a further decrease of the reactive surface area to 3600 m^2/L. In total, the reactive surface area has reduced to 55 % of the original Fe (hydr)oxide fraction and the fraction of adsorbed P is reduced by 40 %, for instance forming a co-precipitate. In the last steps, 90% and 95% of the (hydr)oxide fraction is transformed. In Table 3, the corresponding change of the ion loading of the surface is given.

In order to reach As concentration above 50 μg/L, a strong surface transformation is required. In case of a 90% reduction of the iron (hydr)oxide fraction, i.e. from 3600 to 800 m^2/L (factor 4.5), the As concentrations reach well above 200 μg/L (Fig.10). It is important to note that even in this case, the vast majority (~97 %) of all As is still adsorbed! The R_d ($\rho A\Gamma/C$) value is still high. If all As is released, the concentration would reach 6000 μg/L in the average sediment.

In Table 3, the calculated loading of the iron (hydr)oxide fraction is given. The As/P value is about 1/190 mole/mole in the first steps. When a formation of a P-precipitate limits the P-concentration, the As/P ratio changes to 1/110 mole/mole in the step with 55% ΔA_{sed}.

Table 3. The change of the ion loading of the surface for the processes mentioned in Fig.10.

Scenario	loading μmol/m^2						
	P	As(V)	As(III)	Si	Ca	Mg	Fe(II)
River	1.85	0.0097	0	0.42	1.21	0.09	0
pH=8-7	1.85	0.0097	0	0.41	1.07	0.02	0
Soil	2.26	0.0125	0	0.12	1.21	0.02	0
*[1]Fe-Redox	3.09	0.0170	0	0.00	1.42	0.00	0.59
*[1]As(III) 50%	3.09	0.0085	0.0085	0.00	1.41	0.00	0.60
*[2]ΔA= 55%	3.10	0	0.028	0.00	1.41	0.00	0.62
*[2]ΔA= 90%	3.08	0	0.120	0.00	1.37	0.00	0.68
*[2]ΔA= 95%	3.06	0	0.230	0.00	1.33	0.00	0.76

*[1] ΔA ≈ 25%, *[2] 100% As(III).

The calculated amount of co-precipitated P is 40% of the initial P loading. If this co-precipitate dissolves in the oxalate extract, than our approach is consistent in the sense that the lower As/P concentration in the river water explains the As/P oxalate ratio and this ratio originates from the initial Fe (hydr)oxide fraction. If the phosphate co-precipitate does not dissolve in the oxalate extract, the average amount of P bound to the Fe oxide fraction is not a good measure for the amount of phosphate bound at the surface of the initial oxide Fe-fraction. This initial P-fraction will then be underestimated and the lower average value will result in the calculation of a lower SSA. This may be the case in 40 % of the samples, in particular when high As concentrations are present in the pore water.

In the calculations, we have focused on the average sediment. As discussed, natural variation exists, like a higher SSA and or another As/P ratio. Assuming a higher reactive surface A_{sed} hardly changes the results, if the same PO_4^{-3} level in solution is to be reached. In that case, the same relative change of the reactive surface area is required. In terms of eq.[4c] this means that the total amount T will be higher (higher A_{sed}), but the relative change in A_{sed} is the same, and so is the change in the As concentration. In case of a higher As/P ratio a significant change will occur. An increase of the As concentration by for instance a factor three at the same As/P ratio, results in 0.9 μg As/L in the soil, 55 μg As/L at Fe-reduction, 82 μg As/L at 50% As(V) reduction, 190 μg As/L at 55% ΔA_{sed} with 100% reduction to As(III), 899 μg As/L at 90% ΔA_{sed} with 100% As(III), and 1902 μg As/L at 95% ΔA_{sed} with 100% As(III). The concentrations goes

up with the same factor of 3 as long as a linear isotherm applies in the various steps. It implies that under this condition, the variation that is observed in the As/P ratio (Fig.4c), will also be the calculated variation in the scenarios.

Example

The variation in the reactive surface area of a sediment (A_{sed}) can be estimated if the experimental pore water chemistry is combined with a measured As loading (As_{ads} mol/kg sediment). If additionally also the corresponding amount of iron (hydr)oxide is known, the specific surface area of the iron (hydr)oxide fraction can be calculated too. Swartz et al. (2004) have provided such a data set, as already used above (Figs.2 and 8). They measured in detail the pore water composition and characterized the sediment with sequential extractions. The cumulative amounts of As and Fe extracted in the sequence up to oxalate, excluding the 1 M HCl extraction, is considered as "reactive" (see Fig.2). These numbers will be indicated here as respectively Fe_{ox} and As_{ox}. The reactive surface area of the sediment (A_{sed} m^2/kg sediment) can be found from:

$$A_{sed} = As_{ads} / \Gamma_{As} \approx As_{ox} / \Gamma_{As} \qquad [5a]$$

in which Γ_{As} is the calculated As-loading (mol/m^2). Combination of A_{sed} and the above fraction of sequentially extracted Fe (Fe_{ox} in g FeOOH per kg sediment) results in a SSA of the (hydr)oxide fraction (m^2/g):

$$SSA = A_{sed} / Fe_{ox} \qquad [5b]$$

In Fig.11a, the As concentrations are given in a combination with the lithography. Very high concentrations are found in the upper part of the Holocene aquifer. The Holocene aquifer is mainly sand, bounded by an upper and lower layer of clay. The Pleistocene aquifer is below. The calculated reactive surface area of the sediment is given in Fig.11b. On average, it is about A_{sed} = 1000 m^2/kg sediment, but the number varies very strongly. The lowest values ($A_{sed} \approx 30$ m^2/kg sediment) are found in the upper part of the sandy aquifer at 25-46 m. Deeper in the upper aquifer profile (46-100 m), the average A_{sed} is about 160 m^2/kg. The corresponding SSA are respectively

~15 and 90 m^2/g, which contrasts with the SSA in the upper clay layer (~350±250 m^2/g) and the Pleistocene sand (250 m^2/g). These low numbers are also much smaller than the average initial SSA obtained from analysis of the data fig.2

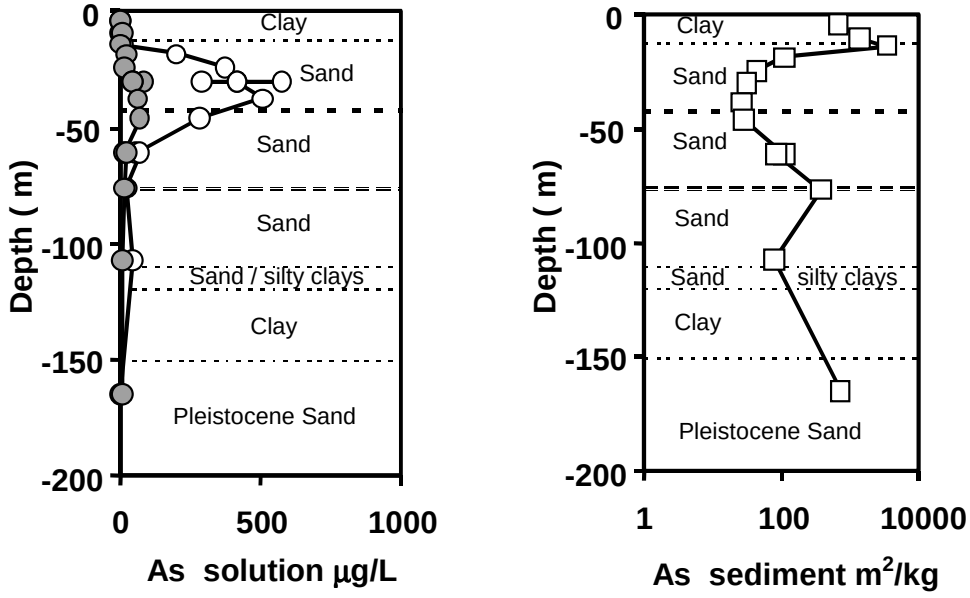

Fig 11a. The As(V) and As(III) concentrations (colored and open sphere respectively) and b) the calculated effective reactive surface area A_{sed} of the sediment, with in addition, the lithography of a Holocene and Pleistocene aquifer. Data from Swartz et al. (2004).

The SSA obtained might be due to in-situ diagenesis or may originate from different conditions at sedimentation and burial. Let's assume that diagenesis plays a role and that the original sandy material had at the time of deposition a much higher SSA of for instance 350 m^2/g, the value found as the average in Fig.2 and in the top clay layer of the present profile. This implies that in the most extreme case, the SSA has decreased with about 95%. Application of this number (ΔA=95%) in the above scenario using in the last step with 100% As(V) reduction, leads to 560 µg As/L, which approximately fits with the highest measured As concentrations (Fig.11a). An effective SSA of about 90 m^2/g results in values in the order of around 30 µg As/L. However, it is important to realize that the calculated concentrations follow from the assumptions made, which are partly based on calculations in which the As concentrations itself were used as input.

Nevertheless, the scenario sketches a possible explanation for the high As concentrations in this profile.

From these scenario calculations, we learn that very high levels of As may be reached due to strong decrease of the reactive surface area and that small differences in a large ΔA like 80%, 90% or 95% lead in each step to doubling of the As concentrations (in the example from 140 to 280 and 560 μg As/L). It illustrates that small local differences may have a large impact leading to a large variation, which is experienced in field surveys. If the above scenario is realistic, the low value of SSA in the upper aquifer (~15 m^2/g) suggests that all fine particles have disappeared during diagenesis.

4. Conclusions

- The river waters of Bangladesh have a fairly constant As/P ratio but a variable As (≈ 0.5 - 2.5 μg As /L) and P concentration (≈ 0.02-0.08 mg P/L), probably due to PO_4^{3-}-AsO_4^{3-} ion competition with suspended (hydr)oxide particles.
- The As/P ratio during sediment formation is probably lower than the present As/P ratio in river waters of Bangladesh. The difference might be due to a high P concentration related to soil formation but a lower As concentration in ancient river waters is more likely. The average concentration might be about 0.3 μg As/L.
- The average As and P loading of the Fe (hydr)oxide fraction extracted with oxalate can be explained with an average initial SSA of about 350 m^2/g. This value can be considered as the initial value at sedimentation. This calculated initial SSA varies between about 200-600 m^2/g.
- The natural range of the P loadings on the Fe (hydr)oxide fraction is predominantly caused by a variation in the initial SSA. The natural span of the As loadings is additionally related to a variation in the As/P loading during sediment formation.
- In sediments, the main ions adsorbed by the natural Fe (hydr)oxide fraction are PO_4^{3-} (≈ 2.5 ±0.4 μmol/m^2), Ca^{2+} (≈ 1.3±0.1 μmol/m^2), Fe^{2+} (≈ 0-0.7 μmol/m^2) and Si (≈ 0-0.2 μmol/m^2). The adsorption of Mg^{2+} and HCO_3^- is negligible. The average As loading varies between ≈0.01-0.2 μmol/m^2. The adsorption of As(V) is favored over As(III) by Fe

(hydr)oxides, which may lead to a relatively high fraction of As(V) adsorbed even if the solution is dominated by As(III).

- The adsorption isotherms of As(III) and As(V) bound by iron (hydr) oxides are usually linear in natural systems due to the dominant effect of phosphate.
- The NH_4^+ and PO_4^{3-} concentrations resulting from reductive dissolution can be understood from a combination of ion exchange (NH_4^+) on clay/organic matter and P adsorption to the iron (hydr)oxides. The corresponding Fe^{2+} concentrations are strongly buffered by precipitation reactions like the formation of (amorphous) siderite. This fraction is probably extractable in 1 M HCl. In 60% of the Bangladesh samples this fraction is 25% or less.
- In the scenario analysis for average sediments the reductive dissolution with concomitant release of PO_4^{3-} was identified as the first factor that may increase very low As concentrations to levels that are beyond the WHO standards for drinking water. Reduction of As(V) to As(III) may approximately double these values and further doubling may occur each time that the surface area decreases by a factor of 2. The average concentration of 55 μg As/L (data base BGS/DPHE) may result from a transformation of about 50 % of the iron (hydr)oxides and 50 % reduction of the As(V) to As(III) assuming that limitation of the phosphate and ferrous ion concentration occurs due to (co) precipitation reactions.
- Even at a 95%- transformation (and more) of the iron oxide fraction, the vast majority of As is still adsorbed!
- The variation in the As/P ratio due to local variation in the conditions during sedimentation leads to the same variation in the sediments if the same events take place. The original amount of Fe (hydr)oxide and its SSA is not very relevant for the development of elevated As concentrations, except that a low amount of Fe (hydr)oxide may be easier transformed at a given degradation of organic matter (less active organic matter is required).

5. Appendix

The ion adsorption reactions for goethite have been described with a combination of the CD model (Hiemstra and van Riemsdijk, 1996) and the MUSIC model (Hiemstra et al., 1989; Hiemstra et al., 1996) using the extended Stern layer model (Hiemstra and van Riemsdijk, 2006). The capacitances of the inner- and outer-Stern layer are 0.85 F/m^2 and 0.75 F/m^2. The primary surface charge is developed by the protonation of two types of surface groups, $\equiv FeOH^{-1/2}$ and $\equiv Fe_3O^{-1/2}$ with effective site density of respectively 3.45 nm^{-2} and 2.7 nm^{-2}.

Table A1. The formation reactions of surface species determining the primary charge (Hiemstra and van Riemsdijk, 2006)

Surface species	$\equiv FeOH$	$\equiv Fe_3O$	Δz_0	Δz_1	Δz_2	H^+	Na^+	K^+	Cl^-	log*K*
$\equiv FeOH^{-1/2}$	1	0	0	0	0	0	0	0	0	0.00
$\equiv FeOH_2^{+1/2}$	1	0	1	0	0	1	0	0	0	9.20
$\equiv FeOH^{-1/2} \cdots Na^+$	1	0	0	1	0	0	1	0	0	-0.60
$\equiv FeOH^{-1/2} \cdots K^+$	1	0	0	1	0	0	0	1	0	-1.71
$\equiv FeOH_2^{+1/2} \cdots Cl^{-1}$	1	0	1	-1	0	1	0	0	1	8.76
$\equiv Fe_3O^{-1/2}$	0	1	0	0	0	0	0	0	0	0.00
$\equiv Fe_3OH^{+1/2}$	0	1	1	0	0	1	0	0	0	9.20
$\equiv Fe_3O^{-1/2} \cdots Na^+$	0	1	0	1	0	0	1	0	0	-0.60
$\equiv Fe_3O^{-1/2} \cdots K^+$	0	1	0	1	0	0	0	1	0	-1.71
$\equiv Fe_3OH^{+1/2} \cdots Cl^{-1}$	0	1	1	-1	0	1	0	0	1	8.76

Table A2. The formation reactions for the surface species of As(III) and As(V) (Stachowicz et al., 2006).

Species	$\equiv FeOH$	$\equiv Fe_3O$	Δz_0	Δz_1	Δz_2	H^+	$As(OH)_3^0$	AsO_4^{3-}	log*K*
$\equiv FeOAs(OH)_2$	1	0	0.16	-0.16	0	0	1	0	4.91
$\equiv Fe_2O_2\,AsOH$	0	1	0.34	-0.34	0	0	1	0	7.26
$\equiv FeOAsO_2OH$	1	0	0.30	-1.30	0	2	0	1	26.60
$\equiv Fe_2O_2\,AsO_2$	1	0	0.47	-1.47	0	2	0	1	29.27
$\equiv Fe_2O_2\,AsOOH$	2	0	0.58	-0.58	0	3	0	1	33.00

Table A3. The formation reactions for the surface species of PO_4^{3-} (Rahnemaie et al., 2007b).

Species	≡ FeOH	≡ Fe_3O	Δz_0	Δz_1	Δz_2	H^+	PO_4^{-3}	log*K*
≡ $Fe_2O_2PO_2$	2	0	0.46	-1.46	0	2	1	29.77
≡ $FeOPO_2OH$	1	0	0.28	-1.28	0	2	1	27.65

Table A4. The formation reactions for the surface species of Ca^{2+} and Mg^{2+} (Stachowicz et al., 2007b).

Species	≡ FeOH	≡ Fe_3O	Δz_0	Δz_1	Δz_2	H^+	Ca^{2+}	Mg^{2+}	log*K*
≡ $FeOH^{-1/2}\cdots Ca^{2+}$	1	0	0	2	0	0	1	0	3.00
≡ $Fe_3O^{-1/2}\cdots Ca^{2+}$	0	1	0	2	0	0	1	0	3.00
≡ FeOHCa	1	0	0.32	1.68	0	0	1	0	3.65
≡ FeOHCaOH	1	0	0.32	0.68	0	-1	1	0	-9.25
≡ $(FeOH)_2Mg$	2	0	0.71	1.29	0	0	0	1	4.90
≡ $(FeOH)_2MgOH$	2	0	0.71	0.29	0	-1	0	1	-6.47

Table A5. The formation reaction for the surface species of CO_3^{-2} (Stachowicz et al., 2007a).

Species	≡ FeOH	≡ Fe_3O	Δz_0	Δz_1	Δz_2	H^+	CO_3^{2-}	log*K*
≡ Fe_2O_2CO	2	0	0.68	-0.68	0	2	1	22.33

Table A6. The formation reactions for the surface species of Fe^{2+} and Fe(II)-As(III) (Hiemstra, 2007).

Species	≡ FeOH	≡ Fe_3O	Δz_0	Δz_1	Δz_2	H^+	Fe^{2+}	$As(OH)_3^0$	log*K*
≡ $(FeO)_2\ Fe_{II}$	2	0	0.73	1.27	0	0	1	0	8.47
≡ $(FeO)_2Fe_{III}(OH)_2$	2	0	0.17	-0.17	0	-2	1	0	-9.31
≡ $FeOAs_{III}(OH)_3Fe_{II}$	1	0	0.08	0.92	0	-1	1	1	3.35

Table A7. The formation reactions for the surface species of H_4SiO_4 (Hiemstra et al., 2007).

Species	≡ FeOH	≡ Fe_3O	Δz_0	Δz_1	Δz_2	H^+	$H_4SiO_4^0$	log*K*
≡ $Fe_2O_2\ Si(OH)_2$	2	0	0.29	-0.29	0	0	1	5.85
≡ $Fe_2O_2\ SiOHOSi_3(OH)_9$	2	0	0.29	-0.29	0	0	4	13.98
≡ $Fe_2O_2\ SiOHOSi_3(OH)_8$	2	0	0.29	-1.29	0	-1	4	7.47

Table A8. Representative Gaines-Thomas ion exchange reactions and constants used.

Reaction			K_{GT}
½ X_2Ca + NH_4^+	⇔	XNH_4 + ½ Ca^{2+}	2.5
½ X_2Ca + K^+	⇔	XK + ½ Ca^{2+}	2.5
½ X_2Ca + ½ Mg^{2+}	⇔	½ X_2Mg + ½ Ca^{2+}	0.7
½ X_2Ca + ½ Fe^{2+}	⇔	½ X_2Fe + ½ Ca^{2+}	0.7

References

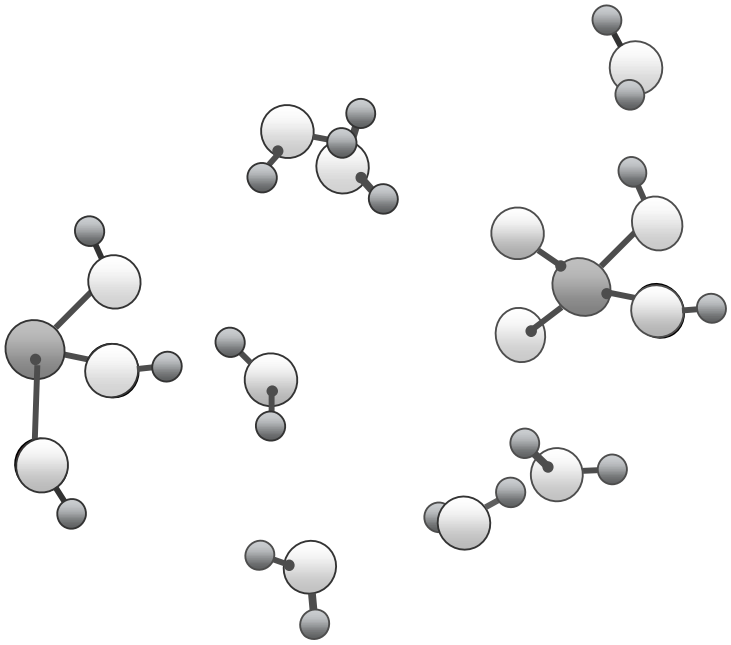

References

Ahmann D., Krumholz L. R., Hemond H. F., Lovley D. R., and Morel F. M. M. (1997) Microbial mobilization of arsenic from sediments of the Aberjona Watershed. *Environ. Sci. Technol.* **31**(10), 2923-2930.

Ali M. A. and Dzombak D. A. (1996) Effects of simple organic acids on sorption of Cu2+ and Ca2+ on goethite. *Geochim. Cosmochim. Acta* **60**(2), 291-304.

Anawar H. M., Akai J., and Sakugawa H. (2004) Mobilization of arsenic from subsurface sediments by effect of bicarbonate ions in groundwater. *Chemosphere* **54**(6), 753-762.

Antelo J., Avena M., Fiol S., Lopez R., and Arce F. (2005) Effects of pH and ionic strength on the adsorption of phosphate and arsenate at the goethite-water interface. *J. Colloid Interface Sci.* **285**(2), 476-486.

Appelo C. A. J., Weiden V. D., M. J. J. T., and C. C., L. (2002) Surface Complexation of Ferrous Iron and Carbonate on Ferrihydrite and the Mobilization of Arsenic. *Environ. Sci. Technol.* **36**(14), 3096 - 3103.

Arai Y. and Sparks D. L. (2001) ATR-FTIR spectroscopic investigation on phosphate adsorption mechanisms at the ferrihydrite-water interface. *J. Colloid Interface Sci.* **241**(2), 317-326.

Arai Y., Sparks D. L., and Davis J. A. (2004) Effects of dissolved carbonate on arsenate adsorption and surface speciation at the hematite-water interface. *Environ. Sci. Technol.* **38**(3), 817-824.

Arienzo M., Adamo P., Chiarenzelli J., Bianco M. R., and De Martino A. (2002) Retention of arsenic on hydrous ferric oxides generated by electrochemical peroxidation. *Chemosphere* **48**(10), 1009-1018.

Bargar J. R., Brown J., G. E., and Parks G. A. (1997) Surface complexation of Pb(II) at oxide-water interfaces: I. XAFS and bond-valence determination of mononuclear and polynuclear Pb(II) sorption products on aluminum oxides. *Geochim. Cosmochim. Acta* **61**(13), 2617-2637.

Bargar J. R., Kubicki J. D., Reitmeyer R., and Davis J. A. (2005) ATR-FTIR spectroscopic characterization of coexisting carbonate surface complexes on hematite. *Geochim. Cosmochim. Acta* **69**(6), 1527-1542.

Barrow N. J. and Bowden J. W. (1987) A comparison of models for describing the adsorption of anions A on a variable charge mineral surface. *J. Colloid Interface Sci.* **119**(1), 236-250.

Betancur J. D., Barrero C. A., Greneche J. M., and Goya G. F. (2004) The effect of water content on the magnetic and structural properties of goethite. *J. Alloy Compd.* **369**(1-2), 247-251.

BGS and DPHE. (2001) Arsenic contamination of groundwater in Bangladesh. In *Technical Report*, Vol. WC/00/19. BGS.

Blakey B. C. and James D. F. (2003) The viscous behaviour and structure of aqueous suspensions of goethite. *Colloids Surf., A* **231**(1-3), 19-30.

Boily J. F. (2003) AIM and ELF analyses and gas-phase acidities of some main-group oxyacids (HzXO4, X = Cl, S, P, Si and Br, Se, As, Ge). *J. Phys. Chem. A* **107**(21), 4276-4285.

Boily J. F., Sjoberg S., and Persson P. (2005) Structures and stabilities of Cd(II) and Cd(II)-phthalate complexes at the goethite/water interface. *Geochim. Cosmochim. Acta* **69**(13), 3219-3235.

Brown I. D. (1978) Bond Valences - Simple Structural Model for Inorganic-Chemistry. *Chem. Soc. Rev.* **7**(3), 359-376.

Brown I. D. and Altermatt D. (1985) Bond-Valence Parameters Obtained from a Systematic Analysis of the Inorganic Crystal-Structure Database. *Acta Crystallogr. Sect. B Struct. Sci.* **41**, 244-247.

Buffle J. (1990) *Complexation Reactions in Aquatic Systems. An Analytical Approach.* Ellis Horwood Limited.

Burleson D. J. and Penn R. L. (2006) Two-step growth of goethite from ferrihydrite. *Langmuir* **22**(1), 402-409.

Catalano J. G., Park C., Zhang Z., and Fenter P. (2006) Termination and water adsorption at the alpha-Al2O3 (012) - Aqueous solution interface. *Langmuir* **22**(10), 4668-4673.

Chakraborti D., Biswas B. K., Chowdhury T. R., Basu G. K., Mandal B. K., Chowdhury U. K., Mukherjee S. C., Gupta J. R., Chowdhury S. R., and Rathore K. C. (1999) Arsenic groundwater contamination and sufferings of people in Rajnandgaon district, Madhya Pradesh, India. *Curr. Sci.* **77**(4), 502-504.

Chakraborti D., Rahman M. M., Paul K., Chowdhury U. K., Sengupta M. K., Lodh D., Chanda C. R., Saha K. C., and Mukherjee S. C. (2002) Arsenic calamity in the Indian subcontinent: What lessons have been learned? *Talanta* **58**(1), 3-22.

Chowdhury T. R., Basu G. K., Mandal B. K., Biswas B. K., Samanta G., Chowdhury U. K., Chanda C. R., Lodh D., Lal Roy S., Saha K. C., Roy S., Kabir S., Quamruzzaman Q., and Chakraborti D. (1999) Arsenic poisoning in the Ganges delta. *Nature* **401**(6753), 545-546.

Combes J. M., Manceau A., Calas G., and Bottero J. Y. (1989) Formation of Ferric Oxides from Aqueous-Solutions - a Polyhedral Approach by X-Ray Absorption-Spectroscopy .1. Hydrolysis and Formation of Ferric Gels. *Geochim. Cosmochim. Acta* **53**(3), 583-594.

Cornell R. M., Posner A. M., and Quirk J. P. (1974) Crystal Morphology and Dissolution of Goethite. *J. Inorg. Nucl. Chem.* **36**(9), 1937-1946.

Das D., Samanta G., Mandal B. K., Chowdhury T. P., Chanda C. R., Chowdhury P. P., Basu G. K., and Chakraborti D. (1996) Arsenic in groundwater in six districts of West Bengal, India. *Environ. Geochem. Health* **18**(1), 5-15.

Davis J. A. (1977) Adsorption of trace elements and complexing ligands at the oxide/water interace. PhD thesis, Stanford University.

Davis J. A. and Leckie J. O. (1978) Surface Ionization and Complexation at Oxide-Water Interface .2. Surface Properties of Amorphous Iron Oxyhydroxide and Adsorption of Metal-Ions. *J. Colloid Interface Sci.* **67**(1), 90-107.

Deschamps E., Ciminelli V. S. T., Weidler P. G., and Ramos A. Y. (2003) Arsenic sorption onto soils enriched in Mn and Fe minerals. *Clay. Clay Miner.* **51**(2), 197-204.

Devlin J. P. and Buch V. (1997) Vibrational spectroscopy and modeling of the surface and subsurface of ice and of ice-adsorbate interactions. *Journal of Physical Chemistry B* **101**(32), 6095-6098.

Dixit S. and Hering J. G. (2003) Comparison of Arsenic(V) and Arsenic(III) Sorption onto Iron Oxide Minerals: Implications for Arsenic Mobility. *Environ. Sci. Technol.* **37**(18), 4182-4189.

Dixit S. and Hering J. G. (2006) Sorption of Fe(II) and As(III) on goethite in single- and dual-sorbate systems. *Chem. Geol.* **228**(1-3), 6-15.

Dzombak D. A. and Morel F. M. M. (1990) *Surface complexation modeling: Hydrous Ferric Oxide*.

Eggleston C. M., Hug S., Stumm W., Sulzberger B., and Afonso M. D. (1998) Surface complexation of sulfate by hematite surfaces: FTIR and STM observations. *Geochim. Cosmochim. Acta* **62**(4), 585-593.

Elzinga E. J. and Sparks D. L. (2007) Phosphate adsorption onto hematite: An in situ ATR-FTIR investigation of the effects of pH and loading level on the mode of phosphate surface complexation. *J. Colloid Interface Sci.* **308**(1), 53-70.

Farquhar M. L., Charnock J. M., Livens F. R., and Vaughan D. J. (2002) Mechanisms of Arsenic Uptake from Aqueous Solution by Interaction with Goethite, lepidocrocite, Mackinawite, and Pyrite: An X-ray Absorption Spectroscopy Study. *Environ. Sci. Technol.* **36**(8), 1757-1762.

Fendorf S., Eick M. J., Grossl P., and Sparks D. L. (1997) Arsenate and Chromate Retention Mechanisms on Goethite. 1. Surface Structure. *Environ. Sci. Technol.* **31**(2), 315 -320.

Fenter P. and Sturchio N. C. (2004) Mineral-water interfacial structures revealed by synchrotron X-ray scattering. *Progress Surf. Sci.* **77**, 171-258.

Foster A. L., Brown G. E., Tingle T. N., and Parks G. A. (1998) Quantitative arsenic speciation in mine tailings using X-ray absorption spectroscopy. *Am. Mineral.* **83**(5-6), 553-568.

Frankerberger W. T. (2002a) Environmental Chemistry of Arsenic. *published by Marcel Dekker, Inc,*.

Frankerberger W. T. (2002b) *Environmental Chemistry of Arsenic*. Chapter 8, Arsenic (V)/(III) Cycling in Soils and Natural Waters: Chemical and Microbiological Processes by Inskeep, W.P., McDermott, T.R., Fendorf, S., Marcel Dekker, Inc,.

Gaboriaud F. and Ehrhardt J.-J. (2003) Effects of different crystal faces on the surface charge of colloidal goethite ([alpha]-FeOOH) particles: an experimental and modeling study. *Geochim. Cosmochim. Acta* **67**(5), 967-983.

Gao Y. and Mucci A. (2001) Acid base reactions, phosphate and arsenate complexation, and their competitive adsorption at the surface of goethite in 0.7 M NaCl solution. *Geochim. Cosmochim. Acta* **65**(14), 2361-2378.

Garcia-Sanchez A., Moyano A., and Mayorga P. (2005) High arsenic contents in groundwater of central Spain. *Environmental Geology* **47**(6), 847-854.

Geelhoed J. S., Hiemstra T., and Riemsdijk W. H. V. (1998) Competetive Interaction between Phosphate and Citrate on Goethite. *Environ. Sci. Technol.* **32**(14), 2119-2123.

Geelhoed J. S., Hiemstra T., and Van Riemsdijk W. H. (1997) Phosphate and sulfate adsorption on goethite: Single anion and competitive adsorption. *Geochim. Cosmochim. Acta* **61**(12), 2389-2396.

Goldberg S. and Johnston C. T. (2001) Mechanisms of Arsenic Adsorption on Amorphous Oxides Evaluated Using Macroscopic Measurements, Vibrational Spectroscopy, and Surface Complexation Modeling. *J. Colloid Interface Sci.* **234**(1), 204-216.

Gomez-Ariza J. L., Sanchez-Rodas D., Beltran R., Corns W., and Stockwel P. (1998) Evaluation of atomic fluorescence spectrometry as a sensitive detection technique for arsenic speciation. *Appl. Organomet. Chem.* **12**(6), 439-447.

Gomez-Caminero A., Howe P., Hughes M., Kenyon E., Lewis D. R., Moore M., Ng J., Aito A., and Becking G. (2001) Arsenic and Arsenic Compounds. In *Environmental Health Criteria 224*. World Health Organization.

Grafe M. and Sparks D. L. (2005) Kinetics of zinc and arsenate co-sorption at the goethite-water interface. *Geochim. Cosmochim. Acta* **69**(19), 4573-4595.

Gustafsson J. P. (2001) Modelling competitive anion adsorption on oxide minerals and an allophane-containing soil. *Eur. J. Soil Sci.* **52**(4), 639-653.

Han B., Zimbron J., Runnells T., Shen Z., and Wickramasinghe S. R. (2003) New arsenic standard spurs search for cost-effective removal techniques. *J. Amer. Water Works Associat.* **95**(10), 109-118.

Harvey C. F., Swartz C. H., Badruzzaman A. B. M., Keon-Blute N., Yu W., Ali M. A., Jay J., Beckie R., Niedan V., Brabander D., Oates P. M., Ashfaque K. N., Islam S., Hemond H. F., and Ahmed M. F. (2002) Arsenic mobility and groundwater extraction in Bangladesh. *Science* **298**, 1602-1606.

Harvey C. F., Swartz C. H., Badruzzaman A. B. M., Keon-Blute N., Yu W., Ali M. A., Jay J., Beckie R., Niedan V., Brabander D., Oates P. M., Ashfaque K. N., Islam S., Hemond H. F., and Ahmed M. F. (2005) Groundwater arsenic contamination on the Ganges Delta: biogeochemistry, hydrology, human perturbations, and human suffering on a large scale. *Compt. Rend. Geosci.* **337**(1-2), 285-296.

Hawthorne F. C. (1976) Hydrogen Positions in Scorodite. *Acta Crystallogr. Sect. B Struct. Sci.* **32**(OCT15), 2891-2892.

Hayes K. F., Roe A. L., Brown G. E., Hodgson K. O., Leckie J. O., and Parks G. A. (1987) Insitu X-Ray Absorption Study of Surface Complexes - Selenium Oxyanions on Alpha-Feooh. *Science* **238**(4828), 783-786.

Hazemann J. L., Bérar J. F., and Manceau A. (1991) Rietveld Studies of the Aluminium-Iron Substitution in Synthetic Goethite. *Mater. Sci. Forum* **79**, 821-826.

Hiemstra T. (2007) Adsorption and surface oxidation of Fe(II) on metal (hydr)oxides. *Geochem. Cosmochim. Acta* **submitted**.

Hiemstra T., Barnett M. O., and Riemsdijk W. H. v. (2007) Interaction of Silicic Acid with Goethite. *J. Colloid Interface Sci.* **accepted**.

Hiemstra T., de Wit J. C. M., and van Riemsdijk W. H. (1989a) Multisite Proton Adsorption Modeling at the Solid-Solution Interface of (Hydr)Oxides - a New Approach .2. Application to Various Important (Hydr)Oxides. *J. Colloid Interface Sci.* **133**(1), 105-117.

Hiemstra T., Rahnemaie R., and van Riemsdijk W. H. (2004) Surface complexation of carbonate on goethite: IR spectroscopy, structure and charge distribution. *J. Colloid Interface Sci.* **278**(2), 282-290.

Hiemstra T. and Riemsdijk W. H. V. (2007) Surafce complexation of selenite on goethite: MO/DFT geometry and charge distribution. *Croatica Chemica Acta* **accepted**.

Hiemstra T. and van Riemsdijk W. H. (1996) A Surface Structural Approach to Ion Adsorption: The Charge Distribution (CD) Model. *J. Colloid Interface Sci.* **179**(2), 488-508.

Hiemstra T. and van Riemsdijk W. H. (1999) Surface Structural Ion Adsorption Modeling of Competitive Binding of Oxyanions by Metal (Hydr)oxides. *J. Colloid Interface Sci.* **210**(1), 182-193.

Hiemstra T. and van Riemsdijk W. H. (2000) Fluoride Adsorption on Goethite in Relation to Different Types of Surface Sites. *J. Colloid Interface Sci.* **225**(1), 94-104.

Hiemstra T. and van Riemsdijk W. H. (2006) On the relationship between charge distribution, surface hydration and the surface of the interface of metal hydroxides. *J. Colloid Interface Sci.* **301**, 1-18.

Hiemstra T., van Riemsdijk W. H., and Bolt G. H. (1989b) Multisite proton adsorption modeling at the solid/solution interface of (hydr)oxides: A new approach : I. Model description and evaluation of intrinsic reaction constants. *J. Colloid Interface Sci.* **133**(1), 91-104.

Hiemstra T., Venema P., and van Riemsdijk W. H. (1996) Intrinsic Proton Affinity of Reactive Surface Groups of Metal (Hydr)oxides: The Bond Valence Principle. *J. Colloid Interface Sci.* **184**(2), 680-692.

Hingston F. J., Posner A. M., and Quirk J. P. (1971) Competitive Adsorption of Negatively Charged Ligands on Oxides Surfaces. *Diss. Faraday Soc.* **52**, 334-342.

Hingston F. J., Posner A. M., and Quirk J. P. (1974) Anion adsorption by goethite and gibbsite II. Desorption of anions from hydrous oxide surfaces. *J. Soil Sci.* **25**, 16-26.

Holm T. R. (2002) Effects of CO3(2-), Si and PO4(3-) on Arsenic sorption to HFO. *J. Am. Water Works Assoc.* **94**(4), 174-181.

Horneman A., van Geen A., Kent D. V., Mathe P. E., Zheng Y., Dhar R. K., O'Connell S., Hoque M. A., Aziz Z., and Shamsudduha M. (2004) Decoupling of As and Fe release to Bangladesh groundwater under reducing conditions. Part I: Evidence from sediment profiles. *Geochim. Cosmochim. Acta* **68**(17), 3459-3473.

Hsi C.-k. D. and Langmuir D. (1985) Adsorption of uranyl onto ferric oxyhydroxides: Application of the surface complexation site-binding model. *Geochim. Cosmochim. Acta* **49**(9), 1931-1941.

Hsia T. H., Lo S. L., and Lin C. F. (1992) As(V) Adsorption on Amorphous Iron-Oxide - Triple Layer Modeling. *Chemosphere* **25**(12), 1825-1837.

Inskeep W. P., McDermott T. R., and Fendorf S. (2002) Arsenic (V)/(III) Cycling in Soils and Natural Waters: Chemical and Microbiological Processes. In *Environmental Chemistry of Arsenic*, Vol. Chapter 8 (ed. W. T. Frankerberger), pp. 186. Marcel Dekker, Inc,.

Islam F. S., Gault A. G., Boothman C., Polya D. A., Charnock J. M., Chatterjee D., and Lloyd J. R. (2004) Role of metal-reducing bacteria in arsenic release from Bengal delta sediments. *Nature* **430**(6995), 68-71.

Israelachvili J. and Wennerstrom H. (1996) Role of hydration and water structure in biological and colloidal interactions. *Nature* **379**(6562), 219-225.

Jain A. and Loeppert R. H. (2000) Effect of Competing Anions on the Adsorption of Arsenate and Arsenite by Ferrihydrite. *J. Environ. Qual.* **29**, 1422-1430.

Jain A., Raven K. P., and Loeppert R. H. (1999) Arsenite and Arsenate Adsorption on Ferrihydrite: Surface Charge Reduction and Net OH- Release Stoichiometry. *Environ. Sci. Technol.* **33**(8), 1179-1184.

Jambor J. L. and Dutrizac J. E. (1998) Occurrence and constitution of natural and synthetic ferrihydrite, a widespread iron oxyhydroxide. *Chem. Rev.* **98**(7), 2549-2585.

Katsoyiannis I. A. and Zouboulis A. I. (2002) Removal of arsenic from contaminated water sources by sorption onto iron-oxide-coated polymeric materials. *Water Res.* **36**(20), 5141-5155.

Keizer M. G. and van Riemsdijk W. H. (1998) Ecosat. In *Technical Report*. Department Soil Science and Plant Nutrition, Wageningen Agricultural University.

Kim M. J., Nriagu J., and Haack S. (2000) Carbonate ions and arsenic dissolution by groundwater. *Environ. Sci. Technol.* **34**(15), 3094-3100.

Kinniburgh D. G. (1993) Fit. In *Technical Report*. BGS.

Kitahama K., Kiriyama R., and Baba Y. (1975) Refinement of Crystal-Structure of Scorodite. *Acta Crystallogr. Sect. B Struct. Sci.* **B 31**(JAN15), 322-324.

Kong J., White C. A., Krylov A. I., Sherrill D., Adamson R. D., Furlani T. R., Lee M. S., Lee A. M., Gwaltney S. R., Adams T. R., Ochsenfeld C., Gilbert A. T. B., Kedziora G. S., Rassolov V. A., Maurice D. R., Nair N., Shao Y. H., Besley N. A., Maslen P. E., Dombroski J. P., Daschel H., Zhang W. M., Korambath P. P., Baker J., Byrd E. F. C., Van

Voorhis T., Oumi M., Hirata S., Hsu C. P., Ishikawa N., Florian J., Warshel A., Johnson B. G., Gill P. M. W., Head-Gordon M., and Pople J. A. (2000) Q-chem 2.0: A high-performance ab initio electronic structure program package. *J. Comput. Chem.* **21**(16), 1532-1548.

Kosmulski M., Durand-Vidal S., Maczka E., and Rosenholm J. B. (2004) Morphology of synthetic goethite particles. *J. Colloid Interface Sci.* **271**(2), 261-269.

Kosmulski M., Maczka E., Jartych E., and Rosenholm J. B. (2003) Synthesis and characterization of goethite and goethite-hematite composite: experimental study and literature survey. *Adv. Colloid Interface Sci.* **103**(1), 57-76.

Kostka J. E. and Luther G. W. (1994) Partitioning and Speciation of Solid-Phase Iron in Salt-Marsh Sediments. *Geochim. Cosmochim. Acta* **58**(7), 1701-1710.

Kubicki J. D. (2005) Comparison of As(III) and As(V) complexation onto Al- and Fe-hydroxides. In *Advances in Arsenic Research*, Vol. 915, pp. 104-117.

Kwon K. D. and Kubicki J. D. (2004) Molecular orbital theory study on surface complex structures of phosphates to iron hydroxides: Calculation of vibrational frequencies and adsorption energies. *Langmuir* **20**(21), 9249-9254.

Ladeira A. C. Q., Ciminelli V. S. T., Duarte H. A., Alves M. C. M., and Ramos A. Y. (2001) Mechanism of anion retention from EXAFS and density functional calculations: Arsenic (V) adsorbed on gibbsite. *Geochim. Cosmochim. Acta* **65**(8), 1211-1217.

Ler A. and Stanforth R. (2003) Evidence for surface precipitation of phosphate on goethite. *Environ. Sci. Technol.* **37**(12), 2694-2700.

Manceau A. (1995) The Mechanism of Anion Adsorption on Iron-Oxides - Evidence for the Bonding of Arsenate Tetrahedra on Free Fe(O,Oh)(6) Edges. *Geochim. Cosmochim. Acta* **59**(17), 3647-3653.

Manceau A. and Charlet L. (1994) The Mechanism of Selenate Adsorption on Goethite and Hydrous Ferric-Oxide. *J. Colloid Interface Sci.* **168**(1), 87-93.

Manceau A. and Combes J. M. (1988) Structure of Mn and Fe Oxides and Oxyhydroxides - a Topological Approach by Exafs. *Phys. Chem. Miner.* **15**(3), 283-295.

Manceau A., Nagy K. L., Spadini L., and Ragnarsdottir K. V. (2000) Influence of anionic layer structure of Fe-oxyhydroxides on the structure of Cd surface complexes. *J. Colloid Interface Sci.* **228**(2), 306-316.

Mandal B. K., Chowdhury T. R., Samanta G., Basu G. K., Chowdhury P. P., Chanda C. R., Lodh D., Karan N. K., Dhar R. K., Tamili D. K., Das D., Saha K. C., and Chakraborti D. (1996) Arsenic in groundwater in seven districts of West Bengal, India—The biggest aresenic calamity in the world. *Curr. Sci.* **70**(11), 976-986.

Mandal B. K. and Suzuki K. T. (2002) Arsenic round the world: a review. *Talanta* **58**(1), 201-235.

Manna B. R., Dey S., Debnath S., and Gosh U. C. (2003) Removal of arsenic from groundwater using crystalline hydrous ferric oxide (CHFO). *Water Qual. Res. J. Canada* **38**(1), 193-210.

Manning B. A., Fendorf S. E., and Goldberg S. (1998) Surface Structures and Stability of Arsenic(III) on Goethite: Spectroscopic Evidence for Inner-Sphere Complexes. *Environ. Sci. Technol.* **32**(16), 2383 - 2388.

Manning B. A. and Goldberg S. (1996) Modeling competitive adsorption of arsenate with phosphate and molybdate on oxide minerals. *Soil Sci. Soc. Am. J.* **60**(1), 121-131.

Manning B. A., Hunt M. L., Amrhein C., and Yarmoff J. A. (2002) Arsenic(III) and Arsenic(V) reactions with zerovalent iron corrosion products. *Environ. Sci. Technol.* **36**(24), 5455-5461.

Manning B. A. and Suarez D. L. (2000) Modeling of arsenic (III) adsorption and heterogeneous oxidation kinetics in soils. *Soil Sci Soc Am J* **64**(1), 128-137.

McNeill L. A., Chen H. W., and Edwards M. (2002) Aspects of Arsenic Chemistry in relation to occurrence, health, and treatment. In *Environmental chemistry of Arsenic*. Marcel Dekker Inc.

Meng X., Korfiatis G. P., Bang S., and Bang K. W. (2002) Combined effects of anions on arsenic removal by iron hydroxides. *Toxicol. Lett.* **133**(1), 103-111.

Moreno E., Camara C., Corns W. T., Bryce D. W., and Stockwell P. B. (2000) Arsenic speciation in beverages by direct injection-ion chromatography - hydride generation atomic fluorescence spectrometry. *J. Autom. Methods Manage. Chem.* **22**(2), 33-39.

Murphy P. J., Posner A. M., and Quirk J. P. (1974) Gel Filtration Chromatography of Partially Neutralized Ferric Solutions. *J. Colloid Interface Sci.* **52**(2), 229-238.

Neuberger C. S. and Helz G. R. (2005) Arsenic(III) carbonate complexing. *Appl. Geochem.* **20**(6), 1218-1225.

Nickson R. T., McArthur J. M., Burgess W. G., Ahmed K. M., Ravenscroft P., and Rahman M. T. (1998) Arsenic poisoning of Bangladesh groundwater. *Nature* **395**(6700), 388.

Nickson R. T., McArthur J. M., Ravenscroft P., Burgess W. G., and Ahmed K. M. (2000) Mechanism of arsenic release to groundwater, Bangladesh and West Bengal. *App. Geochem.* **15**(4), 403-413.

Ona-Nguema G., Morin G., Juillot F., Calas G., and Brown G. E. (2005) EXAFS analysis of arsenite adsorption onto two-line ferrihydrite, hematite, goethite, and lepidocrocite. *Environ. Sci. Technol.* **39**(23), 9147-9155.

Pashley R. M. and Israelachvili J. N. (1984) Molecular Layering of Water in Thin-Films between Mica Surfaces and Its Relation to Hydration Forces. *J. Colloid Interface Sci.* **101**(2), 511-523.

Pedersen H. D., Postma D., Jakobsen R., and Larsen O. (2005) Fast transformation of iron oxyhydroxides by the catalytic action of aqueous Fe(II). *Geochim. Cosmochim. Acta* **69**(16), 3967-3977.

Pierce M. L. and Moore C. B. (1982) Adsorption of arsenite and arsenate on amorphous iron hydroxide. *Water Res.* **16**(7), 1247-1253.

Ponthieu M., Juillot F., Hiemstra T., van Riemsdijk W. H., and Benedetti M. F. (2006) Metal ion binding to iron oxides. *Geochim. Cosmochim. Acta* **70**(11), 2679-2698.

Prelot B., Villieras F., Pelletier M., Gerard G., Gaboriaud F., Ehrhardt J.-J., Perrone J., Fedoroff M., Jeanjean J., and Lefevre G. (2003) Morphology and surface heterogeneities in synthetic goethites. *J. Colloid Interface Sci.* **261**(2), 244-254.

Radu T., Subacz J. L., Phillipi J. M., and Barnett M. O. (2005) Effects of Dissolved Carbonate on Arsenic Adsorption and Mobility. *Environ. Sci. Technol.* **39**(20), 7875-7882.

Rahnemaie R., Hiemstra T., and van Riemsdijk W. H. (2006a) Inner- and outer-sphere complexation of ions at the goethite-solution interface. *J. Colloid Interface Sci.* **297**(2), 379-388.

Rahnemaie R., Hiemstra T., and van Riemsdijk W. H. (2006b) A new surface structural approach to ion adsorption: Tracing the location of electrolyte ions. *J. Colloid Interface Sci.* **293**(2), 312-321.

Rahnemaie R., Hiemstra T., and van Riemsdijk W. H. (2007a) Carbonate adsorption on goethite in competition with phosphate. *J. Colloid Interface Sci.*(accepted).

Rahnemaie R., Hiemstra T., and van Riemsdijk W. H. (2007b) Geometry, Charge Distribution, and Surface Speciation of Phosphate on Goethite. *J. Colloid Interface Sci.* **accepted**.

Ramirez-Solis A., Mukopadhyay R., Rosen B. P., and Stemmler T. L. (2004) Experimental and theoretical characterization of arsenite in water: Insights into the coordination environment of As-O. *Inorg. Chem.* **43**(9), 2954-2959.

Raven K. P., Jain A., and Loeppert R. H. (1998) Arsenite and Arsenate Adsorption on Ferrihydrite: Kinetics, Equilibrium, and Adsorption Envelopes. *Environ. Sci. Technol.* **32**(3), 344 - 349.

Rietra R. P. J. J., Hiemstra T., and Riemsdijk W. H. V. (2001a) Interaction between Calcium and Phosphate Adsorption on Goethite. *Environ. Sci. Technol.* **35**(16), 3369-3374.

Rietra R. P. J. J., Hiemstra T., and van Riemsdijk W. H. (2001b) Comparison of Selenate and Sulfate Adsorption on Goethite. *J. Colloid Interface Sci.* **240**(2), 384-390.

Roberts D. R., Ford R. G., and Sparks D. L. (2003) Kinetics and mechanisms of Zn complexation on metal oxides using EXAFS spectroscopy. *J. Colloid Interface Sci.* **263**(2), 364-376.

Roden E. E. and Zachara J. M. (1996) Microbial reduction of crystalline iron(III) oxides: Influence of oxide surface area and potential for cell growth. *Environ. Sci. Technol.* **30**(5), 1618-1628.

Rustad J. R. and Felmy A. R. (2005) The influence of edge sites on the development of surface charge on goethite nanoparticles: A molecular dynamics investigation. *Geochim. Cosmochim. Acta* **69**(6), 1405-1411.

Schwertmann U. and Cornell R. M. (1991). In *Iron Oxides in the Laboratory. Preparation and Characterization*, Vol. Chap. 5. VCH, Weinheim, Germany.

Sherman D. M. and Randall S. R. (2003) Surface complexation of arsenic(V) to iron(III) (hydr)oxides: structural mechanism from ab initio molecular geometries and EXAFS spectroscopy. *Geochim. Cosmochim. Acta* **67**(22), 4223-4230.

Smedley P. L. and Kinniburgh D. G. (2002) A review of the source, behaviour and distribution of arsenic in natural waters. *App. Geochem.* **17**(5), 517-568.

Spadini L., Manceau A., Schindler P. W., and Charlet L. (1994) Structure and Stability of Cd2+ Surface Complexes on Ferric Oxides .1. Results from Exafs Spectroscopy. *J. Colloid Interface Sci.* **168**(1), 73-86.

Spadini L., Schindler P. W., Charlet L., Manceau A., and Vala Ragnarsdottir K. (2003) Hydrous ferric oxide: evaluation of Cd-HFO surface complexation models combining CdK EXAFS data, potentiometric titration results, and surface site structures identified from mineralogical knowledge. *J. Colloid Interface Sci.* **266**(1), 1-18.

Sparks D. L. (1995) Environmental Soil Chemistry.

Stachowicz M., Hiemstra T., and van Riemsdijk W. H. (2006) Surface Speciation of As(III) and As(V) in relation to charge distribution. *J. Colloid Interface Sci.* **302**(1), 62-75.

Stachowicz M., Hiemstra T., and van Riemsdijk W. H. (2007a) Arsenic and bicarbonate adsorption on goethite. *Environ. Sci. Technol.* **41**(16), 5620-5625.

Stachowicz M., Hiemstra T., and van Riemsdijk W. H. (2007b) Multi-Competitive Interaction of As(III) and As(V) Oxy-anions with Ca^{2+}, Mg^{2+}, PO_4^{3-}, and CO_3^{2-} Ions on Goethite. (*submitted)*.

Su C. M. and Puls R. W. (2003) In situ remediation of arsenic in simulated groundwater using zerovalent iron: Laboratory column tests on combined effects of phosphate and silicate. *Environ. Sci. Technol.* **37**(11), 2582-2587.

Sun X. and Doner H. (1996) An Investigation of Arsenate and Arsenite Bonding structures on goethite by FTIR. *Soil Sci.* **161**, 865-872.

Sverjensky D. A. (2005) Prediction of surface charge on oxides in salt solutions: Revisions for 1 : 1 (M+L-) electrolytes. *Geochim. Cosmochim. Acta* **69**(2), 225-257.

Swartz C. H., Blute N. K., Badruzzman B., Ali A., Brabander D., Jay J., Besancon J., Islam S., Hemond H. F., and Harvey C. F. (2004) Mobility of arsenic in a Bangladesh aquifer: Inferences from geochemical profiles, leaching data, and mineralogical characterization. *Geochim. Cosmochim. Acta* **68**(22), 4539-4557.

Tadanier C. J. and Eick M. J. (2002) Formulating the charge-distribution multisite surface complexation model using FITEQL. *Soil Sci. Soc. Am. J.* **66**(5), 1505-1517.

Tejedor-Tejedor M. I. and Anderson M. A. (1990) Protonation of Phosphate on the Surface of Goethite as Studied by CIR-FTIR and Electrophoretic Mobility. *Langmuir* **6**, 602-611.

Thompson A., Chadwick O. A., Rancourt D. G., and Chorover J. (2006) Iron-oxide crystallinity increases during soil redox oscillations. *Geochim. Cosmochim. Acta* **70**(7), 1710-1727.

Toney M. F., Howard J. N., Richer J., Borges G. L., Gordon J. G., Melroy O. R., Wiesler D. G., Yee D., and Sorensen L. B. (1995) Distribution of water molecules at Ag(111)/electrolyte interface as studied with surface X-ray scattering. *Surf. Sci.* **335**, 326-332.

van der Zee C., Roberts D. R., Rancourt D. G., and Slomp C. P. (2003) Nanogoethite is the dominant reactive oxyhydroxide phase in lake and marine sediments. *Geology* **31**(11), 993-996.

van Geen A., Robertson A. P., and Leckie J. O. (1994) Complexation of carbonate species at the goethite surface: Implications for adsorption of metal ions in natural waters. *Geochim. Cosmochim. Acta* **58**, 2073-2086.

Venema P., Hiemstra T., and van Riemsdijk W. H. (1996) Multisite Adsorption of Cadmium on Goethite. *J. Colloid Interface Sci.* **183**(2), 515-527.

Venema P., Hiemstra T., and van Riemsdijk W. H. (1997) Interaction of Cadmium with Phosphate on Goethite. *J. Colloid Interface Sci.* **192**(1), 94-103.

Venema P., Hiemstra T., Weidler P. G., and van Riemsdijk W. H. (1998) Intrinsic Proton Affinity of Reactive Surface Groups of Metal (Hydr)oxides: Application to Iron (Hydr)oxides. *J. Colloid Interface Sci.* **198**(2), 282-295.

Villalobos M. and Leckie J. O. (2000) Carbonate adsorption on goethite under closed and open CO2 conditions. *Geochim. Cosmochim. Acta* **64**(22), 3787-3802.

Villalobos M. and Leckie J. O. (2001) Surface Complexation Modeling and FTIR Study of Carbonate Adsorption to Goethite. *J. Colloid Interface Sci.* **235**(1), 15-32.

Voegelin A. and Hug S. J. (2003) Catalyzed oxidation of arsenic(III) by hydrogen peroxide on the surface of ferrihydrite: An in situ ATR-FTIR study. *Environ. Sci. Technol.* **37**(5), 972-978.

Waychunas G. A., Kim C. S., and Banfield J. F. (2005) Nanoparticulate iron oxide minerals in soils and sediments: unique properties and contaminant scavenging mechanisms. *J. Nanopart. Res.* **7**(4-5), 409-433.

Waychunas G. A., Rea B. A., Fuller C. C., and Davis J. A. (1993) Surface chemistry of ferrihydrite: Part 1. EXAFS studies of the geometry of coprecipitated and adsorbed arsenate. *Geochim. Cosmochim. Acta* **57**(10), 2251-2269.

Weidler P. G., Hug S. J., Wetche T. P., and Hiemstra T. (1998) Determination of growth rates of (100) and (110) faces of synthetic goethite by scanning force microscopy. *Geochim. Cosmochim. Acta* **62**(21-22), 3407-3412.

Weidler P. G., Schwinn T., and Gaub H. E. (1996) Vicinal faces on synthetic goethite observed by atomic force microscopy. *Clays Clay Miner.* **44**(4), 437-442.

Weng L. P., Koopal L. K., Hiemstra T., Meeussen J. C. L., and Van Riemsdijk W. H. (2005) Interactions of calcium and fulvic acid at the goethite-water interface. *Geochim. Cosmochim. Acta* **69**(2), 325-339.

Westall J. and Hohl H. (1980) A comparison of electrostatic models for the oxide/solution interface. *Adv. Colloid Interface Sci.* **12**(4), 265-294.

Wijnja H. and Schulthess C. P. (2000) Vibrational spectroscopy study of selenate and sulfate adsorption mechanisms on Fe and Al (hydr)oxide surfaces. *J. Colloid Interface Sci.* **229**(1), 286-297.

Wilkie J. A. and Hering J. G. (1996) Adsorption of arsenic onto hydrous ferric oxide: effects of adsorbate/adsorbent ratios and co-occurring solutes. *Colloids Surf., A* **107**, 97-110.

Wilkie J. A. and Hering J. G. (1998) Rapid oxidation of geothermal arsenic(III) in streamwaters of the eastern Sierra Nevada. *Environ. Sci. Technol.* **32**(5), 657-662.

Williams A. G. B. and Scherer M. M. (2004) Spectroscopic evidence for Fe(II)-Fe(III) electron transfer at the iron oxide-water interface. *Environ. Sci. Technol.* **38**(18), 4782-4790.

Yoshida T., Yamauchi H., and Fan Sun G. (2004) Chronic health effects in people exposed to arsenic via the drinking water: dose-response relationships in review. *Toxicol. .App. Pharmacol.* **198**(3), 243-252.

Zeng L. (2003) A method for preparing silica-containing iron(III) oxide adsorbents for arsenic removal. *Water Res.* **37**(18), 4351-4358.

Zhang Y., Charlet L., and Schindler P. W. (1992) Adsorption of Protons, Fe(II) and Al(III) on Lepidocrocite (Gamma-FeOOH). *Colloid Surface A* **63**(3-4), 259-268.

Zhao H. S. and Stanforth R. (2001) Competitive adsorption of phosphate and arsenate on goethite. *Environ. Sci. Technol.* **35**(24), 4753-4757.

Zheng Y., van Geen A., Stute M., Dhar R., Mo Z., Cheng Z., Horneman A., Gavrieli I., Simpson H. J., Versteeg R., Steckler M., Grazioli-Venier A., Goodbred S., Shahnewaz M., Shamsudduha M., Hoque M. A., and Ahmed K. M. (2005) Geochemical and hydrogeological contrasts between shallow and deeper aquifers in two villages of Araihazar, Bangladesh: Implications for deeper aquifers as drinking water sources. *Geochim. Cosmochim. Acta* **69**(22), 5203-5218.

Summary

Introduction

The discovery of arsenic contamination in groundwater around the world has stimulated the scientific community to initiate research activities. The data obtained in field studies point to iron oxides as a source of arsenic in water. Besides, most of the water purification and waste treatment techniques related with arsenic contamination are either based on co-precipitation with iron oxides and/or adsorption on iron oxides. For a better understanding of what conditions in nature cause naturally elevated arsenic concentrations as well as for designing better treatment techniques an increase in our fundamental knowledge on the interaction of arsenic in complex environmental matrices with iron oxides is essential.

Surface Speciation of As(III) and As(V) in Relation to Charge Distribution (Chapter 2)

Metal (hydr)-oxides are omnipresent in nature. They may contribute to the control of the mobility and bioavailability of many elements in the environment via adsorption and desorption processes. Ion binding properties of metal (hydr)-oxides are strongly determined by the structure of the surface and the structure of the surface complexes formed. Incorporation of the microscopic information, i.e. the structure(s) of the adsorbed entities, in the interpretation of macroscopic adsorption characteristics, is vital for a valid modeling of transport processes and the bioavailability of toxic elements in the environment.

The adsorption of As(III) and As(V) on goethite has been studied as function of pH and loading. The data can be successfully described with the charge distribution (CD) model (extended Stern option) using realistic species observed by EXAFS. The CD values have been derived theoretically. Therefore, the Brown bond valence approach has been applied to MO/DFT optimized geometries of a series of hydrated complexes of As(III) and As(V) with Fe(III)(hydr)oxide. The calculated ionic CD values have been corrected for the effect of dipole orientation of interfacial water, resulting in overall interfacial CD coefficients that can be used to

describe the surface speciation as function of pH and loading. For As(III), the main surface species is a bidentate complex and a minor contribution of a monodentate species is found, which is in agreement with EXAFS. The CD values have also been fitted. Such an analysis of the adsorption data resulted in the same surface species. The fitted CD values for the bidentate complex points to the presence of strong As-O bonds with the surface and a weaker As-OH bond with the free OH ligand. This agrees quantitatively with the MO/DFT optimized geometry. Interpretation of free fitted CD values for As(V) binding suggests that the main surface species is a non protonated bidentate complex (B) with a contribution of a singly protonated surface complex (MH) at sub neutral pH and high loading. In addition, a protonated bidentate surface complex (BH) may be present. The same species are found if the theoretical CD values are used in the data analysis. The pH dependency of surface speciation is strongly influenced by the charge attribution of adsorbed species to the electrostatic surface plane while the effect of loading is primarily controlled by the amount of charge attributed to the 1-plane, illustrating the different action of the CD value. The MO/DFT geometry optimizations furthermore suggests that for As(V) the B, MH and BH surface complexes may have very similar As-Fe distances which may complicate the interpretation of EXAFS data.

The Arsenic -Bicarbonate Interaction on Goethite Particles (Chapter 3)

A large number of chemical and biogeochemical processes have been proposed that may explain the mobilization of arsenic compounds. High arsenic concentrations in groundwater are often accompanied by (bi)carbonate concentrations exceeding 300 mg/L. So far however, the literature sources give contradictory information on what the relation is, if any. It has been argued that high arsenic concentrations can be explained by the competitive action of bicarbonate. Like arsenate and arsenite, (bi)carbonate may adsorb strongly to iron oxides and therefore, it may influence the speciation and mobility of arsenic. For this reason, the effects of carbonate on the arsenic sorption are particularly important to understand.

The As(V) and As(III) interaction with HCO_3 has been studied for goethite systems using a pH and As concentration range that is relevant for field situations. Our study shows that dissolved bicarbonate may act as a competitor for both As(V) and As(III). In our closed systems, the largest effect of bicarbonate occurs at the lowest experimental pH values (pH~6.5), which is

related to the pH dependency of the carbonate adsorption process. The experimental data have been modeled with the charge distribution (CD) model. The CD-model was separately parameterized for goethite with 'single ion' adsorption data of HCO_3, As(III), and As(V). The competitive effect of HCO_3 on the As(III) and As(V) release could be predicted well. Application of the model shows that the natural As loading of aquifer materials (~ < 0.01-0.1 µmol/m^2 or <1-5 mg/kg) is at least about >1-2 orders of magnitude smaller than the As loading based on the competition of As-HCO_3 alone. It indicates that another, very prominent competitor, like phosphate and natural organic matter, will strongly contribute to the control of As in natural systems.

Multi-Competitive Interaction of As(III) and As(V) Oxy-anions with Ca^{2+}, Mg^{2+}, PO_4^{3-}, and CO_3^{2-} Ions on Goethite (Chapter 4)

Mobility and bioavailability of arsenic in complex natural systems seems to be determined by a combination of factors such as the redox conditions, the presence of mineral surfaces and organic matter. Another factor is the co-occurrence of elements that may enhance or suppress the As concentration of groundwater. For instance, specifically adsorbed inorganic ions, such as Ca^{2+}, Mg^{2+}, PO_4^{3-}, CO_3^{2-} may be relevant for a release of arsenic. These ions are commonly present in natural waters and will interact with As when adsorbed on the sites of metal oxides surfaces, *i.e*. they may suppress or promote the binding of each other.

Complex systems, simulating natural conditions like groundwater, have rarely been studied, since measuring and in particular, the modeling of such systems is very challenging. In this paper, the adsorption of the oxyanions of As(III) and As(V) on goethite has been studied in the presence of various inorganic macro-elements (Mg^{2+}, Ca^{2+}, PO_4^{3-}, CO_3^{2-}). We have used 'single-', 'dual-', and 'triple-ion' systems. The presence of Ca^{2+} and Mg^{2+} has no significant effect on As(III) oxyanion (arsenite) adsorption in the pH range relevant for natural groundwater (pH 5-9). In contrast, both Ca^{2+} and Mg^{2+} promote the adsorption of PO_4^{-3}. A similar effect is expected for the Ca^{2+} and Mg^{2+} interaction with As(V) oxyanions (arsenate). Phosphate is a major competitor for arsenate as well as arsenite. Although carbonate may act as competitor for both types of As oxyanions, the presence of significant concentrations of phosphate makes the interaction of (bi)carbonate insignificant. The data have been modeled with the charge distribution (CD) model

in combination with the extended Stern model option. In the modeling, independently calculated CD values were used for the oxyanions. The CD values for these complexes have been obtained from a bond valence interpretation of MO/DFT (molecular orbital / density functional theory) optimized geometries. The affinity constants (log*K*) have been found by calibrating the model on data from 'single-ion' systems. The parameters are used to predict the ion adsorption behavior in the multi-component systems. This way calibrated model is able to predict successfully the ion concentrations in the mixed 2- and 3-component systems as a function of pH and loading. From a practical perspective, data as well as calculations show the dominance of phosphate in regulating the As concentrations. Arsenite ($As(OH)_3$) is often less strongly bound than arsenate (AsO_4^{3-}) for conditions relevant in nature and arsenite responses less strongly to changes in the phosphate concentration compared to arsenate, *i.e.* $\delta \log C_{As(III)} / \delta \log C_{PO4} \approx 0.4$ and $\delta \log C_{As(V)} / \delta \log C_{PO4} \approx 0.9$ at pH 7.

Linking the Arsenic Binding to Goethite with the Binding to Amorphous Iron (Hydr)oxide (Chapter 5)

Natural systems are complex and thus the mobility and bioavailability of arsenic is affected by the presence of various mineral surfaces as well as other co-occurring elements. The field data support the hypothesis that As bound by iron oxides is a primary source of arsenic in Bangladesh groundwater. Iron oxides present in those sediments include Fe(III)-oxides such as hydrous ferric oxide (HFO), goethite or hematite, and possibly various mixed valence oxides such as magnetite and green rust. The amount of mobile arsenic under field conditions is often linked to the amount of iron found by oxalate extraction. It is believed that the oxalate-extracted Fe is related to oxide material with a high reactive surface area. HFO is seen as an important representative and for this reason it has been considered a useful proxy for the natural Fe (hydr)oxide fraction.

Primary structure of HFO and goethite has similarities, that have been used here as a common basis in the modeling of the proton and arsenic adsorption behavior on both materials. We differentiated between a relative number of the various reactive surface groups. For goethite the apparent fraction of top-end faces at the crystals was assumed to be 5%, while for HFO, a

50% contribution of similar faces was used. As a result, the primary charging behavior of goethite and HFO has been modeled in a coherent manner using the MUSIC model approach.

Adsorption of As(III) on HFO and goethite has been described assuming the formation of 2 species; a bidentate double corner (^{2}C) and a bidentate edge (^{2}E), as found by spectroscopy. In case of the adsorption of As(V) we were not able to identify the surface speciation unambiguously for the different crystal phases. We found a number of possible options. We arbitrary chose the following As(V) surface speciation: three species on the 110+100 face; i.e. a bidentate, a protonated bidentate and a protonated monodentate; and one type of species on the 021+001 face; i.e. a protonated monodentate. The CD values of the different type of As(III) and As(V) complexes were found independently from the MO/DFT optimized geometries of hydrated complexes. The affinity constants were fitted iteratively on adsorption data of goethite and HFO.

The modeling results have been tested on data from competition experiments. The model successfully predicted the competition between arsenic species, As(III) and As(V), on both minerals. For the highest surface loading discrepancies between the data and model predictions were observed for adsorption on HFO. However, it is possible that for such an extreme surface loadings a surface precipitation occurs.

The above suggests that despite the differences in the reactivity of goethite and HFO a link exists between the adsorption behavior of both minerals. Since HFO has been considered representative for 'field' conditions this is of important practical relevance. In future the CD model can be used in to predict adsorption in complex systems simulating natural conditions.

Biogeochemical Key Factors Controlling Arsenic in Groundwater (Chapter 6)

The As distribution in groundwater has been widely studied. Based on the results, a number of hypotheses have been formulated to explain the origin of elevated As concentrations. The large number of different explanations that have been suggested in recent years points to the complex nature of the arsenic contamination and proves that our understanding of the problem is still limited. The identification of processes is often based on speculations using correlations and observed trends as the relevant data, related to the solid phase composition, is unfortunately almost completely absent.

The aim of this study is to discuss quantitatively varies biogeochemical processes that may be involved in the release of As; i.e. the effect of pH and an equilibration with calcite, the release of PO_4^{3-} due to mineralization and reductive dissolution of Fe (hydr)oxides, the reduction of As(V) to As(III), and the effect of additional diagenetic processes that change the reactive surface area of the sediment. Eventually, a scenario has been used to predict the impact of changing conditions on the arsenic concentration in pore waters. In the scenario analysis for average sediments the reductive dissolution with a release of PO_4^{3-} was identified as the first factor that may increase very low As concentrations to levels that are beyond the WHO standards for drinking water. Reduction of As(V) to As(III) may approximately double these values and further doubling may occur each time that the surface area decreases by a factor of 2. The average concentration of 55 μg As/L may result from a transformation of about 50 % of the iron (hydr)oxides and 50 % reduction of the As(V) to As(III) assuming limitation of the phosphate and ferrous ion concentration due to (co) precipitation reactions. The CD model has been used in the calculations as it has been tested for a large number of ion-ion interactions relevant in the As binding process and it can successfully predict competitive effects in 2- and 3- component systems containing As.

Concluding remarks

Groundwater contamination with arsenic quickly became a key-issue on political agendas around the world as it turned out that the number of people affected by this problem worldwide is increasing. As a result of this research large adsorption datasets for mono-component and multi-component systems simulating relevant groundwater field situations were obtained. The data were interpreted with a molecular based adsorption model; i.e. the CD model. The model has been applied in order to predict the adsorption behavior of arsenic for a very wide range of chemical compositions as they are observed in the field. This way the thesis has added into providing quantitative understanding of the behavior of arsenic in natural waters. This knowledge may contribute to the long-term solutions for arsenic problems, such as an optimization of arsenic removal from drinking water as well as a methodology to guide the positioning of new arsenic-free wells.

Samenvatting

Inleiding

Wereldwijde ontdekkingen van arseenverontreinigingen in grondwater hebben de wetenschappelijke gemeenschap aangezet tot het verrichten van onderzoek naar deze problematiek. Veldgegevens wijzen in de richting van ijzeroxides als een bron van arseen in water. De meeste waterzuiveringtechnieken gericht op de verwijdering van arseen zijn trouwens ook gebaseerd op ofwel co-precipitatie met en/of adsorptie aan ijzeroxides. Voor een beter begrip van de condities die natuurlijk verhoogde arseenconcentraties veroorzaken, maar ook voor het ontwerpen van betere behandelingstechnieken, is een toename van onze fundamentele kennis over de interactie van arseen met ijzeroxides in complexe matrices onontbeerlijk.

Oppervlaktespeciatie van As(III) en As(V) in Relatie tot Ladingsverdeling (Hoofdstuk 2)

Metaal(hydr)oxides zijn in overal in de natuur aanwezig. Zij kunnen van invloed zijn op de mobiliteit en de biobeschikbaarheid van vele elementen in het milieu via adsorptie- en desorptieprocessen. Ionbindende eigenschappen van metaal(hydr)oxides worden sterk bepaald door de structuur van het oppervlak en de structuur van de gevormde oppervlaktecomplexen. Het meenemen van de “microscopische informatie”, ofwel de structu(u)r(en) van de geadsorbeerde entiteiten, bij de interpretatie van macroscopische adsorptiekarakteristieken, is essentieel voor een adequate modellering van transportprocessen en de biobeschikbaarheid van toxische stoffen in het milieu.

De adsorptie van As(III) en As(V) aan goethiet is gemodelleerd als een functie van de pH en belasting. De gegevens kunnen met succes worden beschreven met het “charge distribution” (CD) model (met uitgebreide Stern optie), wanneer realistische species, waargenomen met EXAFS, gebruikt worden. De CD-waarden zijn theoretisch afgeleid. Daarom is de zgn. “Brown bond valence”- benadering toegepast op MO/DFT-geoptimaliseerde geometrieën van een reeks van gehydrateerde complexen van As(III) en As(V) met Fe(III)(hydr)oxide. De berekende ionische CD-waarden zijn gecorrigeerd voor het effect van dipooloriëntatie van grensvlakwater,

resulterend in effectieve CD-waarden voor het grensvlak welke gebruikt kunnen worden voor de beschrijving van oppervlaktespeciatie als een functie van pH en belasting. Voor As(III) is een bidentaatcomplex de voornaamste oppervlaktespecies en wordt een kleine bijdrage van een monodentaatspecies gevonden, wat in overeenstemming is met EXAFS. De CD-waarden zij ook gefit. Een dergelijke analyse van de adsorptiedata resulteerde in dezelfde oppervlaktespecies. De gefitte CD-waarden voor het bidentaatcomplex wijzen op de aanwezigheid van sterke As-O-bindingen met het oppervlak en een zwakkere As-OH-binding met de vrije OH-ligand. Dit komt kwantitatief overeen met de MO/DFT-geoptimaliseerde geometrie. Interpretatie van de vrije gefitte CD-waarden voor As(V)-binding suggereert dat de belangrijkste oppervlaktespecies een niet-geprotoneerd bidentaatcomplex (B) is met een bijdrage van een enkelvoudig geprotoneerd oppervlaktecomplex (MH) op een subneutraal pH-niveau en bij een hoge belasting. Ook kan een geprotoneerd bidentaat-oppervlaktecomplex (BH) aanwezig zijn. Dezelfde species worden gevonden indien de theoretische CD-waarden worden gebruikt in de data-analyse. De pH-afhankelijkheid van de oppervlaktespeciatie wordt sterk beïnvloed door de ladingstoekenning van geadsorbeerde species aan het elektrostatische oppervlak, terwijl het effect van de belasting voornamelijk wordt bepaald door de hoeveelheid lading die toegekend wordt aan het “1-plane”, wat de afwijkende werking van de CD-waarde illustreert. De MO/DFT-geometrie-optimalisaties suggereren verder dat voor As(V) de oppervlaktecomplexen B, MH en BH zeer vergelijkbare As-Fe-afstanden kunnen hebben, wat de interpretatie van EXAFS-data kan bemoeilijken.

De Arseen-Bicarbonaat-Interactie op Goethietdeeltjes (Hoofstuk 3)

Er is een groot aantal chemische en biochemische processen voorgesteld die de mobilisatie van arseenverbindingen zouden kunnen verklaren. Hoge arseenconcentraties in grondwater gaan vaak samen met (bi)carbonaatconcentraties van meer dan 300 mg/L. Tot op heden geeft de literatuur echter tegenstrijdige informatie over wat de relatie precies is, als er al een relatie is. Er wordt gespeculeerd dat hoge arseenconcentraties verklaard kunnen worden door de competitieve werking van bicarbonaat. (Bi)carbonaat kan, net als arsenaat en arseniet, sterk adsorberen aan ijzeroxides en daarom kan het de speciatie en mobiliteit van arseen beïnvloeden. Daarom is het van groot belang de effecten van carbonaat op arseensorptie te doorgronden.

De interactie tussen As(V)/As(III) en HCO_3 is bestudeerd voor goethietsystemen met voor veldsituaties relevante ranges van pH en As concentraties. Onze studie laat zien dat opgelost

bicarbonaat competitie kan vertonen met zowel As(V) als As(III). In onze gesloten systemen treedt het grootste effect van bicarbonaat op bij de laagste pH-waarden die in de experimenten zijn gebruikt (pH≈6.5), wat samenhangt met de pH-afhankelijkheid van het carbonaatadsorptieproces. De experimentele gegevens zijn gemodelleerd met het CD-model. Het CD-model is afzonderlijk geparameteriseerd voor goethiet met "single ion"-adsorptiedata van HCO_3, As(III) en As(V). Het competitieve effect van HCO_3 op het vrijkomen van As(III) en As(V) kon goed voorspeld worden. Toepassing van het model laat zien dat de natuurlijke As-belasting van aquifermatrices (≈<0.01-0.1 µmol/m^2 of <1-5 mg/kg) minstens 1-2 ordes van grootte kleiner is dan de As-HCO_3 competitie. Dit laat zien dat een andere, zeer prominente *competitor*, zoals fosfaat en natuurlijk organisch materiaal, het gedrag van As sterk beïnvloedt.

Multi-competitieve Interactie van As(III) en As(V) Oxyanionen met Ca^{2+}, Mg^{2+}, PO_4^{3-} en CO_3^{2-}-ionen aan Goethiet.

De mobiliteit en biobeschikbaarheid van arseen in complexe natuurlijke systemen lijken bepaald te worden door een combinatie van factoren zoals de redoxcondities, de aanwezigheid van minerale oppervlakken en organische stof. Een andere factor is de gelijktijdige aanwezigheid van elementen die de aanwezigheid van arseen in grondwater kunnen verhogen of onderdrukken. Zo kunnen specifiek geadsorbeerde anorganische ionen, zoals Ca^{2+}, Mg^{2+}, PO_4^{3-} en CO_3^{2-}, belangrijk zijn bij het vrijkomen van arseen. Deze ionen komen in natuurlijke wateren voor en zullen de interactie met As aangaan voor adsorptie aan bindingsplaatsen op metaaloxideoppervlakken, d.w.z. ze kunnen elkaars binding aan deze oppervlakken vergemakkelijken of onderdrukken.

Complexe systemen welke de natuurlijke condities, zoals die in grondwater, simuleren, zijn zelden bestudeerd, omdat het meten in en met name ook het modelleren van deze systemen een grote uitdaging vormen. Voor dit hoofdstuk is de adsorptie van de oxyanionen van As(III) en As(V) aan goethiet in de aanwezigheid van verschillende anorganische macro-elementen (Ca^{2+}, Mg^{2+}, PO_4^{3-} en CO_3^{2-}) bestudeerd. We hebben hiervoor 'single-', 'dual-' en 'triple-ion' –systemen gebruikt. De aanwezigheid van Ca^{2+} en Mg^{2+} heeft geen significant effect op de adsorptie van As(III)-oxyanion (arseniet). Daarentegen stimuleren zowel Ca^{2+} als Mg^{2+} de adsorptie van PO_4^{3-}. Een soortgelijk effect wordt verwacht voor de interactie van Ca^{2+} en Mg^{2+} met As(V)-oxyanionen (arsenaat). Fosfaat is een belangrijke concurrent voor zowel arseniet als arsenaat. Hoewel

carbonaat als een concurrent kan fungeren voor beide typen van As-oxyanionen, wordt de interactie met (bi)carbonaat door de aanwezigheid van significante fosfaatconcentraties gemarginaliseerd. De data zijn gemodelleerd met het ladingsverdelingsmodel CD, in combinatie met de uitgebreide Stern-optie. Voor de berekeningen werden onafhankelijk berekende CD-waarden gebruikt voor de oxyanionen. De CD-waarden voor deze complexen zijn verkregen vanuit een bindingswaarde-interpretatie van MO/DFT (molecular orbital/density functional theory)-geoptimaliseerde geometrieën. De affiniteitsconstanten (log*K*) zijn gevonden door het model te calibreren op data van 'single-ion'-systemen. De parameters zijn gebruikt om het ionadsorptiegedrag in de multi-componentsystemen te voorspellen. Het op deze manier gecalibreerde model kan de ionconcentraties in de gemengde 2- en 3-componentsystemen als een functie van pH en belasting met succes voorspellen. Vanuit een praktisch perspectief laten zowel de data als de modelberekeningen de dominantie van fosfaat zien in het reguleren van de As-concentraties. In voor natuurlijke systemen relevante omstandigheden wordt arseniet ($As(OH)_3$) vaak minder sterk gebonden dan arsenaat (AsO_4^{3-}) en reageert arseniet minder sterk op veranderingen in de fosfaatconcentratie dan arsenaat: $\delta \log C_{As(III)} / \delta \log C_{PO4} \approx 0.4$ en $\delta \log C_{As(V)} / \delta \log C_{PO4} \approx 0.9$ bij pH 7.

Het Relateren van de Binding van Arseen aan Goethiet aan de Binding aan Amorf Ijzer(hydr)oxide (Hoofdstuk 5).

Natuurlijke systemen zijn complex en zodoende worden de mobiliteit en de biobeschikbaarheid van arseen beïnvloed door de aanwezigheid van verschillende minerale oppervlakken en de aanwezigheid van andere elementen. Veldgegevens ondersteunen de hypothese dat door ijzeroxides gebonden As een primaire bron is van het arseen in het grondwater van Bangladesh. Onder de in deze sedimenten aanwezige ijzeroxides behoren Fe(III)-oxides zoals HFO, (hydrous ferric oxide), goethiet of hematiet, en mogelijk verschillende *mixed valence* –oxiden zoals magnetiet en *green rust*. De hoeveelheid mobiel arseen is onder veldcondities vaak gerelateerd aan de hoeveelheid oxidemateriaal die gevonden wordt met oxalaatextractie. Er wordt verondersteld dat het oxalaat-geëxtraheerde Fe gerelateerd is aan oxidemateriaal met een hoogreactief oppervlak. HFO wordt gezien als een belangrijke vertegenwoordiger en om deze reden is HFO in beschouwing genomen als een bruikbare proxy voor de natuurlijke Fe (hydr)oxidefractie.

De primaire structuren van HFO en goethiet vertonen overeenkomsten die hier zijn gebruikt als een gemeenschappelijke basis in de modellering van het proton- en arseenadsorptiegedrag aan beide materialen. We hebben onderscheid gemaakt tussen een relatief aantal van de verschillende groepen van reactieve oppervlakken. Voor goethiet werd een aantoonbare fractie van *top-end faces* op de kristallen aangenomen van 5%, terwijl voor HFO een bijdrage van 50% van vergelijkbare faces werd gebruikt. Dit resulteerde in een coherente modellering van het primaire ladingsgedrag van goethiet en HFO met behulp van de MUSIC modelbenadering.

De adsorptie van As(III) aan HFO en goethiet is beschreven met de aanname van de vorming van 2 species: een *bidentate double corner* (^{2}C) en een *bidentate edge* (^{2}E), zoals aangetoond met behulp van spectroscopie. In het geval van de adsorptie van As(V) waren we niet in staat de oppervlaktespeciatie ondubbelzinnig te identificeren voor de verschillende kristalfasen: we vonden een aantal mogelijke opties. We hebben, arbitrair, voor de volgende As(V)-speciatie gekozen: drie species op de 110+100 *face*, namelijk een bidentaat, een geprotoneerde bidentaat en een geprotoneerde monodentaat; en één type species op de 021+001 face, namelijk een geprotoneerde monodentaat. De CD-waarden voor de verschillende typen As(III) en As(V)-complexen werden onafhankelijk verkregen vanuit de MO/DFT-geoptimaliseerde geometrieën van gehydrateerde complexen. De affiniteitsconstanten werden iteratief gefit op adsorptiedata van goethiet en HFO.

De modelresultaten zijn getest op data van competitie-experimenten. Het model voorspelde de competitie tussen de arseenspecies en beide mineralen met succes. Voor de hoogste oppervlaktebelasting werden discrepanties waargenomen tussen de data en de modelvoorspellingen voor de adsorptie aan HFO. Het is echter mogelijk dat bij zulke extreme belastingen oppervlakteprecipitatie optreedt.

Het bovenstaande suggereert dat er, ondanks verschillen in reactiviteit tussen goethiet en HFO, een relatie bestaat tussen het adsorptiegedrag van beide mineralen. Omdat HFO beschouwd wordt als een belangrijke vertegenwoordiger voor veldcondities is dit van groot praktisch belang. In het vervolg kan het CD-model gebruikt worden om adsorptie te voorspellen in complexe systemen die natuurlijke condities simuleren.

Biogeochemische Sleutelfactoren in het Gedrag van Arseen in Grondwater (Hoofdstuk 6)

De verspreiding van As in grondwater is uitgebreid bestudeerd. De resultaten hebben geleid tot een aantal hypotheses die de oorsprong van de verhoogde As-concentraties trachten te verklaren. Het grote aantal uiteenlopende verklaringen dat in recente jaren naar voren is gebracht benadrukt de complexiteit van het vraagstuk en bewijst dat ons begrip van het probleem nog steeds beperkt is. De identificatie van processen is vaak gebaseerd op speculatie, waarbij gebruik gemaakt wordt van correlaties en waargenomen trends: dit omdat de relevante gegevens, met betrekking tot de samenstelling van de vaste fase, helaas vrijwel volledig ontbreken.

Het doel van dit hoofdstuk is de verschillende biogeochemische processen die een rol kunnen spelen in het vrijkomen van As op een kwantitatieve manier te beschrijven, namelijk: het effect van pH en een evenwichtsinstelling met calciet, het vrijkomen van PO_4^{3-} als gevolg van mineralisatie en reductieve oplossing van Fe(hydr)oxides, de reductie van As(V) naar (As(III), en het effect van additionele diagenetische processen die het reactieve oppervlak van het sediment veranderen. Uiteindelijk is een scenario gebruikt om de impact van veranderende condities op arseenconcentraties is poriewater te voorspellen. In de scenarioanalyse werd voor gemiddelde sedimenten de reductieve oplossing met het vrijkomen van PO_4^{3-} geïdentificeerd als de eerste factor die zeer lage As-concentraties kan doen toenemen tot niveaus die boven de WHO-norm voor drinkwater uitstijgen. Reductie van As(V) naar As(III) kan deze waarden ongeveer verdubbelen en elke keer dat het reactieve oppervlak met een factor 2 afneemt kan een verdere verdubbeling optreden. De gemiddelde concentratie van 55 µg/L kan het gevolg zijn van een transformatie van ongeveer 50% van het ijzer(hydr)oxide en 50% reductie van het As(V) naar As(III), aangenomen dat de fosfaat- en Fe^{2+} concentraties gelimiteerd worden door (co)precipitatiereacties. Het CD-model is gebruikt in de berekeningen omdat het is getest voor een groot aantal ion-ion-interacties die relevant zijn in het arseenbindingsproces en het de competitieve effecten in 2- en 3-componentsystemen met As met succes kan voorspellen.

Concluderende opmerkingen

Grondwaterverontreiniging met arseen werd over de gehele wereld snel een belangrijk thema op de politieke agenda toen duidelijk werd dat het aantal mensen dat door dit probleem wordt gedupeerd wereldwijd toeneemt. Door dit onderzoek werd een grote adsorptiedataset verkregen voor mono- en multicomponentsystemen die relevante veldsituaties simuleren. De gegevens werden geïnterpreteerd met een adsorptiemodel met een moleculaire basis: het CD-model. Dit

model is toegepast om het adsorptiegedrag van arseen voor een wijde range van chemische samenstellingen, zoals die voorkomen in het veld, te voorspellen. Op deze manier draagt dit proefschrift bij aan het kwantitatieve begrip van het gedrag van arseen in natuurlijke wateren. Deze kennis kan bijdragen aan lange-termijnoplossingen voor arseenproblemen, zoals bijvoorbeeld optimalisatie van arseenverwijdering uit drinkwater of de ontwikkeling van een methode voor het bepalen van posities van nieuwe, arseen-vrije drinkwaterbronnen.

Epilogue

After 5 years and 7 months this thesis is finally finished! The fact that this promotion is taking place is a combination of pure luck, coincidence, fate, good and bad moments, and a lot of hard work, enthusiasm and frustration. This thesis would not have been finished if it weren't for a number of people, who I would like to thank here.

I start with my friend Anna, with whom I fist arrived in Wageningen. It was her idea to come here, and it was supposed to be for 3 months. None of us ever imagined that we both would be stuck in Wageningen for another 5 years. We shared rooms, clothes, money, some good times and some bad times. In that entirely new, exciting, scary and just unfamiliar situation, it was (and is) very comforting to have a familiar person beside me, and a friend. Thank you for that.

I first arrived in Wageningen on 30 August 2001. I got the job in September. But it took another 7 months before I started this project. Without Winnie van Vark, her will to invest time, effort and persistence in facing the Immigration Office, I would not be able to start working on the project.

The past 6 years of my life have been marked with research. I would like to thank Willem van Riemsdijk and Tijsse Hiemstra for giving me a chance to work on this project, guiding me through it and teaching me "the art of science". I think that I have never met two people with more passion for science. I thank TRIAS for funding this research and the project committee for their time, the support, and their input.

I am very grateful for all the help I received from the lab personnel, when conducting my research; Gerlinde, Peter, Arie, and Andre. I was lucky to have shared my office with some nice

guys: Romulo, Xiaopeng, Odair, and Gerson. Special thanks to Odair and Glaciela, who invited me to Brasil, and provided me with one of the best vacations!

Whenever I had a problem, whether on personal or work level, I could always turn to Nicole, Ellen, Gijs or Liping. I really appreciate all your help in the past years. I hope we can stay friends.

I also want to thank Jac and Erwin, for encouraging Gijs at some point. And I want to thank Gijs for encouraging me for the past 3 years and now.

Special thanks to my family: my mother- Grazyna, my sister- Kamila for their support, and for encouraging me to pull through despite the difficulties.

The time I spent working at the Department of Soil Quality, the work, the people I met, all the things I experienced; it was a life changing experience. When I look at this book, at my life at present almost 6 years later, I can honestly say that it was hard, but it was worth it.

Thank you.

About the Author

Monika Stachowicz was born on 12 March 1978 in Lodz, Poland. After finishing high school in 1996, she went to study Process and Chemical Engineering at the Department of Process and Environmental Engineering at the Technical University of Lodz. She graduated in 2001 and received a Master's Degree. Later that year she came to Wageningen in the Netherlands. In April 2002 she started working at the Soil Quality, a sub-department of Environmental Sciences at the Wageningen University. This thesis presents results of a 5-year research work on arsenic adsorption on iron oxides. After the end of the research project, she started working as a Process Engineer and is currently employed by KH Engineering in Schiedam.

Netherlands Research School for the
Socio-Economic and Natural Sciences of the Environment

CERTIFICATE

The Netherlands Research School for the
Socio-Economic and Natural Sciences of the Environment
(SENSE), declares that

Monika Stachowicz

Born on: 12 March 1978 in: Lodz, Poland

has successfully fulfilled all requirements of the
Educational Programme of SENSE.

Place: Wageningen Date: 1 November 2007

the Chairman of the SENSE board	the SENSE Director of Education
Prof. dr. R. Leemans	Dr. C. Kroeze

The SENSE Research School declares that Ms. Monika Stachowicz has successfully fulfilled all requirements of the Educational PhD Programme of SENSE with a work load of 40 ECTS, including the following activities:

SENSE PhD courses:

- **Environmental Research in Context**
- **Research Context Activity: "Research view on: Solubility/Mobility of Arsenic under Changing Redox Conditions as affected by Multi-Component transport"**
- **Speciation and Bioavailability**
- **Time Planning and Project Management**

Other Phd courses:

- **Speciation and Transport**
- **Water Risk Management**
- **Techniques for Writing and Presenting a Scientific Paper**
- **Scientific Writing**

Scientific Training:

- **Atomic Fluorescence Spectrometer – running Maintenance and Optimalisation of Measurement Techniques**

Activities:

- **PR Officer at WIMEK PhD council**

Presentations:

- **Oral Presentation: SENSE PhD Colloquium, "Solubility / Mobility of Arsenic under Changing Redox Conditions as affected by Multi-Component Transport", 27 March 2003, Ede, The Netherlands**
- **Poster Presentation: Bodem Diep, 4 – 5 June 2003, Zeist, The Netherlands**
- **Oral Presentation: SENSE Summer Symposium, "Contestable Nature-Claims on the Countryside", 17 June 2004, Utrecht, The Netherlands**
- **Oral Presentation: 1st International Conference on Environmental Science and Technology, "Arsenic and Bicarbonate Adsorption on Goethite" 23 – 25 January 2005, New Orleans, Louisiana, USA**

Deputy director SENSE
Dr. A. van Dommelen

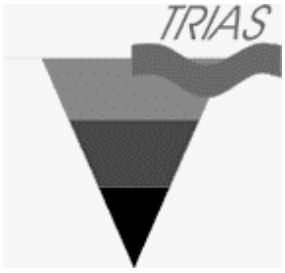

This work was founded by TRIAS project 835.80.006/Delft Cluster 5.17.

TRIAS is het gezamenlijke bodemonderzoeksprogramma van Delft Cluster, NWO en SKB.

Printing: Sieca Repro, Delft

Cover: M. Stachowicz